HYDROMETALLURGY OF METAL SULPHITES:

A STUDY OF LEACHING AND RECOVERY IN THE ZINC SULPHIDE-SULPHUR DIOXIDE SYSTEM

by

DON MARK LARSEN

A thesis submitted for the degree of

Doctor of Philosophy

Department of Chemical Engineering,
The University of Sydney,
New South Wales, Australia

September, 1984

ABSTRACT

Conventional processes for the production of zinc from its sulphide ores have become progressively unsatisfactory owing to the increased complexity of processing low grade ores and environmental pollution problems. As an endeavour to develop a new process, an intensive study was made on the properties of zinc in aqueous sulphurous acid media. The use of sulphur dioxide for precipitating zinc in the form of a sulphite salt was investigated as a potential hydrometallurgical purification or selective extraction process. Thermodynamic Pourbaix and solubility diagrams were developed, from experimental and published data, for the $Zn-S-SO_2-H_2O$ system at temperatures up to 200°C. Kinetic leaching experiments were performed on an iron-free synthetic sphalerite powder by injecting mixtures of sulphur dioxide, oxygen and nitrogen into a stirred slurry of the material in water. Ferric sulphate and sulphuric acid were used as secondary reagents. In the absence of iron and sulphuric acid, sphalerite decomposed by an oxidative dissolution process to form the tetrathionate ion as the principal sulphur product. Oxygen had no role in the dissolution process. In the presence of dissolved iron, however, oxygen was active in the decomposition and the mechanism was dependent on the SO/O_2 ratio of the gas mixture. At mole ratios below 0.5, the leaching proceeded by acidic decomposition and hydrogen sulphide was evolved. At SO_2/O_2 mole ratios above 0.5, elemental sulphur was formed and the oxidation of hydrogen sulphide in-situ was postulated to occur by the Wackenrhoder reaction, or by a mechanism involving the $FeHSO_3^{2+}$ species shown to be present in the medium by the thermodynamic study. The production of elemental sulphur did not impede the reaction kinetics and the process was observed to be surface reaction controlled. The Pourbaix diagrams developed in this work aid in the development of effective process strategies and reveal sulphur dioxide to be an attractive reagent for the leaching of zinc sulphide in an ambient temperature and pressure process.

PREFACE

The work reported in this thesis was carried out in the Hydrometallurgical Laboratories of the Department of Chemical Engineering in The University of Sydney, between May, 1980 and July, 1984. It is the original and independent work of the author except where specifically acknowledged in the text. Neither this thesis, nor any part of it, has been previously presented at this or any other University.

The thermodynamic potential -pH diagrams of the $Zn-SO_2-H_2O$, metastable $S-H_2O$ and $Zn-S-SO_2-H_2O$ systems at temperatures of 25°C to 200°C, and the $Fe-S-SO_2-H_2O$ system at 25°C, are original and previously unpublished. The incorporation of the tetrathionate species into the metastable $S-H_2O$ system, and of the iron bisulphite species into the $Fe-S-SO_2-H_2O$ system, are the original work of the of the author. These diagrams were developed by the author from experimental solubility measurements and from the thermodynamic data available in Kao (1979), Naumov, et al (1974) and Wagman, et al (1982). A computer program package, described by Linkson, et al (1979), was used by the author to aid in the calculation of the thermodynamic equilibrium relationships.

The experimental apparatus, including the reactor lid and sample collection device, was designed and commissioned by the author. Fabrication of the reactor lid and impeller assembly was carried out by the technical staff of the Chemical Engineering Workshop. The experimental procedure was developed by the author. A method for the quantitative estimation of the tetrathionate species in sulphur dioxide leach liquors was developed largely through the work of M. Josephson in the Department of Chemical Engineering.

ACKNOWLEDGEMENTS

The author wishes to thank all those who have been of assistance during the course of this work. In particular, he wishes to thank,

- Associate Professor P.B. Linkson for his consistent, sound advice throughout the course of this project.

- Denis Nobbs, Greg Hopkins and the technical staff of the Department of Chemical Engineering, for their advice and assistance with the laboratory and analytical equipment.

- Marius Josephson for his excellent analytical work.

- Tracy Ashcroft, Sue Hollingsworth and Karen McIlroy, for their patience, diligence and perseverance in transforming the original manuscript into its present form.

- The University of Sydney for providing the Postgraduate Research Scholarship.

TABLE OF CONTENTS

LIST OF TABLES

LIST OF FIGURES

NOMENCLATURE

SYMBOL		UNITS
a_i	activity of species i	mol dm^{-3}
a	concentration of acid	mol dm^{-3}
a	total quantity of acid	mol dm^{-3}
A_a	anodic surface area	m^2
A_c	cathodic surface area	m^2
a,b,c...	general constants or variables	
A,B,C...	general constants or variables	
b	concentration of base	mol dm^{-3}
b	total quantity of base	mol dm^{-3}
b,c,n,m,p,q	stoichiometric coefficients	
C_i	concentration of species i	mol dm^{-3}
C_p°	heat capacity	J mol^{-1} K^{-1}
$\overline{C_p^\circ}\Big\|_{T_1}^{T_2}$	average heat capacity between temperatures T_1 and T_2	J mol^{-1} K^{-1}
$\overline{\Delta C_{p,f}^\circ}\Big\|_{T_1}^{T_2}$	average heat capacity change of the formation reaction	J mol^{-1} K^{-1}
d_i	ionic diameter of species i	
D	diffusivity	
E	electromotive force	V
Eh	potential relative to the SHE	V
%EXTN	percent extraction	
F	Faraday constant = 96487	C mol^{-1}
ΔG	Gibb's free energy change	kJ mol^{-1}
ΔG°	standard free energy change	kJ mol^{-1}
$\Delta G_{f,i}^\circ$	standard free energy change of the formation reaction of species i	kJ mol^{-1}
I	ionic strength	
I_a	anodic current	A
I_c	cathodic current	A
k,k'	rate constant	s^{-1}
k_a	anodic rate constant	
k_c	cathodic rate constant	

SYMBOL		UNITS
k_r	reaction rate constant	ms^{-1}
k_d	diffusion rate constant	ms^{-1}
K	equilibrium constant	
K_{SP}	solubility product	
m_i	molality of species i	mol dm^{-3}
N_i	moles of substance i	mol
P_A	partial pressure of gas A	atm
r	particle radius	m
r_o	initial particle radius	m
R	universal gas constant = 8.314	J mol^{-1} K^{-1}
R_a	rate of anodic reaction	s^{-1}
R_c	rate of cathodic reaction	s^{-1}
rpm	revolutions per minute	min^{-1}
s	surface area	m^2
S°_T	conventional entropy at temperature T	J mol^{-1} K^{-1}
$\overline{S}^\circ_T$	absolute entropy at temperature T	J mol^{-1} K^{-1}
$\Delta S^\circ_{f,T}$	standard entropy change of the formation reaction at temperature T	J mol^{-1} K^{-1}
SHE	standard hydrogen electrode	
SCE	standard calomel electrode	
t	time	s
T	temperature	K
z_i	ionic charge of species i	

GREEK SYMBOLS

α	fraction of material reacted	
$\alpha_1, \alpha_2, \ldots$	ionization fractions	
β_a	anodic charge transfer barrier	
β_c	cathodic charge transfer barrier	
γ_i	activity coefficient of species i	
ν_i	stoichiometric coefficient	
ϕ	charge transfer coefficient	
ϕ	electrode potential	V
ϕ_{ref}	reference electrode potential	V
ρ	molar density	mol cm^{-3}
ρ_i	mass density of substance i	g cm^{-3}
τ	time required for complete reaction	s

CHAPTER ONE

INTRODUCTION AND LITERATURE OVERVIEW

1.1 INTRODUCTION

Historically, the processing of lead-zinc sulphide ores has involved the roasting of high grade ores or concentrates to form a metal-oxide calcine. The roasting process traditionally is followed by either a reduction with coke in a blast furnace, or by acid leaching of the calcine and subsequent electrowinning of the metal values. The smelting of sulphide minerals generates flue gases which contain sulphur dioxide in concentrations ranging from 0.5 to 10 percent. The detrimental effect that releasing these sulphur dioxide laden gases into the environment had in the early days of smelting practice can be witnessed around the world in such areas as Sudbury, Ontario and Queenstown, Tasmania. Fortunately, much of this problem has been alleviated through the introduction of strict pollution control regulations. Conversion to sulphuric acid, generally, is the most common method of recovering the sulphur in waste gas. However, recent environmental legislation continually becoming more stringent, now requires even further treatment for the disposal of acid plant tail gas.

The capital and operating costs of a smelter and the associated dust collection and acid production facilities are extremely high. Although much of the acid generated in an operation can be recycled to on-site hydrometallurgical operations or used in fertilizer manufacture, the handling, storage and transportation of sulphuric acid for sale or disposal can be very costly. These costs are especially high when such operations are located in remote areas.

Currently, the worldwide increase in demand for resources coupled with the depletion of high grade, massive ore bodies has stimulated the development of technology to process low grade, highly disseminated and mineralogically complex ores. The McArthur River deposit located in Australia is, in particular, a very large lead-zinc sulphide deposit with a very complex and fine grained mineralogy. Attempts to develop suitable metallurgy for this ore, since its discovery in 1955, have not been successful (Anon., 1977). The extremely fine grain size and intimate mixture of minerals prevents the achievement of sufficient liberation for an effective differential sulphide flotation. The close association of zinc and iron sulphides in the McArthur River ore leads to the formation of a significant quantity of zinc ferrite in roasting operations. Consequently, production costs are increased and there is a loss in zinc recovery due to the formidable nature in the treatment of these ferrite compounds.

Research interest in recent years, therefore, has been directed toward the removal of sulphur dioxide from smelter gases. An attractive means would be the conversion of sulphur dioxide to the inert form of elemental sulphur. Even more desirable would be the elimination of the need for a roasting step altogether by direct oxidation of the sulphides in aqueous media. The oxidation of sulphide minerals by oxygen in an aqueous medium is thermodynamically favourable. However, at ambient temperatures and pressures the oxidation suffers from slow kinetics. Reasonably high rates of leaching are only obtained in autoclaves at elevated temperatures and high oxygen pressures. An elevated temperature and pressure process, however, is very capital intensive. This greatly increases the overall cost of the operation. Additionally, in the case of highly disseminated ores such as the McArthur River ore, oxygen pressure leaching of lead-zinc concentrates leads to the formation of

lead jarosites. This in turn, creates a formidable problem in the final recovery of the lead content.

Consequently, there is an industrial need for research to be carried out in the area of sulphite chemistry for two major reasons. Firstly, it is no longer acceptable to deposit sulphur dioxide laden waste gases from smelters into the atmosphere. The technology for the elimination of these contaminant gases must be developed. Secondly, the mineral resources of the earth are being depleted of their high grade, coarse grained components. Present technology cannot satisfactorily refine all of the very fine grained and highly disseminated complex ores which remain. Therefore, the technology to process these remaining resources must be developed, because, they will need to be mined in the future.

1.2 LITERATURE OVERVIEW

The usefulness of sulphur dioxide as a hydrometallurgical reagent has been demonstrated in the literature. Various researchers have shown that it can function as an oxidizing agent, a reducing agent or a precipitant in an aqueous solution. However, relatively few studies with sulphur dioxide have been concerned with the methods of extraction of zinc from sulphide ores. Table 1 lists the pertinent works which use sulphur dioxide or sulphite chemistry as the basis for a proposed process.

The two studies by Nobbs and Linkson (1981), and Parker and Muir (1981) both demonstrate the utility of sulphur dioxide as a precipitant and as a reducing agent. Various copper sulphite salts are precipitated with sulphur dioxide from impure copper solutions and, in both of these processes, the salts are subsequently reduced to metallic copper. The sulphite component of the salt is consequently oxidized to the sulphate state.

Sudderth, et al (1978) investigated the production of

TABLE 1

AREAS OF RESEARCH UTILIZING SULPHUR DIOXIDE IN ZINC AND SULPHIDE ORE PROCESSING

RESEARCH AREA	FUNCTION OF SULPHUR DIOXIDE	AUTHOR	TOPIC
Copper Extraction	Precipitant, Reducant	Nobbs & Linkson (1981)	Two-stage process for recovery of metallic copper from sulphite leach liquors.
Copper Extraction	Reducant	Parker & Muir (1981)	Recovery of copper powder from concentrates using sulphur dioxide.
Zinc Extraction	Chemical Reagent	Sudderth, et al (1978)	Selective extraction of zinc from bisulphite leach liquors using solvent extraction.
Zinc Concentrate Leaching	Oxidant	Adams & Matthews (1981)	Leaching of sulphide concentrates at atmospheric pressure using sulphur dioxide/oxygen mixtures.
Zinc Sulphide Leaching	Oxidant	Tiwari (1976)	The kinetics of oxidation of zinc sulphide and hydrogen sulphide by sulphur dioxide in aqueous sulphuric acid.
Zinc-Lead Concentrate Treatment	Chemical Reagent, Precipitant	Esdaile & Walters (1969)	Treatment of McArthur River ore by dissolution and precipitation of various metal sulphites.
Sulphur Dioxide Recovery, Zinc Oxide Treatment	Chemical Reagent	Johnstone & Singh (1940)	Recovery of sulphur dioxide from waste gas by reaction with impure zinc sulphite. Production of pure sulphur dioxide and zinc oxide by sulphite calcination.

a pure zinc sulphate solution suitable for electrolytic reduction of zinc from impure sulphite-bisulphite leach liquors. The selective solvent extraction of zinc from an impure sulphite-bisulphite medium containing iron was found to be superior to the selectivity obtained from a sulphate medium. A process for zinc recovery was proposed comprising the leaching and solvent extraction of zinc in aqueous sulphur dioxide media. Final zinc production by electrolysis could then proceed unhindered by dissolved iron.

The investigation by Adams and Matthew (1981) and that by Tiwari (1976) illustrate the oxidizing properties of sulphur dioxide. Adams and Matthew studied the leaching of zinc sulphide concentrates with mixtures of sulphur dioxide and oxygen in an aqueous medium. Tiwari studied the oxidation kinetics of synthetic zinc sulphide and hydrogen sulphide by sulphur dioxide in a sulphuric acid medium.

Esdaile and Walters (1969) have conducted a pilot scale investigation of a scheme for the treatment of McArthur River ore using sulphite chemistry. Several of the dissolution and precipitation steps tested appeared feasible, however, sufficient purity of the product solution could not be obtained for the electrolytic production of zinc.

Johnstone and Singh (1940) conducted a thorough pilot plant investigation on the recovery of sulphur dioxide from waste gases by precipitation of zinc sulphite. This was followed by calcination of the dried solid to give pure sulphur dioxide and zinc oxide for recycle. Much data are presented on the design of flash calciners for zinc sulphite in this early work.

1.3 OBJECTIVES OF WORK

Despite its dominant position in the industry, the electrolytic process for the winning of zinc has some well recognized problems as previously outlined. The incentive to develop new technology or to modify the existing practice is provided by an increasing necessity to process low grade ores of complex mineralogy, soaring energy costs and the implementation of strict pollution standards. Since few comprehensive studies exist on the application of sulphite chemistry to the extraction of metals, a project was undertaken to examine the use of sulphur dioxide gas in the extraction and recovery of zinc from its sulphide ore. The scope of this thesis, therefore, includes a study of the leaching of zinc sulphide in aqueous sulphur dioxide media and the properties of the resulting leach liquors.

Very little fundamental quantitative information is available on the zinc sulphite system for use in the formulation of process strategy. This work was aimed at evaluating and extending the available thermodynamic data for use in the construction of stability diagrams. These concise and convenient diagrams, it was envisaged, would highlight the features of the zinc - sulphur dioxide - water system, and therefore, identify the conditions for mineral decomposition and solids precipitation. Such information would provide a sound basis for the proposed experimental investigation. Consequently, the resulting dissolution kinetics and extent of reaction data would allow the formulation of a process for the direct dissolution of zinc sulphide in aqueous sulphurous acid media at atmospheric pressure, followed by precipitation of any insoluble species from the resultant leach liquors.

CHAPTER TWO

THERMODYNAMICS OF THE ZINC-SULPHUR DIOXIDE-WATER SYSTEM

The industrial application of hydrometallurgy over a span of several decades has evolved a great variety of processing schemes whose operational practices have become a well established art. However, in many cases the understanding of the fundamental chemical principals involved in governing the operation of those processes is limited. Hydrometallurgical operations can be conveniently classified into three major areas: specifically, the dissolution of the desired element from a solid, purification of the resulting leach liquor and finally, the recovery of the desired element from the purified pregnant liquor. The study of thermodynamics makes it possible to define the equilibrium state in each of these three heterogeneous chemical processes and to predict how this equilibrium will shift by changing conditions such as temperature, pressure, concentration and pH, etc. Consequently, knowledge of the physical chemistry of heterogeneous aqueous solutions has rapidly advanced with the appearance of vast quantities of theoretical and experimental thermodynamic data.

2.1 LITERATURE REVIEW

The copious quantities of available thermodynamic data have been considered so indigestible that many workers, with a few notable exceptions, have not been prepared to utilize them. Pourbaix (1949) in a major work, describes a method to condense this great volume of data into concise and functional stability diagrams. The resulting potential-pH (Eh-pH) diagram, as developed by Pourbaix, represents one type of thermodynamic diagram which describes the theoretical oxidation, reduction, dissolution and hydrolysis reactions occuring in

heterogeneous aqueous solutions. Pourbaix (1966) also published an atlas of metal-water Eh-pH diagrams for all of the more common metal-water systems at 25°C.

The sulphur-water system as first published by Valensi (1950) shows only three sulphur valence states to be stable at room temperature. These stable species of sulphur are sulphate-bisulphate, elemental sulphur and the sulphides (H_2S,HS^-,S^{2-}). Valensi, in the same paper, also published an Eh-pH diagram incorporating the metastable species of thiosulphate ($HS_2O_3^-$,$S_2O_3^{2-}$)and sulphite (H_2SO_3,HSO_3^-,SO_3^{2-}) while omitting the sulphate species. This metastable sulphur-water diagram by Valensi is reproduced on page 64 of the Pourbaix (1966) Atlas. A diagram of this type permits the analysis of systems where metastable species are formed and persist in solution. Peters and Majima (1968) and Peters (1976) later followed this idea by assembling together metal-water and sulphur-water diagrams and incorporating into them the metal sulphide species. The resultant Eh-pH diagrams were used to study the solution properties of several sulphide minerals. Table 2 presents a summary of some of those researchers who have contributed to the development of the metal-sulphur-water, potential-pH diagram.

The reaction of a sulphide with aqueous sulphur dioxide solution was shown by Thorne and Roberts (1948) to yield finely divided elemental sulphur. However, it is recorded in Schroeter (1966) that this reaction also produces a complex distribution of sulphur compounds. This complex mixture of sulphur oxyanions produced by the reaction of hydrogen sulphide with aqueous sulphurous acid is known as Wackenroder's Solution. The preparation, composition and properties of Wackenroder's Solution is discussed in detail by Debus (1888).

A metastable sulphur-water diagram such as the one presented by Peters (1976) can define the conditions under which such species might form. The capability of predicting intermediate reaction products and metastable

TABLE 2

REPORTED STUDIES ON POTENTIAL-pH THERMODYNAMIC DIAGRAMS

AUTHOR	SUBJECT OF RESEARCH
Pourbaix (1949)	Described the method of constructing potential-pH diagrams.
Valensi (1950)	First to publish the sulphur-water diagram and to produce the metastable sulphur-water system.
Garrels & Christ (1965)	Combined metal-water diagrams with the sulphur-water diagram for interpreting geological systems.
Pourbaix (1966)	Published an atlas of metal-water stability diagrams to the interpretation of leaching characteristics.
Burkin (1966)	Applied metal-sulphur-water diagrams to the interpretation of leaching characteristics.
Peters & Majima (1968)	Applied metal-sulphur-water diagrams to the interpretation of leaching results for various metal sulphides. Constructed iron-sulphur-water diagrams at elevated temperatures up to 200°C.
Biernat & Robins (1969)	Presented potential-pH diagrams for the sulphur-water system at temperatures up to 300°C.
Lowson (1971)	Compiled the available methods of extrapolating thermodynamic data to elevated temperatures for the construction of Eh -pH diagrams.
Biernat & Robins (1972)	Presented potential-pH diagrams for the iron-water and iron-sulphur-water systems at temperatures up to 300°C.
McDonald, et al (1972)	Presented potential-pH diagrams for the water and water-copper systems at elevated temperatures.
Ferreira (1975)	Presented potential-pH diagrams for the sulphur-water, copper-sulphur-water and iron-sulphur-water systems at temperatures up to 150°C.
Peters (1976)	Described thermodynamically feasible decomposition paths for several sulphide minerals using metal-sulphur-water potential-pH diagrams.

species aids in the identification of the mechanism of a chemical reaction between a mineral and its aqueous environment. As Peters (1976) points out, there are four types of media in which a sulphide mineral can decompose. These four media types are:

1) Oxidizing solutions, where the sulphide is oxidized to elemental sulphur or sulphate.
2) Strong acid solutions, leading to hydrogen sulphide evolution and dissolved metal ion.
3) Reducing solutions, where an aqueous sulphide is produced (H_2S,HS^- or S^{2-}) and metal or metal ions are formed.
4) Strong basic solutions, leading to sulphide ions and metal hydroxides in solution.

The metastable Pourbaix diagram shows directly the reaction products that can form when any of the four solution conditions listed above are applied to sulphide mineral systems.

The Pourbaix Atlas (1966) contains diagrams for the zinc-water system at 25°C. However, an investigation of the dissolution of zinc sulphide and other metal sulphides in aqueous sulphurous acid requires a more complex diagram. Preliminary experiments have shown that zinc sulphite can precipitate from sulphurous solutions containing zinc. Consequently, in any equilibrium compilation, this solid, as well as zinc sulphide, zinc hyrdoxide and elemental zinc, must be considered. Despite the knowledge for a century of the formation of solid zinc sulphite (Heuston, 1890), very little quantitative information is available on its properties. The incorporation of zinc sulphite into the zinc-water system will define the conditions for precipitation and stability of this salt in sulphur dioxide media. Similarly, the incorporation of zinc sulphide into the zinc-water system will predict the plausible dissolution routes for the mineral in a sulphite medium. Peters (1976) has incorporated zinc sulphide into the zinc-sulphur water system. However, Peters (1976) only considered the sulphate species and neglected the sulphite and other

metastable species. Therefore, any compound of sulphur which may form by the reaction of aqueous sulphur dioxide and zinc sulphide must be considered for a comprehensive diagram.

Generally, there is a lack of thermodynamic data for ionic species at temperatures other than 25°C. Many recent hyrdometallurgical schemes, however, have employed high temperatures and pressures to overcome kinetic difficulties. Hence, it is desirable to have diagrams available which depict the equilibria at elevated temperatures where many of the applications may be of interest. Table 2 also lists the major works on high temperature stability diagrams. Lowson (1971) has compiled most of the available methods for extrapolating thermodynamic data to elevated termperatures. These methods have been employed by other researchers such as Peters and Majima (1968), McDonald, et al(1972) and Ferreira (1975) to construct diagrams up to 200°C for the systems involving iron, copper, sulphur and water. Biernat and Robins (1972) have constructed stability diagrams up to temperatures as high as 300°C for the systems involving iron, sulphur and water. Studies on the zinc-sulphur-water system, however, are very limited. The utility of high temperature equilibrium diagrams in process studies has been demonstrated. It is important to note however, that the potential-pH diagram depicts only thermodynamic feasibility and cannot be used to predict the velocity of attaining the equilibrium state.

2.2 DEVELOPMENT OF THE POTENTIAL -pH DIAGRAM

2.2.1 Mathematical Development

The general equilibrium equation representing electrochemical reactions in aqueous solutions containing a metallic species is given by

$$pAq + cH^{+} + ne^{-} = qBp + mH_2O \qquad (1)$$

when written in the form of a reduction. Aq and Bp are

the particular metallic species where p and q define the number of metal atoms associated with each species. Equation (1) can be written in the more concise form

$$\Sigma\nu_i M_i - ne^- = 0 \qquad (2)$$

where n is the number of electrons, i an identification or index of a species, and ν_i the stoichiometric coefficient of species M_i. ν_i is positive for product and negative for reactant species. Thus for Equation (1)

$$\nu_{Aq} = -p,\ \nu_{H^+} = -C,\ \nu_{B_p} = q,\ \nu_{H_2O} = m$$

where p, q, c and m are positive integers.

Electrochemical reactions are brought about by the coupling of two electrodes at which takes place reduction and oxidation, respectively. It is generally convenient to consider any electrochemical reaction as part of a galvanic cell made up of one electrode where the reaction of interest takes place and the other a reversible reference electrode. The reversible reference electrode defines a state of the thermodynamic equilibrium against which all reactions are measured. The reaction for any reference electrode can be written as

$$\Sigma\nu_{ref} M_{ref} - ne^- = 0\ . \qquad (3)$$

Then the overall reaction for the galvanic cell considered is

$$\Sigma\nu_i M_i - \Sigma\nu_{ref} M_{ref} = 0 \qquad (4)$$

A general electrochemical reaction, $\Sigma\nu_i M_i - ne^- = 0$, is in equilibrium if the difference between the potential ϕ of the electrode on which this reaction is taking place and the potential ϕ_{ref} of the reference electrode has a fixed value. This equilibrium value is given by

$$\phi - \phi_{ref} = -\frac{\Delta G}{RT} \qquad (5)$$

where ΔG is the change in the Gibbs free energy for the overall reaction, defined as

$$\Delta G = \Sigma \nu_i \Delta G_{f,i} - \Sigma \nu_{ref} \Delta G_{f,ref} \cdot \qquad (6)$$

$\Delta G_{f,i}$ and $\Delta G_{f,ref}$ are the free energy of formation of species M_i and M_{ref} respectively. F is the Faraday constant, equal to 96487 coulombs/mole. $\phi - \phi_{ref}$ is called the electrode potential, with respect to the reference electrode used.

If the reference electrode used is the standard hydrogen electrode (SHE), i.e.,

$$2H^+ + 2e^- = H_2(g) \quad (a_{H^+} = P_{H_2} = 1)$$

then, $\phi_{ref} = \phi_{SHE} = 0$ by definition and $\phi - \phi_{SHE} = Eh$.

Eh is defined as the electrode potential relative to the SHE. Equation (6) then becomes, for the case of the general electrochemical reaction of Equation (1),

$$\Delta G = (p\Delta G_{f,Aq} - C\Delta G_{f,H^+} + q\Delta G_{f,B_p} + m\Delta G_{f,H_2O}) - (n\Delta G_{f,H^+} + \frac{n}{2} \Delta G_{f,H_2}) \cdot \qquad (7)$$

The free energy of formation, $\Delta G_{f,i}$, can be related to the standard free energy of formation, $\Delta G^\circ_{f,i}$, and the activity of species i, a_i, by

$$\Delta G_{f,i} = \Delta G^\circ_{f,i} + RT \ln a_i \cdot$$

For the general electrochemical reaction (1), then

$$\Delta G_{f,Aq} = \Delta G^\circ_{f,Aq} + RT \ln a_{Aq}$$

$$\Delta G_{f,B_p} = G^\circ_{f,B_p} + RT \ln a_{B_p}$$

etc.,

and for the standard hydrogen electrode, with the reaction,

$$2H^+ + 2e^- = H_2 \quad (a_{H^+} = P_{H_2} = 1) \tag{8}$$

$$\Delta G_{f,H^+} = \Delta G^\circ_{f,H^+} + RT \ln a_{H^+} = \Delta G^\circ_{f,H^+}$$

$$\Delta G_{f,H_2} = \Delta G^\circ_{f,H_2} + RT \ln P_{H_2} = \Delta G^\circ_{f,H_2} .$$

Then, Equation (7) gives

$$\Delta G = -p\Delta G^\circ_{f,Aq} - (c-n)\Delta G^\circ_{f,H_2} + q\Delta G^\circ_{f,B_p} + m\Delta G^\circ_{H_2O} + RT \ln \frac{a^q_{Bp} a^m_{H_2O}}{a^p_{Aq} a^c_{H^+}} . \tag{9}$$

If the standard Gibbs free energy change for the overall cell reaction is defined as

$$\Delta G^\circ = \Delta G^\circ_f \text{ (products)} - \Delta G^\circ_f \text{ (reactants)}$$

$$= -p\Delta G^\circ_{f,Aq} - (c-n)\ \Delta G^\circ_{f,H^+} - \frac{n}{2}\ \Delta G^\circ_{f,H_2} + q\Delta G^\circ_{f,B_p} + m\Delta G^\circ_{f,H_2O} , \tag{10}$$

Equation (9) can be written as

$$\Delta G = \Delta G^\circ + RT \ln \frac{a^q_{Bp}\ a^m_{H_2O}}{a^p_{Aq}\ a^c_{H^+}} . \tag{11}$$

Combining Equations (5) and (11) yields

$$Eh = -\frac{\Delta G^\circ}{nF} - \frac{RT}{nF} \ln \frac{a^q_{B_p}\ a^m_{H_2O}}{a^p_{Aq}\ a^c_{H^+}} \tag{12}$$

or,

$$Eh = -\frac{\Delta G^\circ}{nF} - \frac{RT}{nF} \ln \frac{a^q_{B_p}}{a^p_{Aq}} - 2.303\ \frac{RT}{nF} c\ pH - \frac{RT}{nF} m \ln a_{H_2O} . \tag{13}$$

Equations (10) and (13) form the working relation for the calculation of Eh. If Equation (10) is used to calculate ΔG° from thermodynamic ΔG_f° data, Equation (13) yields Eh as a linear function of pH for the reaction studied, at a specific temperature and a given ratio of activities. Examples of these calculations are presented in detail in Appendix 3.

Each line defined by Equation (13) represents equilibrium coexistance between two species, or in the case of the general electrochemical reaction of Equation (1), the species Aq and Bp. One of these species becomes energetically more favourable over the other when this line is crossed. Each line therefore delineates a boundary between two adjacent areas on a diagram. If the generated lines for all possible equilibria in the system under study are plotted on the same diagram, there will be competing equilibria and the elimination of some species as thermodynamically unstable will result. By elimination of lines or parts of lines which have no significance, a composite diagram which shows the relative areas of predominance for the various species is obtained. The thermodynamic significance of such an area is that the species predominant in it has the lowest Gibbs free energy of any species in the system and is therefore the most stable.

Two special cases of Equation (13) are to be noted. When no oxidation or reduction is involved but hydrolysis occurs, n is equal to zero. Thus, ΔG equals zero by Equation (5) and Equation (11) reduces to

$$\Delta G^\circ = -RT \ln K \frac{a^q_{B_p}}{a^p_{Aq}\, a_{H^+}} \quad . \tag{14}$$

The lines generated, in this case, are parallel to the Eh axis. For oxidation or reduction with no hydrolysis, c in Equation (13) is equal to zero and the lines are parallel to the pH axis.

Since pure solid species by definition have an activity equal to one, the boundary between two solid

species as given by Equation (13) is fixed. It is convenient to define the boundary between two dissolved species as the line corresponding to equal activities of those species. In the case of one solid- one dissolved species, the boundary must be defined in terms of some arbitrary activity of the dissolved species. In hydrometallurgical applications, contours corresponding to activities of 10^0 and 10^{-3} mol dm^{-3} are usually drawn on the same diagram. These activities relate to the approximate concentrations of metal species in pregnant leach liquors and barren raffinate solutions common to hydrometallurgical operations, respectively. Such processes would include electrolytic tank houses, cementation and precipitation operations along with ion exchange or solvent extraction plants.

2.2.2 Stability of Water

The lines corresponding to the oxidation and reduction of water are usually included in the final composite diagram. The electrode reactions are (see Appendix 1):

Reaction 64, $2H^+ + 2e^- = H_2$

Reaction 65, $O_2 + 4H^+ + 4e^- = H_2O$

representing the reduction and oxidation of water respectively. At 25°C, Equation (13) yields the following lines:

$$Eh = -0.0592\ pH - 0.0295 \log P_{H_2}$$

$$Eh = 1.228 - 0.0592\ pH + 0.0148 \log P_{O_2}\ .$$

For PH_2 = 1 atm and P_{O_2} = 1 atm these equations become:

$$Eh = -0.0592\ pH$$

$$Eh = 1.229 - 0.0592\ pH.$$

The region enclosed by these two lines corresponds to an equilibrium pressure of hydrogen and oxygen less than 1 atm. Hence, this represents the area of thermodynamic stability of water under a pressure of 1 atm and at a temperature of 25°C.

2.2.3 Elevated Temperatures

Equations (10), (13) and (14) derived above are applicable at any temperature and pressure. All that is required for the generation of a stability diagram is sufficient thermodynamic data. However, thermodynamic data for species in aqueous solution at temperatures other than 25°C are scarce. Generally, high temperature data must be estimated using extrapolation techniques. A number of such techniques have been proposed and these are summarized by Lowson (1971). The various estimation techniques, particularly the "Correspondence Principal" proposed by Criss and Cobble (1964) are referred to in the next section (2.2.4) and within the sample calculations of Appendix 3.

The calculation of Eh_T (the electrode potential with respect to the SHE at temperature T) from Equations (10) and (13) requires that $G^\circ_{f,T}$ (the standard free energy of formation at temperature T) be known for all species of the electrochemical reaction under study. The Gibbs free energy of a chemical reaction at a temperature T is related to that at 25°C by the equation

$$\Delta G^\circ_T = \Delta G^\circ_{298} - \Delta S^\circ_{298}\,(T-298.15) + \int_{298.15}^{T} \Delta C^\circ_p\, dT - T \int_{298.15}^{T} \Delta C^\circ_p\, d(\ln T) \qquad (17)$$

The derivation of Equation (17) from basic thermodynamic relations is given by Linkson, et al (1979). This equation can be simplified by using average values of heat capacities over the range of 25°C to T. If the average heat capacity values are incorporated, Equation (17) in the case of a formation reaction of a species from its elements reduces to

$$\Delta G^\circ_{f,T} = \Delta G^\circ_{f,298} - \Delta S^\circ_{f,298}(T-298.15) + \overline{\Delta C^\circ_{p,f}}\,\Big|_{298}^{T} \left(T-298.15 - T \ln \frac{T}{298.15}\right) . \qquad (18)$$

Thus, $\Delta G^\circ_{f,T}$ can be calculated from $\Delta G^\circ_{f,298}$ with the appropriate entropy and heat capacity data. Subsequently, Eh_T is found for the reaction of interest from Equations (10) and (13). Additionally, it is important to note that

in this work all electrode potentials at elevated temperature, Eh_T, are measured relative to the SHE at that same temperature.

2.2.4 Thermodynamic Data

The thermodynamic data available in the scientific literature are, in general, given at a temperature of 25°C. The only data required for the construction of a potential-pH diagram at 25°C are free energy of formation values for each species to be included in the diagram. Tables 3 through 7 inclusive list the free energy data for the relevant species of zinc sulphur, iron, lead and water, respectively, at 25°C. This data is used directly in the construction of Eh-pH diagrams at room temperature. The general source of these data is Wagman, et al(1982). Data obtained from alternative sources are indicated in Tables 3 through 7 inclusive by a footnote in parenthesis. The appropriate data sources are referenced in the footnotes. In the case of the metal sulphite salts listed, the free energy of formation was determined experimentally. The experimental determination of the free energy of formation of these salts is the subject of Chapter Three.

The calculation of free energy of formation data at elevated temperatures requires the use of room temperature free energy, entropy and heat capacity data. These data at 25°C are also listed in Tables 3 through 7 inclusive. The absolute entropy, $\bar{S}°$, are calculated from the conventional entropy, S°, in a manner defined by Criss and Cobble (1964). The method of calculation is presented with the sample calculations in Appendix 3. Since entropy and heat capacity data are generally scarce for ionic species, various established estimation techniques have been employed to approximate these data where they are otherwise unavailable. The estimation techniques used are indicated in the footnotes to the tables.

Table 8 presents the thermodynamic data extrapolated to elevated temperatures for the zinc-metastable sulphur-

TABLE 3

THERMODYNAMIC DATA FOR SPECIES OF ZINC

	298.15 K (25°C) and 0.1 MPa (1 bar)			
Species	ΔG_f° kJ mol^{-1}	S° J mol^{-1}K^{-1}	$\bar{S}^\circ$ J mol^{-1}K^{-1}	C_p° J mol^{-1}K^{-1}
Solid Species				
Zn (C)	0. *	41.63	41.63	25.40
ε-$Zn(OH)_2$ (C)	-555.07	81.6	81.6	72.4
$ZnSO_3 \cdot 2\frac{1}{2}H_2O$(C)	-1256. (1)	206.3 (2)	206.3	
ZnS (sph)	-201.29	57.7	57.7	46.0
Dissolved Species				
Zn^{2+} (aq)	-147.06	-112.1	-153.9	46.
$ZnOH^+$ (aq)	-330.10	81.6(3)	60.7	
$Zn(OH)_2^\circ$ (aq)	-522.73	0. (3)	0.	
$Zn(OH)_3^-$ (aq)	-694.22	144. (4)	165.	
$Zn(OH)_4^{2-}$ (aq)	-858.52	61.9(4)	104.	

* Defined reference state

(1) Experimentally determined from solubility data.

(2) Entropy estimated by the method of Latimer (1951).

(3) Entropy estimated by the method of Cobble (1953).

(4) Entropy estimated by the method of Couture and Laidler (1957).

TABLE 4

THERMODYNAMIC DATA FOR SPECIES OF SULFUR

298.15 K (25°C) and 0.1 MPa (1 bar)

Species	ΔG_f° kJ mol^{-1}	S° J $mol^{-1}K^{-1}$	$\bar{S}^\circ$ J $mol^{-1}K^{-1}$	C_p° J $mol^{-1}K^{-1}$	
Solid Species					
S (rhombic)	0. *	31.80	31.80	22.64	
Dissolved Species					
SO_2 (aq)	-300.676	161.9	161.9	105.	(1)
HSO_3^- (aq)	-527.73	139.7	160.6	-69.9	(1)
SO_3^{2-} (aq)	-486.5	-29.	12.8	-268.	(1)
$H_2S_2O_4$ (aq)	-616.6				
$HS_2O_4^-$ (aq)	-614.5				
$S_2O_4^{2-}$ (aq)	-600.3	92.	134.		
$S_4O_6^{2-}$ (aq)	-1040.4	257.3	341.0	-67.8	
$H_2S_2O_3$ (aq)	-526.2(1)	242.2(1)	242.2	173.	(1)
$HS_2O_3^{2-}$ (aq)	-523.6(1)	162.8(1)	183.7	-84.9	(1)
$S_2O_3^{2-}$ (aq)	-513.8(1)	37.2(1)	79.1	-300.	(1)
H_2S (aq)	-27.83	121.	121.	132.	(1)
HS^- (aq)	12.08	62.8	83.7	-141.	(1)
S^{2-} (aq)	85.8	-14.6	27.2	-400.	(1)
Gaseous Species					
SO_2 (g)	-300.194	248.22	248.22	39.87	
H_2S (g)	-33.56	205.79	205.79	34.23	

* Defined reference state

(1) Data obtained from Naramov, et al (1974).

TABLE 5

THERMODYNAMIC DATA FOR SPECIES OF IRON

295.15 K (25°C) and 0.1 MPa (1 bar)

Species	ΔG_f° kJ mol^{-1}	S° J mol^{-1}K^{-1}	$\bar{S}^\circ$ J mol^{-1}K^{-1}	C_p° J mol^{-1}K^{-1}
Solid Species				
Fe (C)	0. *	27.28	27.28	25.10
$Fe(OH)_2$ (C)	-486.5	88.	88.	
$Fe(OH)_3$ (C)	-696.5	106.7	106.7	
FeS_2 (py)	-166.9	52.93	52.93	62.17
α-FeS (C)	-100.4	60.29	60.29	50.54
$FeSO_3 \cdot 3H_2O$(C)	-1306. (1)			
Dissolved Species				
Fe^{2+} (aq)	-78.90	-137.7	-179.5	33.1 (2)
$FeOH^+$ (aq)	-277.4	-29.	-49.9	
$Fe(OH)_2^\circ$ (aq)	-459.2(2)			
$Fe(OH)_3^+$ (aq)	-614.9			
$Fe(OH)_4^{2+}$ (aq)	-769.7			
Fe^{3+} (aq)	-48.5	-315.9	-378.6	24.7 (2)
$FeOH^{2+}$ (aq)	-229.41	-142.	-184.	
$Fe(OH)_2^+$ (aq)	-438.0			
$Fe(OH)_3^\circ$ (aq)	-659.3			
$Fe(OH)_4^-$ (aq)	-843.9 (2)			
$FeHSO_3^+$ (aq)	-615.8 (3)			
$FeSO_3^\circ$ (aq)	-599.2 (3)			
$FeHSO_3^{2+}$ (aq)	-543.2 (3)			
$FeSO_3^+$ (aq)	-532.1 (3)			

* Defined reference state

(1) Experimentally determined from solubility data.

(2) Data obtained from Naramov, et al (1974).

(3) Data calculated from formation constants given by Kao (1979).

TABLE 6

THERMODYNAMIC DATA FOR SPECIES OF LEAD

298.15 K (25°C) and 0.1 MPa (1 bar)

Species	ΔG_f° kJ mol^{-1}	S° J $mol^{-1}K^{-1}$	$\bar{S}^\circ$ J $mol^{-1}K^{-1}$	C_p° J $mol^{-1}K^{-1}$
Solid Species				
Pb (C)	0. *	64.81	64.81	26.44
PbO_2 (C)	-217.33	68.6	68.6	64.64
$Pb(OH)_2$ (C)	-452.2			
PbS (galena)	-98.7	91.2	91.2	49.50
$PbSO_3$ (C)	-541. (1)			
Dissolved Species				
Pb^{2+} (aq)	-24.43	10.5	-31.34	-52.7
$PbOH^+$ (aq)	-226.3			
$Pb(OH)_2^\circ$ (aq)	-452.2			
$Pb(OH)_3^-$ (aq)	-575.6			

* Defined reference state

(1) Experimentally determined from solubility data.

TABLE 7

THERMODYNAMIC DATA FOR SPECIES OF WATER

298.15 K (25°C) and 0.1 MPa (1 bar)

Species	ΔG_f^o kJ mol^{-1}	S^o J $mol^{-1}K^{-1}$	$\bar{S}^o$ J $mol^{-1}K^{-1}$	C_p^o J $mol^{-1}K^{-1}$
Aqueous Species				
H_2O (ℓ)	-237.129	69.91	69.91	75.291
H^+ (aq)	0.*	0.	-20.92	0
OH^- (aq)	-157.244	-10.75	10.17	-148.5
Gaseous Species				
O_2 (g)	0. *	205.138	205.138	29.355
H_2 (g)	0. *	130.684	130.684	28,824

* Defined reference state

TABLE 8

THERMODYNAMIC DATA FOR THE Zn-S-SO_2-H_2O SYSTEM AT ELEVATED TEMPERATURES

Species	$C_p^o\|_{25}^{60}$	$C_p^o\|_{25}^{100}$	$C_p^o\|_{25}^{150}$	$C_p^o\|_{25}^{200}$		ΔG_f^o, T			
						60°C	100°C	150°C	200°C
	J $mol^{-1}K^{-1}$					kJ $mol^{-1}K^{-1}$			
Solid Species									
Zn (C)	25.52	25.69	25.90	26.15	(1)	0. *	0. *	0. *	0. *
$Zn(OH)_2$ (C)	72.4	72.4	72.4	72.4	(2)	-545.2	-533.3	-518.3	-503.1
$ZnSO_3 \cdot 2\frac{1}{2}H_2O$ (C)	189.	189.	189.	189.	(3)	-1229.	-1199.	-1161.	-1122.
ZnS (Sph)	46.02	46.65	47.28	47.86	(1)	-203.2	-202.6	-201.7	-200.6
S (C)	23.14	23.56	25.82	30.46	(1)	0. *	0. *	0. *	0. *
Dissolved Species									
Zn^{2+} (aq)	209.	276.	285.	305.	(4)	-146.5	-145.7	-144.7	-144.1
$ZnOH^+$ (aq)	121.	159.	155.	172.	(4)	-331.0	-328.4	-324.9	-321.5
$Zn(OH)_2^o$ (aq)					(5)	-522.5	-506.9	-487.2	-468.0
$Zn(OH)_3^-$ (aq)	-108.	-113.	-147.	-157.	(4)	-688.1	-668.9	-643.2	-617.0
$Zn(OH)_4^{2-}$ (aq)	-452.	-506.	-490.	-544.	(4)	-843.0	-809.0	-764.6	-715.9
SO_2 (aq)	105.	105.	105.	105.	(6)	-298.2	-295.5	-292.5	-289.5
HSO_3^- (aq)	-67.	-46.	-88.	-88.	(4)	-516.1	-502.9	-485.4	-468.0
SO_3^{2-} (aq)	-506.	-548.	-527.	-573.	(4)	-468.3	-445.8	-416.1	-382.5

TABLE 8 (Continued)

THERMODYNAMIC DATA FOR THE Zn-S-SO_2-H_2O SYSTEM AT ELEVATED TEMPERATURES

Species	C_p^o 60	C_p^o 100	C_p^o 150	C_p^o 200		ΔG_f^o, T 60°C	100°C	150°C	200°C
	C_p 25	C_p 25	C_p 25	C_p 25					
	J $mol^{-1}K^{-1}$					kJ $mol^{-1}K^{-1}$			
$S_4O_6^{2-}$ (aq)	-67.8	-67.8	-67.8	-67.8	(2)	-1021.6	-1000.4	-973.7	-946.7
$H_2S_2O_3$ (aq)	173.	173.	173.	173.	(6)	-518.1	-508.1	-495.7	-483.3
$HS_2O_3^-$ (aq)	-85.	-85.	-85.	-85.	(6)	-511.5	-497.6	-479.6	-461.2
$S_2O_3^{2-}$ (aq)	-377.	-402.	-377.	-406.	(4)	-498.4	-479.8	-455.7	-429.0
H_2S (aq)	132.	132.	132.	132.	(6)	-26.59	-25.48	-24.53	-23.85
HS^- (aq)	-218.	-243.	-259.	-276.	(4)	15.88	20.96	28.58	37.71
S^{2-} (aq)	-200.	-243.	-256.	-273.	(4)	92.09	99.36	108.7	118.5
$H_2O(\ell)$	75.23	75.44	75.81	76.44	(1)	-231.53	-225.22	-217.53	-210.04
H^+ (aq)	96.	130.	138.	146.	(4)	0. *	0. *	0. *	0. *
OH^- (aq)	-197.	-243.	-255.	-272.	(4)	-148.5	-137.6	-123.1	-107.3
Gaseous Species									
O_2 (g)	29.6	29.9	30.1	30.4	(1)	0. *	0. *	0. *	0. *
H_2 (g)	28.8	28.8	28.9	28.9	(1)	0. *	0. *	0. *	0. *

* Defined reference state
(1) Data obtained from Barin, et al (1977).
(2) Data obtained from Wagman, et al (1982) and assumed constant with temperature.
(3) Estimated by the rule of Kopp (1864) and assumed constant with temperature.
(4) Estimated by the method of Criss and Cobble (1964).
(5) High temperature free energy data estimated by the method of Barner and Scheuerman (1978).
(6) Data obtained from Naramov, et al (1974) and assumed constant with temperature.

water system. The average heat capacity data were calculated by integrating known heat capacity functions over the given temperature ranges where possible. Otherwise, the average heat capacity was estimated as explained in the footnotes. The Correspondence Principle of Criss and Cobble (1964), in most cases, was used to estimate these average heat capacity values. Table 8 also presents the free energy of formation data calculated by Equation (18) at four elevated temperatures. The method of entropy estimation, heat capacity extrapolation and calculation of high temperature free energy data are explained with sample calculations in Appendix 3.

2.3 THE POTENTIAL-pH DIAGRAM

The equilibria existing between aqueous ionic species and crystalline solids in the zinc-water, sulphur-water and iron-water systems have been evaluated using Equation (13) and the thermodynamic data in Tables 3 to 8 inclusive. The equilibrium between each pair of species in a system establishes a single chemical reaction. A complete list of all the possible equilibrium reactions between species of the zinc-sulphur-water system is given in Appendix 1. The corresponding potential-pH activity relationship obtained from Equation (13) for each reaction is presented in Appendix 2. Appendix 2 lists the resultant Eh-pH equations for the zinc-sulphur-water system at 25°C plus four elevated temperatures (60°C, 100°C, 150°C, 200°C). The potential-pH activity equations which subsequently appear as lines on the Pourbaix diagrams are identified by the corresponding reaction number found in Appendix 1 placed adjacent to the line.

2.3.1 The Zinc-Water System

The diagram constructed for the zinc-water system which corresponds to the simple type of Eh-pH diagram found in the Pourbaix (1966) Atlas, is presented in

Figure 1(a). This potential -pH diagram summarizes all the reactions that can occur between the various zinc species in an aqueous environment. Zinc metal, crystalline zinc hydroxide, the aqueous species Zn^{2+} ion and its hydrolysis components $ZnOH^{+}$, $Zn(OH)_2^0$, $Zn(OH)_3^-$ and $Zn(OH)_4^{2-}$ are the species considered for this diagram. Contour lines corresponding to three different activities of the dissolved species (10^0,10^{-3}, 10^{-5} mol dm^{-3}) in equilibrium with zinc metal and zinc hyrdoxide, are shown in Figure 1(a). Since a barren liquor is usually defined as having a dissolved species activity of 10^{-3} mol dm^{-3}, it can be seen from this diagram that zinc hydroxide is precipitated from solution in the pH range of approximately 7 to 13. Below this range zinc hydroxide will dissolve as Zn^{2+} in acid media. Similarly, in the alkaline range of pH zinc hydroxide is in equilibrium with soluble zinc species in the form of $Zn(OH)_3^-$. Ultimately at high alkalinity, zinc hydroxide will dissolve as $Zn(OH)_4^{2-}$. Figure 1 also shows that as the pH of a 1 mol dm^{-3} Zn^{2+} liquor is raised by adding alkali, zinc hydroxide will begin to precipitate at a pH of approximately 6. The solution, as the pH continues to rise, will be essentially barren with only 10^{-3} mol dm^{-3} Zn^{2+} remaining at a pH of approximately 7.

Figure 1(b) represents another form of solubility diagram which gives a more quantitative assessment of the solubility of a solid metallic species and the corresponding concentration of the dissolved species in equilibrium with it. The solubility of zinc hydroxide, it can be seen, passes through a minimum of approximately $10^{-5.7}$ mol dm^{-3} (0.14 mg dm^{-3}) of soluble zinc in the pH range of 9 to 11. In this minimum solubility range, the predominant form of dissolved zinc is the aqueous complex $Zn(OH)_2^0$.

The relationship between Figure 1(a) and Figure 1(b) is demonstrated by the dashed arrows superimposed on these figures. The 10^0 and 10^{-3} mol dm^{-3} activity contours, Lines 9 and 13 in Figure 1(a), each correspond

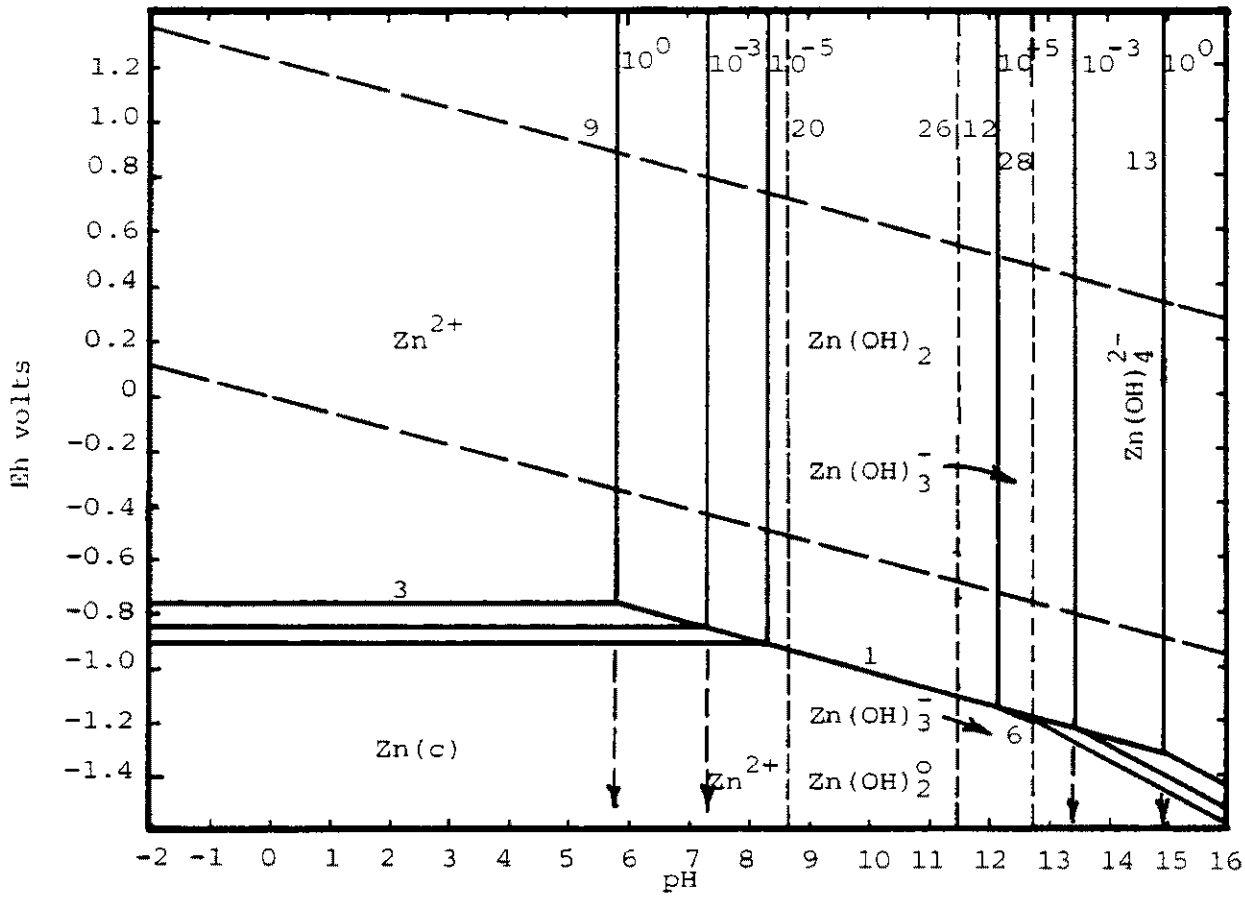

FIGURE 1(a) Potential -pH diagram of the $Zn-H_2O$ system at 25°C

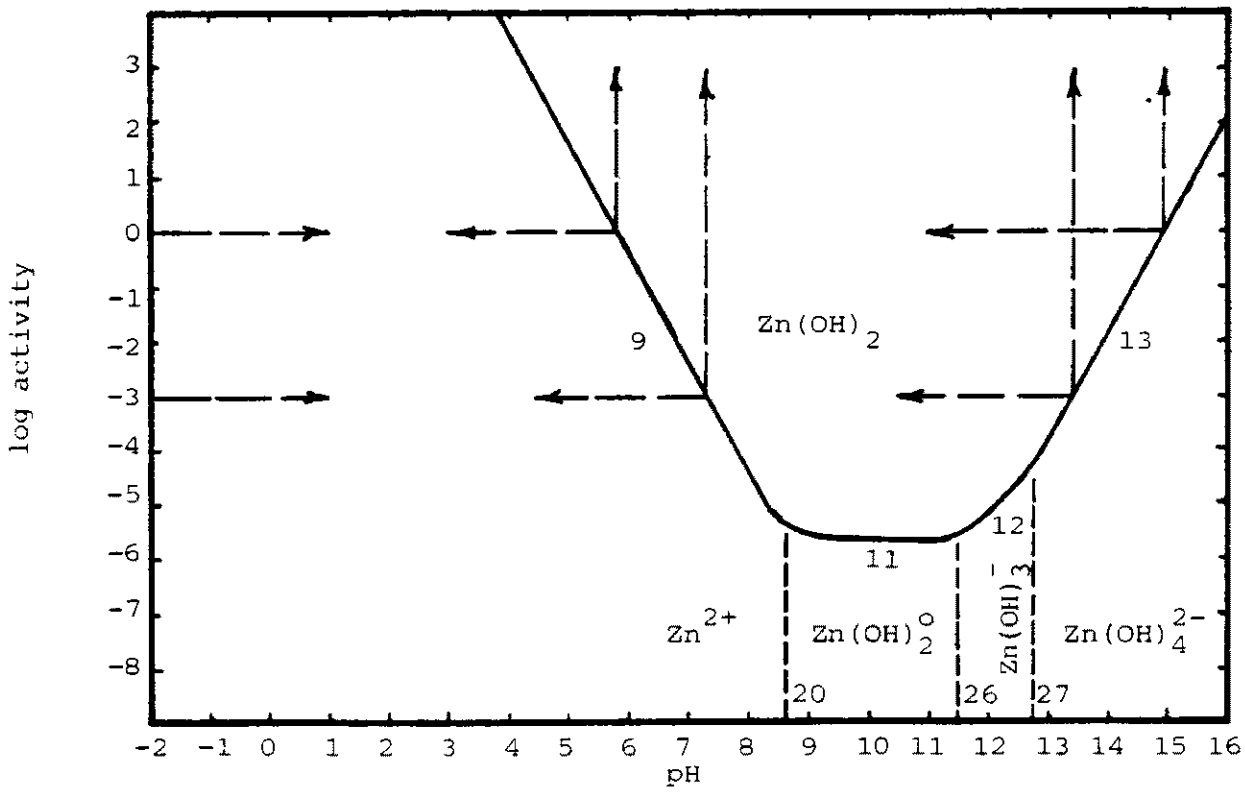

FIGURE 1(b) Activity -pH diagram of the $Zn-H_2O$ system at 25°C

to a point on the solubility curve in Figure 1(b) at the same dissolved zinc activity. The amphoteric nature of zinc is quantified in Figure 1(b) where zinc hyrdoxide redissolves at high pH. The extent of dissolution of the zinc hydroxide and the species resulting can be read directly from Figure 1(b).

Pourbaix diagrams show directly the relative nobility of metals. Noble metals such as gold or platinum are predominant over a large portion of the stability region of water. Zinc cannot be classed as a noble metal since as Figure 1(a) shows, it has no predominance within the stability limits of water. In fact, Figure 1(a) shows zinc to be a very active metal that is not thermodynamically stable in water. Since the reduction potential for zinc described by Lines 1, 3 and 7 lies well below the lower stability limit of water, it can be concluded that any attempt to reduce Zn^{2+} from solution to metallic zinc will result in the generation of hydrogen gas. However, the success of the industrial electrolytic zinc process has shown this conclusion to be invalid. The zinc electrode, fortunately, has a large associated hydrogen overvoltage due to the high activation energy required for nucleation of hydrogen gas on the zinc surface. This saving kinetic feature of the electrolytic process allows efficient cathodic deposition of zinc contrary to the thermodynamic findings. Thus, the thermodynamics of an aqueous system must ultimately be considered in conjunction with the process kinetics. The thermodynamics of the zinc system allow assessment of the feasibility of certain interactions and provide guidelines to an experimental investigation. However, the thermodynamics must then be considered along with the appropriate measured kinetics.

2.3.2 The Sulphur-Water System

Figure 2 presents the stable sulphur-water equilibria as given in the Pourbaix (1966) Atlas. This diagram shows that ultimately over long periods of time, bisulphate,

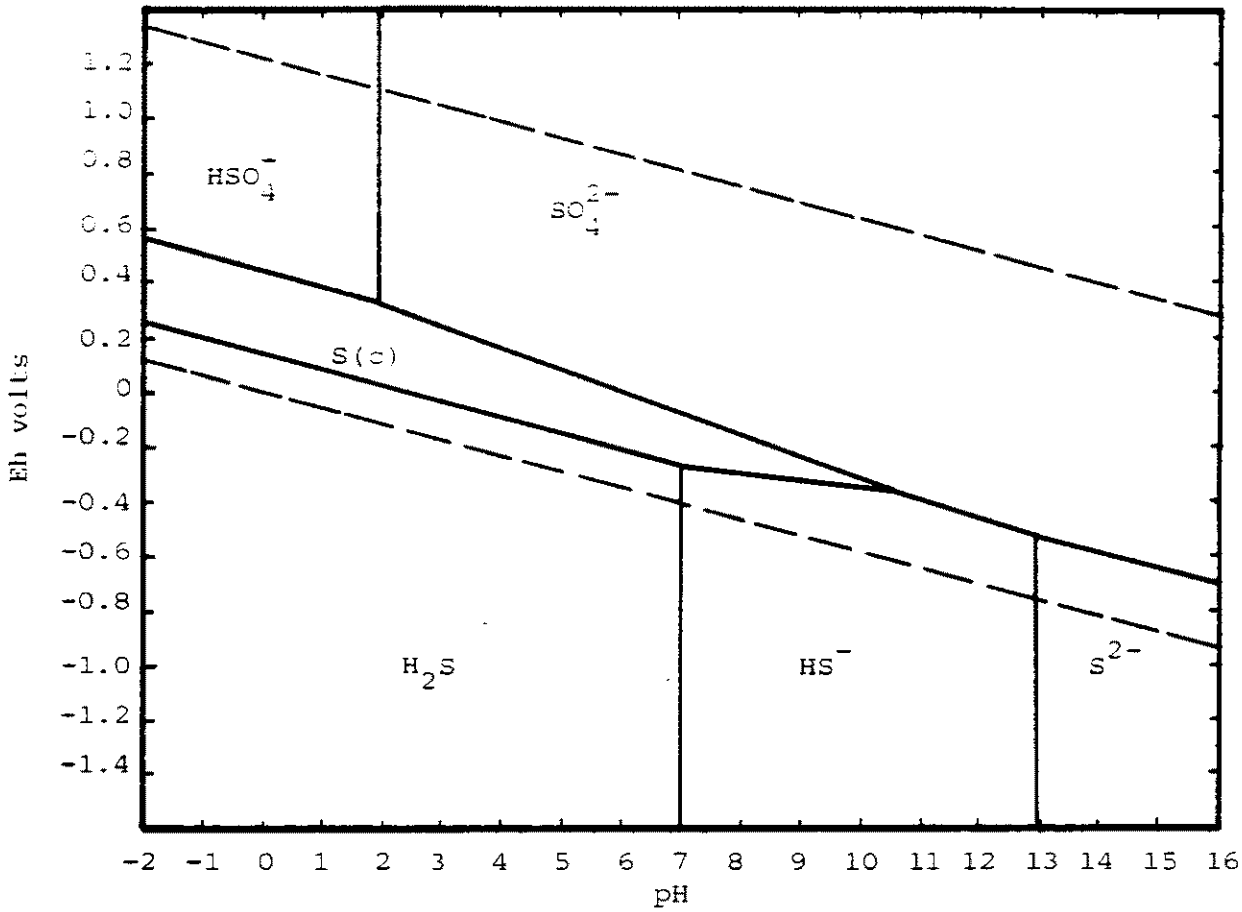

FIGURE 2 Potential -pH diagram of the stable S-H_2O system at 25°C

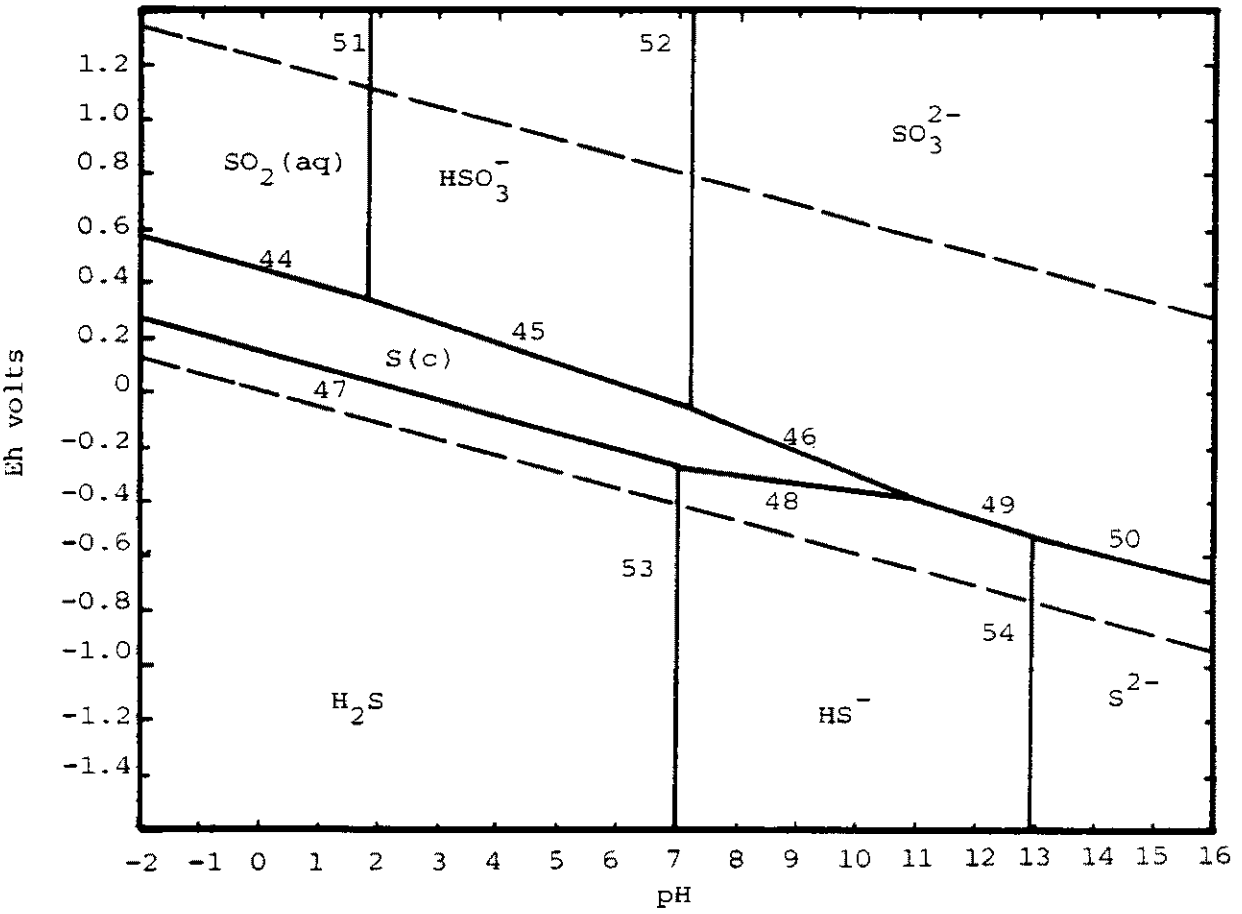

FIGURE 3 Potential -pH diagram of the metastable S-H_2O system at 25°C

sulphate and the aqueous sulphides ($H_2S(aq), HS^-, S^{2-}$) are the only species of sulphur that can exist in true equilibrium with elemental sulphur in an aqueous medium. Generally, this has been the diagram appropriately used in hydrometallurgical studies. However, the present study involves injection of sulphur dioxide gas directly into heterogenous aqueous media containing metals and minerals. In the absence of any strong oxidizing agents, sulphur dioxide is quite stable in such media. Therefore, a better representation of the characteristics and properties of sulphite media are obtained by considering the equilibria between the metastable sulphur species.

2.3.3 The Metastable Sulphur-Water System

Figure 3 presents the metastable sulphur-water diagram obtained by considering all the equilibria between the sulphite species, elemental sulphur and the sulphide species. This diagram is quite similar to the stable sulphur-water diagram but with the sulphites occupying the upper portion of the diagram rather than the sulphates. Early in this century it was discovered that the reaction between aqueous sulphur dioxide and hydrogen sulphide produces a complex series of oxygenated sulphur anions known as Wackenroder's Solution (Schroeter, 1966; Debus, 1888). Consequently in an effort to summarize the complex chemistry of this system, a stability diagram was constructed incorporating all of the sulphur species known to exist and for which, free energy of formation data are available. Figure 4 shows the metastable sulphur-water diagram resulting from the incorporation of all the sulphur species listed in Table 4.

The Eh-pH diagram presented in Figure 4 was constructed by considering all the possible equilibria between the species of sulphur with a sulphur valence state from +4 to -2. This includes sulphur dioixde (+4), the sulphur oxyanions, elemental sulphur and the sulphides (-2) respectively. Thus in both Figure 3 and Figure 4, the

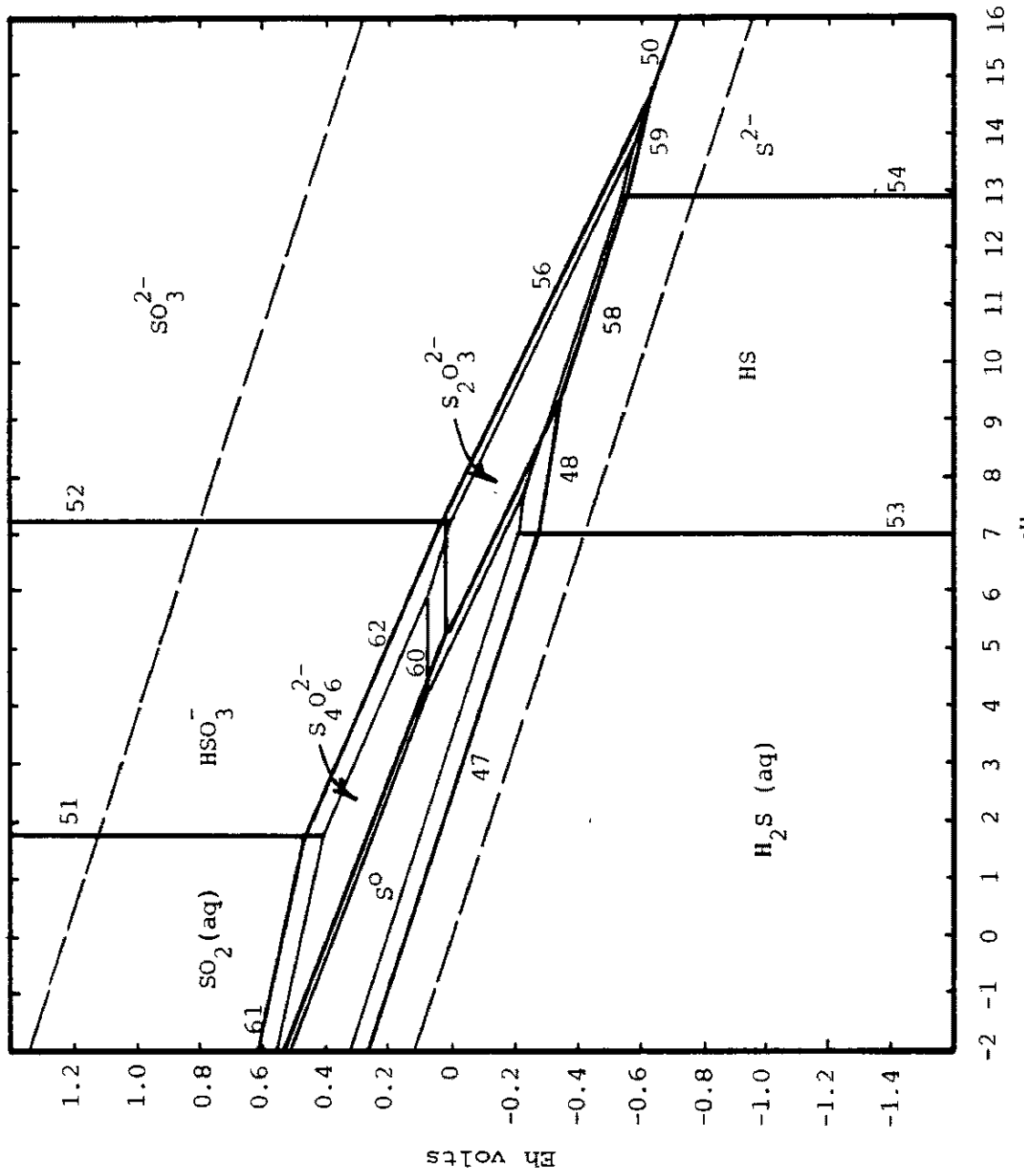

FIGURE 4 Potential -pH diagram of the metastable S-H_2O system at 25°C

most stable valence of state of sulphur (sulphate, with the lowest Gibbs free energy) has not been considered and the pseudoequilibria at higher free energy states than true equilibrium are shown. It can be seen in Figure 3 that the species which exist in metastable equilibrium with sulphur and the aqueous sulphides ($H_2S(aq)$,HS^-,S^{2-}) are aqueous sulphur dioxide and its hyrdolysis component species HSO_3^- and SO_3^{2-}. Additionally in Figure 4, the tetrathionate ($S_4O_6^{2-}$) and thiosulphate ($S_2O_3^{2-}$) species appear.

Figure 3 is drawn for a total sulphite activity of 1.0 mol dm^{-3}. The predominance areas occupied by each sulphite species define the pH ranges over which each hydrolysis component has the highest activity. The vertical boundaries (Lines 51 and 52) define the pH at which the two competing species have equal activities. Aqueous sulphur dioxide, $SO_2(aq)$, is predominant at a pH less than 1.76. Bisulphite, HSO_3^-, has the highest activity in the pH range of 1.76 to 7.22 and sulphite, SO_3^{2-}, is likewise predominant above the pH of 7.22. Figure 4 is drawn with two different activity levels shown for the ionic sulphur species. The bold lines represent a total dissolved sulphur activity of 1.0 mol dm^{-3} and the light lines represent an activity of 0.1 mol dm^{-3}.

Situated between the predominance areas of the sulphite species and elemental sulphur are the regions of stability of two metastable sulphur oxyanions, tetrathionate and thiosulphate. It can be seen from the diagram that thiosulphate ($S_2O_3^{2-}$) is not stable below a pH of approximately 5.5. Thiosulphate, below this pH, will disproportionate to elemental sulphur and bisulphite by the reaction

$$S_2O_3^{2-} + H^+ = S^\circ + HSO_3^-$$

A reaction of this type has been previously reported by Valensi (1950) and Debus (1888). However, Figure 4 shows that, under slightly oxidizing conditions in acidic media, thiosulphate should form tetrathionate by the reaction of Line 60 which is,

$$S_4O_6^{2-} + 2e^- = 2S_2O_3^{2-}.$$

The appearance of a predominance region for the tetrathionate species among the metastable equilibria of the sulphur-water system has not previously been reported.

2.3.4 The Zinc-Sulphur Dioxide-Water System

A number of diagrams have been constructed to consider the consequences of adding sulphur dioxide to the aqueous zinc-water system. These diagrams show the effect of superimposing the predominance regions of various sulphur compounds on the zinc-water system. Figure 5(a), a zinc-sulphur dioxide-water Eh-pH diagram at 25°C, represents the simplest of these combined diagrams. The stable crystalline sulphite salt of zinc, $ZnSO_3.2\frac{1}{2}H_2O$, has been incorporated this diagram. Since there is no existing thermodynamic data available in the literature for this sulphite compound, the Gibbs free energy of formation was determined experimentally through solubility measurements. A detailed discussion of the solubility measurements carried out on zinc sulphite can be found in Chapter Three.

Figure 5(a), which was derived from Figure 1(a), along with Figure 5(b) conveniently describe the characteristics of zinc in sulphite media. Figures 5(a) and 5(b) are both drawn with a total sulphite activity of 1.0 mol dm^{-3} which corresponds, approximately, to a saturated solution. The predominance region of zinc sulphite, as shown in Figure 5(a), intrudes into a portion of the predominance areas of both Zn^{2+} ion and zinc hydroxide. If sulphur dioxide is bubbled into a slurry of zinc hydroxide suspended in water, the slurry will become acidic and as Figure 1(a) shows, the hydroxide will dissolve. Upon subsequent neutralization of the media, a precipitate of zinc sulphite is formed as predicted by Figure 5(a). This precipitation of zinc sulphite from acidic media containing zinc, or pregnant zinc leach liquors, occurs at a much lower pH than the precipitation of zinc hydroxide. As Figure 5(b) shows,

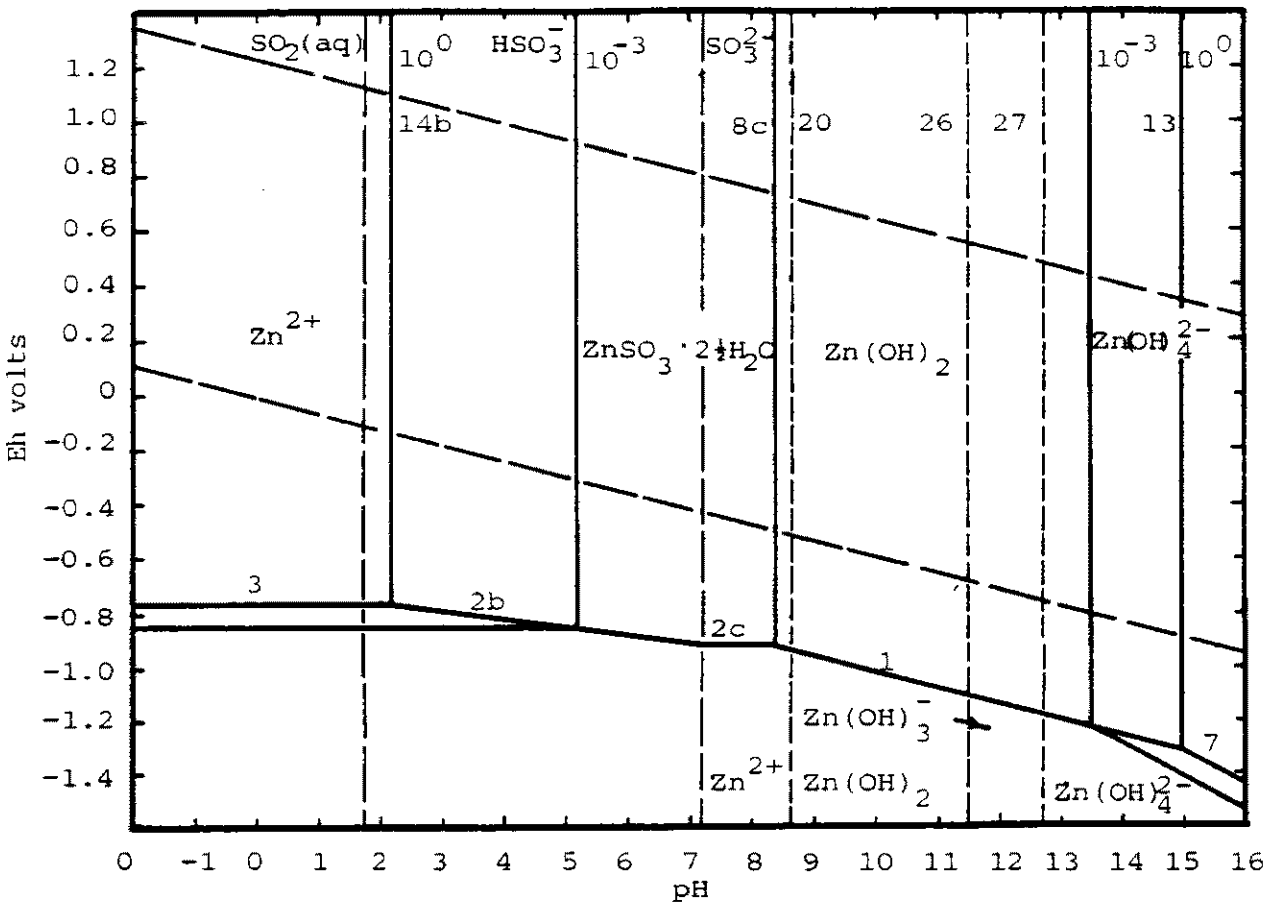

FIGURE 5(a) Potential -pH diagram of the $Zn-SO_2-H_2O$ system at 25°C

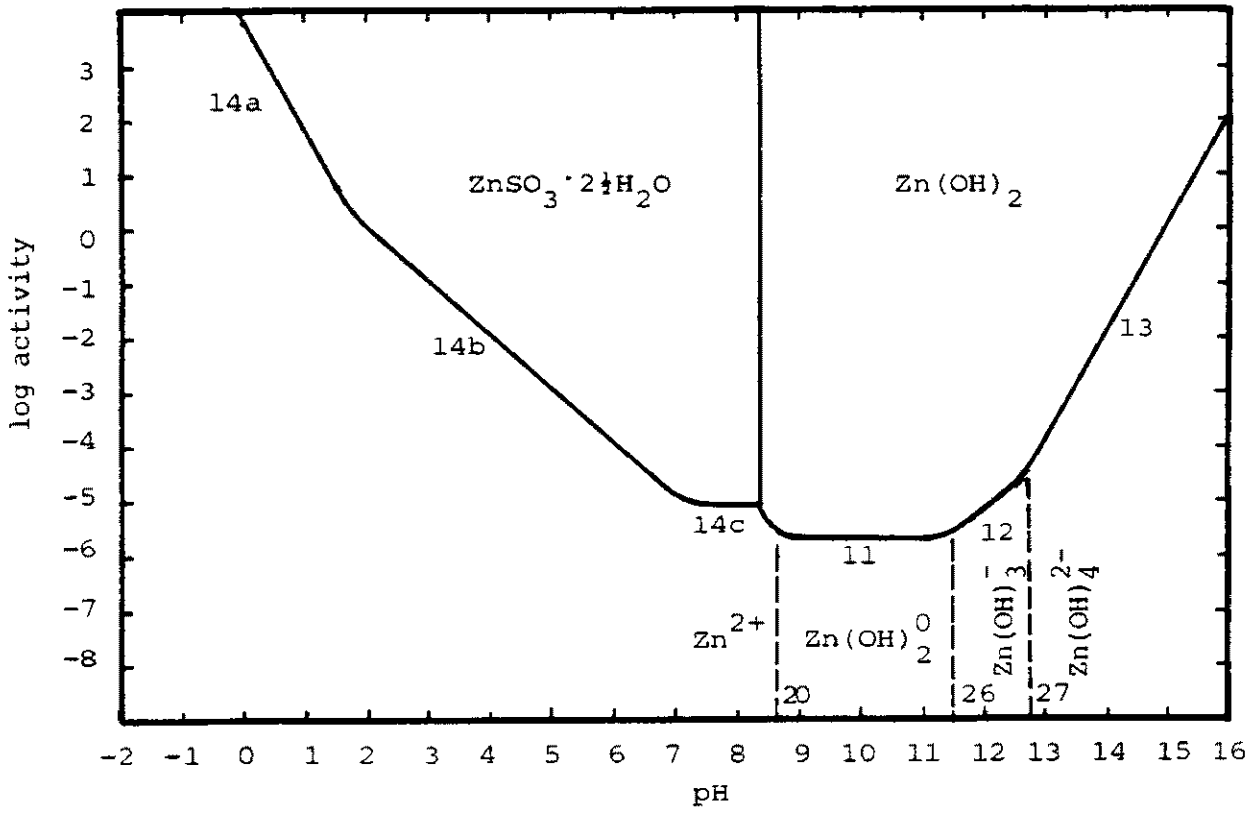

FIGURE 5(b) Activity -pH diagram of the $Zn-SO_2-H_2O$ system at 25°C

the maximum depletion of zinc from aqueous media by precipitation of zinc sulphite is nearly as great as by the precipitation of zinc hydroxide. The minimum solubility of zinc sulphite in a solution, with a total aqueous sulphite activity of 1 mol dm^{-3}, occurs in the pH range of approximately 7 to 8. The aqueous zinc activity in this range of maximum depletion is $10^{-5.1}$ mol dm^{-3} (0.53 mg dm^{-3}), whereas, the zinc activity by precipitation of zinc hydroxide is only slightly less at $10^{-5.7}$ mol dm^{-3} (0.15 mg dm^{-3}).

The precipitation of the zinc sulphite is demonstrated in Figure 5(a) to be a feasible purification step in the hydrometallurgical processing of zinc. For example, an impure zinc hydroxide or zinc oxide calcine could be upgraded by the use of sulphur dioxide. The impure material could first be slurried in water and dissolved by injecting sulphur dioxide gas. From the resulting liquor, a pure zinc sulphite salt could be precipitated and filtered leaving the contaminates in the barren liquor. The sulphite could then be calcined to produce a purified zinc oxide and sulphur dioxide for recycle.

2.3.5 The Zinc-Sulphur-Sulphur Dioxide-Water System

The standard Pourbaix diagram is sufficient to give an appreciation of the equilibria involved in the study of metals, oxides and calcine materials in aqueous media. However, the study of mineral systems, most notably the sulphides, requires the construction of a more complex diagram to represent the equilibria involved. Figure 6 presents a diagram which was developed by superimposing the zinc-sulphur dioxide-water system of Figure 5(a) over the metastable sulphur-water diagram of Figure 3 and including one additional phase, the mineral sphalerite (ZnS). This complex diagram will be referred to in this work as the $Zn-S-SO_2-H_2O$ system. A diagram of this type aids in determining the feasible hydrometallurgical dissolution paths of the mineral in aqueous sulphur dioxide media and allows a valuable insight into the possible reaction mechanisms.

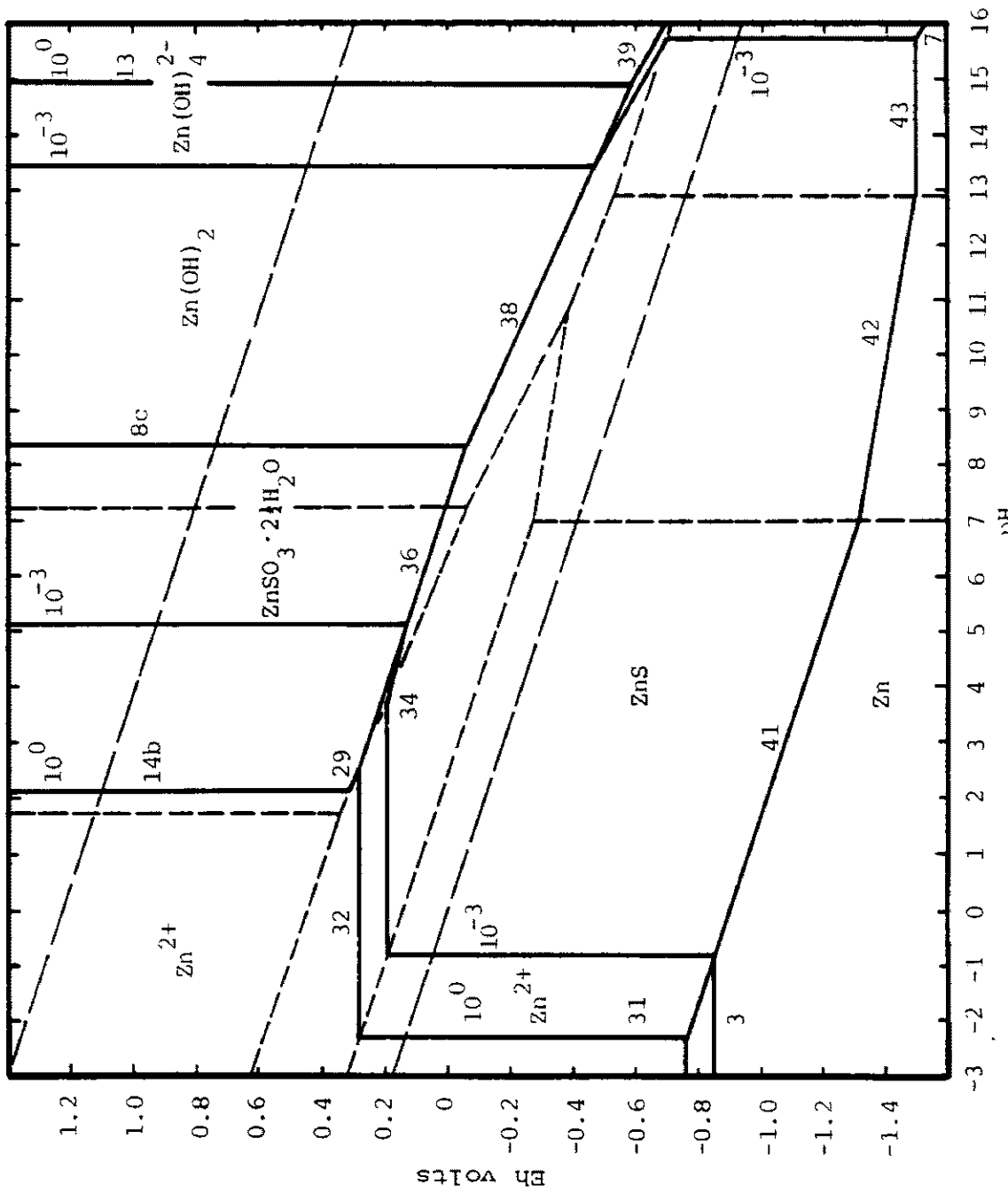

FIGURE 6 Potential -pH diagram of the Zn-S-SO_2-H_2O system at 25°C

The diagram of the $Zn-S-SO_2-H_2O$ system presented in Figure 6 shows the four routes available for the dissolution of sphalerite in sulphurous acid media. They are as follows:

1. In strong acid solutions, sphalerite can decompose to Zn^{2+} ion with the evolution of hydrogen sulphide. The contours represented by Line 31 of Figure 6 indicate the possible degree of dissolution of sphalerite as a function of pH by this mechanism. It is known that sphalerite reacts incompletely in very strong sulphuric acid solutions. The extremely low pH required prevents complete dissolution. In sulphurous acid solutions alone, this reaction can occur only to a very limited extent. The equilibrium pH of a saturated solution of sulphur dioxide under atmospheric pressure is in the range of 1 to 2, which yields a corresponding small dissolution of sphalerite.

2. No practical application of the reactions represented by the lower limits of the sphalerite predominance region are known (Peters, 1976). Lines 41, 42 and 43 indicate that zinc sulphide will decompose under sufficiently strong reducing conditions to metallic zinc and a sulphide species. However, in acidic media this boundary (Line 41) lies far below that for the reduction of water. It is highly likely that the hydrogen overvoltage on the zinc or mercury cathode is too low to prevent the decomposition of water with hydrogen evolution. This is especially true in the presence of all the impurities introduced by the concentrates which can lower the overvoltage. The reduced difference in voltage between the ZnS-Zn boundary (Line 43) and lower water stability limit at high pH values makes it possible for reductive decomposition to occur at a mercury cathode. However, there would have to be a market for the alkaline sodium sulphide solution produced.

3. The sphalerite boundary represented by Line 40 indicates that sphalerite can decompose into $Zn(OH)_4^{2-}$ and S^{2-} ions under very alkaline conditions. However, the existing technology for the electrolytic production of zinc, which occurs in neutral to acid solutions, restricts the practical application of this reaction. Additionally, the pH required for this type of process is inaccessibly high.

4. The upper left hand portion of the $Zn-S-SO_2-H_2O$ diagram indicates several possible mechanisms for the decomposition of sphalerite under neutral to acid and oxidizing conditions. It can be seen in Figure 6 that below a pH of 2, ZnS is unstable above a potential of 0.2 to 0.3 volts (depending on concentration) at Line 32. Under slightly oxidizing conditions, sphalerite can be oxidized to form Zn^{2+} and elemental sulphur. This is consistent with the known processes for acid pressure leaching of zinc concentrates with oxygen at elevated temperatures and pressures which are known to yield elemental sulphur (Forward and Veltman, 1959; Stanczyk and Rampacek, 1961; Scott and Dyson, 1968; Dewing and Cochran, 1978; Veltman and Bolton, 1980; Bolton et al, 1981; Dewing et al, 1982). If the stable sulphur-water equilibria are considered, as in Figure 2, the bisulphate and sulphate species predominate in the entire region above elemental sulphur. Therefore above a pH of about 2 and in an oxidizing medium, sphalerite will decompose to Zn^{2+} and SO_4^{2-} ions in an oxygen acid pressure leaching process.

The complex diagram in Figure 6 was utilized to this point only to predict the end products of the decomposition of sphalerite when placed in a certain type of medium. No predictions have been made for how the media itself will subsequently be altered. However, Figure 6 does elucidate the interplay between sphalerite and the aqueous sulphurous acid medium. The top left corner of Figure 6 shows that sulphur dioxide can act as an oxidizing agent on sphalerite.

Suppose, that sulphur dioxide gas is injected into a slurry of sphalerite suspended in water. Since the predominance region for aqueous sulphur dioxide lies at a higher potential than that of sphalerite, the mineral phase is being subjected to an oxidizing and acidic environment. The aqueous sulphur dioxide will act as an oxidizing agent and be reduced to elemental sulphur by the reaction corresponding to Line 44. The sphalerite will be oxidized to Zn^{2+} ion and elemental sulphur by the reaction corresponding to Line 32. Thus, both phases react toward the equilibrium condition in the area bounded by Lines 32 and 44. Therefore, Figure 6 demonstrates the thermodynamic basis for the oxidative dissolution of sphalerite in aqueous sulphurous acid media. The reactions for the decomposition predicted by Figure 6 are:

$$ZnS = Zn^{2+} + S^{\circ} + 2e^{-} \qquad 32$$

and $$SO_2(aq) + 4H^{+} + 4e^{-} = S^{\circ} + 2H_2O, \qquad 44$$

to yield a corresponding overall reaction

$$ZnS + 0.5SO_2 + 2H^{+} = Zn^{2+} + 1.5S^{\circ} + H_2O.$$

A second reaction path yielding the same overall reaction as discussed above also is predicted in Figure 6. If an acid decomposition of sphalerite occurs by the reaction corresponding to Line 31,

$$ZnS + 2H^{+} = Zn^{2+} + H_2S\ (aq), \qquad 31$$

then aqueous hydrogen sulphide will be produced within the leaching medium. The presence of sulphur dioxide in the leaching medium will result in the oxidation of hydrogen sulphide to elemental sulphur by the reactions corresponding to Lines 44 and 47.

$$SO_2\ (aq) + 4H^{+} + 4e^{-} = S^{\circ} + 2H_2O \qquad 44$$

$$H_2S\ (aq) = S^{\circ} + 2H^{+} + 2e^{-} \qquad 47$$

The overall reaction corresponding to this sequence of reactions is the same as the oxidative dissolution discussed above. However, it is to be noted (as previously outlined) that this second reaction path requires a very low pH for dissolution to occur with any appreciable concentration of zinc present.

2.4 HIGH TEMPERATURE POTENTIAL-pH DIAGRAMS

The utility of potential-pH diagrams in describing and predicting the characteristics of hydrometallurgical processes at room temperature has been demonstrated. Modern hydrometallurgy in many cases has moved toward the use of elevated temperature processing to achieve kinetic efficiency. The extention of the potential-pH diagrams initially established for 25°C to higher temperatures is the most efficient way to obtain direct information on the feasibility of a high temperature process. The various potential-pH diagrams of the zinc and sulphur systems at 25°C have been developed. Also, the obstacle of obtaining reliable high temperature thermodynamic data has been surmounted by employing the various extrapolation techniques of other researchers. The free energy of formation of all the species of zinc and sulphur, appearing at least in the room temperature metastable diagrams, have been calculated at elevated temperatures as described in Section 2.2.3. This calculated thermodynamic free energy data is listed in Table 8. Hence, Equations (10),(13) and (14) were subsequently used to calculate the Eh-pH relationships at elevated temperatures. These equations are compiled along with those for 25°C in Appendix 2.

The first and most apparent effect that raising the temperature has on Eh-pH diagrams is the change in shape of the water stability region. The overall size of this region decreases with temperature under 1 atm pressure of hydrogen and oxygen. Also, the reduction and oxidation reactions of water become more highly pH dependant at elevated temperatures. This effect was most recently demonstrated by Pourbaix and Yang (1981) who also show the influence of temperature on the neutrality of water. The pH of neutrality of water decreases from 7.00 to 5.85 as the temperature increases from 25°C to 300°C, passing through a minimum value of 5.74 at 225°C.

Figures 7 and 8 present the potential-pH diagrams of the zinc-water system at 100°C and 200°C respectively.

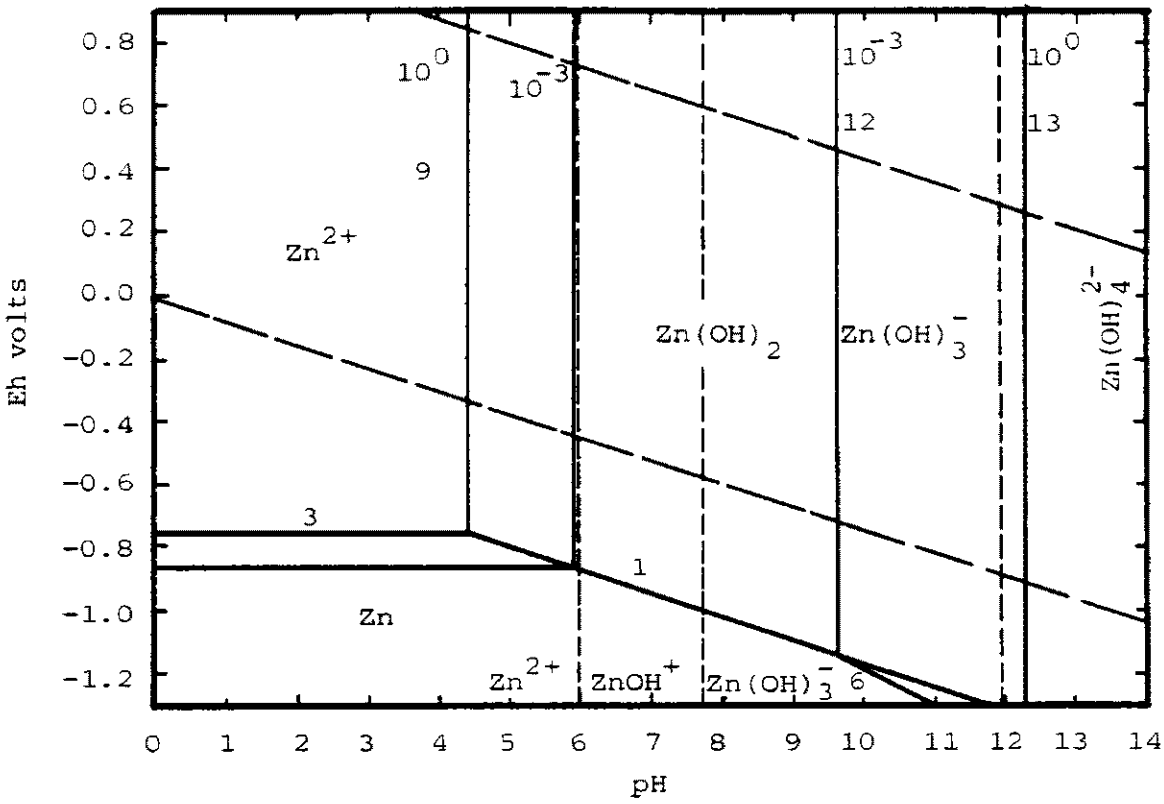

FIGURE 7 Potential -pH diagram of the $Zn-H_2O$ system at 100°C

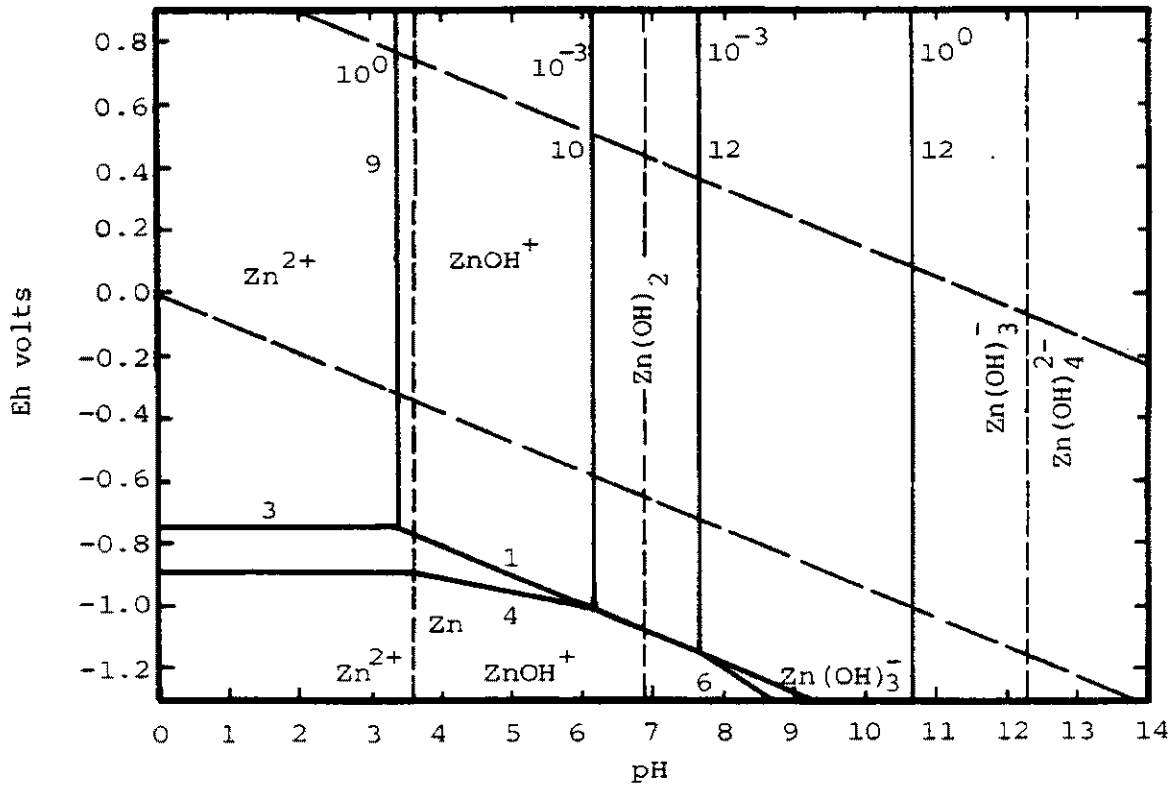

FIGURE 8 Potential -pH diagram of the $Zn-H_2O$ system at 200°C

It can be seen in these diagrams that temperature does not have a significant effect on the hydrogen overvoltage required to reduce zinc from solution at temperatures up to 200°C. The range of pH for stability of zinc hydroxide is reduced along with an overall shift in all the stability regions toward more acidic media. The expansion of the stability regions of the complex zinc ions in aqueous media at higher temperatures is not unusual. These effects form the basis of "hydrothermal precipitation" as proposed by Kwok and Robins (1973). A solution containing zinc in a mild acidic media can precipitate zinc hydroxide upon heating. This is shown by the shift of the equilibrium lines between Zn^{2+} ion and zinc hydroxide to the left (toward lower pH) with an increase in temperature.

Figures 9(a), 10(a) and 11(a) present the zinc-sulphur dioxide-water system at temperatures of 60°C, 100°C and 200°C, respectively, with a total sulphite activity of 1.0 mol. dm^{-3}. Figures 9(b), 10(b) and 11(b) show the corresponding diagrams at a total sulphite activity of 0.1 mol dm^{-3} respectively. It can be seen in these diagrams that like the zinc-water system, the stability region of the complex zinc ions expands and that for zinc hydroxide contracts with increasing temperature. All of the equilibria between the zinc species moves toward more acid media while the equilibria between the aqueous sulphite species slides toward greater pH values. Consequently, the stability region of zinc hydroxide intrudes into the zinc sulphite stability region with higher temperatures and the zinc sulphite predominance region is subsequently reduced. Comparison of Figure 5(a) with Figures 9(a), 10(a) and 11(a) reveals that heating an acid medium containing zinc and sulphite ions up to 100°C will result in hydrothermal precipitation of zinc sulphite instead of zinc hydroxide. Above 100°C, there is a reversal of this trend shown by Lines 14(a) and 14(b) and the sulphite becomes more soluble with further heating. The precipitation of zinc sulphite from solutions containing zinc and aqueous sulphur by heating the solution below 100°C was experimentally observed by Esdaile and Walters (1969).

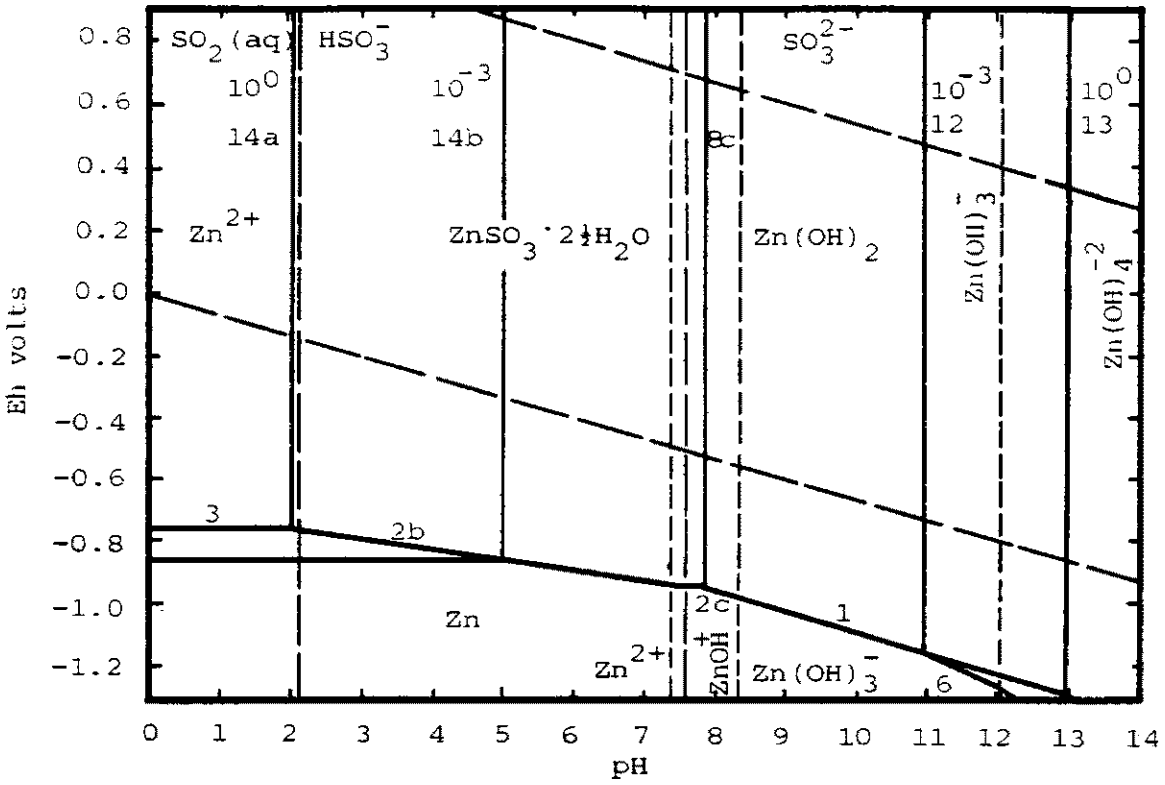

FIGURE 9(a) Potential -pH diagram of the $Zn-SO_2-H_2O$ system at 60°C. Total sulphite activity of 1.0 mol dm^{-3}

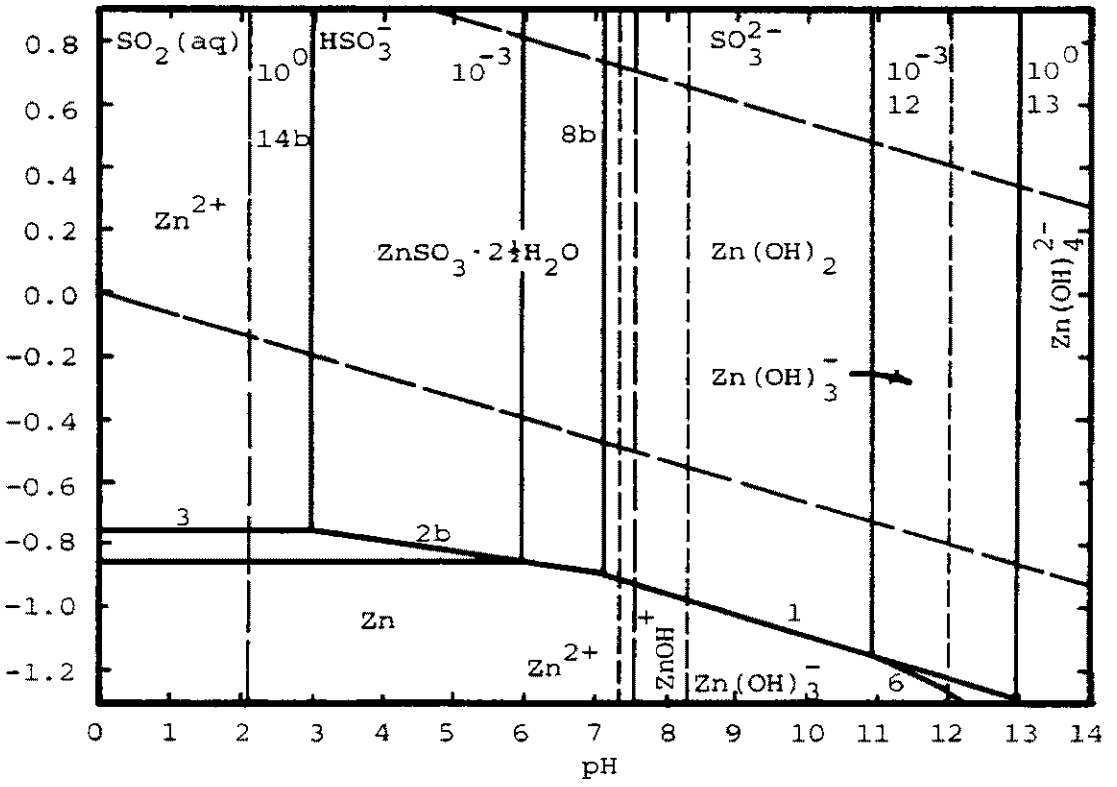

FIGURE 9(b) Potential -pH diagram of the $Zn-SO_2-H_2O$ system at 60°C. Total sulphite activity of 0.1 mol dm^{-3}

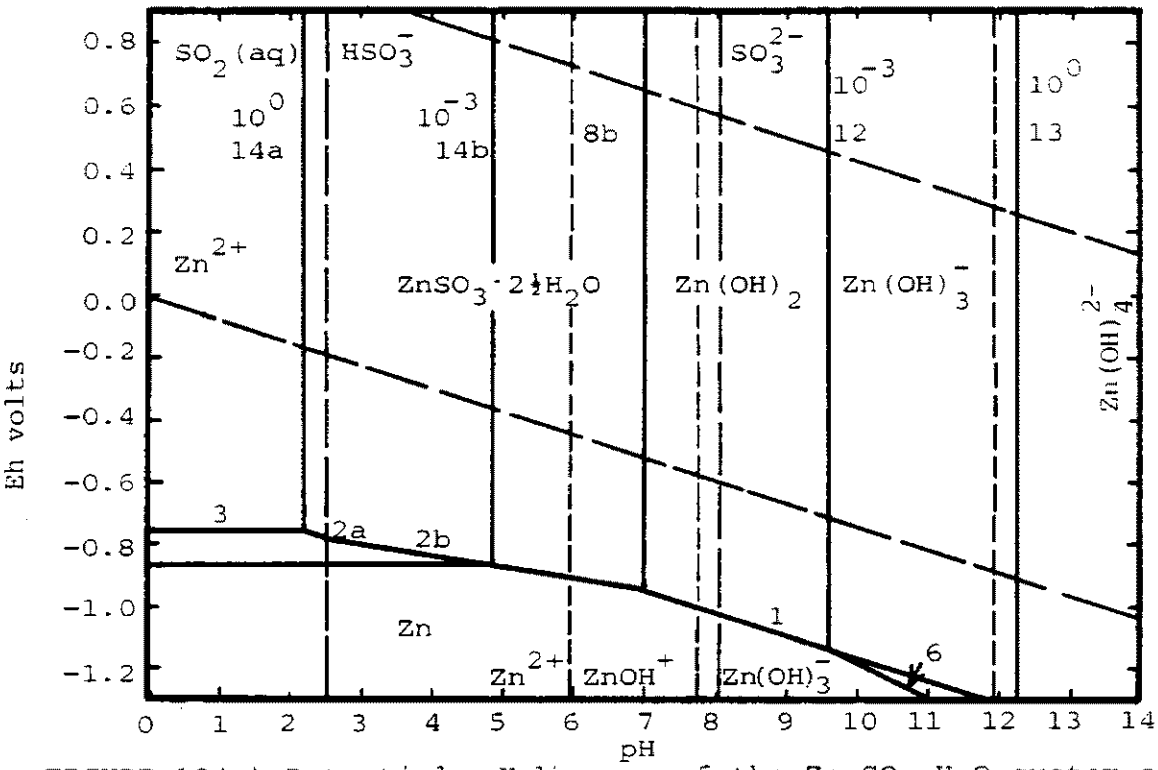

FIGURE 10(a) Potential -pH diagram of the Zn-SO_2-H_2O system at 100°C. Total sulphite activity of 1.0 mol dm^{-3}.

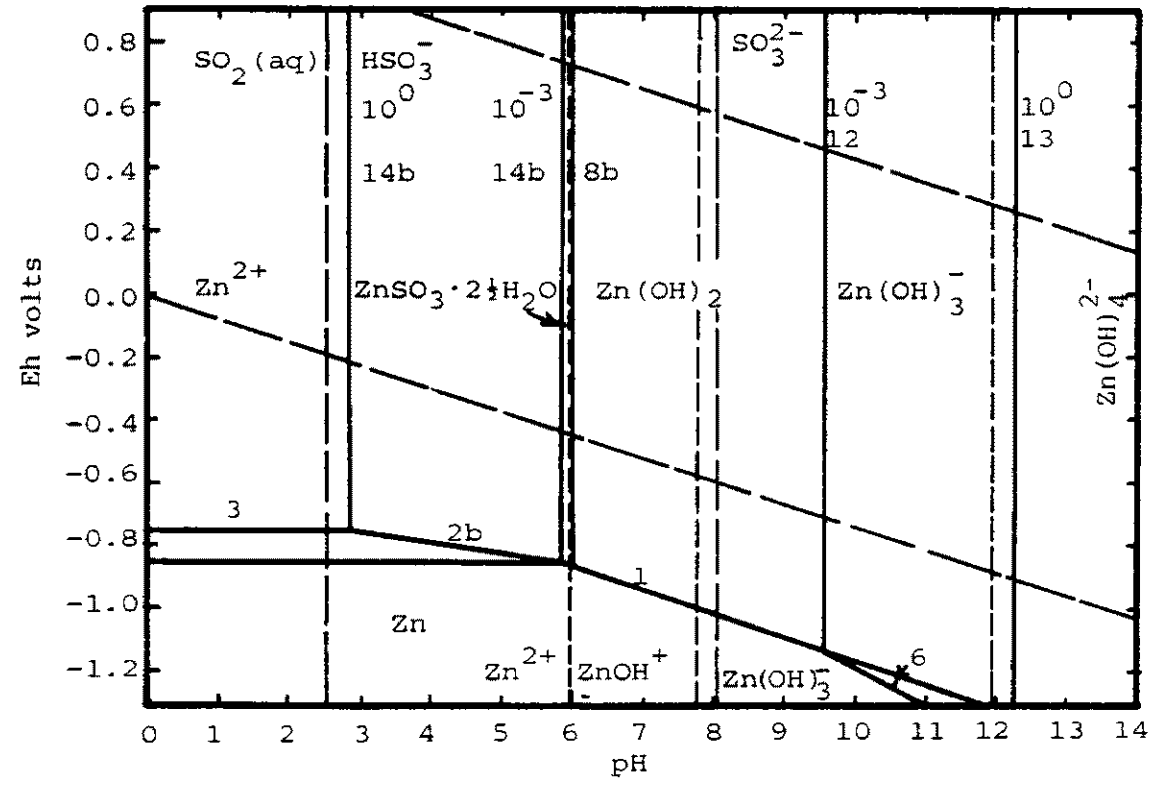

FIGURE 10(b) Potential -pH diagram of the Zn-SO_2-H_2O system at 100°C. Total sulphite activity of 0.1 mol dm^{-3}

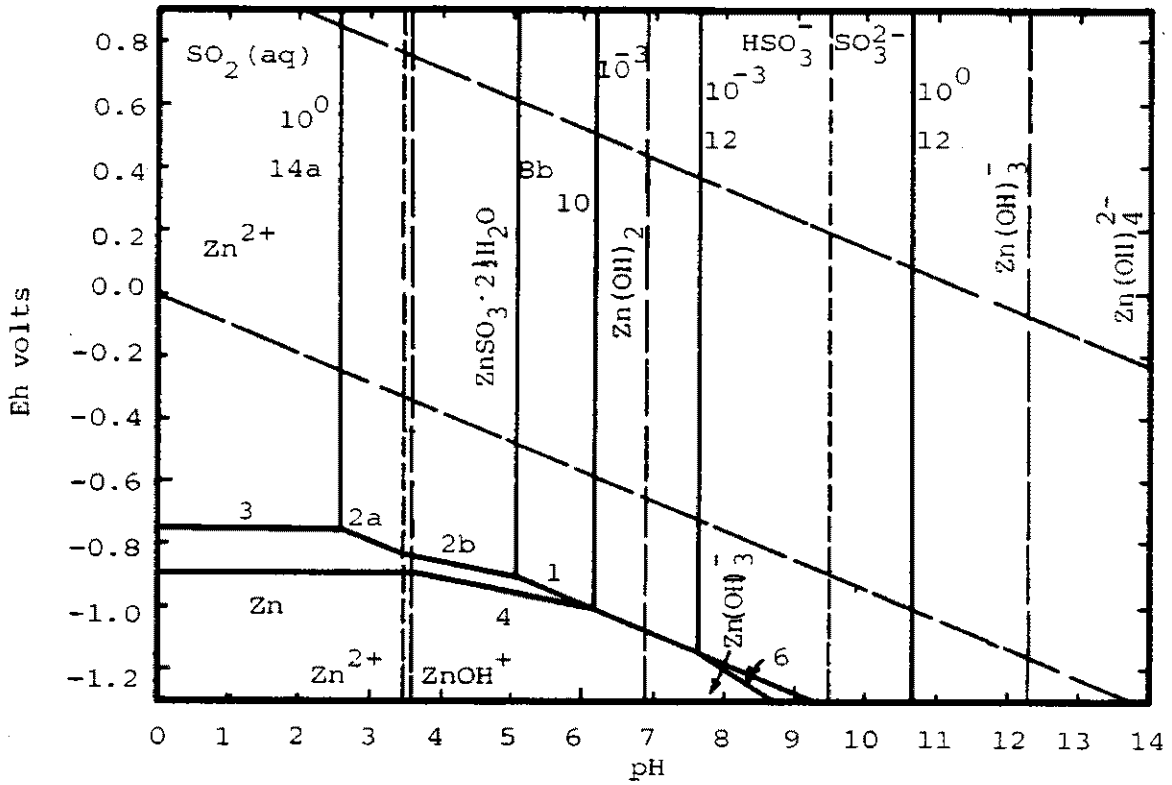

FIGURE 11(a) Potential -pH diagram of the Zn-SO_2-H_2O system at 200°C. Total sulphite activity of 1.0 mol dm^{-3}

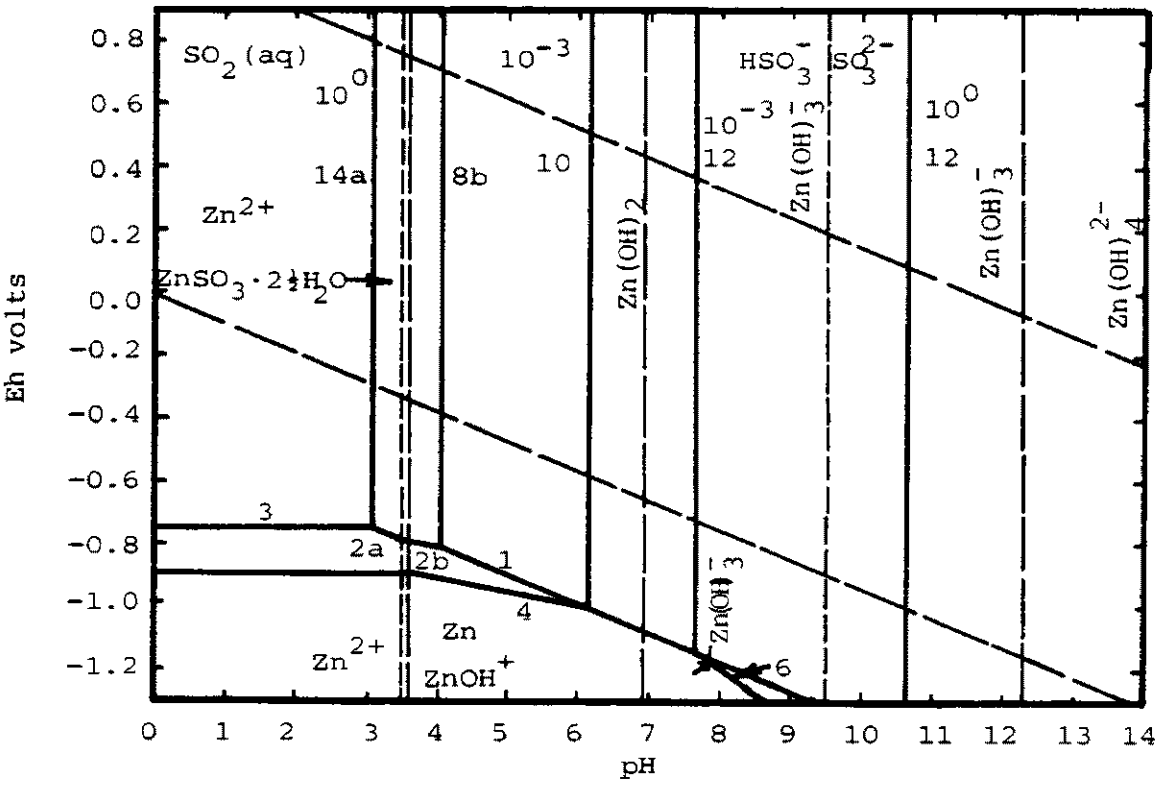

FIGURE 11(b) Potential -pH diagram of the Zn-SO_2-H_2O system at 200°C. Total sulphite activity of 0.1 mol dm^{-3}

Figure 12 presents the high temperature (200°C) equivalent of Figure 5(b). Figure 12 is drawn for two different total sulphite activities. A total sulphide activity of 1.0 mol dm^{-3} is shown by the bold lines and the light lines represent an activity of 0.1 mol dm^{-3}. This diagram shows more clearly the intrusion of zinc hydroxide into the stability region of zinc sulphite at high temperatures and the overall size reduction of the zinc sulphide predominance region. This observation from Figure 12 is important to note since the solubility product of zinc sulphite decreases at high temperatures. Equation A.2.14(c) (Appendix 2) shows that the solubility product of zinc sulphite decreases (i.e., log K_{SP} becomes more negative) with increasing temperature. However, Figure 12 shows that the equilibrium reaction of Line 14(c) is not a relevant reaction under these conditions. Line 14(c) does not appear in the diagram due to the shift of the stability regions of the complex zinc ions toward more acidic media at high temperatures. Consequently, Line 15(b) represents the relevant reaction, and the solubility product of zinc sulphite increases at the elevated temperatures.

Figures 13, 14 and 15 present potential-pH diagrams of the zinc-sulphur-sulphur dioxide-water system at temperatures of 60°C, 100°C and 200°C respectively. These diagrams show that the area of stability of zinc sulphide in aqueous media contracts with increasing temperature along with the general shift of all zinc equilibria toward more acidic media. The potential required for the oxidation of sphalerite in acidic media remains relatively constant with increasing temperature. Additionally, the extremely high acid strength required for direct acid dissolution of sphalerite is somewhat reduced at elevated temperatures. However, the pH required for such a process still remains very low.

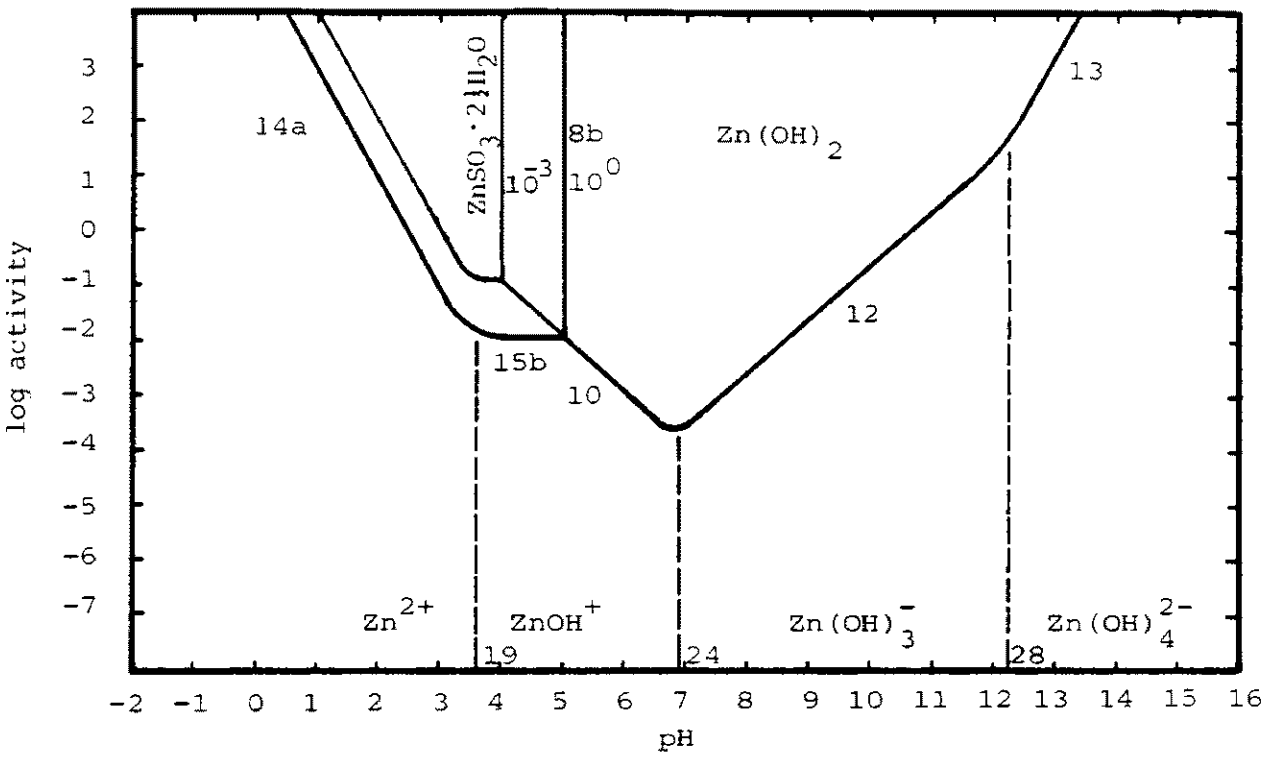

FIGURE 12 Activity -pH diagram of the $Zn-SO_2-H_2O$ system at 200°C.

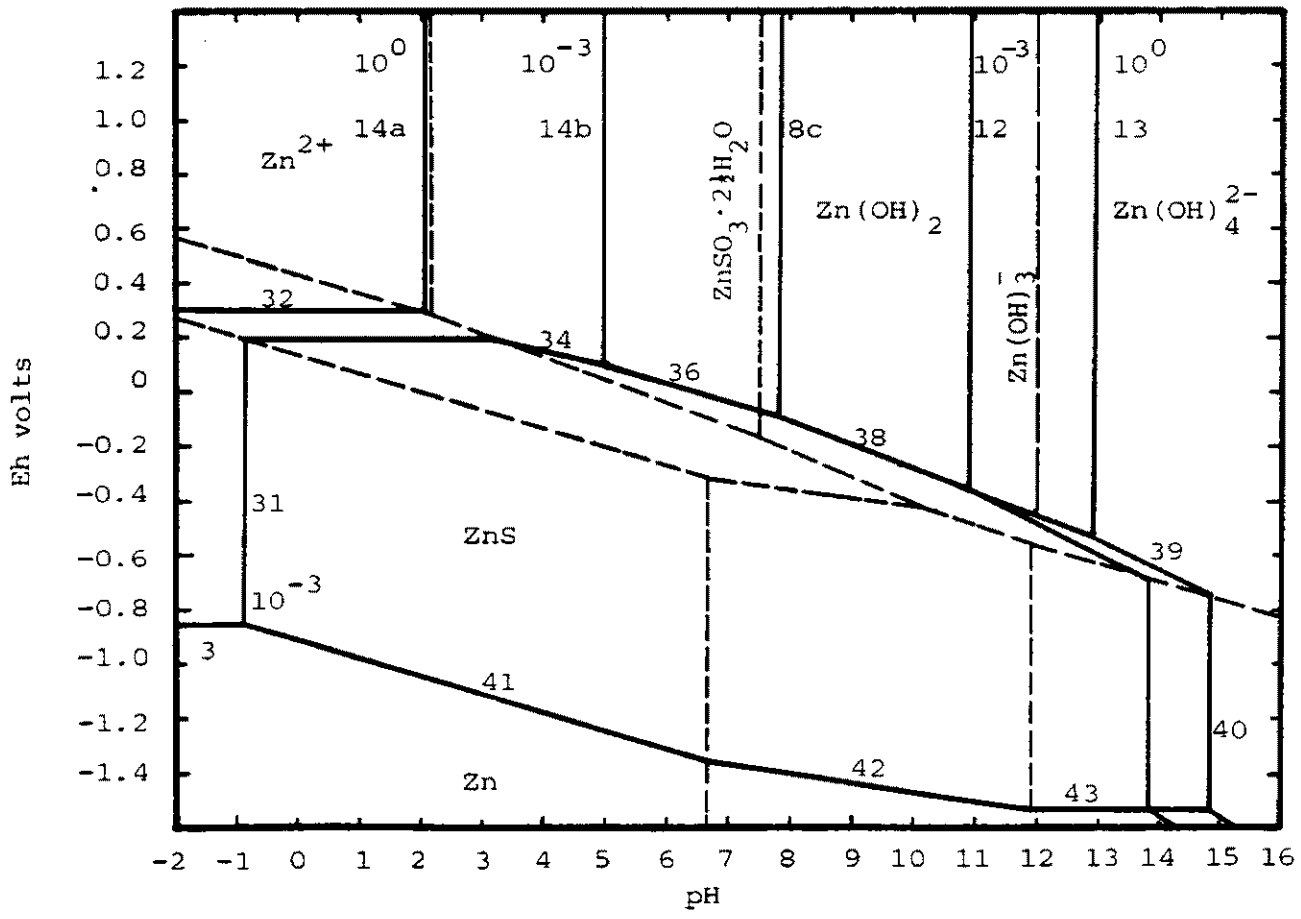

FIGURE 13 Potential -pH diagram of the $Zn-S-SO_2-H_2O$ system at 60°C.

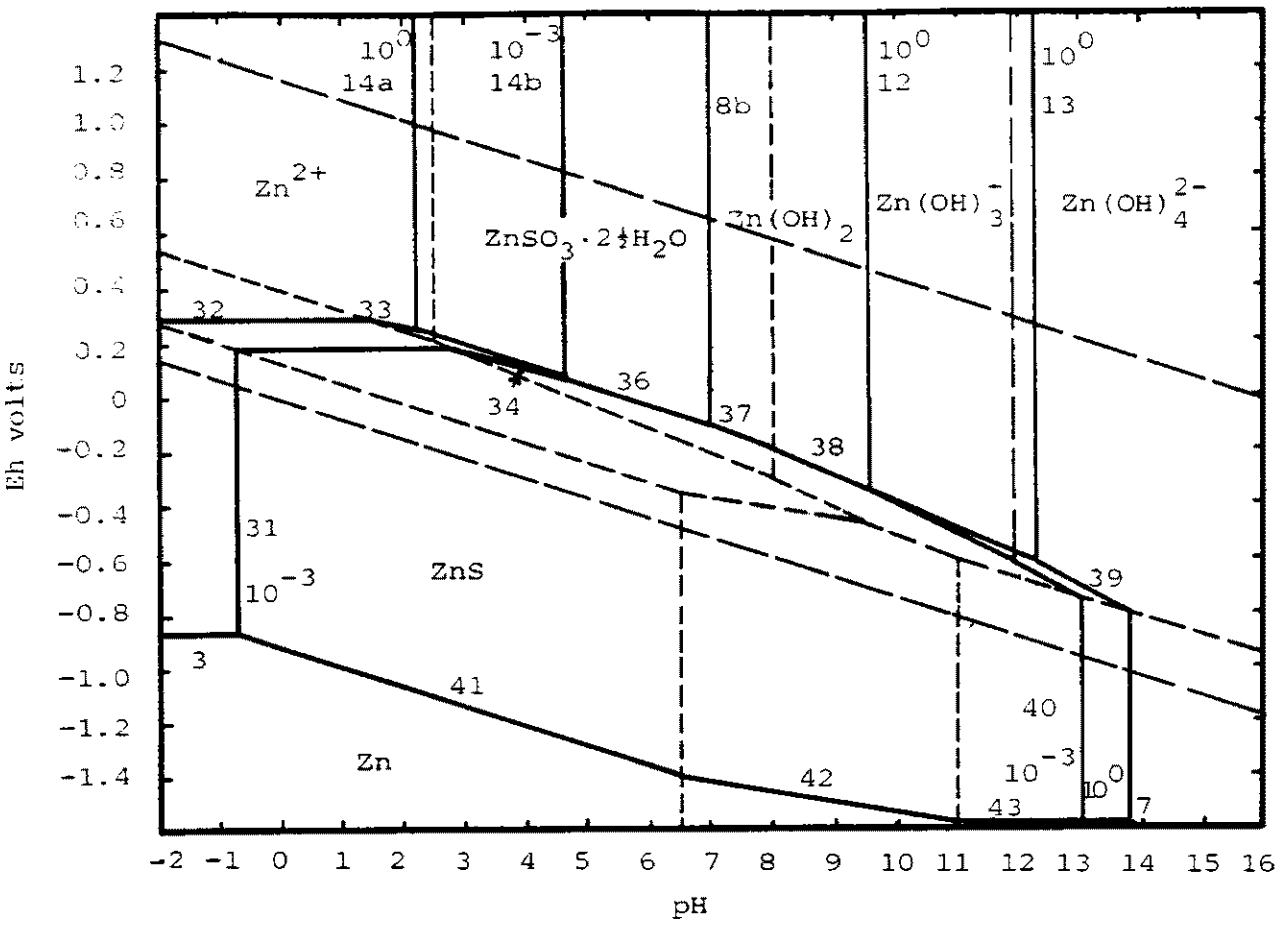

FIGURE 14 Potential -pH diagram of the $Zn-S-SO_2-H_2O$ system at 100°C.

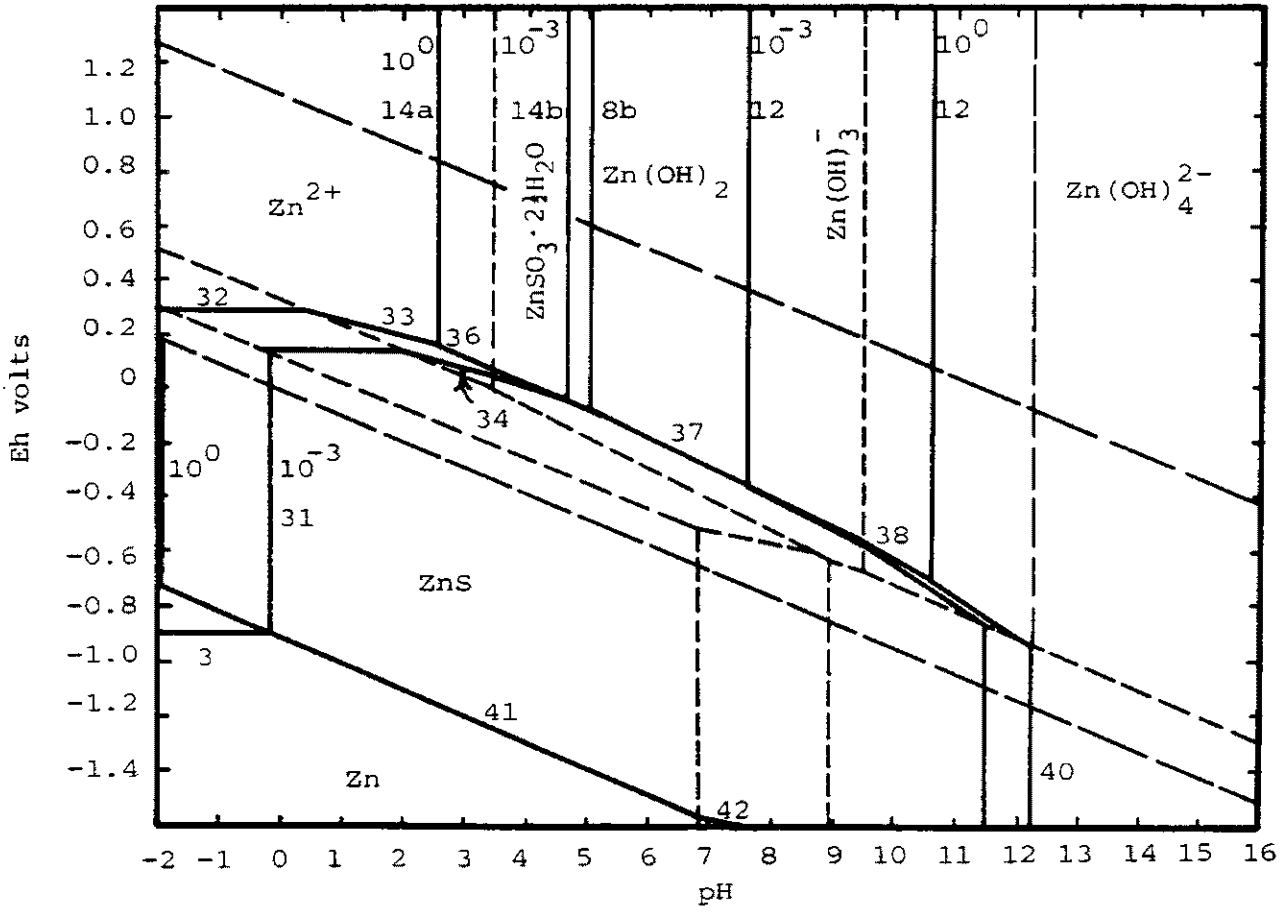

FIGURE 15 Potential -pH diagram of the $Zn-S-SO_2-H_2O$ system at 200°C.

CHAPTER THREE

SOLUBILITY OF ZINC SULPHITE IN THE ZINC-SULPHUR DIOXIDE-WATER SYSTEM

The aim of the work in this chapter is to investigate the properties of zinc sulphite in an aqueous media and to present, in a concise form, its solubility in an aqueous environment. It is expected that such data will allow rationalization of the scattered and meagre literature information. Subsequently this data will permit the prediction of the conditions necessary to achieve a given degree of depletion of zinc from solution by precipitation of the insoluble sulphite. The first task then, was to obtain a reliable value for the standard free energy of formation of zinc sulphite, so that a model for its solubility can be devised in the form of phase diagrams.

3.1 BACKGROUND AND AVAILABLE LITERATURE DATA

Although a process for the preparation of crystalline zinc sulphite salt was first recorded more than a century ago, little information is presently available on the physical and chemical properties of this material. The meagre data available in the literature for the solubility of this salt can ultimately be traced to the original publicaton of Heuston and Tichborne (1890). This paper describes the use of zinc sulphite as a non-poisonous, non-irritative, antiseptic surgical dressing. The sulphite of zinc is stated in this work to be a stable compound with the composition of $ZnSO_3.2H_2O$. Furthermore, the salt is reported as very insoluble in water, being soluble in that medium only to the extent of 0.16 percent.

More recently, Johnstone and Singh (1940) have made a study on the use of zinc sulphite in the recovery of

sulphur dioxide from waste gases. This study was concerned with the filtering properties of zinc sulphite, and therefore, the crystal habits of this salt were investigated. It was reported that precipitation of zinc sulphite from mixtures of zinc oxide and sodium sulphite can yield at least four types of solid compounds depending on the sulphur dioxide to sodium ratio employed. The four compounds include a basic sulphite, $ZnO \cdot 2ZnSO_3 \cdot 3H_2O$, two hydrated sulphite forms, $ZnSO_3 \cdot 2H_2O$ and $ZnSO_3 \cdot 2.5H_2O$, plus a double salt with sodium $Na_2SO_3 \cdot 3ZnSO_3 \cdot 4H_2O$. A powder diffraction pattern for each of the compounds was also supplied, but no line identification or indexing was reported.

Another recent study by Feitknecht and Schindler (1963) summarizes the methods of expressing and determining the various solubility constants for metal oxides, hydroxides and basic salts. These researchers carried out a very careful experimental study of the solubility of zinc hydroxide in conjunction with an analysis of all of the available solubility data. Five crystalline and one amorphous forms of zinc hydroxide are listed. The most stable hydroxide form is the eta phase (ε-$Zn(OH)_2$). Zinc oxide is stated by Feitknecht and Schindler (1963) to have the same solubility as ε-$Zn(OH)_2$ within experimental error, and the latter seems to be the stable phase at 25°C. Since the hydrometallurgical processes dealt with here take place in aqueous solution, thermodynamic data for the ε-$Zn(OH)_2$ phase was consequently selected for use in this present work.

A review of the X-ray diffraction patterns listed in the Joint Committee on Powder Diffraction Standards (JCPDS) card file reveals that it is possible to produce zinc sulphite in various crystalline forms. Six powder patterns are listed for various hydrates of zinc sulphite: one pattern for each of the $ZnSO_3$ (anhydrous), $ZnSO_3 \cdot 0.5H_2O$ and $ZnSO_3 \cdot H_2O$ forms plus three patterns for the $ZnSO_3 \cdot 2.5H_2O$ phase.

It was decided, in view of the imprecise and divergent nature of the available data, to investigate the crystal structure and habits of precipitated zinc sulphite. The prepared zinc sulphite then would be used for subsequent solubility measurements to obtain the required free energy data.

3.2 DETERMINATION OF THE FREE ENERGY OF FORMATION OF ZINC SULPHITE

The free energy of formation of zinc sulphite was experimentally determined by studying the equilibria of the following reactions:

$$Zn^{2+} + HSO_3^- + 2\tfrac{1}{2}H_2O = ZnSO_3.2\tfrac{1}{2}H_2O + H^+ \quad (14b)$$

$$Zn^{2+} + SO_3^{2-} + 2\tfrac{1}{2}H_2O = ZnSO_3.2\tfrac{1}{2}H_2O \quad (14c)$$

Two different methods were employed. The first method involved the measurement of the potential of a zinc electrode immersed in a medium consisting of crystalline zinc sulphite suspended in an aqueous solution of sodium sulphite. The second method involves suspending crystalline zinc sulphite in sulphite solutions of various concentrations. The solubility of the solid was directly measured by analysing solution samples for dissolved zinc and sulphite content as the equilibrium of Reaction 14(b) was established.

3.2.1 Preparation of Zinc Sulphite Powder

Crystalline zinc sulphite powder was prepared for these experiments by dissolving analytical reagent grade zinc oxide (see Appendix 4) in a saturated solution of aqueous sulphur dioxide. A rigorous effort was made to eliminate all extraneous dissolved gases from the solution by using distilled, deionized, boiled water purged with high purity nitrogen gas during cooling. The solid zinc sulphite then precipitates from the zinc bisulphite solution upon removal of the excess aqueous

sulphur dioxide. Sulphur dioxide removal was accomplished by reducing the partial pressure of sulphur dioxide above the solution. This action effectively increases the pH of the solution yielding precipitation of the solid salt from a supersaturated solution. This principal is well illustrated by Figure 5(b) (Chapter Two) where an increase in pH yields precipitation of the sulphite at Line 14(b) i.e., Reaction 14(b).

3.2.2 Electrochemical Measurement

The first method of studying the various equilibria of Reaction 14 utilizes the Princeton Applied Research Corporation (PARC) model K47 corrosion cell system. Approximately 10 grams of crystalline zinc sulphide was suspended in 700 ml of 0.010 molar sodium sulphite solution. The sulphite solution was prepared with Merck sodium sulphite reagent (see Appendix 4) and distilled, deionized, boiled water. The one litre reaction vessel was thermostatically maintained at (25 ± 0.1) $^{\circ}$C, magnetically stirred and purged with high purity nitrogen gas. The potential of a zinc metal electrode, freshly polished with 1200 grit abrasive paper, was measured relative to saturated calomel electrode via a Luggin capillary. Potential measurements were made with the PARC model 173 potentiostat/galvanostat at various times while the system approached equilibrium. The solution pH was measured after the zinc electrode had attained a steady state potential.

The steady state potential of the zinc electrode is a measurement of the equilibrium zinc ion activity in the solution by virtue of Reaction 3:

$$Zn^{2+} + 2e^{-} = Zn\ (c). \qquad (3)$$

The zinc ion activity is therefore related by Equation (12) (Chapter Two) which in this case is,

$$E = E^{\circ} - \frac{RT}{nF} \ln \frac{1}{a_{Zn^{2+}}} \qquad (12)$$

where E is the measured potential and E° = 0.763 volts

(Latimer, 1952) both relative to the standard hydrogen electrode. E° represents the potential of the electrochemical Reaction 3 in the standard state of $a_{Zn}2+ = 1$. The potential of the saturated calomel electrode (SCE) with respect to the standard hydrogen electrode (SHE) is +0.242 volts (Latimer, 1952).

A series of four experiments were carried out as described. The results, which show a high degree of reproducibility, are shown in Table 9. Using the mean result for test nos. T-1, T-2 and T-3, the cell voltage obtained relative to the standard hydrogen electrode (SHE) is:

$$E_{(SHE)} = E_{(SCE)} + E_{(measured)}$$
$$= +0.242 - 1.073$$
$$= -0.831 \pm 0.005 \text{ volts}$$

The corresponding zinc ion activity, calculated from Equation (12) for the conditions of this experiment, is

$$a_{Zn}2+ = 0.005 \pm 0.001 \text{ mol dm}^{-3}.$$

3.2.3 Calculation of $\Delta G°_f$ for Zinc Sulphite

The overall free energy change, ΔG, of a chemical reaction which has attained a steady state dynamic equilibrium is defined to be zero. At steady state then, Equation (11) (Chapter Two) simplifies to Equation (14).

$$G° = -RT \ln K \qquad (14)$$

For the case of Reaction 14(c) at equilibrium,

$$Zn^{2+} + SO_3^{2-} + 2½H_2O = ZnSO_3.2½H_2O \qquad (14c)$$

Equation (14) can be written as

$$\Delta G^\circ = RT \ln K_{SP}$$
$$= RT \ln a_{Zn}2+ \, a_{SO_3}2- \qquad (19)$$

where K_{SP} represents the solubility product of zinc sulphite and $\Delta G°$ is the standard free energy of the reaction. If the activities of the zinc ion and sulphite ion species are measured for Reaction 14(c) at equilibrium, then the standard free energy of the reaction, $\Delta G°$, can be calculated from Equation (19).

TABLE 9

MEASURED POTENTIAL OF A ZINC ELECTRODE IN SULPHITE MEDIA

Test No.	Temp. deg.C	Na_2SO_3 Concentration mol dm^{-3}	Time to Steady State Hours	E measured Volts	Total Sulphite Concentration mol dm^{-3}	pH
T-1	25	0.01	3.5	-1.078		6.77
T-2	25	0.01	2	-1.068	0.0191	6.28
T-3	25	0.01	3.5	-1.073	0.0200	6.31
T-4	25	0.05	3	-1.125	0.0573	7.36

TABLE 10

CONSTANTS FOR THE DEBYE-HÜCKEL EXPRESSION AT 25°C

CONSTANT	VALUE
A	0.509
B	0.328×10^{-8}
$a^{o}_{Zn^{2+}}$	6×10^{8}
$d_{SO_3^{2-}}$	4.5×10^{8}
$d_{HSO_3^{-}}$	$4\text{-}4.5 \times 10^{8}$
$d_{Na^{+}}$	$4\text{-}4.5 \times 10^{8}$

SOURCE : Garrels and Christ, 1965, pp. 61-63.

Consequently with a value for $\Delta G°$, the standard free energy of formation of zinc sulphite can be calculated using the free energy data in Tables 3, 4 and 7 with Equation (10). Equation (10) written for Reaction 14c is:

$$\Delta G^{\circ}=\Delta G^{\circ}_{f,ZnSO_3.2\frac{1}{2}H_2O} - \Delta G^{\circ}_{f,Zn^{2+}} - \Delta G^{\circ}_{f,SO_3^{2-}} - 2\frac{1}{2}\Delta G^{\circ}_{f,H_2O} \qquad (10)$$

The measurement of the zinc ionic activity, $a_{Zn^{2+}}$, has been described in the previous section, 3.2.2. The sulphite ion activity must now be found from the experimental data in Table 9.

The activity of an ionic species, i, in solution is related to its concentration, m_i, by the equation:

$$a_i = \gamma_i m_i \qquad (20)$$

where, γ_i is the activity coefficient of species i. The activity coefficient of a species is given by the Debye-Hückel expression:

$$-\log \gamma_i = \frac{A z_i^2 \, I^{\frac{1}{2}}}{1+d_i \, BI^{\frac{1}{2}}} \qquad (21)$$

where, z_i is the charge on the ionic species and d_i is related to the diameter of the ion in solution. The values for the constants A, B and d_i, relevant to the present study, are listed in Table 10. A comprehensive list of values of d_i can be found in Kielland (1937) or Garrels and Christ (1965). Also, the ionic strength of a solution, I in Equation (21), is given by,

$$I = (\Sigma m_i \, z_i^2)^{\frac{1}{2}} \qquad (22)$$

The total sulphite concentration data given in Table 9 represents the measurement of C_T using the idiometric titration described in Appendix 5.2. C_T, defined here as

$$C_T = [H_2SO_3(aq)]+[HSO_3^-]+[SO_3^{2-}] \qquad (23)$$

is the sum of the concentrations of each of the sulphite species. However in the experiments of Table 9, the concentration of the H_2SO_3 (aq) species is negligible in the near neutral pH media shown. The C_T measured then represents,

$$C_T = [HSO_3^-] + [SO_3^{2-}] \quad (24)$$

The equilibria existing between the sulphite and bisulphite species is given by Reaction 52 as,

$$HSO_3^- = SO_3^{2-} + H^+. \quad (52)$$

The equation corresponding to Reaction 52 (Equation A.2.52) in Appendix 2 yields the ratio of sulphite to bisulphite in a solution of measured pH. At 25°C the equation is:

$$pH = 7.22 + \log \frac{[SO_3^{2-}]}{[HSO_3^-]} \quad (A.2.52)$$

Using the data in Table 9, Equations (20), (21), (23) and (A.2.52) can be solved for the sulphite ion activity by iteration. Such an iterative method would begin by assuming all activity coefficients equal to one. The concentrations and activities of all species are then found with Equations (20) and (A.2.52). The ionic strength of the media is then calculated by Equation (22). Finally, the activity coefficient of all species are found from Equation (21) and a new iterative cycle is begun. Using this method of analysis, the data in Table 9 yields for the solubility product of zinc sulphite:

$$\begin{aligned} K_{SP} &= a_{Zn^{2+}}\, a_{SO_3^{2-}} \\ &= 0.005 \times 0.0017 \text{ (mol dm}^{-3})^2 \\ &= (8.5 \pm 0.5) \times 10^{-6} \text{ mol}^2 \text{ dm}^{-6} \end{aligned}$$

or, $\log K_{SP} = -5.06 \pm 0.05$

Equations (19) and (10) then yield the standard free energy of formation of zinc sulphite. At 25°C this value is:

$$\Delta G^\circ_{f,ZnSO_3.2\frac{1}{2}H_2O} = -1256 \pm 4 \text{ kJ mol}^{-1}$$

3.2.4 Solubility of Zinc Sulphite by Direct Measurement

The second method of studying the equilibria of Reaction 14 involves the direct measurement of the zinc and total sulphite concentration of a medium in which Reaction 14(b) has attained a steady state equilibrium. This involved the same procedures as the preparation of

zinc sulphite powder in Section 3.2.1. Analytical reagent grade zinc oxide was dissolved in a solution of pure water saturated with sulphur dioxide. Crystalline zinc sulphite was forced to precipitate from the solution by the removal of the excess sulphur dioxide, as was explained in Section 3.2.1. The removal of the excess sulphur dioxide was achieved by connecting the erlenmeyer flask, containing approximately 500 ml of the zinc bisulphite solution, to a water aspirator vacuum pump. The solution was magnetically stirred and the flask was submerged in a water bath thermostatically controlled at (25 ± 0.1)°C. After a period of time ranging from 18 to 240 hours, the vacuum was disconnected, the pH was measured and the solution was quantitatively analysed for zinc and total sulphite concentration. The methods of analysis are described in Appendix 5. By varying the initial quantity of zinc oxide dissolved into solution from 2.0 to 14.0 grams, the equilibrium of Reaction 14(b) was established at several different zinc ion concentrations and pH values. The crystalline zinc sulphite formed in the experiments was of very high purity since the only components entering the system were pure zinc oxide, sulphur dioxide and purified water. This material, upon removing the vacuum, was rapidly filtered, washed with acetone and allowed to air dry.

The crystalline zinc sulphite powder produced in this manner was used, additionally, to measure the solubility of the salt by direct dissolution in water. Approximately 10 grams of the salt was suspended in 500 ml of distilled, deionized, boiled water in a one litre glass reaction vessel purged with high purity nitrogen gas. This reactor, fitted with a two blade paddle stirrer and ground glass fittings, was placed in a water bath thermostatically controlled at (25 ± 0.1)°C. The solution pH in the reaction vessel was continuously monitored. Solution samples were withdrawn at 2 hour intervals for analysis of zinc and

total sulphite concentration. Six experiments were performed at 25°C in this manner. All six experiments yielded an identical result for the equilibrium pH, zinc concentration and total sulphite concentration measured by the analysis techniques described in Appendix 5. This highly reproducible data is tabulated in summarized form in Appendix 7 along with all the other experimental data resulting from direct solubility measurements on crystalline zinc sulphite. This entire set of experimental data is also plotted in Figure 16 and is discussed in the following section.

3.2.5 Discussion of the Zinc Sulphite Solubility Measurements

Figure 16 presents a graph of the zinc activity -pH equations of Reactions 14(a), 14(b) and 14(c) of Appendix 1 as indicated. The zinc sulphite equilibria shown in Figure 16 closely resembles that shown in Figure 5(b) of Chapter Two. Figure 5(b) was constructed with the total sulphite species activity fixed at 1.0 mol dm^{-3}. Figure 16, on the other hand, is drawn assuming a fixed ratio of total sulphite activity to zinc activity. The dissolution equilibria reactions of zinc sulphite shown in Figure 16 are:

$$Zn^{2+} + SO_2(aq) + 3\tfrac{1}{2}H_2O = ZnSO_3.2\tfrac{1}{2}H_2O + 2H^+ \qquad 14(a)$$

$$Zn^{2+} + HSO_3^- + 2\tfrac{1}{2}H_2O = ZnSO_3.2\tfrac{1}{2}H_2O + H^+ \qquad 14(b)$$

$$Zn^{2+} + SO_3^{2-} + 2\tfrac{1}{2}H_2O = ZnSO_3.2\tfrac{1}{2}H_2O \; . \qquad 14(c)$$

A simplified form of the equations from Appendix 2 for these reactions at 25°C are:

$$pH = 1.95 - \log (Zn^{2+}) - 0.5 \log n \qquad 14(a)$$

$$pH = 2.13 - 2 \log (Zn^{2+}) - \log n \qquad 14(b)$$

$$\log (Zn^{2+}) + 0.5 \log n = -2.53, \qquad 14(c)$$

where n is defined as the ratio of the total sulphite activity to the zinc activity. The bold lines (14(a), 14(b) and 14(c)) in Figure 16 are drawn assuming that the zinc activity equals the total sulphite activity

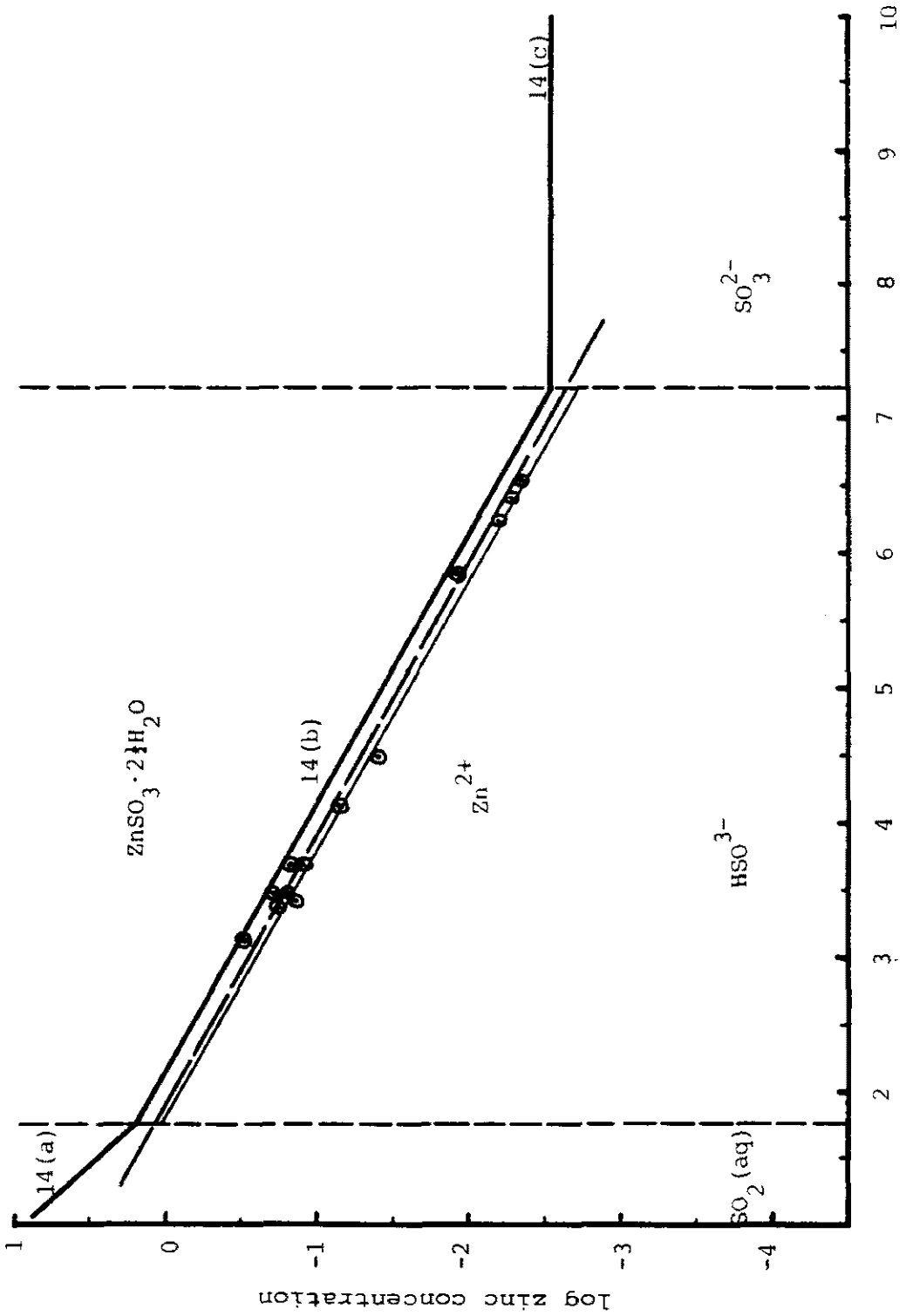

FIGURE 16 Experimental results for the solubility of zinc sulphite by direct measurement.

(i.e., n=1). The light line for Reaction 14(b) is drawn assuming the bisulphite activity to equal twice the zinc activity (i.e., n=2). These three lines then represent the solubility of zinc sulphite as a function of pH. It is important at this point to recall, however, that these equations are based on the thermodynamic data derived from the results of the electrochemical measurement of the solubility of zinc sulphite as described in Section 3.2.3.

Superimposed on Figure 16 are the data points obtained from the solubility measurements on zinc sulphite. The numerical data for these measurements tabulated in Appendix 7, show that the ratio n in most cases has a value between 1.5 and 1.8. The only species present in solution for the conditions of these experiments are zinc ion and aqueous sulphur dioxide. Under equilibrium conditions, therefore, the solution must establish electroneutrality by the following ionic charge balance,

$$2[Zn^{2+}] + [H^{+}] = [HSO_3^{-}] + 2[SO_3^{2-}].$$

Since the equilibrium pH in all cases lies well within the predominance regions of both the Zn^{2+} ion and the bisulphite species, the charge balance indicates that the bisulphite concentration must be approximately equal to twicethe zinc ion concentration. The observed ratio for n (1.5 to 1.8) supports this conclusion. Ionic effects such as the possible formation of a complex zinc-bisulphite ion can account for any apparent deviation from the above charge balance.

The line of best fit by the least-squares method of linear regression for the thirteen data points plotted in Figure 16 is shown by a dashed line in the same figure. A high degree of correlation was found for this linear regression. The correlation coefficient obtained was 0.995. The equation of the best fit line calculated in the form of Equation 14(b) given above is:

$$pH = 2.13 - 2.02 \log(Zn^{2+}) - \log 1.72$$

which, within experimental error, is an exact fit of

Equation 14(b) with the ratio n equal to 1.72. The calculated bisulphite to zinc ion concentration ratio of 1.72 is in very close agreement with the observed experimental ratios given in Appendix 7.

The measurement of the solubility of zinc sulphite in water by chemical analysis, therefore, directly confirms the results obtained by electrochemical means. Thus, the calculated free energy of formation of crystalline zinc sulphite has been derived and substantiated by two completely different measurement techniques.

A study of the physical properties of a precipitated compound naturally should include an investigation into the crystal structure of such a material. A preliminary investigation revealed that various hydrates of zinc sulphite could be formed by precipitating the salt from a solution at various temperatures. Since the thermodynamic data was desired at 25°C, the study of the crystal structure of zinc sulphite is limited to the material precipitated at that temperature.

Figure 17 presents two scanning electron microscope photographs of zinc sulphite at a magnification of 470X. The top photomicrograph (a) shows the freshly precipitated crystalline material after being filtered and dried in a vacuum desiccator. This photograph shows the precipitated material to be well developed crystals with the majority being at least 30μm in the shortest dimension. The bottom photomicrograph (b) shows the same material after being subjected to a solubility experiment where the crystals were suspended in water until dissolution equilibrium was achieved. This photomicrograph shows evidence of the original crystal structure remaining intact, but, with dissolution and reprecipitation having occured.

Table 11 presents a chemical analysis of the zinc sulphite material before and after the solubility experiment along with theoretical analysis for $ZnSO_3.2\frac{1}{2}H_2O$. Zinc and sulphite were quantitatively

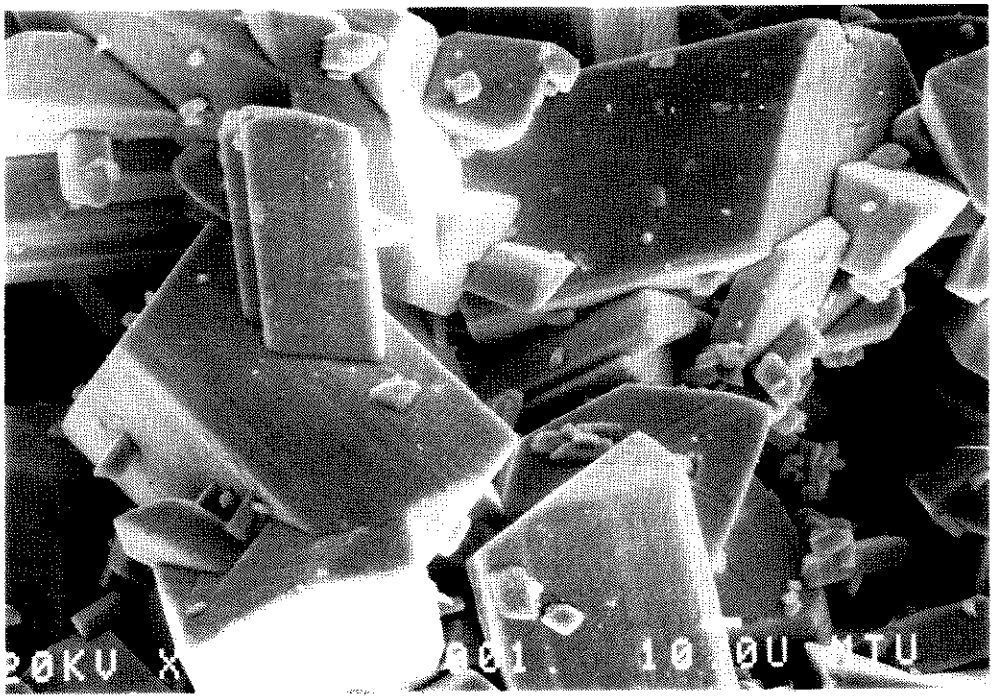

(a) Freshly precipitated zinc sulphite

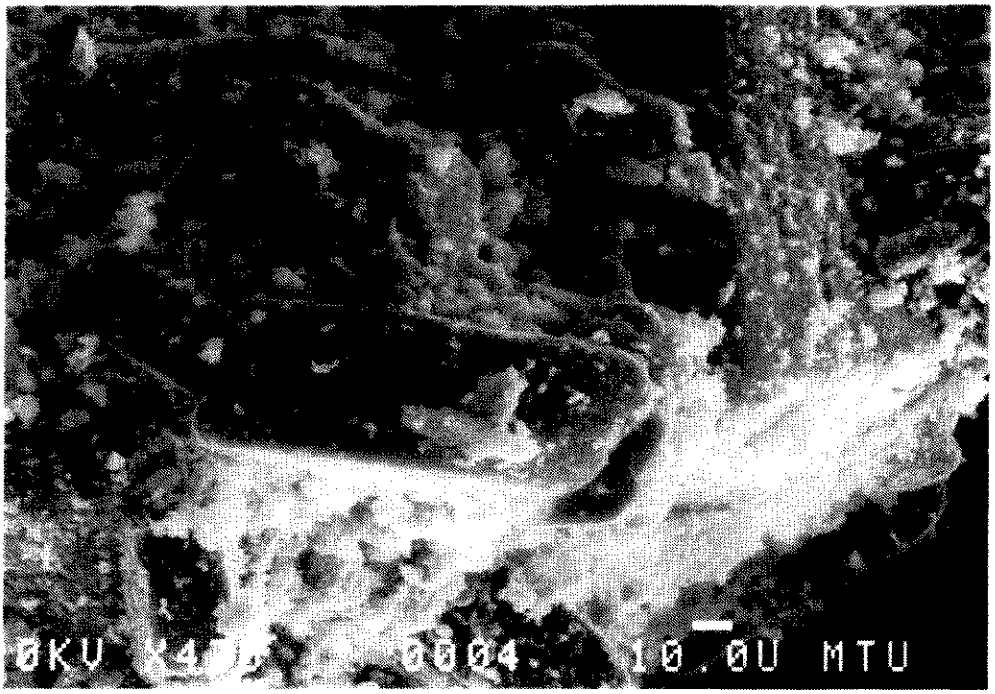

(b) Material remaining from solubility experiment

FIGURE 17 SEM photomicrograph of zinc sulphite

TABLE 11

CHEMICAL ANALYSIS OF CRYSTALLINE ZINC SULPHITE

Precipitated Zinc Sulphite

	Percent Weight	Mole Ratio
Zn	34.0	1.00
SO_3^{2-}	40.8	0.98
H_2O	26.1	2.68

Material After Solubility Experiment

	Percent Weight	Mole Ratio
Zn	35.2	1.00
SO_3^{2-}	39.5	0.92
H_2O	25.3	2.61

Theoretical Analysis of $ZnSO_3 . 2.5H_2O$

	Percent Weight	Mole Ratio
Zn	34.32	1.00
SO_3^{2-}	42.03	1.00
H_2O	23.64	2.50

analysed by the methods given in Appendix 5. The water of hydration was assumed to make up the difference from 100 percent. The analysis in Table 11 shows that the freshly precipitated material, within experimental error, matches the theoretical analysis for $ZnSO_3.2\frac{1}{2}H_2O$. It is possible that all of the moisture may not have been removed from the solids by the desiccator before analysis. This would account for the slightly low assay for zinc and sulphite. The analysis presented for the material remaining from the solubility test shows an assay high in zinc and low in sulphite compared to the theoretical analysis. This suggests that some zinc hydroxide may have been reprecipitated after the dissolution of zinc sulphite. This conclusion is further substantiated by the ratio of approximately 1.5 for bisulphite to zinc found in the solution in equilibrium with the solid material. The reprecipitation of zinc hydroxide following dissolution of zinc sulphite is discussed in further detail in the following section.

The crystal structure of zinc sulphite was investigated by X-ray diffraction. The interplanar spacing versus relative line intensity data is presented in Table 12. This data was obtained on a Phillips PW1050 X-ray diffractometer using Cu_{K_α} radiation (λ =1.541838Å). Upon comparison with the diffraction patterns in the Powder Diffraction File (of the JCPDS), it was found that several of the diffraction peaks shown in Table 12 matched various peaks in each of the published diffraction patterns. No general agreement, however, could be made with any single pattern contained in the Powder Diffraction File.

The solubility of the crystalline zinc sulphite precipitated from a solution containing zinc and aqueous sulphur dioxide has been measured at 25°C and confirmed. This data formed the basis for the calculation of the thermodynamic free energy of formation of $ZnSO_3.2\frac{1}{2}H_2O$. Use of this molecular formula in the

TABLE 12

X-RAY DIFFRACTION DATA
FOR ZINC SULPHITE PRECIPITATED AT 25°C

Interplanar Spacing d Å	Relative Intensity I/Io
6.55	95
4.63	95
4.17	100
3.32	60
2.95	90
2.62	25
2.60	95
2.54	10
2.35	50
2.30	10
2.27	15
2.22	5
2.17	5
2.11	10
2.10	5
2.05	5
1.97	5
1.880	15
1.783	15
1.752	20
1.742	10
1.675	15
1.662	20

thermodynamic calculations is justified by the analysis of the chemical composition of the precipitated zinc sulphite material. Although the atomic structure of this material could not be identified, its crystal structure has been investigated and reported. It is possible that the zinc sulphite precipitated at 25°C could be composed of a mixture of various hydrate forms. However, this ambiguity does not affect the construction of Pourbaix diagrams since the free energy of this zinc sulphite material was established by direct physical property measurement.

3.3 CONGRUENCY OF SOLUBILITY

Equilibrium solubility relationships between solid compounds and an aqueous medium can be described by a number of methods. Most commonly and simply this is achieved through the use of phase diagrams. One form of such diagrams are presented in Figures 1(b) and 5(b) of Chapter Two. The principal variables of these two diagrams are metal ion concentration versus media pH at a constant activity of aqueous sulphur dioxide. Ricci (1952) in a formidable treatise has given a thorough mathematical description of the solubility relationships that apply to generalized acid-base-water systems. The principal variables used by Ricci (1952) are total moles of acid versus total moles of base contained in a system. The type of diagram developed from these relationships elucidate physical properties of solid compounds in an aqueous medium that are not shown in the diagrams of Chapter Two. The present section develops these diagrams for the zinc-sulphur dioxide-water system, in a simplified fashion, after Ricci's work. The relevant material required to investigate the solubility in the zinc-sulphur dioxide-water system is presented using the same notation as Ricci (1952).

3.3.1 General Diagrammatic Relationships

The degree of solubility of metal hydroxides and normal metal salts in the system acid-base-water can be mathematically described in a quantitative manner by fundamental relationships based on equilibria and solution electroneutrality. The acid-base-water system can be denoted by, in the case dibasic acids and divalent bases, H_2X-$M(OH)_2$-H_2O respectively. The symbol H_2X represents a dibasic acid and $M(OH)_2$ is a divalent base. Solutions of the two may form an insoluable normal salt MX. Solubility relationships in such a system can best be presented through equilbrium phase diagrams.

Figure 18 is a general schematic diagram of the acid-base-water system. Plotted along the horizontal axis is **a** which is defined as the number of moles of the acid in the system whether or not completely dissolved. The actual concentration of acid in the solution is denoted by a. Similarly, **b** is the number of moles of base plotted along the vertical axis and b is the concentration of base in solution. S_1 and S_2 represent the aqueous solubility of the base and acid respectively. The curve S_1x is the solubility of the base as acid is added to the system. Conversely, the curve S_2x is the solubility curve of the acid as the base is added to the system. Point x, therefore, is a hypothetical solution saturated with both solids.

The area shown as L in Figure 18 is the set of all solutions with unsaturated compositions. A system whose composition lies in the area above the curve S_1x will contain the solid base in equilibrium with a saturated solution. The saturated solution will have a composition corresponding to a point of curve S_1^x that lies vertically below the system composition. Likewise, a system with a composition lying to the right of curve S_2x contains the solid acid in equilibrium with the corresponding saturated solution on curve S_2^x.

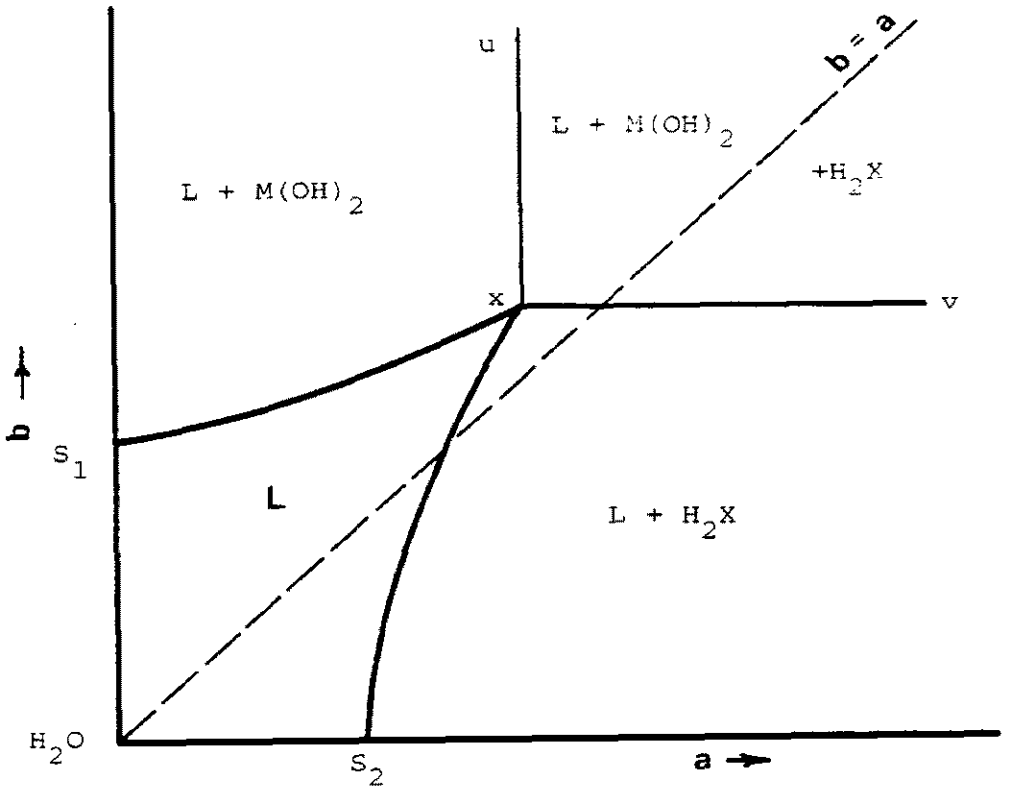

FIGURE 18 Schematic diagram of the $M(OH)_2$-H_2X-H_2O system.

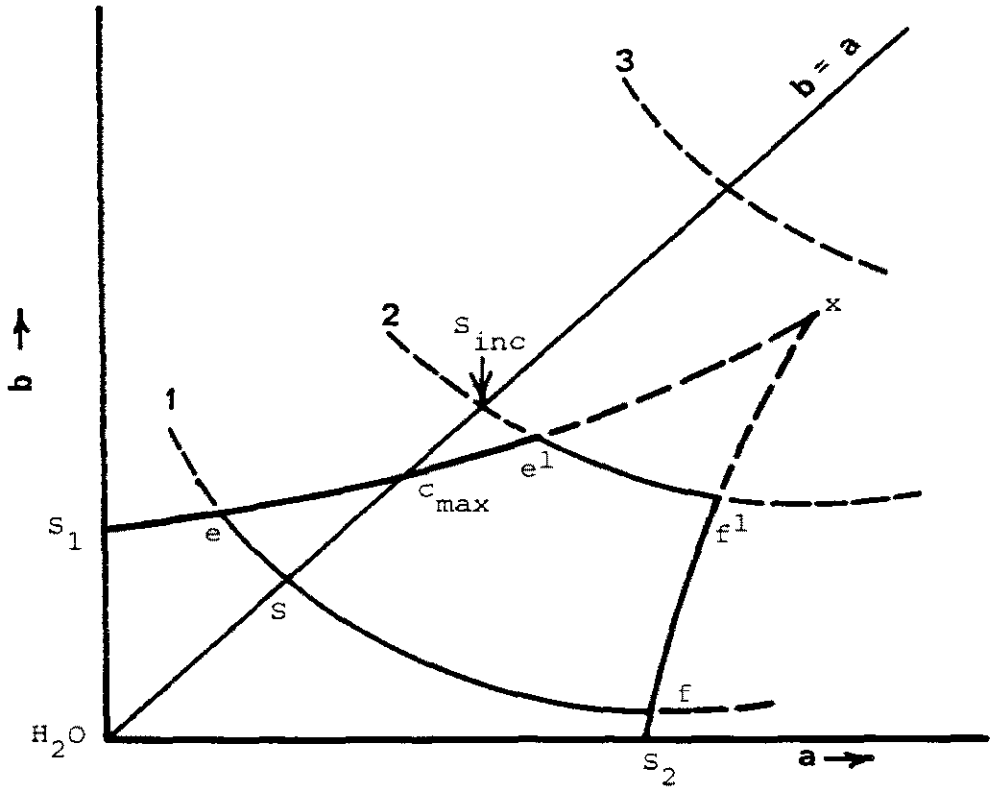

FIGURE 19 Congruent and incongruent solubility relationships.

A system with a composition in the region between lines ux and xv contains a mixture of both solids in equilibrium with a solution of composition x. The dashed line labelled **b=a** represents an equal concentration of acid and base in a system.

Figure 18, however, represents only one specific case. A solid salt of the acid and the base, MX, may in many cases precipitate from a solution saturated with both acid and base. Figure 19 shows three possible curves, labelled 1, 2 and 3, for the solubility of the salt MX. Curve 3 is the case of the system shown in Figure 18. The solubility of the salt MX exceeds the solubility of the solid acid and solid base such that the solution can never be concentrated enough to precipitate MX. Either the solid base $M(OH)_2$ or the solid acid H_2X will precipitate first in preference to MX. Curve 1, on the other hand, shows a system where the salt MX has a much lower solubility. The pure salt placed in water will dissolve to an extent such that the liquid will have the composition at point S. The branch eS of Curve 1 represents the solubility of the salt in an excess of base and branch Sf, its solubility in an excess of acid. Point e is the solution saturated with both salt and base, point f is the solution saturated with salt and acid while point S is the solution saturated with salt.

The point labelled c_{max} in Figure 19 represents the maximum concentration of the pure salt dissolved into solution without precipitating either the solid base or acid. If the solubility curve of the salt cuts the **b=a** line above c_{max}, such as Curve 2 in Figure 19, then the solid salt may exist as a stable phase only when in equilibrium with a solution containing an excess of acid (or base). The salt with solubility Curve 2 is stable only along section e'f' which has an excess of acid over the stoichiometric ratio of a=b. The solution saturated with salt and acid is point f'. Only dilute solutions of the salt, those

with concentrations less than c_{max} are stable in pure water. If a salt solution is allowed to evaporate such that the salt concentration begins to exceed c_{max}, the solid base will begin to precipitate. As the evaporation continues, the composition of the solution moves along curve $c_{max}e'$ as the base precipitates. The solid salt then precipitates when the solution composition has reached point e'. Similarly, if an excess of the solid salt is added to pure water, equilibrium is established with not only the solid salt, but with the base (hydroxide) phase as well. The solution would establish, in this case, a composition of e' at equilibrium.

A salt with a solubility curve resembling Curve 1 in Figure 19 (i.e., a curve such that S is less than c_{max}) is defined as being congruently soluble in water. The stable segment of its solubility curve intersects the **b=a** line which represents the composition of a pure salt. A congruently soluble salt has several distinguishing properties. A saturated solution in equilibrium with the solid salt only, can be prepared from the solid salt and water without an excess of either the acid or base. Evaporation of this pure salt solution leads to precipitation of only the pure salt. Furthermore, the solid salt may be washed with water without decomposition.

A salt, on the other hand, with a solubility curve such as Curve 2 of Figure 19 is defined as being incongruently soluble in water. The distinguishing factor of incongruency in Figure 19 is that the **b=a** line intersects Curve 2 above c_{max}. That is, the segment of Curve 2 in which the salt is in stable equilibrium with the solution, does not intersect the **b=a** line. If salt is added to the system above c_{max} the solid base will be precipitated. A saturated solution of the salt is only possible in an excess of the acid (or in an excess of base if x lies to the left of **b=a**) along curve e'f'. Additional

properties of an incongruently soluble salt are that the evaporation of the pure salt solution leads to precipitation of the solid base rather than the salt. The pure salt solution can not be concentrated and the solid salt can not be washed with water without heterogenous decomposition resulting in precipitation of the solid base.

Figures 18 and 19 are idealized schematic diagrams. Most real situations encountered in the study of hydrometallurgy or geochemistry, will have an acid, H_2X, that does not form a solid and is completely miscible in aqueous solution. The curve S_2X, therefore, in most situations, does not appear in diagrams at ambient temperatures and pressures. Figures 20 and 21 present diagrams that are more representative of congruent and incongruent solubility, respectively, for the normal salt of dibasic acids. The curve S_1e represents, in both figures, the solubility of the hydroxide and the curve ef represents the solubility of the salt. Point e is the solution saturated with both $M(OH)_2$ and MX and is the solution in equilibrium with all system compositions (both solution and solids) lying between lines ej and ek. The $L+M(OH)_2$ and L+MX phase fields lie adjacent to either side of the dual phase field in both the congruent and incongruent diagrams. The region marked L represents unsaturated solutions.

3.3.2 Mathematical Development of Diagrams

The equations necessary for the calculation of the solubility curves are easily developed from solution equilibria and electroneutrality considerations. The symbols and notation used here are the same as that used by Ricci (1952) for the ease of those readers wishing to investigate this type of analysis in greater detail. The first necessary equation is the electroneutrality balance where the sum of positive charges in solution

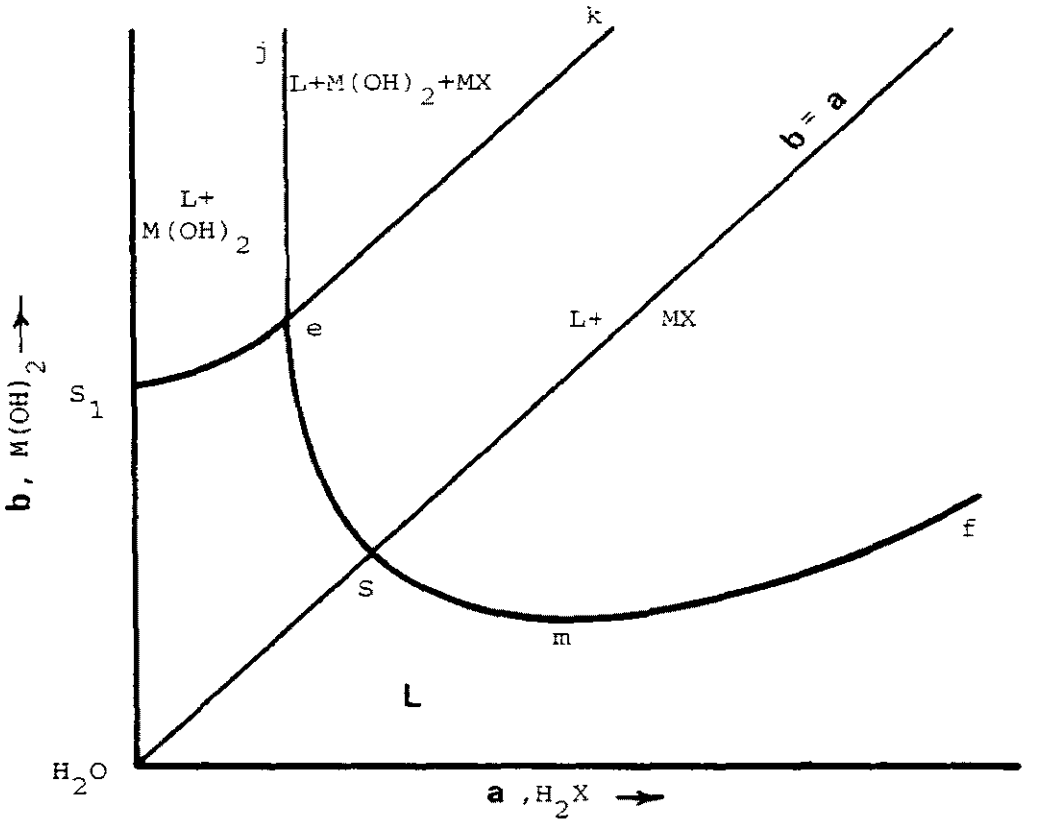

FIGURE 20 Congruent solubility of a normal salt of dibasic acid.

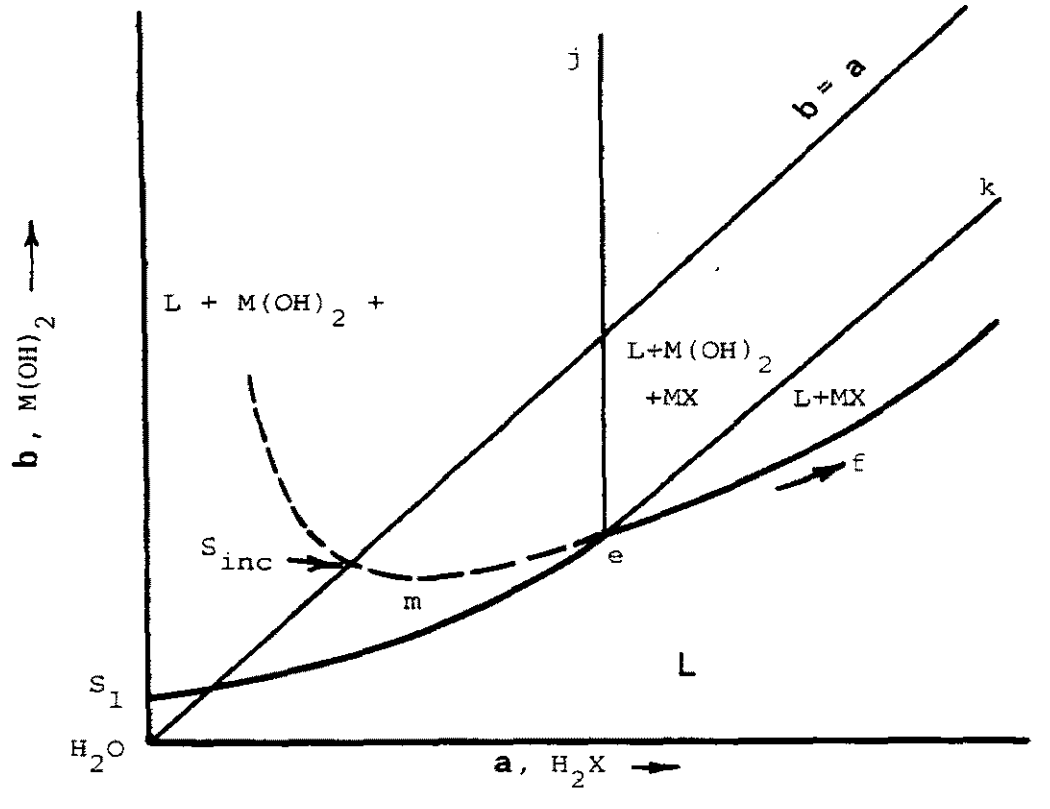

FIGURE 21 Incongruent solubility of a normal salt of dibasic acid.

must equal the sum of negative charges:

$$[H^+] + 2[M^{2+}] = [HX^-] + 2[X^{2-}] + [OH^-]$$

Upon rearrangement,

$$[H^+] - [OH^-] = [HX^-] + 2[X^{2-}] - 2[M^{2+}] .$$

Ricci (1952) makes the following definitions:

a, the total concentration of acid in solution is given by

$$a = [H_2X] + [HX^-] + [X^{2-}]$$

and b, the concentration of base in solution is given by

$$b = [M^{2+}] .$$

Furthermore, α_1 and α_2 are the ionization fractions of the acid

$$\alpha_1 = \frac{[HX^-]}{a} \quad \text{and} \quad \alpha_2 = \frac{[X^{2-}]}{a}$$

In some of the equations it is convenient to define $[H^+]$ as simply H and $[OH^-]$ as OH. Combining the definitions above, yields for the electroneutrality balance

$$H - OH = a\alpha_1 + 2a\alpha_2 - 2b$$

or,

$$H - OH = a(\alpha_1 + 2\alpha_2) - 2b . \qquad (25)$$

The solubility product for the salt MX is

$$P = [M^{2+}] \; [X^{2-}]$$

or,

$$P = b \; a \; \alpha_2 \qquad (26)$$

The water equilibrium equation is

$$W = [H^+] \; [OH^-] \qquad (27)$$

or,

$$W = H \cdot OH$$

The equilibria of the dibasic acid involves two ionizations. The first ionization reaction is

$$H_2X = H^+ + HX^-$$

where the ionization constant is defined as,

$$K_1 = [H^+][HX^-]/[H_2X]$$

and the ionization fraction is

$$\alpha_1 = [HX^-]/a$$

The second ionization reaction of the acid is

$$HX^- = H^+ + X^{2-} ,$$

where the corresponding relationships are

$$K_2 = \frac{[X^{2-}][H^+]}{[HX^-]} \quad \text{and} \quad \alpha_2 = \frac{[X^{2-}]}{a}$$

These relationships when combined yield for the first ionization,

$$\alpha_1 = \frac{1}{1+[H^+]/K_1+K_2/[H^+]} \qquad (28)$$

and for the second ionization,

$$\alpha_2 = \alpha_1 K_2/H \qquad (29)$$

The final relationship required for the calculation of the complete solubility diagram is the solubility product of the metal hydroxide or base. The relationship is

$$P_1=[M^{2+}][OH^-]^2$$

or,

$$P_1=b \times OH^2 \qquad (30)$$

Three separate calculations are required to completely identify plots such as Figures 20 and 21. Equations (25) through (29) inclusive are all necessary for the calculation of curve ef, the solubility of salt. Solving Equations (25) and (27) through (30) inclusive will yield the curve S_1e which is the solubility of the solid base. Point e can be located exactly by solving all six equations simultaneously.

3.3.3 Calculation of Curve ef

The solubility of the salt MX can be calculated from Equations (25) through (29) inclusive after a few algebraic manipulations. The substitution of Equation (27) into Equation (25) yields

$$H-\frac{W}{H}=a(x_1=2x_2)-2b$$

From Equation (26),

$$a = \frac{P}{b\alpha_2}$$

Elimination of a from these two gives,

$$H^2b\alpha_2-b\alpha_2W=HP\alpha_1+2PH\alpha_2-2b^2H\alpha_2$$

Further, eliminating α_2 with the use of Equation (29) and rearrangement then yields

$$(P-bK_2)H^2-2K_2(b^2-P)H+bWK_2=0. \qquad (31)$$

Equation (31) represents the condition for a solution saturated with salt MX. The system variables are b and H while the rest are constants for a given system. Equation (31) can then be solved for H using a selected value for b in the following manner:

$$H = \frac{(b^2-P) \pm \sqrt{(b^2-P)^2-(P/K_2-b)bW}}{(P/K_2-b)} \qquad (32)$$

The a value(s) corresponding to the selected value of b can then be calculated as summarized in Table 13. Following this method, a set of points (a,b) can be calculated to establish the solubility curve ef of salt MX.

Since Equation (32) is of the quadratic form, several types of roots can be obtained. If for a selected value of b two real positive roots are obtained, then, the lower value of H can be interpreted as the precipitation point of the salt MX as the acid (a) is added to a solution with a M^{2+} concentration of b. The higher value of H corresponds to the redissolving of MX upon continued addition of acid a. If Equation (32) yields one positive root, then a precipitate is obtained which never redissolves. If the roots are complex or both negative, the selected value of b is below a certain minimum value denoted in Figures 20 and 21 by point m. For normal salts of dibasic acids, the point m will coincide with the point S or S_{inc}.

3.3.4 Calculation of Curve S_1e and Point e

The curve S_1e can be established without any further manipulation of Equations (25) and (27) through (30) inclusive. A method for calculating a point (a,b) for a selected value of b is summarized in Table 13. The point e can be calculated exactly using Equations (25) through (30) inclusive. A combination of Equations (25) through (29) inclusive yields as previously shown,

$$(P-bK_2)H^2-2K_2(b^2-P)H+bwK_2=0. \qquad (31)$$

Substitution of Equation (27) into Equation (30) gives,

$$b = P_1H^2/W^2 \qquad (33)$$

Substitution of Equation (33) into Equation (31) and some rearrangement yields,

$$2H^4P_1/W^2 + H^3 - HW(1+PW/P_1K_2) - 2PW^2/P_1 = 0. \qquad (34)$$

Equation (34) can be solved for H using an iterative cycle. A procedure for calculating (a,b) for point e

TABLE 13

CALCULATION METHODS FOR SOLUBILITY DIAGRAMS

Solubility curve ef for salt MX

STEP	OBJECTIVE	EQUATION
1	Select b value for point (a,b)	
2	Calculate H value(s)	32
3	Find x_1	28
4	Find x_2	29
5	Calculate a value for point (a,b)	26

Solubility curve S_1e for base $M(OH)_2$

STEP	OBJECTIVE	EQUATION
1	Select b value for point (a,b)	
2	Calculate OH	30
3	Calculate H	27
4	Find x_1	28
5	Find x_2	29
6	Calculate a value for point (a,b)	25

Composition of invarient point e

STEP	OBJECTIVE	EQUATION
1	Solve for H value	34
2	Find OH	27
3	Calculate b value for point (a,b)	30
4	Find x_1	28
5	Find x_2	29
6	Calculate a value for point (a,b)	26

is summarized in Table 13. The point e thus calculated corresponds to the intersection of curve S_1e with curve ef and represents the condition for equilibrium with both the salt MX and base $M(OH)_2$ phases.

3.3.5 Construction of Solubility Diagrams

A computer program, which employs the methods outlined in Table 13, was used to calculate the solubility diagrams for three systems. The well known $Ca(OH)_2$-CO_2-H_2O and $Mg(OH)_2$-CO_2-H_2O systems were constructed along with the $Zn(OH)_2$-SO_2-H_2O system. Ricci (1952, p.412) has calculated the significant points of the $Ca(OH)_2$-CO_2-H_2O and $Mg(OH)_2$-CO_2-H_2O systems and presents this data in tabular form. However, Ricci (1952) does not construct the diagrams. The complete solubility diagrams for the calcium and magnesium carbonate systems are presented in Figures 22 and 23. These diagrams are in close agreement with the data presented by Ricci (1952). Figure 22 clearly shows calcium carbonate to be a congruently soluble salt, whereas in Figure 23, magnesium carbonate is an incongruently soluble salt. Ricci (1952), in the schematic diagrams presented, used no scales on the axis. It was found however, that a logarithmic scale is the most appropriate for illustrating the entire range of concentration.

Figure 24 presents the solubility diagram for the $Zn(OH)_2$-SO_2-H_2O system. It can be seen that this system closely resembles in form the $Mg(OH)_2$-CO_2-H_2O system demonstrating that zinc sulphite is an incongruently soluble salt. The incongruent solubility of zinc sulphite, based on the analysis of incongruently soluble systems by Ricci (1952), suggests several physical characteristics for the behaviour of zinc sulphite in pure water. First, pure zinc sulphite cannot be precipitated from a pure water solution containing the stoichiometric ratio of zinc to aqueous sulphur dioxide. Concentration

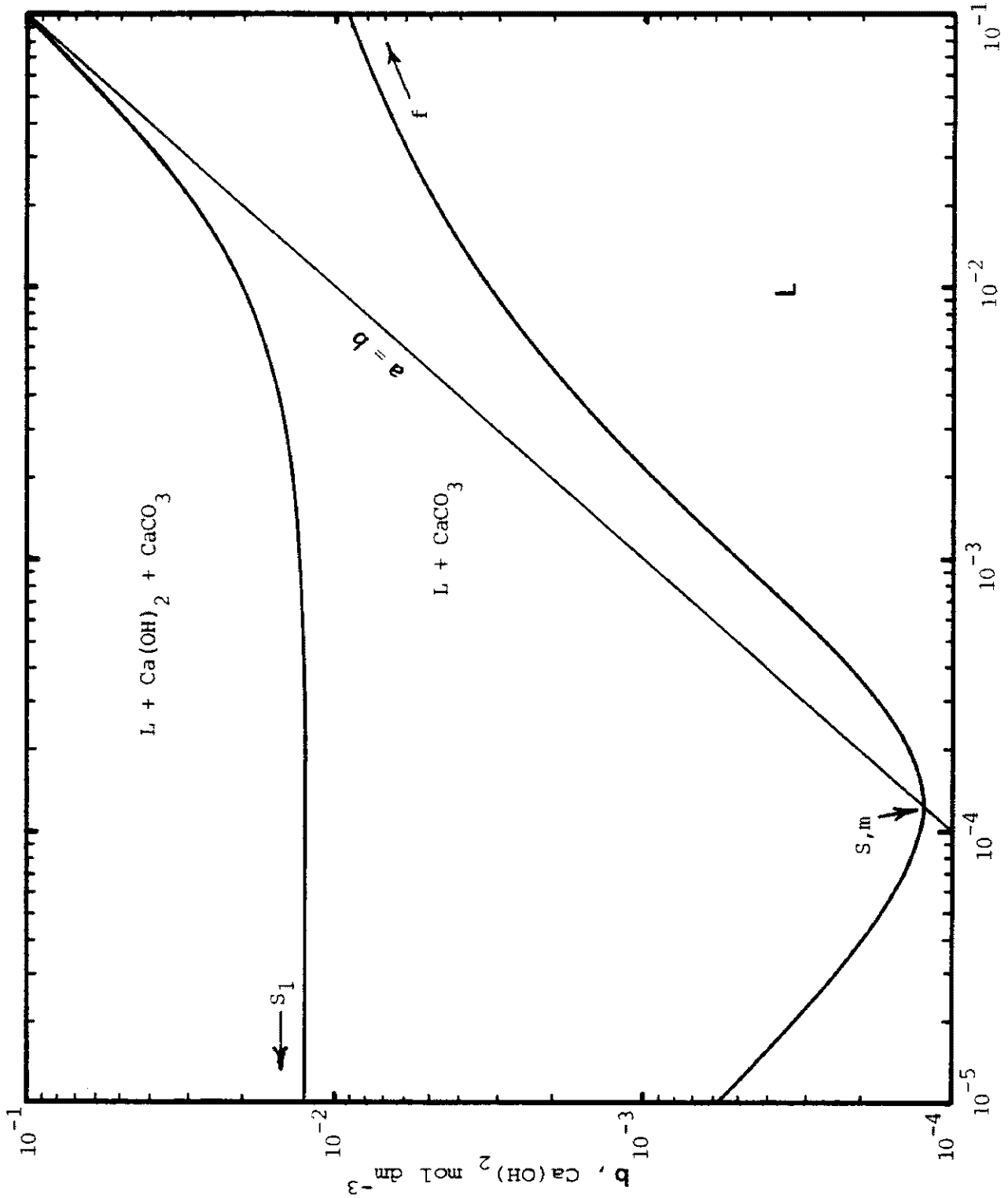

FIGURE 22 Congruent solubility in the $Ca(OH)_2$-CO_2-H_2O system

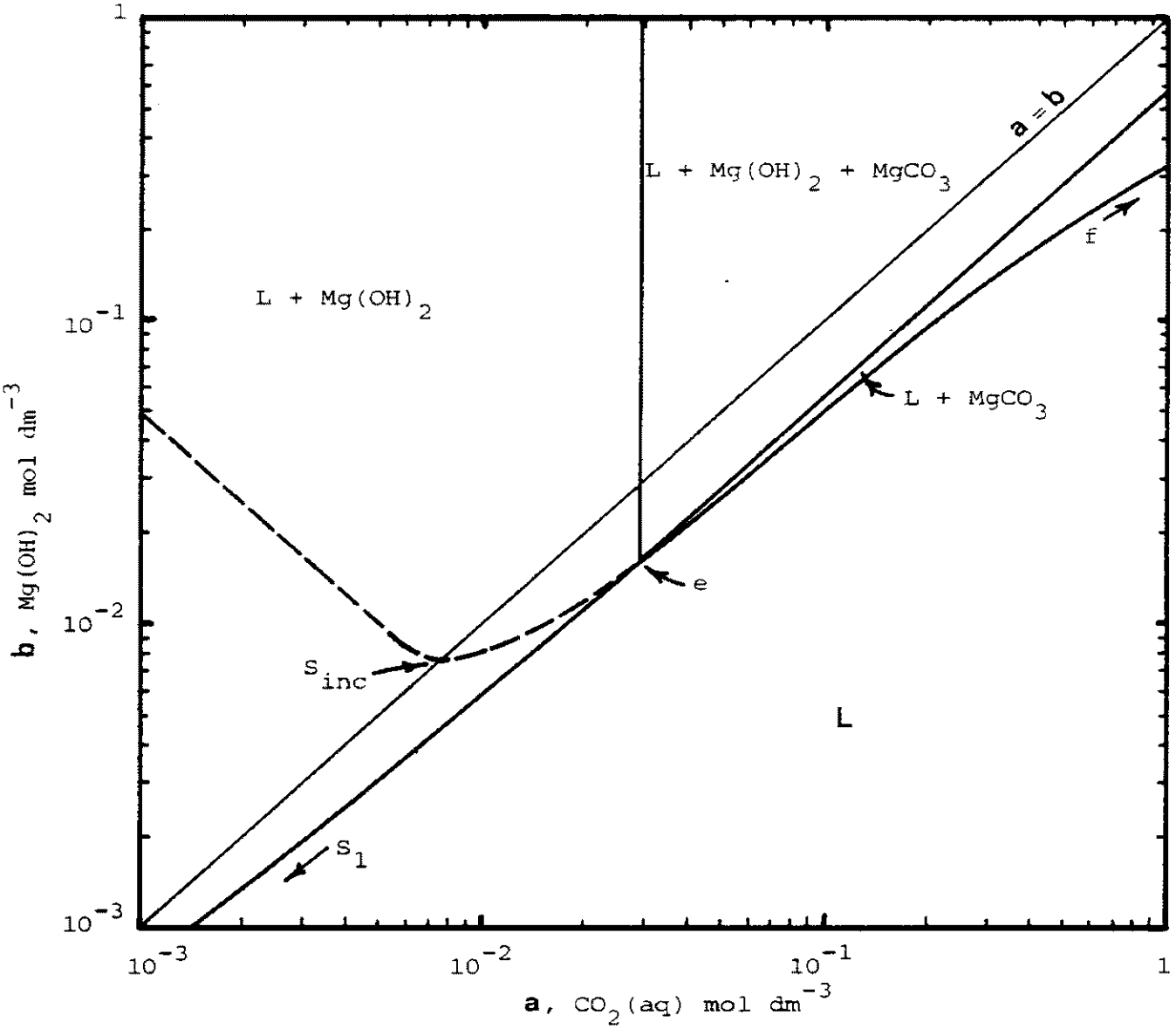

FIGURE 23 Incongruent solubility in the $Mg(OH)_2$-CO_2-H_2O system

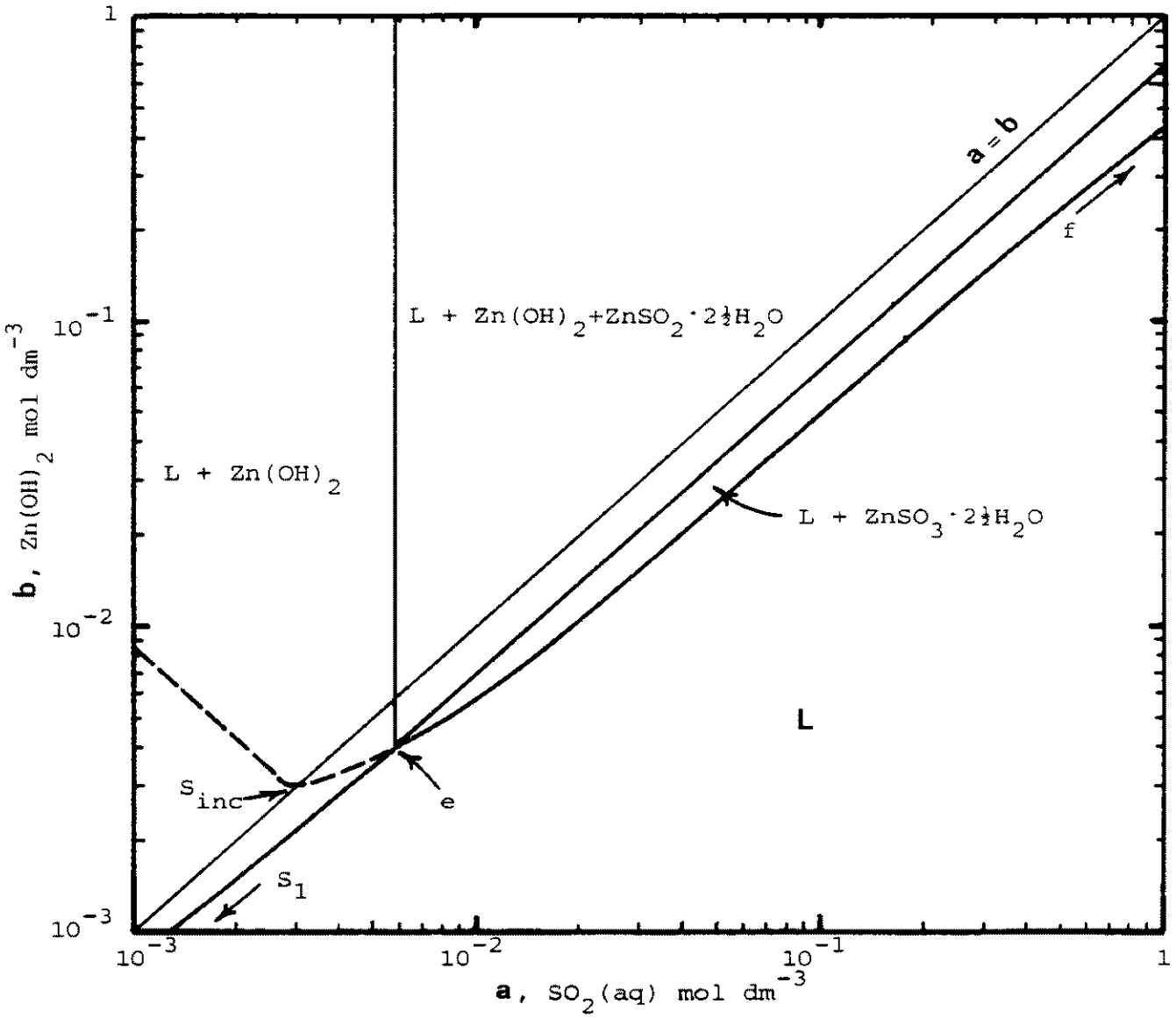

FIGURE 24 Incongruent solubility in the $Zn(OH)_2$-SO_2-H_2O system

of such a solution by evaporation (or by boiling under a vacuum) will result in the precipitation of zinc hydroxide along with zinc sulphite. An excess of sulphite over zinc is required to prevent precipitation of zinc hydroxide. Secondly, zinc sulphite salt cannot be washed with water without heterogenous decomposition resulting in preciptation of zinc hydroxide. A solubility experiment, such as that outlined in Section 3.2.4, will result in reprecipitation of zinc hydroxide following dissolution of the sulphite. The solution in equilibrium with the solid material will subsequently contain an excess of sulphite over the zinc concentration.

The incongruent solubility of zinc sulphite demonstrated in Figure 24 is directly confirmed by experimental observation. As previously outlined, Table 11 shows, for the material remaining from a solubility experiment, an assay that is high in zinc and low in sulphite. Also, the solution in equilibrium with the suspended zinc sulphite shows an excess of sulphite over zinc, as expected from simple dissolution of the salt. Therefore it is apparent, as expected from an incongruently soluble salt, that zinc hydroxide was precipitated at the expense of zinc sulphite. This is necessary to achieve the excess of acid over the base required for stability of the incongruently soluble zinc sulphite salt. As a result of this deposition of zinc hydroxide, the remaining material has the observed deviation from the theoretical composition. Further evidence of this zinc hydroxide deposition is also shown, as previously mentioned, by the photomicrograph of the remaining material in Figure 17(b) which shows zinc hydroxide precipitated on the original zinc sulphite crystals.

3.4 DISCUSSION OF THERMODYNAMIC PHASE DIAGRAMS

Chapter Two and Chapter Three present, in a concise and convenient form, the thermodynamics of the zinc-

sulphur dioxide-water system with a detailed investigation of the solubility of zinc sulphite in this system. The importance of the various types of phase diagrams produced through this study is found in the development of process strategy. All of the Pourbaix diagrams presented, plus solubility diagrams such as Figures 5(b), 12 and 24, allow precise prediction of the optimum conditions for the precipitation of zinc sulphite and the maximum depletion obtainable, from a number of process variables such as temperature, sulphurous acid concentration and media pH. The relationship of zinc sulphite to zinc hydroxide under these process variables is also precisely shown to allow selective or coprecipitation of zinc sulphite as an intermediate or final product in a metal extraction scheme. The diagrams developed also add to the fundamental knowledge of the heterogeneous chemical processes involved in hydrometallurgical processing and facilitate the study of the leaching characteristics of sulphite systems.

Figure 25(a) shows the type of data previously available on sulphite systems. This diagram, reproduced from the work of Esdaile and Walters (1969), shows experimental data on the solubility of zinc and other metal sulphites in water. Information of this type, previously the only information available, formed the basis for process strategy development by Esdaile and Walters. A diagram of equal value, constructed from the recently available thermodynamic data of Linkson (1983), is shown in Figure 25(b). This diagram, rapidly developed from thermodynamic data like that of Esdaile and Walters, shows the relative solubility of several metal sulphites. However, these data are of a very limited nature. They cannot predict the process conditions for precipitation of metal sulphites and they give no indication of the degree of depletion obtainable under specific process conditions. Diagrams of this nature, in reality, only depict a small part of the overall spectrum

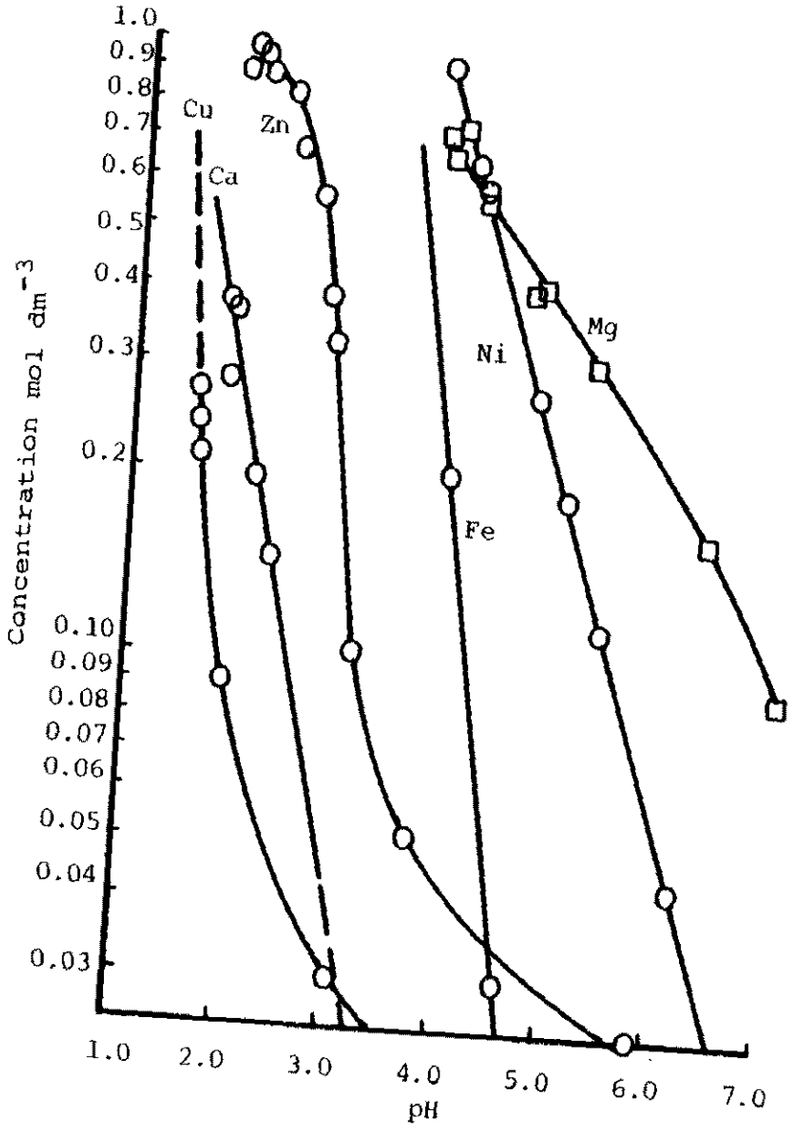

FIGURE 25(a) Solubility of metal sulphites in relation to pH at room temperature.
Reproduced from Esdaile and Walters (1969)

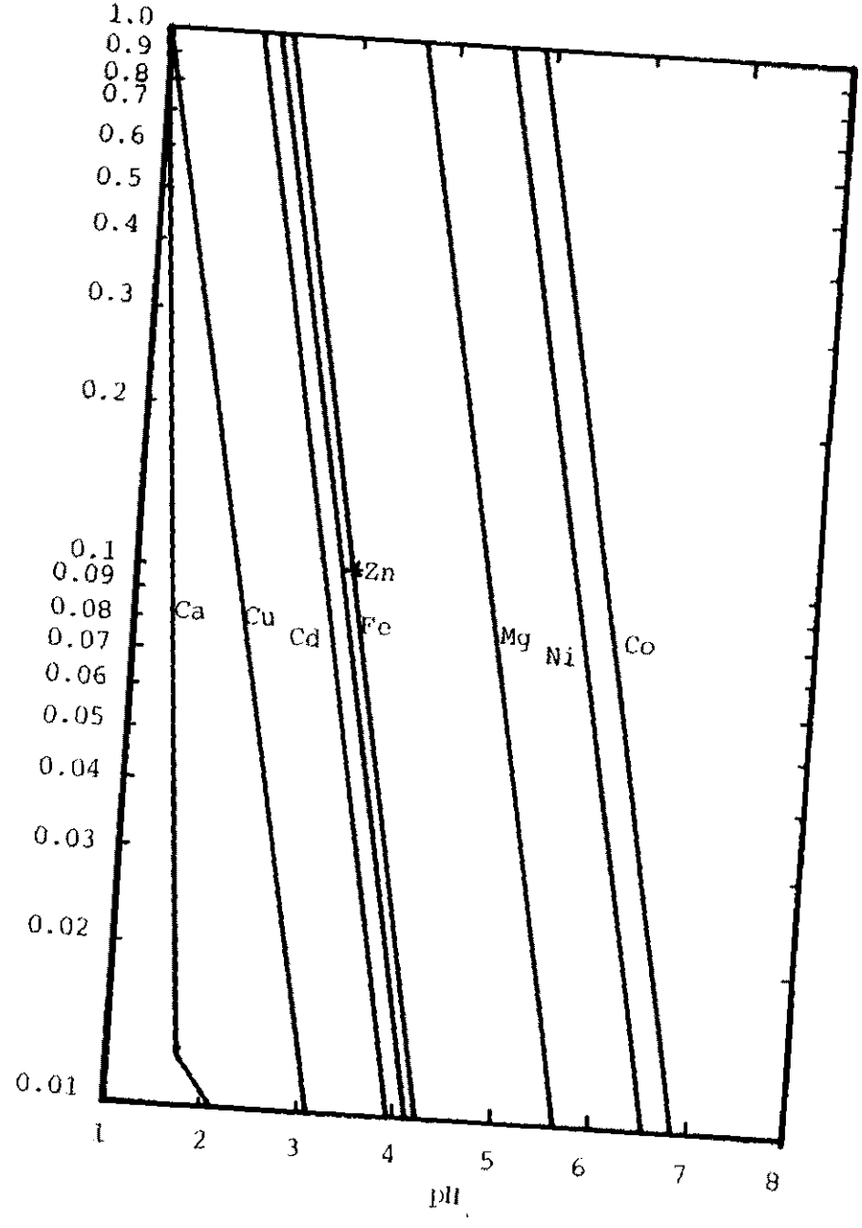

FIGURE 25(b) Solubility of metal sulphites at 25°C.
Derived from thermodynamic data.

of information required to effectively evolve a process scheme. Potential -pH and solubility diagrams, such as those developed in this work for zinc, could easily be constructed from the data used in Figure 25(b) for other metal sulphites. Potential -pH diagrams and their associated solubility diagrams summarize the entire spectrum of process information. Shown clearly are the conditions for selective precipitation or coprecipitation of related phases. The residual metal species concentration and form can be read directly from these diagrams with the appropriate conditions to achieve a given metal depletion from the parent liquor. Such diagrams then facilitate the prediction of selective precipitation of various metals as sulphites under typical process conditions, and form an ideal basis for effective process strategy development.

The zinc sulphite precipitated in this work was found to form coarse crystals with many desirable properties. The precipitated material, it was found, settled rapidly in its parent liquor and could be easily filtered. Once separated from solution and dried, zinc sulphite is a free flowing, highly stable compound. Precipitated zinc hydroxide, on the other hand, was found to form a heavy gelatinous slurry which was very difficult to filter. The maximum depletion of zinc from solution by precipitation of the sulphite was found to yield a residual zinc concentration of 0.53 mg dm^{-3}. Since this maximum depletion is nearly as great as that for zinc hydroxide, the precipitation of zinc sulphite could have application in effluent water quality control. The reduced reagent costs by precipitation of zinc sulphite at a lower pH from acidic media than zinc hydroxide, combined with the enhanced filtering characteristics, makes zinc sulphite precipitation highly desirable in such a process.

The potential use of zinc sulphite precipitation as a hydrometallurgical process for the primary production of zinc is very great. The sulphite could be produced

as a final product or as an intermediate form for further treatment. Zinc, once separated in a sulphite form, can be calcined to yield a high grade zinc oxide product and sulphur dioxide for reuse. Selective precipitation from other metals can be achieved by careful pH control. Furthermore, a high degree of selective extraction of zinc from a sulphite medium containing iron can be obtained with the General Mills Chemicals, Inc. sulphite process (Sudderth, et al, 1978). Therefore, the selective extraction of zinc using sulphite media is an attractive alternative to existing hydrometallurgical processes. The use of scientific data necessarily has an integral role in the development of such a process. Consequently, the careful selection and use of the appropriate thermodynamic phase diagrams will greatly aid in the development of complete hydrometallurgical processing schemes.

CHAPTER FOUR

REVIEW ON THE LEACHING OF ZINC SULPHIDE

The chemistry involved in the leaching of metal sulphide minerals is more complicated than that of metallic elements or metal oxides owing to the complex chemistry of sulphur and the great variety of reaction products that can be formed. Table 14 illustrates this complex sulphur chemistry. Shown are the various oxidation states that sulphur may obtain and the great variety of sulphur oxyanions that can be formed in leaching reactions. Consequently, progress toward the understanding of sulphide leaching has been more limited. A number of publications reviewing the present knowledge and recent advances in sulphide leaching have been presented.

Halpern (1957) reviewed some of the aspects of the physical chemistry involved in leaching processes. Foreward and Warren (1960) reviewed the extraction of metals from sulphide ores by hydrometallurgical processes and discussed the feasibility of a large number of possible chemical lixiviants. Woodcock (1961) discussed various aspects of the oxidation of sulphide minerals including crystal structure, lattice bonding and solution composition. He also pointed out the various oxidation products formed with reference to the kinetics of reaction and rate limiting steps.

Peters and Majima (1968) discussed the physical chemistry of leaching of sulphide minerals with the use of thermodynamic phase diagrams. Some of the complex sulphur chemistry was elucidated and electrochemical reaction mechanisms were postulated to explain their kinetic observations. Wadsworth (1972) reviewed the recent advances in the leaching of various sulphide minerals. Dissolution reactions of many sulphides and

TABLE 14

THE VARIOUS OXIDATION STATES OF SULPHUR

Anion Name	Formula	Sulphur Oxidation State
Permonosulphate	SO_5^{2-}	+8
Dipersulphate	$S_2O_8^{2-}$	+7
Sulphate	SO_4^{2-}	+6
Dithionate	$S_2O_6^{2-}$	+5
Sulphite	SO_3^{2-}	+4
Trithionate	$S_3O_6^{2-}$	+3.33
Dithionite	$S_2O_4^{2-}$	+3
Tetrathionate	$S_4O_6^{2-}$	+2.50
Thiosulphate	$S_2O_3^{2-}$	+2
Pentathionate	$S_5O_6^{2-}$	+2
Sulphur	S	0
Disulphide	S_2^-	-1
Sulphide	S^{2-}	-2

their electrochemical nature were discussed in detail. The kinetics of several leaching systems were explained using diffusion and electrochemical type models. Dutrizac and MacDonald (1974) reviewed the leaching of base metal sulphides by acidic ferric ion media. Presented is a description of the preparation, regeneration and properties of such a leaching medium along with a discussion of several proposed commercial processes. Peters (1976) discussed the chemistry and applications of the direct leaching of sulphide minerals. Thermodynamic Eh-pH diagrams were used to describe feasible decomposition paths. Several recently proposed hydrometallurgical processes are discussed with regard to their scientific basis.

A review of these general papers elucidates several points about the direct leaching of zinc sulphide. Firstly, there are a wide variety of reagent systems that can be applied to the oxidative or non-oxidative dissolution of sphalerite. Secondly, the dissolution of sulphide minerals exhibit many electrochemical characteristics. Since natural sphalerite is a semi-conducting mineral, it is likely that sphalerite dissolution may display an electrochemical nature. Finally, there are many types of kinetic models that may have application in zinc sulphide leaching.

4.1 REVIEW OF LEACHING SYSTEMS APPLIED TO ZINC SULPHIDE

Table 15 presents a summary of the available work on the chemical leaching of zinc sulphide. A great variety of reagent systems, as shown in Table 15, have been investigated by previous researchers. All reagent systems employ the use of a strong acid, most commonly, sulphuric acid and to a lesser extent, hydrochloric acid. Combined with the acid, an additional oxidizing agent is often used. Commonly, Fe^{3+} ion or oxygen have been applied as the oxidizing agent in these reagent systems.

TABLE 15

RESEARCH ON THE LEACHING OF ZINC SULPHIDE

REFERENCE	REAGENT	MATERIAL	FUNDAMENTAL OR PROCESS STUDY	KINETIC MODEL AND COMMENTS	RESULTANT S FORM
Romankiw & De Bruyn (1964)	H_2SO_4	Synthetic ZnS	Fundamental	Chemical reaction control established rate expression	H_2S
Dewing & Cochran (1978)	H_2SO_4	ZnS Concentrate	Process Bench Scale	Chemical reaction control 1st order dependence on [ZnS]	S° or SO_2
Dewing, et al (1982)	H_2SO_4	ZnS Concentrate	Process Pilot Plant		S°
Jackson & Strickland (1958)	HCl/Cl_2	Various Sulphides	Fundamental	Controlled by transport of chlorine in solution	S° and sulphur monochloride
Mizoguchi & Habashi (1983)	HCl/O_2	ZnS Concentrate	Fundamental	Activation energy demonstrates diffusion controlled process. Propose galvinic mechanism with pyrite.	S°
Rath et al (1981)	$HCl/FeCl_3$	ZnS Concentrate	Fundamental	Product layer diffusion control data fits shrinking core model.	S°

TABLE 15 (Continued)

REFERENCE	REAGENT	MATERIAL STUDIED	FUNDAMENTAL OR PROCESS STUDY	KINETIC MODEL AND COMMENTS	RESULTANT S FORM
Venkataswamy & Khangaonkar (1981)	$HCl/FeCl_3$	ZnS Concentrate	Fundamental	In presence of solvent for S°. No conclusion from shrinking core model.	S°
Kuzminkh & Yakhontova (1950) a.	$H_2SO_4/Fe_2(SO_4)_3$	ZnS Concentrate	Fundamental	Greater $[Fe^{3+}]$ accelerates reaction.	S°
Kuzminkh & Yakhontova (1950) b.	$H_2SO_4/Fe_2(SO_4)_3$	Mixed Sulphide Concentrate	Fundamental	Rate hindered by Zn^{2+} accumulation.	S°
Verhulst (1974)	$H_2SO_4/Fe_2(SO_4)_3$	Synthetic ZnS	Fundamental	Chemical reaction control developed expression of Romankiw & de Bruyn	S°
Scott & Nicol (1978)	$H_2SO_4/Fe_2(SO_4)_3$	ZnS Concentrates	Fundamental	Chemical reaction control by oxidative and non-oxidative processes.	H_2S or S°
Verbaan (1980)	$H_2SO_4/Fe_2(SO_4)_3$	Zns Concentrates	Fundamental	Empirical electrochemical based model.	H_2S or S°
Foreward & Veltman (1959)	H_2SO_4/O_2	ZnS Concentrate	Process study		S°
Stanczyk & Rampacek (1961)	H_2SO_4/O_2	ZnS Concentrate	Process study		SO_4^{2-}

TABLE 15 (Continued)

REFERENCE	REAGENT	MATERIAL STUDIED	FUNDAMENTAL OR PROCESS STUDY	KINETIC MODEL AND COMMENTS	RESULTANT S FORM
Majima & Peters (1966)	H_2SO_4/O_2	Various Sulphide Concentrates	Fundamental	Measured relative rates of oxidation	SO_4^{2-}
Gerlach & Pawlek (1968)	H_2SO_4/O_2	Synthetic sulphides	Fundamental	Measured relative dissolution rates	S° or SO_4^{2-}
Scott & Dyson (1968)	H_2SO_4/O_2	Synthetic ZnS	Fundamental	Tested various catalysts. Propose galvanic mechanism.	S° or SO_4^{2-}
Veltman & Bolton (1980)	H_2SO_4/O_2	Zns Concentrate	Process review		S°
Bolton et al (1981)	H_2SO_4/O_2	ZnS Concentrate	Process review		S°
Sobol & Frash (1974)	H_2SO_4/SO_2	Ni containing FeS Concentrate	Process study	Activation energy demonstrates diffusion nature of process	S°
Tiwari (1976)	H_2SO_4/SO_2	Synthetic ZnS	Fundamental	S° layer diffusion control data fits shrinking core model	S°
Adams & Matthew (1981)	SO_2/O_2	ZnS Concentrate	Fundamental	Chemical reaction control data fits shrinking core model	S° or SO_4^{2-}

However, a limited number of studies have tested the application of sulphur dioxide or chlorine gas as oxidizing reagents.

Only one of the reagent systems listed in Table 15 constitutes a direct non-oxidative dissolution of sphalerite. This study by Romankiw and de Bruyn (1964) makes use of moderate to strong sulphuric acid solutions in the direct acid dissolution of synthetic zinc sulphide. The only form of sulphur resulting from this dissolution is hydrogen sulphide. The production of hydrogen sulphide by the non-oxidative decomposition of sphalerite in strong acid solutions is one of the routes available for the dissolution of this sulphide mineral, as discussed in thermodynamic terms in Section 2.3.5. The Eh-pH diagram of Figure 6 shows the maximum Zn^{2+} concentration obtainable in the leach liquor (Line 31) for a given acid strength or pH. The other two studies, Dewing and Cochran (1978) and Dewing, et al (1982) which employ only sulphuric acid as a reagent, use the acid in concentrated form at elevated temperatures. Sulphuric acid, under these conditions can act as an oxidizing agent. Consequently, the form of sulphur reported as a reaction product in these two studies is elemental sulphur.

The following nine studies presented in Table 15 make use of hydrochloric or sulphuric acid with an additional oxidizing agent, most commonly ferric ion. All of these studies report elemental sulphur as the resulting sulphur product. Again the Eh-pH diagram in Figure 6 illustrates this zinc sulphide decomposition path as described in Section 2.3.5. Under acid and oxidizing conditions, Figure 6 shows that sphalerite can be oxidized to form Zn^{2+} ion and elemental sulphur. The two studies by Scott and Nicol (1978) and Verbaan (1980) both report hydrogen sulphide as a decomposition product along with the elemental sulphur. This demonstrates that the dissolution reaction mechanism

can be composed of a non-oxidative acid dissolution reaction to yield hydrogen sulphide followed by oxidation of the hydrogen sulphide to elemental sulphur by reaction with the oxidizing agent.

Recently, much interest has been placed in the use of sulphuric acid-gaseous oxidant reagent systems in autoclave reactors at elevated temperatures and pressures. Ten of the major studies in this area are presented in Table 15, the majority employing oxygen as the oxidant. As Table 15 shows, all of these studies report elemental sulphur or sulphate as the primary product of sulphide decomposition. The production of either elemental sulphur or sulphate, depending upon the particular leaching conditions, is shown in the Eh-pH diagram of Figure 6. The leaching conditions and reactions predicted on a thermodynamic basis are discussed in Section 2.3.5.

The intense research effort into the direct leaching of zinc sulphide over the past 30 years, as summarized in Table 15, has led to the development of only one commerical application of these leaching systems. Recently, the sulphuric acid-oxygen direct pressure leaching process (Sherritt Gordon Process) has been put into practice at the Cominco plant in Trail, B.C. This autoclave process treats zinc concentrates in H_2SO_4/O_2 solutions at a temperature of 150°C and an oxygen pressure of 350 to 1000 kPa. Despite the high capital cost of an autoclave process and the difficulty of iron removal for zinc electrowinning, this process appears to be economically feasible for the treatment of zinc concentrates as reported by Veltman and Bolton (1980).

4.2 REVIEW OF ZINC SULPHIDE LEACHING WITH AQUEOUS SULPHUR DIOXIDE

Sulphur dioxide gas is a highly attractive and readily available leaching reagent. If incorporated into

a direct sulphide leaching process, sulphur dioxide may eliminate the necessity of using high temperature and pressure autoclave equipment. A process operating at ambient temperatures and pressures would create great savings in the required capital investment compared to an autoclave process. The present research is intended to develop the basis for an atmospheric pressure leaching process employing sulphur dioxide as the principal chemical reagent.

A very limited number of studies have been carried out in the area of sulphur dioxide leaching of zinc sulphide. The reported studies are presented in Table 15. The earliest work applying the use of sulphur dioxide in the direct leaching of sulphides, Sobol and Frash (1974), demonstrates the potential use of sulphur dioxide in the pressure leaching of nickel containing pyrrhotite concentrates. Elemental sulphur and sulphate are reported to be the forms of sulphur resulting from the leaching reaction. The formation of thiosulphuric acid is theorized and a reaction mechanism is proposed based on the Wackenroder Reaction. Furthermore, the dissolution reaction is reported to display a "diffusion nature". A flowsheet is proposed for the production of elemental sulphur, iron products and a non-ferrous sulphide concentrate from this pyrrhotite concentrate.

Tiwari (1976) investigated the kinetics of oxidation of zinc sulphide and hydrogen sulphide by sulphur dioxide in aqueous sulphuric acid. Under the conditions of Tiwari's experiments, elemental sulphur is reported to be the form of sulphur resulting from both the oxidation of zinc sulphide and hydrogen sulphide. The stoichiometry of the overall dissolution reaction was found to be,

$$ZnS + 2H^+ + \tfrac{1}{2}SO_2(aq) = Zn^{2+} + 1\tfrac{1}{2}S^\circ + H_2O.$$

The dissolution, it was demonstrated, proceeds by a two step reaction process. Initially, the acid dissolution of zinc sulphide occurs to produce hydrogen sulphide

$$ZnS + 2H^+ = Zn^{2+} + H_2S(aq).$$

This is followed by the oxidation of hydrogen sulphide by sulphur dioxide to form elemental sulphur.

$$H_2S(aq) + \tfrac{1}{2}SO_2(aq) = 1\tfrac{1}{2}S^\circ + H_2O.$$

The initial rate of dissolution was found to be directly proportional to the hydrogen ion concentration. The elemental sulphur produced was shown, under the conditions of Tiwari's experiments, to form a tenacious film on the zinc sulphide particles. A kinetic model was developed for the leaching process on the basis that the film of sulphur impedes further reaction by creating a barrier on the zinc sulphide surface through which reactants and products must diffuse. The apparent activation energy of the dissolution was evaluated to be 49.0 kJ mol^{-1} below a sulphuric acid concentration of 0.45 mol dm^{-3} and 87.0 kJ mol^{-1} above an acid concentration of 3.0 mol dm^{-3}.

The investigation by Tiwari (1976) into the kinetics of hydrogen sulphide oxidation revealed that the reaction between hydrogen sulphide and sulphur dioxide does not occur in the gas phase at room temperature. However, it proceeds at a very high rate on a wetted surface with the production of a sulphur film. The rate of reaction is directly proportional to both the hydrogen sulphide and sulphur dioxide concentration. Furthermore, the oxidation rate reported was so great that the reaction between hydrogen sulphide and sulphur dioxide could not be considered as the rate controlling step of the zinc sulphide dissolution process.

More recently, Adams and Matthew (1981) made an investigation into the leaching of zinc sulphide concentrates with gaseous mixtures of sulphur dioxide and

oxygen at atmospheric pressure in aqueous solution. Elemental sulphur and sulphate are reported as reaction products. Since the sphalerite concentrates used in this experimentation inherently contain iron, the leaching media also contained both ferrous and ferric iron. Subsequently, the iron was found to catalyze the oxidation of sulphur dioxide by oxygen to produce sulphuric acid. The stoichiometry of the overall dissolution process was found in this study to be represented by the following reaction:

$$2ZnS + 3SO_2 + 2\tfrac{1}{2}O_2 + H_2O = 2ZnSO_4 + 2S^\circ + H_2SO_4$$

The authors proposed that the overall reaction was made up of two competing reactions for the consumption and production of sulphuric acid:

$$2ZnS + H_2SO_4 + SO_2 + 1\tfrac{1}{2}O_2 = 2ZnSO_4 + H_2O + 2S^\circ$$

and

$$2SO_2 + O_2 + 2H_2O = 2H_2SO_4.$$

These two reactions account for the initial consumption of acid followed by the generation of acid as observed by Adams and Matthew during their experiments.

Adams and Matthew (1981) found their experimental kinetic data to be chemical reaction controlled and to fit a kinetic model based on the reaction of a shrinking particle. No interference to the reaction by the formation of a sulphur film was found in this investigation. The activation energy for the dissolution process was estimated to be 154.5 ± 7.5 kJ mol^{-1} which is consistent with a chemically controlled surface reaction.

This review has summarized the state of the knowledge of the chemical leaching of zinc sulphide. Despite the considerable number of investigations made into the dissolution of zinc sulphide, few have studied the use of sulphur dioxide as a lixiviant. Furthermore, these studies present conflicting views on the

fundamental manner in which sulphur dioxide acts upon zinc sulphide. The thermodynamic data and discussion presented in Chapter Two of this work have laid the foundation for an understanding of the possible phases participating in the dissolution process. It remains then, to incorporate these thermodynamic ideas into an experimental study of the dissolution kinetics of the sulphur dioxide leaching process and develop a kinetic leaching model which will provide a basis for process design.

4.3 DISCUSSION OF KINETIC MODELS APPLICABLE TO ZINC SULPHIDE LEACHING

A number of descriptive kinetic models have been applied to zinc sulphide leaching. They include classical chemical reaction rate equations, descriptive physical rate models and models based on electrochemical dissolution mechanisms. Although a generalized electrochemical kinetic model for sulphides has been described by both Wadsworth (1981) and Hiskey and Wadsworth (1981) and the electrochemical nature of sulphide dissolution has been often suggested, no electrochemical models have been reported specifically for zinc sulphide dissolution. The models developed in leaching studies mainly consist of chemical reaction rate equations or physical models such as the shrinking core model.

The leaching of zinc sulphide in aqueous sulphurous acid consists of reacting finely ground particles, which generally can be approximated as spheres, with reagents dissolved in an aqueous medium. As the leaching reaction proceeds a residue or product layer, such as a film of elemental sulphur, may be deposited on the zinc sulphide particle surface. This residue layer, in effect, shields the particle from its aqueous environment. Since reactants and products must pass between the reacting

particle and the aqueous medium, the rate of the dissolution reaction may be hindered. Also, as dissolution proceeds, the unreacted core of the particle shrinks in size and the net reaction surface area decreases. This consequently affects the overall leaching rate. These physical effects have been mathematically analyzed for various ideal situations and are known collectively as the shrinking core model. The complete development of the shrinking core model has been well documented: Habashi (1969), Levenspiel (1974), and is summarized in Appendix 3.4 of this work.

Figure 26 illustrates the shrinking core model for the reaction of spherical particles and presents the resulting mathematical expressions. As Figure 26 shows, there are five steps occurring simultaneously in a dissolution process. These five steps are:

1. Diffusion of the dissolved reactant through the solution film surrounding the particle to the surface of the solid.

2. Diffusion of the reactant through the residue layer to the surface of the unreacted core.

3. Reaction of the solid with the leaching reagent at the reaction surface.

4. Diffusion of the reaction products through the residue back to the exterior surface of the solid.

5. Diffusion of the products through the solution film back into the bulk solution.

Any single step listed, could be the limiting factor in the overall rate of dissolution.

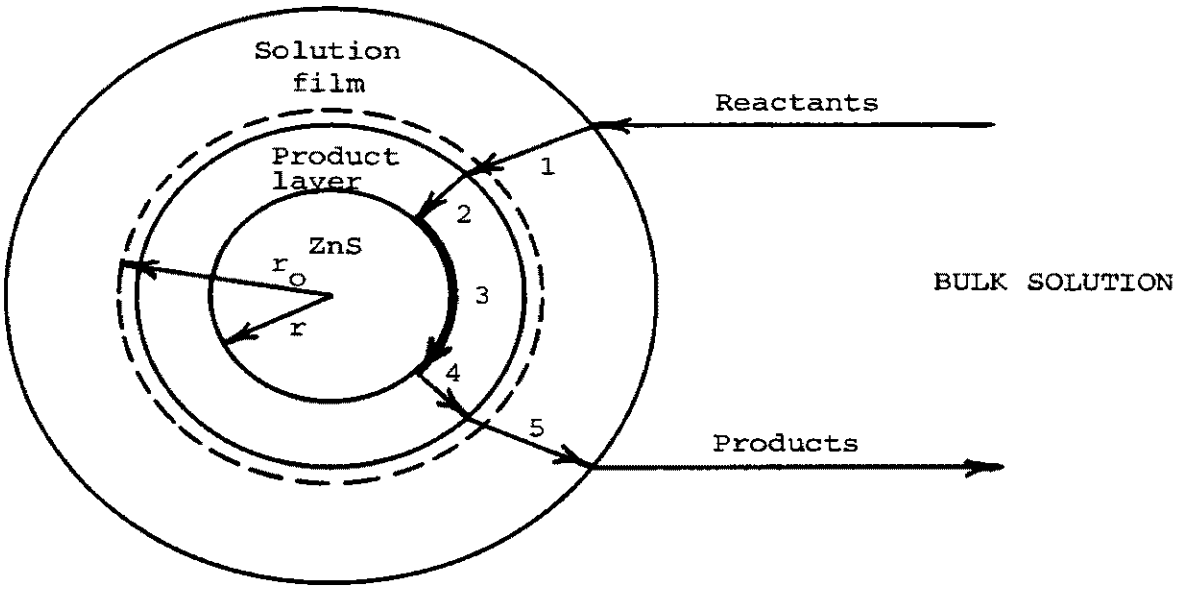

I Solution Film Diffusion Controls

(1) Constant Size Particle

$$\frac{3bk_dCt}{r_o\rho} = \alpha$$

(2) Shrinking Particle (no product layer, constant k_d)

$$\frac{bk_dCt}{r_o\rho} = 1 - (1-\alpha)^{\frac{1}{3}}$$

II Product Layer Diffusion Controls

(1) Jander's Approximation

$$\frac{2k't}{r_o^2} = [1-(1-\alpha)^{\frac{1}{3}}]^2$$

(2) General Solution of Crank, Ginstling and Brounshtein

$$\frac{2bDCt}{r_o^2\rho} = 1 - \frac{2}{3}\alpha - (1-\alpha)^{\frac{2}{3}}$$

III Dissolution Reaction Controls

$$\frac{bk_rCt}{r_o\rho} = 1-(1-\alpha)^{\frac{1}{3}}$$

FIGURE 26. Shrinking Core Model for Reaction of a Spherical Particle: after Habashi (1969).

Each equation derived for the shrinking core model relates the time (t) as a function of α, the fraction of material reacted at that time. The other symbols shown in Figure 26 are the initial particle radius (r_o), the molar density of the solid (ρ), a diffusion constant (k_d), a reaction rate constant (k_r), the diffusivity (D), a reactant concentration (C) and a stoichiometry factor (b). A possible expression describing the rate limiting factor in the dissolution process is one of the equations in Figure 26. The rate controlling step is identified by finding whether the appropriate function of α yields a straight line when plotted against time for a given set of experimental data.

Figure 26 presents the equations for two different situations when overall rate of the dissolution process is limited by diffusion through the solution film. The first equation applies to the situation where a product layer forms as the reaction proceeds and the overall particle size remains constant. The second equation applies to the situation where no product layer is formed and the particle decreases in size as the reaction proceeds. This second situation is also known as the shrinking particle model.

Two different expressions are presented in Figure 26 for product layer diffusion being the rate limiting step. The first is an approximate solution derived by Jander (1927) [Habashi (1969)p.154]. This expression was derived for a thin film on a flat reaction surface and applies only when the product layer is very thin compared to the particle radius. The second expression is a general solution developed by Crank (1957), Ginstling and Brounshtein (1950) [Habashi (1969)p.156] and applies to all situations when the change in volume of the particle during the reaction is small. The final equation in Figure 26 is derived for the situation where the rate of the chemical reaction, occurring at the surface of the unreacted core, controls the kinetics of the dissolution

process. A first-order chemical reaction is assumed in the derivation of this expression.

Industrial leaching of finely ground mineral concentrates generally takes place in closed stirred tanks with moderate agitation. If care is taken to design an efficient gas dispersion system and if sufficient agitation is supplied, the adverse effects of solution diffusion can be kept to a minimum. In laboratory situations practically any degree of agitation can be achieved and the effect of solution diffusion can be eliminated. Generally then, there are two limiting factors of a leaching process that have been considered in the development of kinetic models, product layer diffusion and the rate of the dissolution reaction.

4.3.1 Reported Kinetic Leaching Models

A number of investigations into the kinetics of zinc sulphide leaching have attempted to develop or actually report a kinetic model which describes the rate of dissolution. Generally, the dissolution kinetics have been described as being sulphur layer diffusion controlled or reaction rate controlled. The shrinking core model, in several instances, has been used to correlate experimental data. However, a few studies report a chemical reaction rate equation which correlates the data. Such rate equations provide a more exact description of the rate controlling reaction than the shrinking core model which assumes a first-order irreversible reaction.

Although no mathematical models were developed, Pawlek (1969) summarized some valuable kinetic interpretations derived from his work on the pressure leaching of zinc sulphide. Four important parameters in pressure leaching were identified as follows: (1) the efficient dispersion of gases; (2) the suspension of the solid; (3) the phase-boundary reaction, and (4) the removal of

reaction products. The phase-boundary reaction was investigated and an electrochemical model was proposed in which zinc sulphide reacts anodically according to the reaction:

$$ZnS = Zn^{2+} + S^{\circ} + 2e^{-}.$$

The cathodic reduction of chemisorbed oxygen, the presence of which may increase the number of charge carriers within the zinc sulphide owing to its semi-conductor properties, occurs by the reaction:

$$2H^{+} + \tfrac{1}{2}O_2 + 2e^{-} = H_2O.$$

This semi-conductor model was tested by introducing ultraviolet radiation into the system which, in the case of doped ZnS, showed an appreciable increase in the rate of dissolution. The overall kinetics were not explained on the basis of electronic conduction alone, indicating that other rate processes were involved.

The initial dissolution of zinc sulphide was found to result in the formation of hydrogen sulphide. A build up of hydrogen sulphide severely retards the kinetics of dissolution. The following are proposed reactions for the oxidation of hydrogen sulphide:

$$H_2S + H_2SO_4 = H_2SO_3 + H_2O + S^{\circ}$$

$$2H_2S + O_2 = 2S^{\circ} + 2H_2O$$

$$H_2S + 2O_2 = SO_4^{2-} + 2H^{+}$$

The first reaction occurs only in very high strength acid solutions and the third reaction is favourable only at high temperatures. The second reaction occurs only very slowly and the problem is to accelerate it. The addition of activated carbon was found to accelerate the kinetics of dissolution of several sulphides. This was attributed to an acceleration of the second reaction removing hydrogen sulphide at an increased rate, thus limiting the

back-reaction kinetics.

Earlier, Romankiw and de Bruyn (1964) investigated the kinetics of dissolution of zinc sulphide in aqueous sulphuric acid. The kinetics were found to be chemical reaction controlled where the decomposition of synthetic zinc sulphide proceeds by the reaction:

$$ZnS + 2H^{+} = Zn^{2+} + H_2S.$$

If sufficient agitation is used to eliminate diffusion effects, the overall dissolution rate may be expressed by the relation:

$$\frac{d[Zn^{2+}]}{dt} = A_o(k_f[H^{+}] - k_r[Zn^{2+}]^{\frac{1}{2}} P_{H_2S}^{\frac{1}{2}}) \qquad (35)$$

where A_o is the initial surface area of the zinc sulphide, k_f is the forward reaction rate constant and k_r is the reverse reaction rate constant. An activation energy of 46.4 ± 4.1 kJ mol^{-1} was determined for the dissolution reaction and of 7.8 ± 4.1 kJ mol^{-1} for the reverse reaction.

Verhulst (1974) investigated the kinetics of oxidation of hydrogen sulphide and zinc sulphide by ferric iron in sulphuric acid solution. Like Romankiw and de Bruyn (1964), Verhulst found the dissolution kinetics to be chemical reaction controlled. Moreover, the rate of acid dissolution of zinc sulphide was found to be represented by the same rate equation proposed by Romankiw and de Bruyn (1964). However, the measured rate was more closely proportional to the square root of the surface area ($A_o^{\frac{1}{2}}$) rather than the first power proposed by Romankiw and de Bruyn (1964). A mechanism for the acid dissolution of zinc sulphide in the presence of ferric iron was proposed. This mechanism involved the acid dissolution of zinc sulphide to produce hydrogen sulphide followed by the reaction of hydrogen sulphide with ferric iron.

Scott and Nicol (1978) studied the kinetics of leaching of zinc sulphide concentrates in acidic solutions containing ferric sulphate. This study showed that the nature of the sphalerite significantly influences both the rate of dissolution and the effect of solution variables (Fe^{3+} and H_2SO_4 concentration) on the kinetic behaviour. The authors concluded that it was not possible for a single general mechanism to be derived for the dissolution reaction that could be expected to apply to any given concentrate. However, they proposed that both non-oxidative and oxidative processes were operative in the leaching system.

Verbaan (1980) followed up the work of Scott and Nicol (1978) in a study on the leaching of sphalerite in acidic ferric sulphate media in the absence of elemental oxygen. Verbaan found a close correlation between the rate of leaching of the sphalerite and the measured electrochemical potential of the solution (Eh). This was regarded as evidence that the leaching mechanism was electrochemical in nature. An empirical relation was developed from the experimental kinetic data to describe the rate of dissolution of sphalerite. The empirical relation is:

$$\frac{d[Zn^{2+}]}{dt} = 49.29 \exp\left(\frac{-57.64 \times 10^6}{RT}\right) [M_o A_o (1-X_{Zn^{2+}})^{2/3}] \frac{[Fe^{3+}]^{0.4}}{[Fe^{2+}]^{0.25}}$$

where M_o and A_o are the initial mass of sphalerite and the specific surface area respectively and $X_{Zn^{2+}}$ is the fraction of zinc in solution.

Venkataswamy and Khangonkar (1981) studied the ferric chloride leaching of sphalerite in the presence of an organic solvent for sulphur. Their objective was to ascertain whether the dissolution kinetics were reaction controlled or product layer diffusion controlled. The experimental kinetic data, obtained in both the presence and absence of the organic solvent, was analyzed in terms

of the shrinking core model. Since the organic solvent should remove a sulphur product layer, it was expected that in the presence of the solvent, the kinetics should be chemical reaction controlled. On the other hand, without solvent, the diffusion through the product layer should control the kinetics. Both sets of data showed a high degree of correlation with both the chemical reaction control equation and the product layer diffusion control equation. Hence, no definitive choice of mechanism could be made on the basis of this result. The shrinking core model is valid only for a narrow range of particle size. The diameter ratio of the upper and lower limits must not exceed $2^{\frac{1}{2}}$. This study was performed with a -200 mesh concentrate, the size range of which exceeded the limit. The authors suggested that this large particle size range may account for the ambiguous result.

Roth, et al (1981) also investigated the kinetics of zinc sulphide dissolution in ferric chloride media. Like Venkataswamy and Khangonkar (1981), Roth, et al found a close correlation of the experimental kinetic data with the product layer diffusion control equation of the shrinking core model. Roth, et al, however, did not comment on the correlation of their data with the reaction control equation. It was proposed that a film of elemental sulphur was formed on the zinc sulphide during its dissolution with ferric chloride. Inward diffusion of the ferric ion through this layer was suggested by the authors to be the rate controlling step. No justification was given for this proposed mechanism. The activation energy of the dissolution process was found to be 90.0 ± 12.5 kJ mol^{-1}.

Mizoguchi and Habashi (1983) studied the aqueous oxidation of zinc sulphide and pyrite by oxygen in hydrochloric acid solutions. Hydrogen sulphide was found to be generated in the absence of oxygen. However, with the introduction of oxygen, elemental sulphur was formed.

The proposed oxidation reaction is

$$ZnS + 2H^+ + \tfrac{1}{2}O_2 = Zn^{2+} + S^\circ + H_2O$$

for which an activation energy of about 25 kJ mol^{-1} was found. Due to this low activation energy and a dependence of the reaction on the stirring speed, the authors proposed that the oxidation reaction was diffusion controlled. The addition of pyrite to the reaction increased the oxidation rate of the zinc sulphide. The authors suggested that this was due to a galvanic action in which pyrite acted as a cathode where oxygen was reduced and zinc sulphide acted as an anode.

4.3.2 Models Applied to Sulphur Dioxide Leaching

Tiwari (1976), in his study on the kinetics of oxidation of zinc sulphide and hydrogen sulphide by sulphur dioxide in aqueous sulphuric acid, used Jander's approximate solution for product layer diffusion control to correlate his experimental results. Tiwari proposed that the dissolution and oxidation of zinc sulphide by sulphur dioxide in aqueous sulphuric acid proceeds by the following reactions:

$$ZnS + 2H^+ = Zn^{2+} + H_2S$$

$$H_2S + \tfrac{1}{2}SO_2 = \tfrac{3}{2}S^\circ + H_2O$$

The acid dissolution of the zinc sulphide in the first reaction produces hydrogen sulphide which is rapidly oxidized by sulphur dioxide in the second reaction. Elemental sulphur, subsequently, is deposited on the particle surface creating a diffusion barrier. Tiwari justifies applying Jander's approximation to the correlation of his kinetic data by stating that most of his experiments involved less than 25 percent dissolution of the zinc sulphide, which resulted in less than 10 percent reduction in the size of the zinc sulphide

particles. In other words, Tiwari implied that the thickness of the sulphur film was small in comparison with the size of the particles, as was required by the Jander approximation. However, Tiwari showed that Jander's approximation provided a better fit to the experimental data than the more rigorous model of Crank, Ginstling and Brounshtien when more than 50 percent of the zinc sulphide was dissolved. It is inconsistent with the assumptions made, to apply the Jander approximation to the results at this degree of dissolution. An adherent sulphur film at this point could no longer be thin compared to the radius of the unreacted core. Above 50 percent dissolution the sulphur would no longer resemble a thin film on a flat reaction surface which is the initial assumption of the Jander approximation. Therefore, it is difficult to conclude that Tiwari's kinetic data validates a product layer diffusion controlled dissolution process.

Adams and Matthew (1981), in their study on the leaching of zinc sulphide concentrates with sulphur dioxide/oxygen mixtures at atmospheric pressure, also found elemental sulphur to adhere to the zinc sulphide particles. However, in contrast to the work of Tiwari (1976), much evidence was presented by these authors which demonstrates that the presence of the elemental sulphur does not hinder the dissolution process. A scanning electron microscope photograph was presented clearly showing the deposited sulphur layer on partially leached zinc sulphide particles. The sulphur deposit shown had a porous, nodular structure that did not form a cohesive layer and should not present a significant barrier to diffusion of dissolved reactants or products. Partially leached solids, in another reported test, were withdrawn from the reaction vessel at a point when no further leaching was occurring. The elemental sulphur was removed from the solids by carbon disulfide extraction and the sulphur-free solids were then subjected to

further treatment. The results indicated that removal of the elemental sulphur did not lead to any further significant attack on the partially-leached solids. The experimental kinetic data presented in this study showed a high degree of correlation with the chemical reaction control equation of the shrinking core model presented in Figure 26. These results supply further evidence that the rate of the dissolution reaction is the limiting step in this leaching process and not diffusion through a tenacious sulphur film.

Adams and Matthew also conducted a few experiments using an iron-free reagent grade zinc sulphide material. The reaction of the synthetic material was slow compared to that for the naturally occurring zinc sulphide concentrates which contain iron. Very little elemental sulphur was formed in the experiments with reagent grade zinc sulphide but the evolution of hydrogen sulphide was quite evident. The authors suggested that iron present in naturally occurring zinc sulphide concentrates has an activating effect in the dissolution reaction and proposed that ferric iron may act as an intermediate oxidant by the reaction

$$2Fe^{3+} + H_2S = 2Fe^{2+} + S^\circ + 2H^+.$$

However, in view of the adherence of elemental sulphur to the reacting particles, the authors added that the electrochemical formation of S° by the reaction

$$ZnS + 2Fe^{3+} = Zn^{2+} + S^\circ + 2Fe^{2+}$$

is probably the dominant reaction occurring. In either case, the authors suggested that these reactions may be an oversimplistic assessment of the real situation.

CHAPTER FIVE

EXPERIMENTAL STUDY OF THE LEACHING OF ZINC SULPHIDE WITH SULPHUR DIOXIDE

An experimental investigation was undertaken to explore the kinetics of dissolution of sphalerite in aqueous sulphurous acid media. As highlighted in the literature review of the preceeding chapter, a wide variety of zinc sulphide materials have been used in previous leaching studies. These materials include natural ores, commercial sphalerite concentrates, naturally occurring pure sphalerite and synthetically prepared zinc sulphide laboratory reagents. As reported, the nature and composition of these materials can greatly influence the rate and the manner of the dissolution process. Naturally occurring sphalerite intrinsically contains significant quantities of iron either in the form of non-liberated iron sulphides or substitutional impurity atoms. Since iron can have a major effect on leaching behavior, it was decided to use in this study a high purity synthetic sphalerite material. The use of an iron-free sphalerite is necessary to isolate and determine the role of iron in the dissolution process.

Synthetically prepared laboratory reagent grade zinc sulphide was obtained from several chemical suppliers including BDH Chemicals Ltd., England, Ajax Chemicals Ltd., Australia and Fisher Scientific Co., U.S.A. Since it was reported by Scott and Nicol (1978) that the structure of the zinc sulphide, as well as its composition, may influence the leaching behavior, an x-ray diffraction pattern was obtained for each material. This revealed the zinc sulphide supplied by each of the companies above to be composed entirely or almost entirely of wurtzite, the high temperature polymorph of sphalerite. It is interesting to note at this point that, the zinc sulphide

used by Tiwari (1976) in his leaching studies was a reagent grade material supplied by Fisher Scientific Co. and therefore, may have consisted mainly of wurtzite. Tiwari (1976) did not report on the structure of his zinc sulphide material.

A very high purity electronic grade zinc sulphide powder was obtained from Ventron GMBH. This material was shown by x-ray diffraction to be composed entirely of sphalerite. Also, no iron could be detected in the Ventron material by chemical analysis. Therefore, this zinc sulphide possessed the desired properties and was selected for use in the present experimental investigation. A specific surface area of 17.3 m^2g^{-1} was determined on this material by nitrogen adsorption according to the B.E.T. method. A particle size distribution for the Ventron sphalerite is presented in Appendix 4 along with the method of determination. The Ventron sphalerite used in the experimental work was a very fine, free flowing powder with approximately 90 percent of the mass lying in the size range of 2 to 6 μm.

Highlighted also in the literature review of the previous chapter is the importance of proper reactor design. Romankiw and de Bruyn (1964) state that sufficient agitation must be maintained to eliminate the effects of solution diffusion. Both Pawlek (1969) and Adams and Matthew (1981) point out the importance of efficient gas distribution in leaching systems employing gaseous reactants. Pawlek states that the solids must be well suspended so that the reaction can occur over the entire surface of the particles. Furthermore, he suggests that the gases must be well dispersed so that dissolution of the gas can occur over as great a surface area as possible. Adams and Matthew add, that in systems using more than one gas, the gases should be well mixed before entering the reactor and that it is important to achieve a small bubble size for efficient gas dissolution.

Sixty preliminary two hour leaching experiments were carried out in an all glass, one litre reactor with a paddle stirrer. Although this exercise was useful in developing the procedures and techniques to be used in the experimental work, it was found impossible to determine whether sufficient agitation and efficient gas dispersion were occurring. Due to the vibrations incurred in attempting to achieve high agitation in this leaching reactor, much glassware was broken. Additionally, no satisfactory sampling system could be devised without opening the reactor to the atmosphere. Therefore, a leaching reactor was designed and constructed to eliminate all these experimental difficulties and yield reliable test results. The design of this reactor system along with the entire experimental arrangement is presented in the following section.

5.1 EXPERIMENTAL APPARATUS

Figure 27 presents a schematic diagram of the experimental leaching apparatus used in this study. Specifications of the individual items of equipment, identified with a number in Figure 27, are given in Table 16. The stirrer drive system consisted of a 250 W electric motor coupled to a variable speed drive box. Power was transferred to the reactor impeller through a flexible drive shaft. The drive box was linked to the flexible shaft via a v-belt and pulley arrangement as shown. The drive system, in this manner, was capable of operating the reactor impeller at speeds of 0 to 1500 rpm. A tachometer directly coupled to the drive shaft was used to monitor the exact impeller speed. The 1.6 m long flexible drive shaft allowed the stirrer drive system to be mounted on the laboratory wall outside of the exhaust hood, away from the reactor and associated equipment. This layout minimized the motor vibrations and any electrical interference with the electronic equipment.

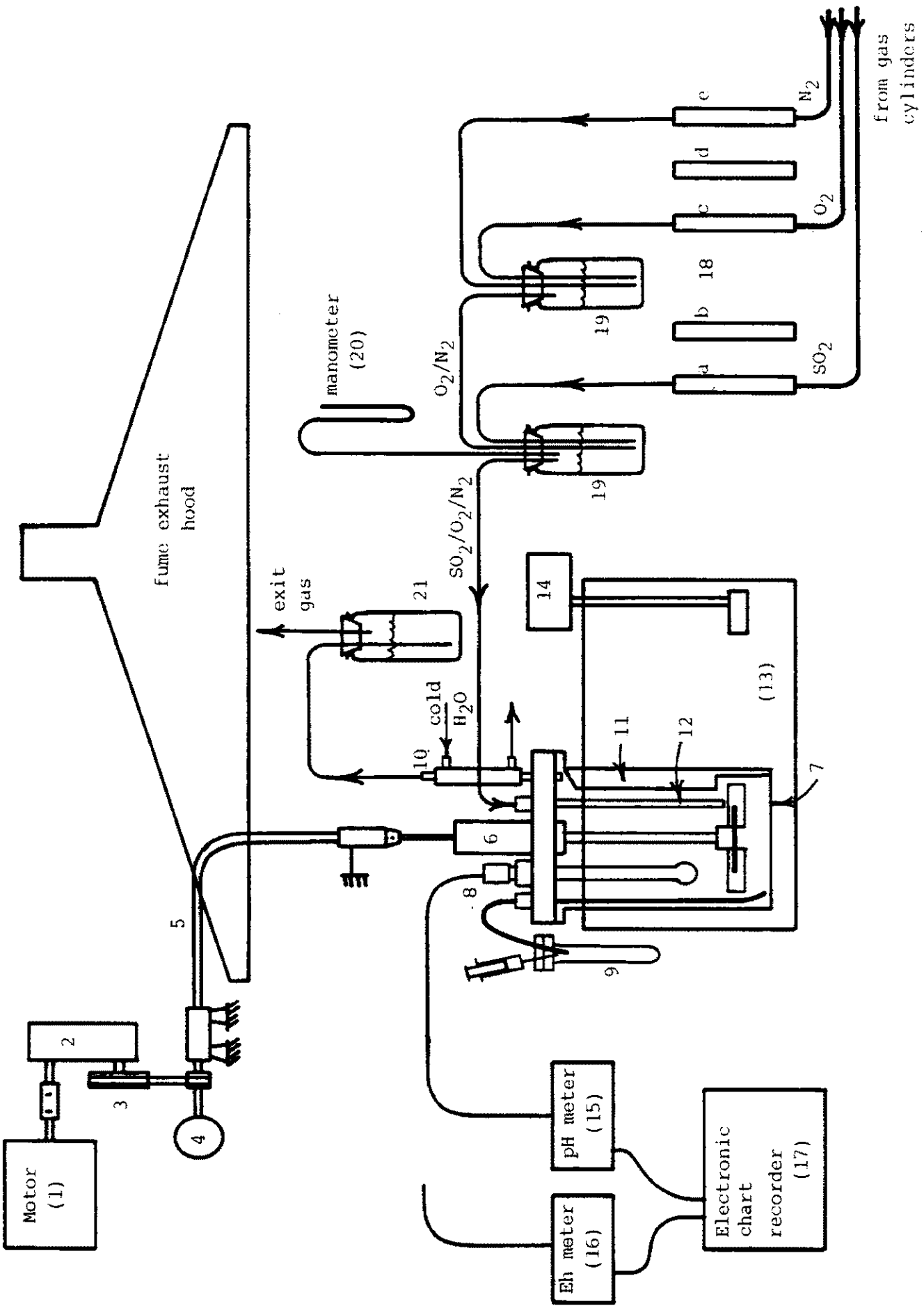

FIGURE 27. Schematic diagram of the experimental leaching apparatus.

TABLE 16

SPECIFICATIONS OF THE EXPERIMENTAL EQUIPMENT SHOWN IN FIGURE 27

NUMBER	DESCRIPTION
1	250W Electric Motor
2	Variable speed drive : ZERO-MAX model E-1
3	V-belt and drive pulleys, 76mm dia (drive box) to 20mm dia.
4	Tachometer: Auto Tempo Instrumentation Ltd., London
5	Flexible tool shaft: Flexdrive Pty.Ltd., Sydney
6	Reactor lid, bearing and impeller assembly
7	Reactor, Pyrex glass, 1.3 litre, cylindrical, flat bottom
8	pH probe: Phillips CH21 combination glass electrode
Not Shown	Eh probe: TPS Ionode, Brisbane, Ag/AgCl electrode
9	Sampling device with 100mm x 12mm test-tube
10	Condenser, exit gas stream, water cooled jacket
11	Baffle (1 of 4 shown only), TEFLON
12	Gas injection tube
13	Water bath
14	Water bath heater/stirrer: Braun Thermomix No.1441
15	pH meter: Orion Research model 611 digital pH/millivolt meter
16	Eh meter: Anax pH/millivolt meter
17	Chart recorder: Rikadenki Kogyo Model B-24
18	Flowmeters: Fischer and Porter 10A3237 Flowrator (a), (c), (e) flow tube: FP-$\frac{1}{8}$-20 with ruby float (b), (d) flow tube: FP-$\frac{1}{16}$-20 with ruby float
19	Inlet gas bubblers
20	Water filled open manometer
21	Exit gas bubbler
Not Shown	Thermometer (in reactor) 0-100°C glass/Hg
Not Shown	pH and Eh probe protection shrouds (see Fig.30)

Reagent gases were supplied to the reactor from commercial gas cylinders. Industrial grade sulphur dioxide and oxygen were used along with high purity, oxygen-free nitrogen. Flow rates of the individual gases were measured with calibrated rotameters. Specifications of these flowmeters are given in Table 16. The flow rates were controlled by adjusting the regulators on the gas cylinders and the needle valves on the rotameters. The wide range of gas flow rates employed in the experimentation required the calibration of two flowmeters for each gas as shown in Figure 27. Rotameters with FP-1/8-20 tubes and ruby floats were used to meter gas flow rates in the range of 100 to 1000 cm^3min^{-1}. Alternatively, if flow rates in the range of 15 to 150 cm^3min^{-1} were required, the gas lines could be switched to rotameters with FP-1/16-20 tubes and ruby floats. Hence, five calibrated flowmeters were required to regulate any desired combination of the three gases. All gas lines were Nylex 1/4 in. o.d. nylon pressure tubing and all gas connections were made with Swagelok stainless steel fittings.

The metered reagent gases were mixed and humidified in sealed bubbler jars filled with distilled water as shown. Oxygen and nitrogen were first mixed in one bubbler before being mixed with sulphur dioxide in a second bubbler. The mixed and humidified reagent gases were then injected into the reactor media through the gas injection tube as shown in Figure 27. A water filled, U-tube, open end manometer was connected to the second inlet gas bubbler to monitor the reactor back pressure. The manometer also acted as a safety relief valve should the reactor gas inlet or outlet become clogged. Unreacted and product gases were vented from the reactor via a water cooled condenser to minimize evaporative losses. The exit gas stream, after passing through the condenser, was vented to the exhaust hood as shown in Figure 27.

Figure 28 presents a detailed drawing of the reactor

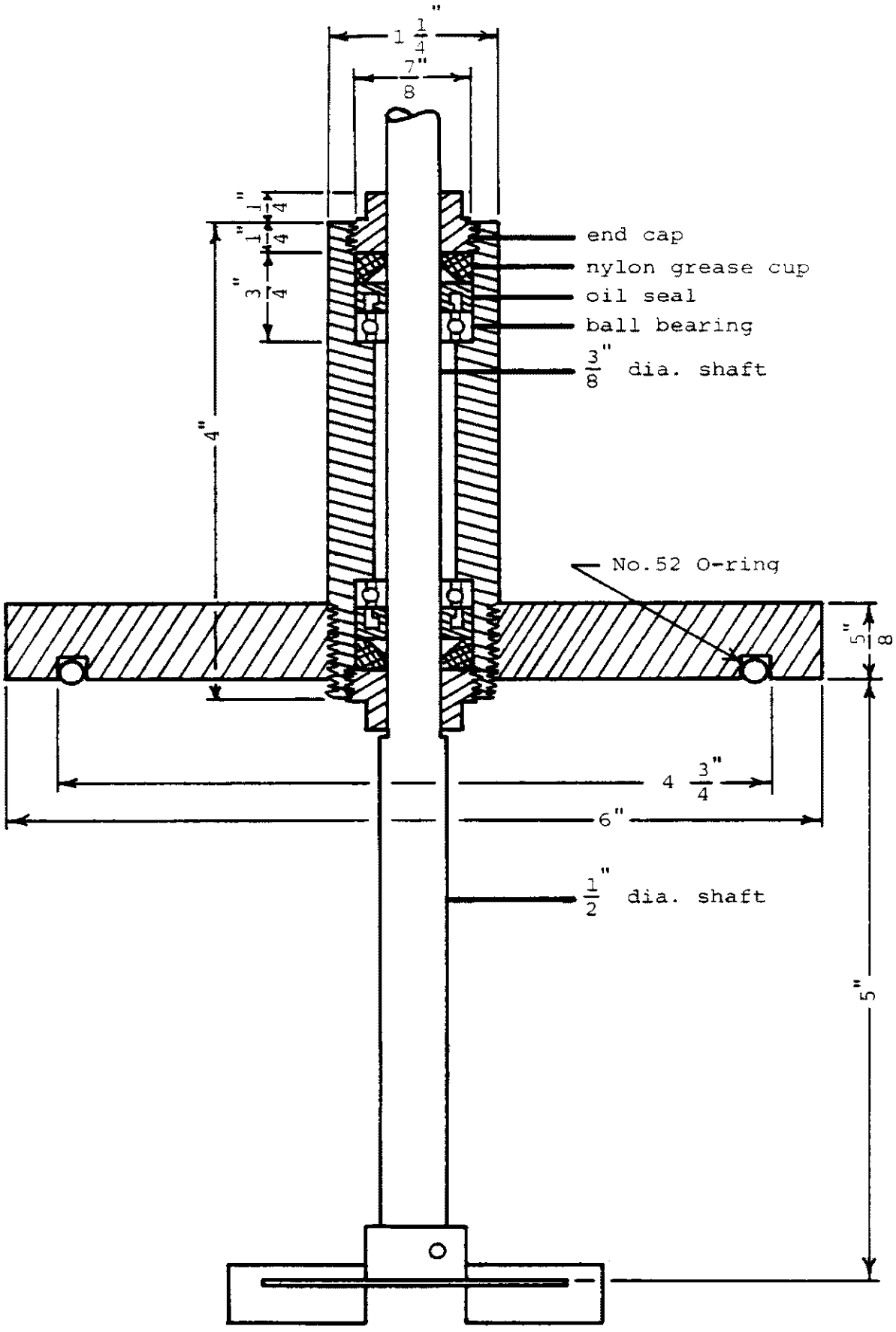

FIGURE 28. Reactor lid, bearing and impeller assembly.

lid, bearing housing and impeller assembly. All parts shown, except the bearings and seals, were fabricated from 316 stainless steel stock material. Special care was taken to ensure the bearing housing was completely sealed from the reactor contents as the leaching media could rapidly corrode the bearings. The inset rubber o-ring formed a seat between the reactor lid and the wide, ground glass lip of the reactor vessel. The reactor vessel itself, was a cylindrical, flat bottom pyrex glass vessel with a 1.3 dm^3 (litre) capacity. The lid assembly was held in place on the reactor vessel by four screw clamps. Several reactor access ports were provided in the lid. The layout of the access ports and their function are shown in Figure 29.

The three ports labelled (A) in Figure 29 were designed to accommodate glass electrodes. Two of these openings were used for the Eh and pH electrodes. The third electrode port, used for charging material to the reactor, was sealed during the experiments. The Eh and pH electrodes were fastened to the lid by a cap and protection shroud assembly which is illustrated in Figure 30. The electrode is inserted into the reactor through the central hole of the cap and shroud. As the cap is screwed tight, the rubber o-ring, compressed between the cap and shroud, grips the electrode and forms a gas tight seal. This same design principal was used to secure the thermometer to the reactor lid in port (D) shown in Figure 29. Unlike the electrodes, however, a shroud was not used to protect the thermometer.

The two reactor lid openings labelled (B) in Figure 29 were drilled and tapped to accept the NPT thread of a 3/8 in. Swagelok stainless steel tube to male pipe connector. One of these two openings, being a spare, was sealed off. The other opening held the exit gas stream condenser in the Swagelok fitting. The condenser consisted of a 25 cm length of 9.53 mm (3/8 in.) stainless steel

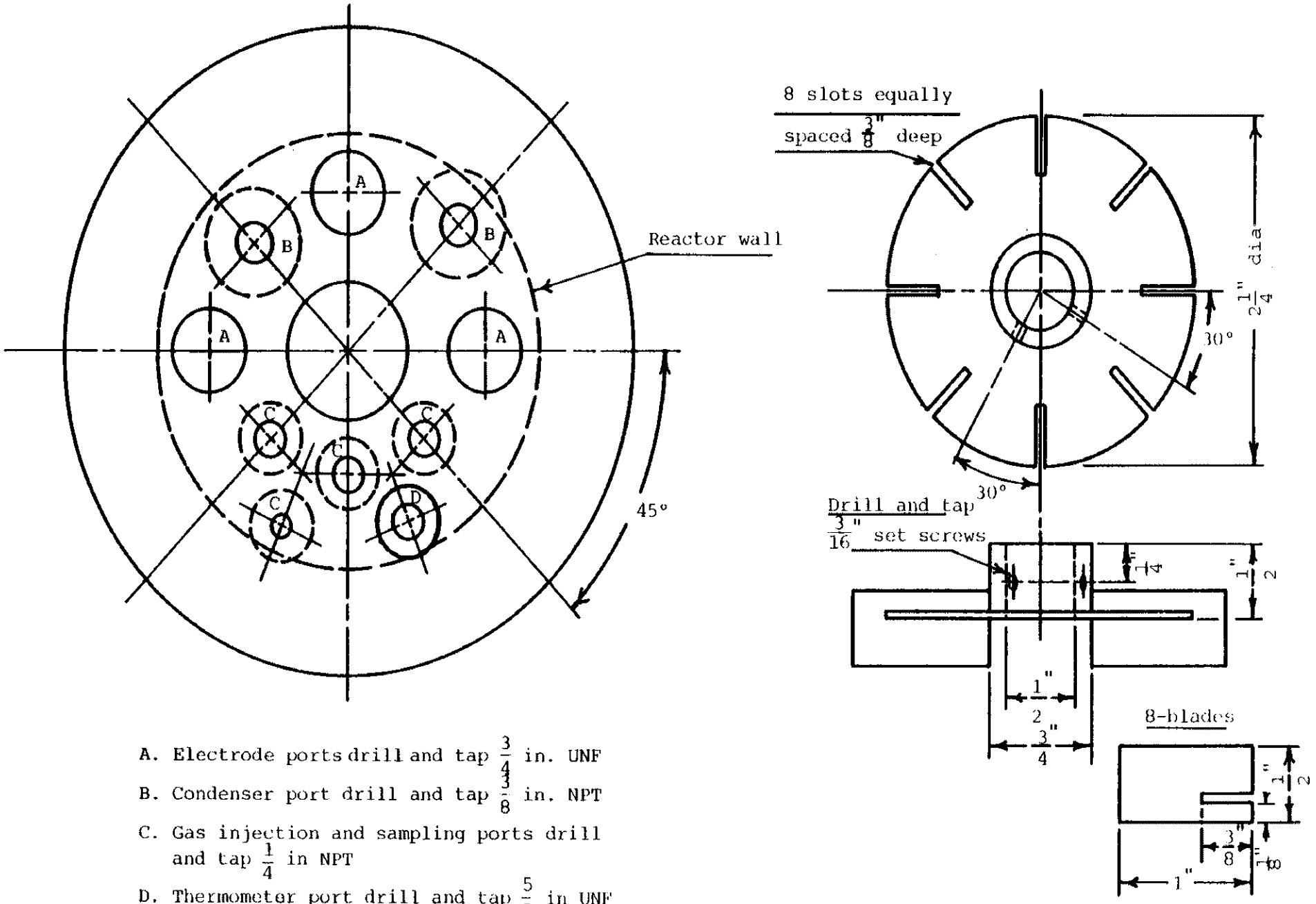

A. Electrode ports drill and tap $\frac{3}{4}$ in. UNF

B. Condenser port drill and tap $\frac{3}{8}$ in. NPT

C. Gas injection and sampling ports drill and tap $\frac{1}{4}$ in NPT

D. Thermometer port drill and tap $\frac{5}{8}$ in UNF

FIGURE 29. Reactor lid port configuration and turbine impeller.

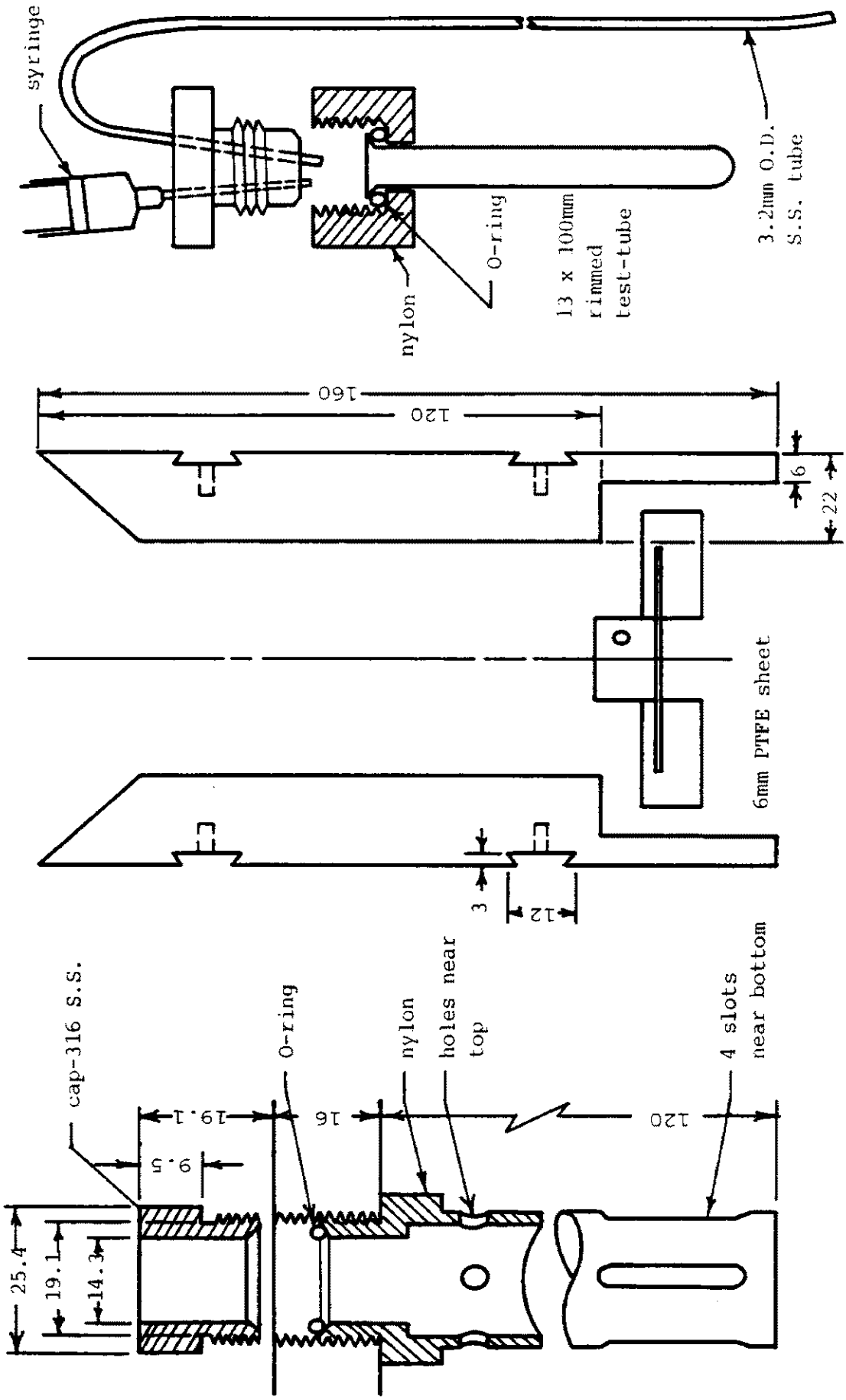

FIGURE 30. Electrode port and shroud assembly, baffle design and sampling device. All dimensions in mm.

tubing, through which the exit gas passed from the reactor, with a 15 cm long concentric shell of 19.05 mm (3/4 in.) tubing forming a water jacket. The exit gas stream condenser can be seen in the photograph of the reactor lid in Figure 31. Cooling water for the condenser was provided by a tap water service. The water was first circulated through a coil of copper tubing kept in a bucket of ice before entering the condenser.

The remaining four openings in the reactor lid labelled (C) in Figure 29, were made to accept 1/4 in. Swagelok tube to male NPT stainless steel connectors. The inside three openings were designed to accommodate gas injection tubes, whereas, the perimeter opening held the sample collection device. Since the reagent gases were fed to the reactor premixed, only one gas injection tube was required and the other two openings were plugged. The gas injection tube was fabricated from a 12.7 cm length of 6.35 mm (1/4 in.) stainless steel tubing butt welded to the NPT end of the Swagelok fitting. The fitting was then securely bolted to the reactor lid such that the stainless steel tube protruded into the reactor and the Nylex gas supply line could be connected to the Swagelok fitting outside the reactor. The gas injection tube can be seen in the reactor lid photograph in Figure 31. The lower end of the gas injection tube was crimped creating several outlet openings that were less than 0.5 mm in size. The length of the injection tube was such that the outlet end was 0.5 mm above the blades of the impeller. Consequently, the reactant gas was injected into the reactor media at a very small bubble size.

Figure 29 presents a detailed drawing of the eight blade turbine impeller used as the agitator. The blades and circular plate of the impeller unit were constructed from 16 gauge 316 stainless steel sheet. All of the various parts of the impeller unit were fastened together by swaging. This eliminated the need for stainless steel

welds which are susceptible to corrosion. The complete impeller assembly was fastened to the stirrer shaft with two titanium alloy set screws.

Figure 30 presents a drawing of the reactor baffles. The baffles were carefully designed to fit with the impeller inside the restricted space of the reactor. Four baffles were used equally spaced around the reactor. The baffles were cut from a 6 mm thick sheet of polytetrafluorethylene (PTFE or teflon). Two retaining strips, attached to the baffles by dovetail slots (Figure 30) and dowel pins, held the baffles tight to the reactor wall. The retaining strips were cut from a 3 mm thick PTFE sheet to a length which fit neatly around the inner circumference of the reactor wall. The baffle assembly could easily be snapped into or removed from the reactor as a single unit.

Figure 31 demonstrates the result of the efficient design of the leaching reactor. The high speed photograph shows the reactor charged with water operating under typical experimental conditions. It can be seen that the injected gas has a very small bubble size and is highly dispersed. This indicates that the reactant gases are dissolved, rapidly as possible, into the leaching media. Also, strong vertical circulation currents can be seen within the leaching media which are indicative of good solids suspension within the reactor pulp.

Figure 30 presents a drawing of the device used for extracting samples of the leach liquor from the reactor. This device was quick and simple in operation as was required by the high rate of sample collection. Also, this apparatus allowed samples to be collected without opening the reactor to the atmosphere. The sampling device consisted of a 3.18 mm (1/8 in.) stainless steel tube through which slurry samples were drawn from near the bottom of the reactor. As shown in Figure 30, the

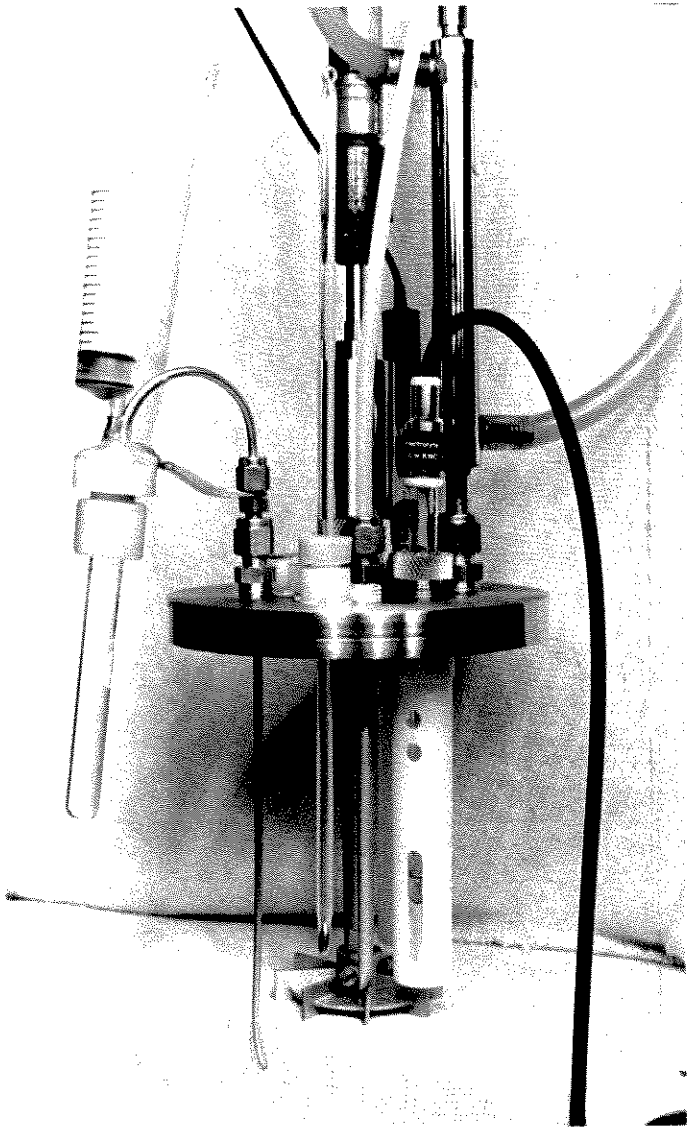

(a) Reactor lid and internal equipment

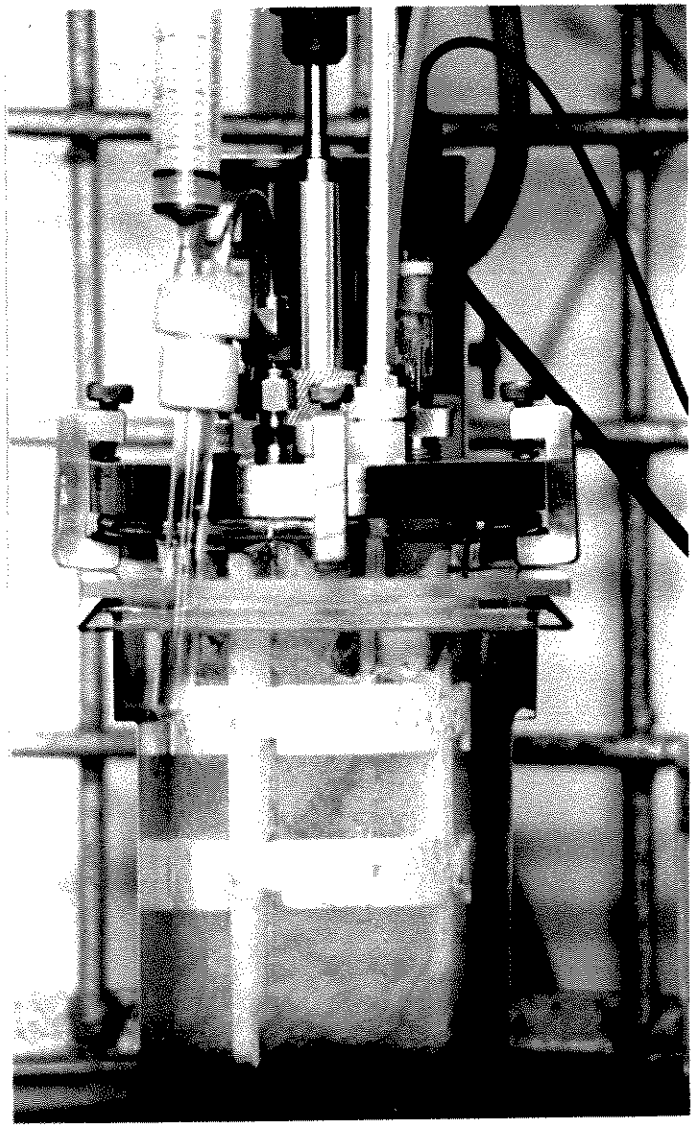

(b) Gas dispersion obtained in reactor

FIGURE 31 Experimental leaching reactor

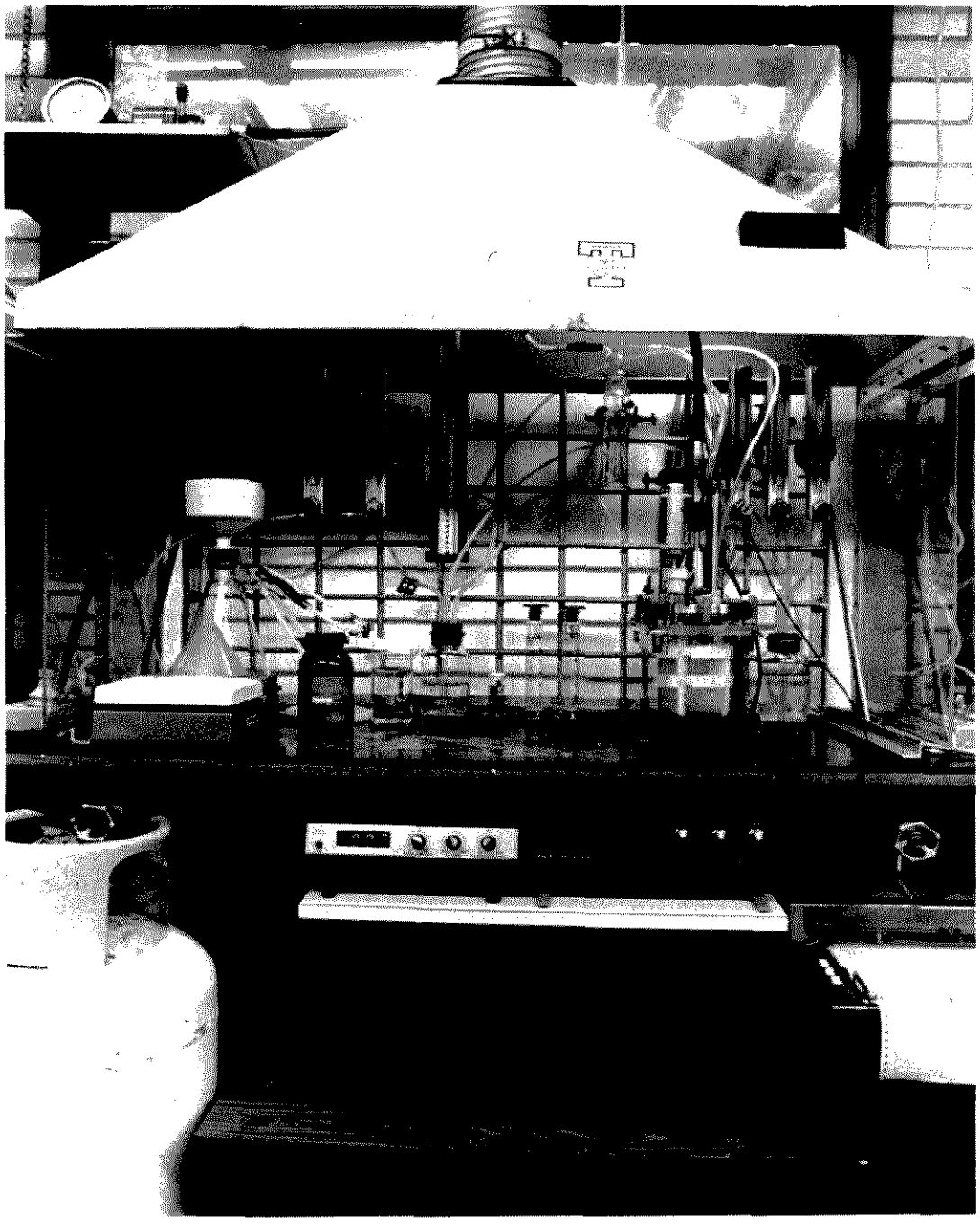

FIGURE 32 Experimental leaching apparatus

test-tube holder, machined from nylon bar stock, seals a test-tube to the end of the sampling tube when the holder is tightly closed. Slurry is then sucked into the test-tube as the plunger of the syringe is drawn back. The screw tight design of the nylon test-tube holder facilitates rapid changing of the test-tubes. Before drawing a sample, all slurry was purged from the sampling tube by injecting a small amount of air.

Figure 32 presents a photograph of the complete experimental set-up. The reactor was immersed in a water bath and kept at a constant temperature throughout an experimental run. The water bath and reactor were maintained at a preset temperature to within ±0.1°C by a thermostatically controlled heating and stirring unit. This unit can be seen behind the reactor in Figure 32. The Eh and pH of the leach medium were continuously monitored and recorded throughout an experimental run with the electronic equipment specified in Table 16. The Eh and pH meters along with the strip chart recorder can be seen in Figure 32. The entire experimental apparatus was set up under a fume exhaust hood to minimize the noxious effects of sulphur dioxide gas.

5.2 EXPERIMENTAL PROCEDURE

The experimental reactor and apparatus described in the previous section were used to perform a number of experiments on the dissolution of a fine sphalerite powder suspended in water with mixtures of sulphur dioxide, oxygen and nitrogen gases. Most of these experimental tests were two hours in duration. Twenty slurry samples were withdrawn from the reactor during each test and analyzed to obtain kinetic dissolution data. This section describes the procedures used to set up and carry out a typical two hour leaching experiment.

5.2.1 Starting a Leaching Test

The assembled reactor is placed in the constant temperature water bath and connected to the stirring motor and gas supply. The reactor is charged with 600.0 cm^3 of distilled, deionized water measured in a volumetric flask at room temperature. If sulphuric acid is to be added to the leaching test, the appropriate volume of an acid stock solution is first measured and added to the volumetric flask which is then made up to the mark with distilled, deionized water. The appropriate gas flow is then initiated and the bath heater and stirring motor are switched on. The Eh and pH electrodes are then calibrated and the strip chart recorder adjusted. The calibration methods for the Eh and pH electrodes are presented in Appendix 6. After the necessary adjustments have been completed, the electrodes are inserted into the reactor and the chart recorder is activated. Time is then allowed for the reactor temperature to attain the desired value and for both the Eh and pH to reach steady state values. Steady state is usually attained within 20 to 30 minutes. The Eh and pH of the leach liquor are noted at this time. If additional compounds such as ferric or ferrous sulphate are to be added to the experiment, the appropriate quantity of the sulphate salt is charged to the reactor at this time and the stopwatch is started. At the end of 15 minutes, the Eh and pH of the leaching medium are manually noted and a 4 cm^3 sample of liquor is withdrawn from the reactor for analysis of Fe^{2+} ion and total dissolved iron concentration. At this point, the measured weight of zinc sulphide powder to be leached is charged to the reactor through a funnel in the side port and the stopwatch is restarted. The remaining 100.0 cm^3 of water are added to the reactor through the funnel to wash any remaining solids into the reactor. The reactor is then quickly sealed and the sampling procedure is begun.

5.2.2 Slurry Sampling

Slurry samples for zinc ion analysis initially are withdrawn from the reactor at one minute intervals for the first six minutes. The sampling interval is then increased to two minutes and then five minutes through the first one-half hour of the run. Thereafter, samples are collected at 15 minute intervals for the duration of of the run. Before a sample is withdrawn, a small volume of air (approximately 1 cm^3) is injected into the reactor to purge all slurry from the sampling tube. The sample is then sucked into the test-tube through air displacement by drawing back the plunger of the syringe. The Eh and pH readings are manually noted and recorded as the sample is taken. The test-tube is then immediately placed in a centrifuge and spun for approximately 15 seconds. The solids free liquor is then decanted directly into a specimen tube for analysis. A 4 cm^3 sample is taken when only a zinc analysis is required. However, an 8 cm^3 sample is extracted when other analyses are desired.

5.2.3 Conclusion of an Experiment

At the conclusion of the run, all equipment is turned off and the gas flow is stopped. The reactor contents are filtered on a Watman no. 40 filter leaf and the filtrate is analyzed for H_2SO_4 and aqueous sulphur dioxide concentration. The filtered solids are washed with distilled water and allowed to air dry. The liquor samples collected are then diluted as appropriate and analysed for zinc ion concentration by atomic absorption spectrophotometry (AAS). All of the analytical methods used for quantitative determination of the concentrations of the various species in the leach liquor are described in detail in Appendix 5.

5.3 EXPERIMENTAL RESULTS

Following the completion of approximately sixty preliminary leaching tests, an experimental programme was undertaken to explore the factors controlling the kinetics of sphalerite dissolution in aqueous sulphurous acid. The preliminary tests were useful in developing the apparatus and procedures described in the previous sections, as well as, defining the basic experimental conditions and parameters to be investigated. As already noted, a high purity sphalerite powder manufactured by Ventron GMBH was used as feed material for the leaching studies. Two bulk samples of this material with different lot numbers were supplied by the manufacturer. Subsequently, twelve leaching tests (test nos. 62 through 73 inclusive) were initially conducted using lot no. 080581 with the remaining tests (test nos. 74 through 131) using lot no. 031220608. The only difference between these two samples was a slight shift of the particle size distribution. The lot no. 080581 sphalerite powder had a more coarse particle size distribution. A particle size distribution and an assay for each lot number is presented in Appendix 4. Consequently, the results of nine leaching tests (test nos. 62 through 70 inclusive) conducted using lot no. 080581 are reported in the results. Although these nine tests cannot be directly compared with the rest of the tests, independently they are informative and for this reason are presented with the results.

The experimental programme, as it is presented here, consists of several series of leaching tests. Each test was designed to investigate the effect of changing a particular leaching parameter or more closely define an observation from a previous experiment. The test series structure was adopted in order to most clearly present the experimental results. However, the way in which the programme was conducted did not correspond to this structure. It evolved naturally by the examination of the

data as it was gathered and the response of certain definitive experiments.

All of the leaching experiments were conducted in an identical manner as described in the previous section. Except where otherwise stated, the reactor in the basic two hour leaching test, was charged with 30.0 g of Ventron sphalerite powder and 700.0 cm^3 of purified water. Thus, a slurry density of 42.86 g dm^{-3} (kg m^{-3}) was used for the majority of the experiments. Likewise, the reactor temperature was maintained at 60 ± 0.1°C and the impeller speed was 800 rpm in most cases. A mixture of sulphur dioxide, oxygen and/or nitrogen gases were fed to the reactor at a total flowrate of 500. $cm^3 min^{-1}$. The composition of the reactant gas is reported in the results as a volume percentage of each gas in the feed mixture. For example, a gas mixture of 10 percent sulphur dioxide and 90 percent oxygen is denoted by 10% SO_2/O_2.

The results of the experimental testwork are presented in this section in tabular and graphical form. Each table summarizes a test series. The percent zinc extraction versus time data of each test in the series are plotted in the corresponding graph. Percent zinc extraction is defined here as the percent of the zinc available in the sphalerite dissolved into solution. The calculation of percent zinc extraction is described in detail along with a sample calculation in Appendix 3.3 Stated at the head of each table are the conditions used for each test in the series. Contained within the tables are the particular conditions of each test along with the zinc concentration in the leach liquor and the percent zinc extraction at both 30 minutes into the test and at the conclusion of each test (2 hours). Also, the concentrations of other components of the leach liquor, such as sulphurous and sulphuric acid, ferrous iron or tetrathionate ion, analyzed at the conclusion of each test are listed. A blank space in the tables indicates the analysis was not

performed for that test. A dash (-) given for an analysis in the tables denotes that no concentration was detected for that particular analysis. Finally, the right hand column of each table indicates whether elemental sulphur was precipitated within the bubbler on the reactor exit gas stream during a test or if the bubbler remained clear. The formation of elemental sulphur in the exit gas bubbler indicates that hydrogen sulphide was formed within the reactor and swept away by the flow of gas through the reactor during the test. The elemental sulphur is a product of the reaction between sulphur dioxide and hydrogen sulphide within the exit gas bubbler. A complete set of kinetic data for each leaching test is tabulated in Appendix 7.

The effect of the degree of agitation on the leaching kinetics was investigated. The impeller and stirring system was capable of being set at any speed between 0 and 1500 rpm (revolutions per minute). It was found, however, that below 200 rpm all of the solids were not suspended and the reactant gas did not appear to be well distributed. Above 900 to 1000 rpm, the agitation became so violent that some solids were expelled from the reactor through the exit gas condenser. Therefore, experiments were conducted varying the impeller speed from 300 rpm to 800 rpm. The tests were run with $SO_2/0_2$ gas mixtures both in the presence and absence of dissolved iron. The results are shown in Figure 33 and Figure 34 for leaching in the presence and absence of dissolved iron, respectively. The corresponding data is summarized in Table 17.

Figure 33 reveals that the kinetics of sphalerite dissolution with $SO_2/0_2$ mixtures in the absence of dissolved iron are independent of the impeller speed in the range of 300 to 800 rpm. However, Figure 34 shows that the dissolution kinetics are dependent on the stirring speed when the leaching is carried out in the presence of dissolved iron. Consequently, in an effort to

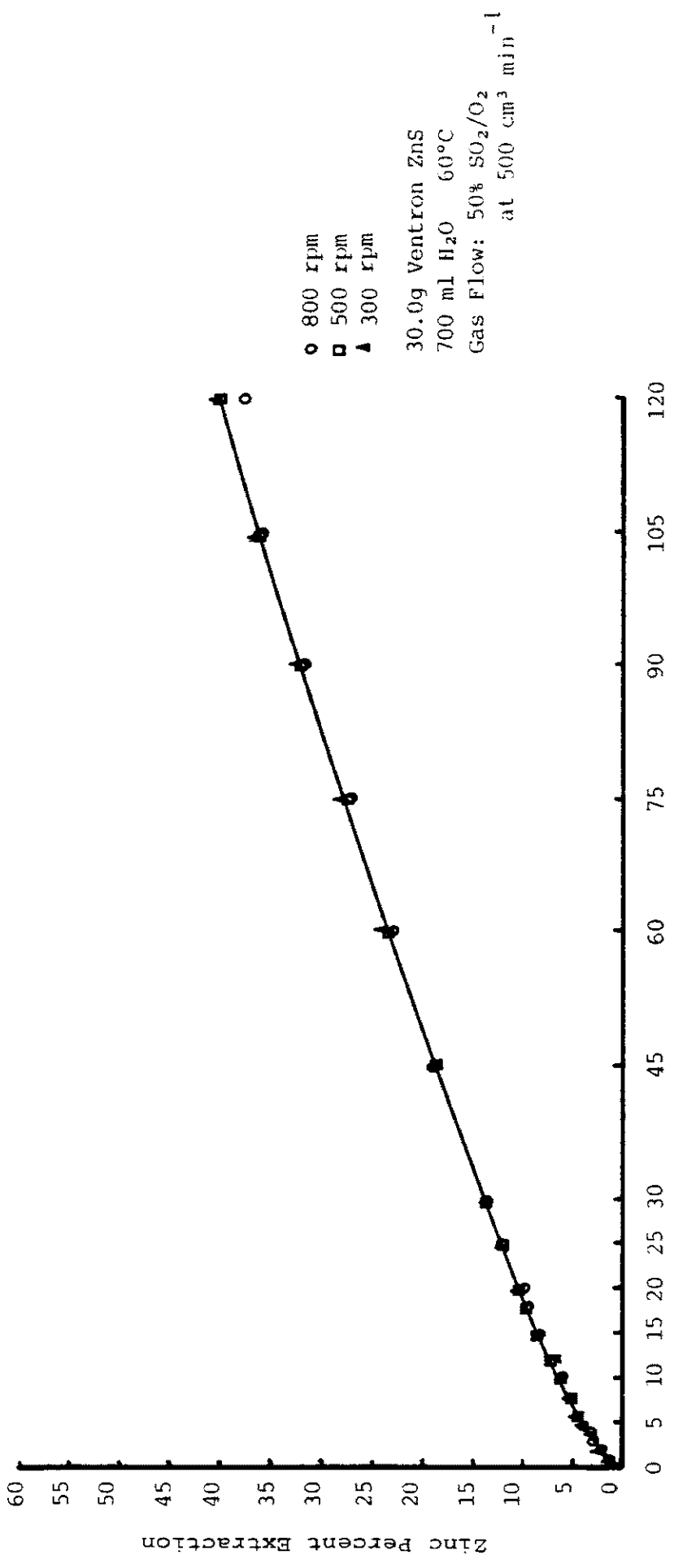

FIGURE 33. Effect of agitation on the kinetics of dissolution of sphalerite in aqueous media with SO_2/O_2 mixtures in absence of dissolved iron.

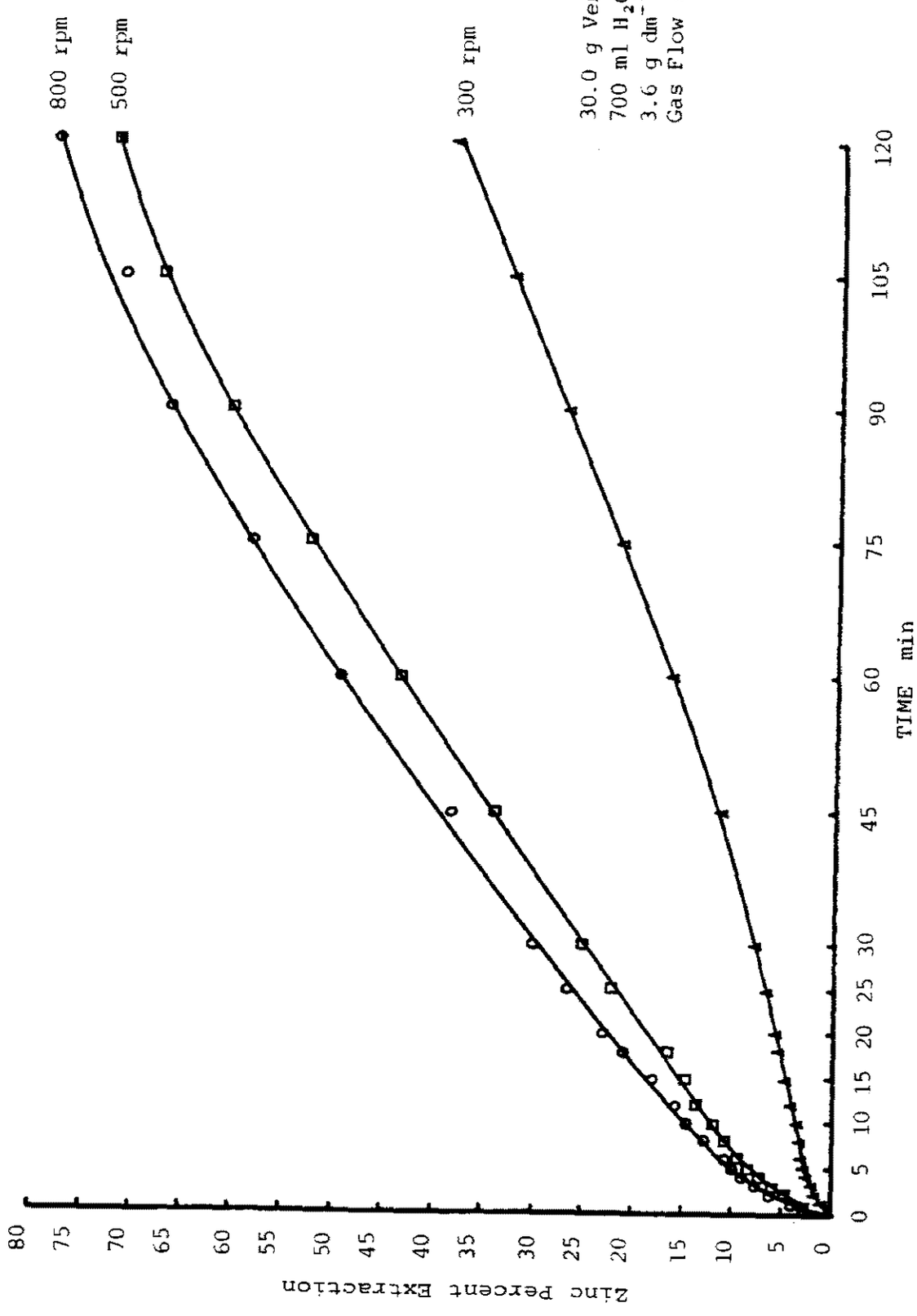

FIGURE 34 Effect of agitation on the kinetics of dissolution of sphalerite in aqueous media with SO_2/O_2 mixtures in presence of dissolved iron.

TABLE 17

VARIATION OF IMPELLER SPEED

Conditions: 30.0 g Ventron sphalerite, 60°C
gas flow = 500 $cm^3 min^{-1}$

TEST NO.	IMPELLER rpm	GAS COMPOSITION	Fe^{2+} Added g dm^{-3}	After 30 min.		After 2 hours leaching							
				Zn^{2+} g dm^{-3}	EXTN %	Zn^{2+} g dm^{-3}	EXTN %	Eh	pH	Fe^{2+} g dm^{-3}	H_2SO_4 g dm^{-3}	SO_2 mol dm^{-3}	EXIT GAS BUBBLER
90	300	50%SO_2/O_2	---	3.81	13.7	11.19	40.3	273	1.26	----	1.6	0.19	Clear
91	500	50%SO_2/O_2	---	3.94	14.2	11.12	40.1	268	1.18	----	0.9	0.18	Clear
74	800	50%SO_2/O_2	---	3.87	13.9	10.41	37.5	273	1.00	----	1.0		Clear
95	300	10%SO_2/O_2	3.6	2.16	7.7	10.71	38.3	615	1.14	3.13	27	0.005	S°
96	500	10%SO_2/O_2	3.6	7.03	25.2	20.10	72.0	728	1.66	0.36	36	----	S°
92	800	10%SO_2/O_2	3.6	8.39	30.1	21.78	78.0	732	0.90	0.53	36	----	S°

minimize the obvious diffusion limitations at low impeller speeds exhibited by the data of Figure 34, all experiments were conducted at an impeller speed of 800 rpm.

The effect of temperature on the dissolution kinetics was investigated in both the presence and absence of dissolved iron. Figure 35 and Figure 36 each present kinetic dissolution curves obtained at five temperatures in the range of 25°C to 90°C. Figure 35 shows that in media containing aqueous sulphur dioxide only, the rate of sphalerite dissolution increases slowly with temperature up to 60°C and then rapidly decreases at higher temperatures. The data corresponding to these experiments are summarized in Table 18. It must be noted here that these five experiments were conducted using the Ventron sphalerite from lot no. 080581 having a large particle size. Figure 36, on the other hand, shows the rate of dissolution to increase with temperature from 25°C to 90°C in tests conducted with SO_2/O_2 mixtures in the presence of dissolved iron. The data corresponding to Figure 36 are summarized in Table 19. Figures 35 and 36 thus demonstrate the reason for conducting all other experiments at a temperature of 60°C.

Table 20 summarizes a series of tests designed to elucidate the role of oxygen in the leaching of sphalerite with aqueous sulphurous acid in the absence of dissolved iron. Six tests were conducted using SO_2/O_2 and SO_2/N_2 mixtures where the partial pressure of sulphur dioxide in the mixtures was 0.50, 0.10 and 0.05 atm. One test was also run using pure sulphur dioxide for comparison. The resulting kinetic dissolution data is plotted in Figure 37.

Table 21 summarizes a similar series of tests designed to show the role of oxygen in the sulphurous acid leaching of sphalerite in the presence of iron. Ferric sulphate was added to the leach liquor at the start of each test to yield a dissolved iron concentration of

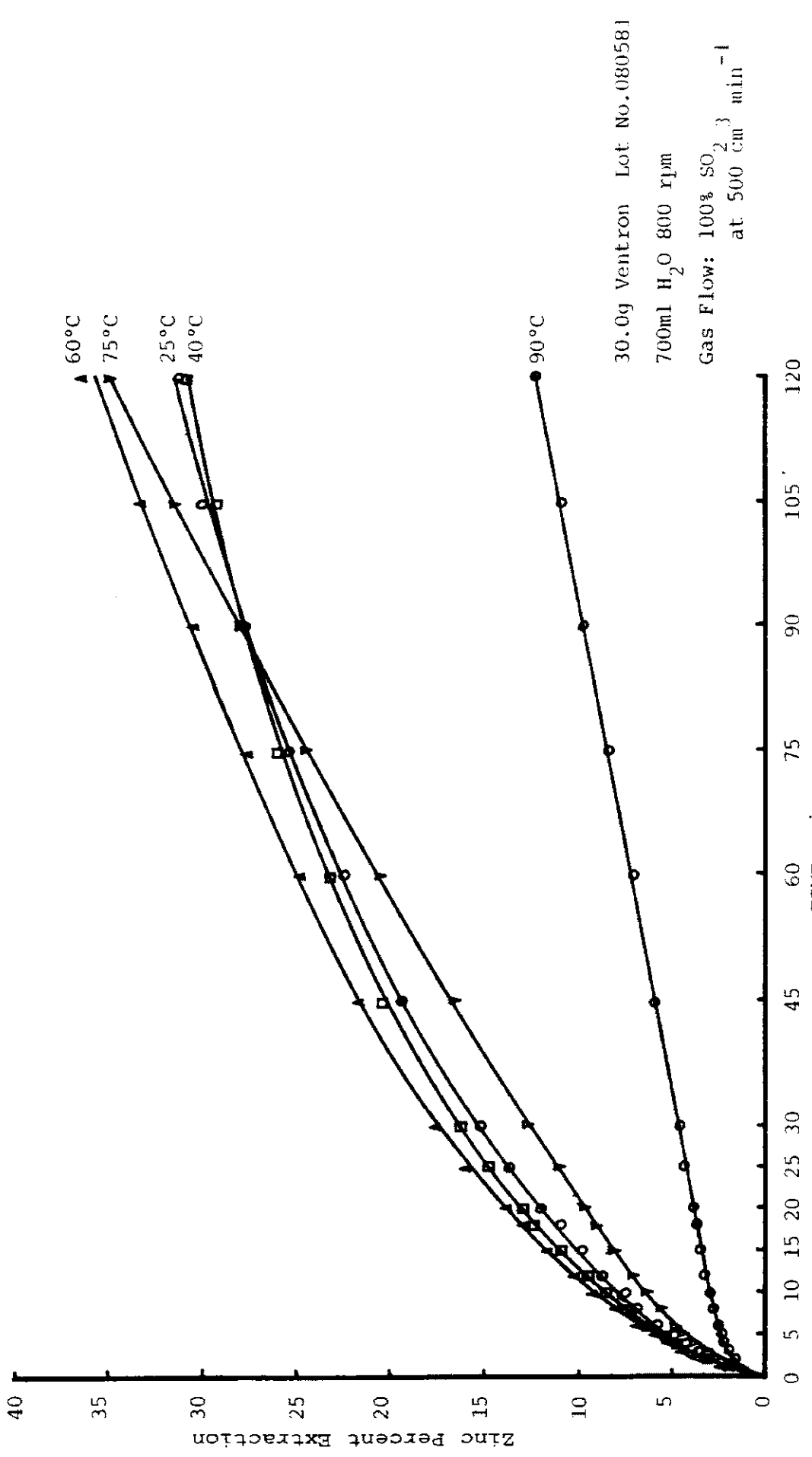

FIGURE 35. Effect of temperature on the kinetics of dissolution of sphalerite in aqueous sulphur dioxide media in absence of dissolved iron.

TABLE 18

VARIATION OF REACTOR TEMPERATURE

Conditions: 30.0g Ventron sphalerite lot no. 080581, 800 rpm
gas flow = 100% SO_2 at 500 cm^3 min^{-1}

		After 30 min.		AFTER 2 Hrs. LEACHING							
TEST NO.	TEMP. °C	Zn^{2+} g dm^{-3}	PERCENT EXTN.	Zn^{2+} g dm^{-3}	PERCENT EXTN.	Eh	pH	H_2SO_4 g dm^{-3}	$S_4O_6^{2-}$ g dm^{-3}	SO_2 mol dm^{-3}	EXIT GAS BUBBLER
64	25	4.21	15.2	8.62	31.1	287	0.90	0.2	11.8	0.96	Clear
65	40	4.53	16.3	8.52	30.7	258	1.02	0.3	20.0	0.99	Clear
68	60	4.89	17.6	10.05	36.2	222	0.74	1.8	29.7	0.35	Clear
66	75	3.52	12.7	9.65	34.8	231	1.11	2.0	26.8	0.19	Clear
67	90	1.94	7.0	3.39	12.2	213	0.93	2.3	9.1	0.076	Clear

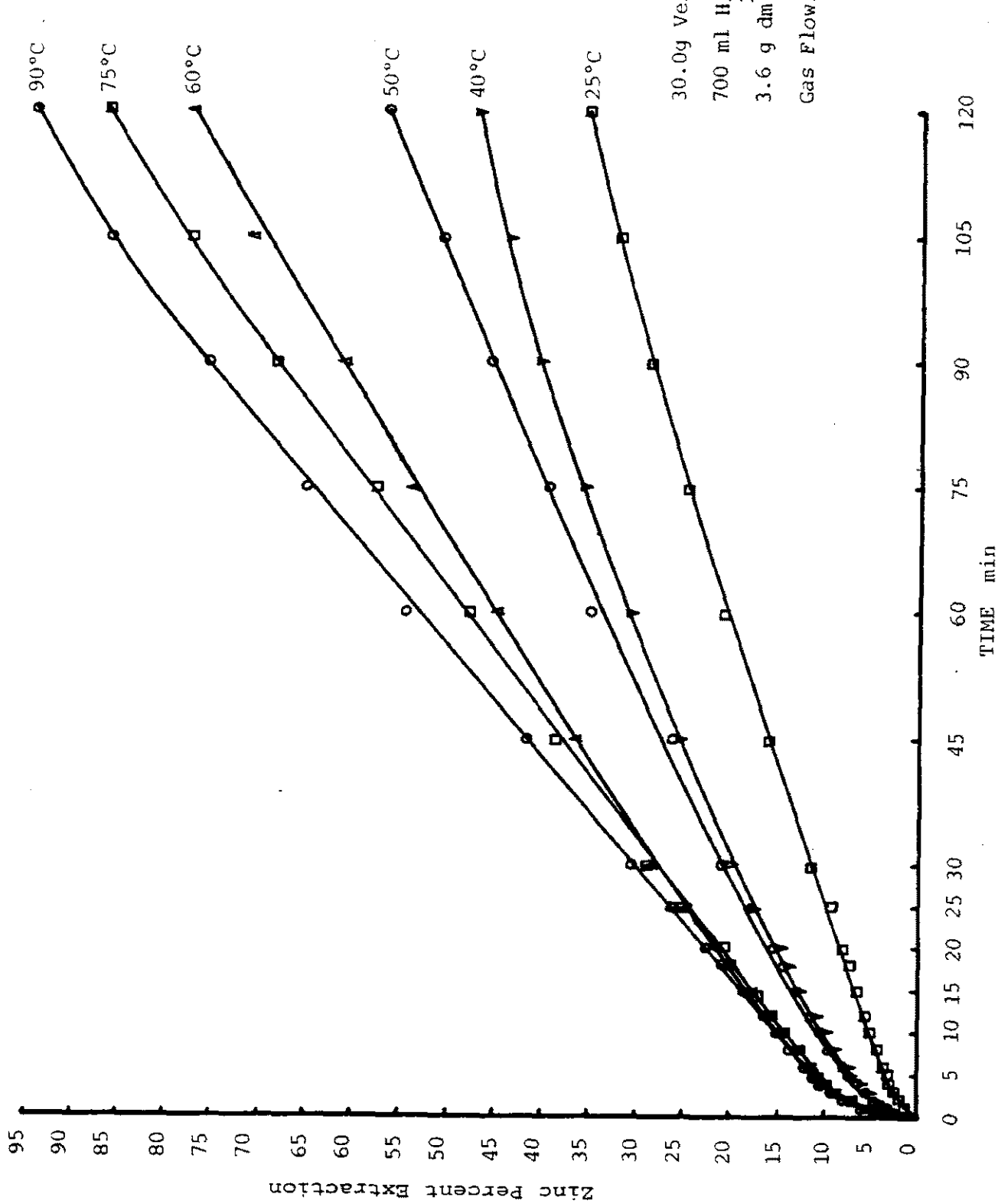

FIGURE 36 Effect of temperature on the kinetics of dissolution of sphalerite with SO_2/O_2 mixtures in presence of dissolved iron.

TABLE 19

VARIATION OF REACTOR TEMPERATURE

TEST NO.	TEMP. °C	After 30 min. Zn^{2+} g dm^{-3}	After 30 min. PERCENT EXTN.	AFTER 2 hrs. LEACHING Zn^{2+} g dm^{-3}	AFTER 2 hrs. LEACHING PERCENT EXTN.	Eh	pH	H_2SO_4 g dm^{-3}	Fe^{2+} g dm^{-3}	SO_2 mol dm^{-3}	EXIT GAS BUBBLER
108	25	3.17	11.4	9.91	35.5	546	1.18	17	3.52	0.060	S°
106	40	5.57	20.0	13.16	47.1	567	1.17	23	3.43	0.024	S°
115	50	5.84	20.9	15.78	56.5	635	1.04	39	2.50	0.0035	S°
75	60	7.72	27.7	21.58	77.2	676	0.56	45		0.0005	S°
107	75	8.03	28.8	24.05	86.1	803	0.90	30	0.22	----	S°
109	90	8.54	30.6	26.21	93.0	820	0.98	26	0.028	----	S°

TABLE 20

VARIATION OF GAS COMPOSITION IN ABSENCE OF IRON

Conditions: 30.0g Ventron sphalerite, 60°C, 800 rpm
gas flow + 500 cm^3 min^{-1}

TEST NO.	GAS COMPOSITION	AFTER 30 min. Zn^{2+} g dm^{-3}	AFTER 30 min. PERCENT EXTN.	AFTER 2 hrs. LEACHING Zn^{2+} g dm^{-3}	AFTER 2 hrs. LEACHING PERCENT EXTN.	Eh	pH	H_2SO_4 g dm^{-3}	$S_4O_6^{2-}$ g dm^{-3}	SO_2 mol dm^{-3}	EXIT GAS BUBBLER
77	100% SO_2	7.85	28.3	16.17	58.3	242	0.69	2.0	29.0	0.33	Clear
74	50% SO_2/O_2	3.87	13.9	10.41	37.5	273	1.00	1.0			Clear
79	10% SO_2/O_2	0.71	2.6	1.88	6.8	330	1.65	0.7	4.20	0.034	Clear
85	5% SO_2/O_2	0.43	1.6	0.88	3.2	335	1.87	0.6	2.24	0.023	Clear
81	50% SO_2/N_2	3.79	13.7	10.24	36.9	225	0.81	0.8	21.8	0.17	Clear
82	10% SO_2/N_2	0.61	2.2	1.54	5.6	220	1.74	0.3	3.60	0.039	Clear
87	5% SO_2/N_2	0.29	1.1	0.68	2.4	228	1.84	0.4	1.48	0.021	Clear

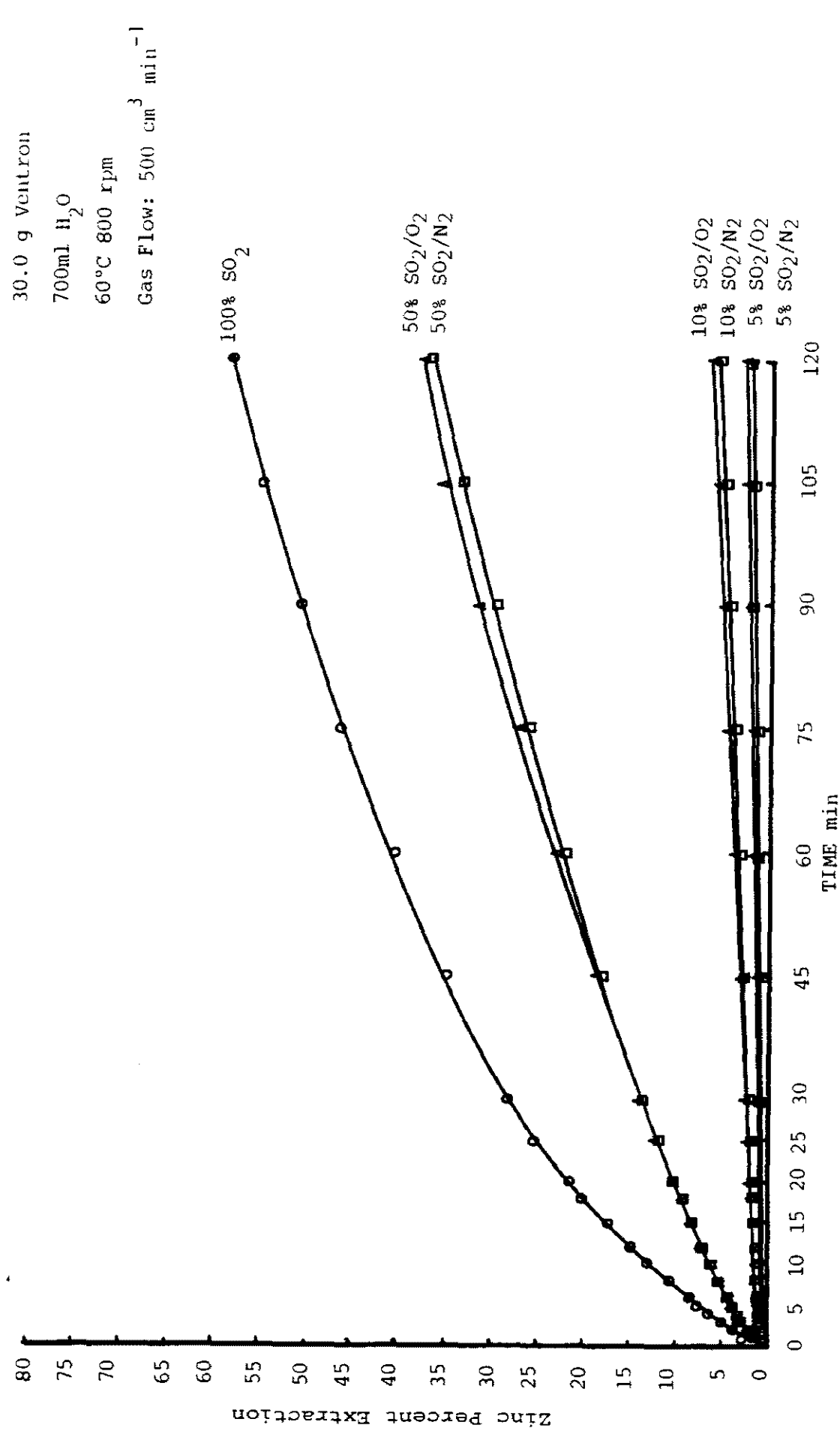

FIGURE 37. Dissolution of sphalerite with SO_2/N_2 and SO_2/O_2 mixtures in the absence of dissolved iron.

TABLE 21

VARIATION OF GAS COMPOSITION IN PRESENCE OF IRON

Conditions: 30.0g Ventron sphalerite, 3.6g dm^{-3} Fe^{3+} added
60°C, 800 rpm, gas flow + 500 $cm^3 min^{-1}$

TEST NO.	GAS COMPOSITION	AFTER 30 min. Zn^{2+} g dm^{-3}	AFTER 30 min. PERCENT EXTN.	AFTER 2 hrs. LEACHING Zn^{2+} g dm^{-3}	AFTER 2 hrs. LEACHING PERCENT EXTN.	Eh	pH	H_2SO_4 g dm^{-3}	$S_4O_6^{2-}$ g dm^{-3}	Fe^{2+} g dm^{-3}	SO_2 mol dm^{-3}	EXIT GAS BUBBLER
104	80% SO_2/O_2	19.00	68.1	25.13	90.0	469	0.59	55			0.21	Clear
123	70% SO_2/O_2	19.78	70.8	25.97	93.0	581	0.67	90		3.27	0.15	Clear
76	50% SO_2/O_2	18.81	67.8	25.64	92.4	675	0.10	132			0.05	S°
110	30% SO_2/O_2	11.77	42.2	26.82	96.0	648	0.85	88		2.21	0.026	S°
111	20% SO_2/O_2	10.15	36.4	24.00	85.6	663	0.55	71		1.87	0.007	S°
75	10% SO_2/O_2	7.72	27.7	21.58	77.2	676	0.56	45			0.001	S°
84	5% SO_2/O_2	7.42	26.7	17.77	64.0	667	0.90	29	1.68		0.001	S°
78	100% SO_2	10.70	38.6	19.92	71.8	232	0.90	7.4	53.6		0.29	Clear
80	50% SO_2/N_2	6.37	23.0	15.55	56.0	220	1.37	6.2	40.5		0.097	Clear
83	10% SO_2/N_2	1.96	7.1	4.34	15.6	265	1.53	5.8	8.68		0.023	Clear
86	5% SO_2/N_2	1.53	5.5	2.87	10.4	248	1.56	5.8	2.24		0.014	Clear

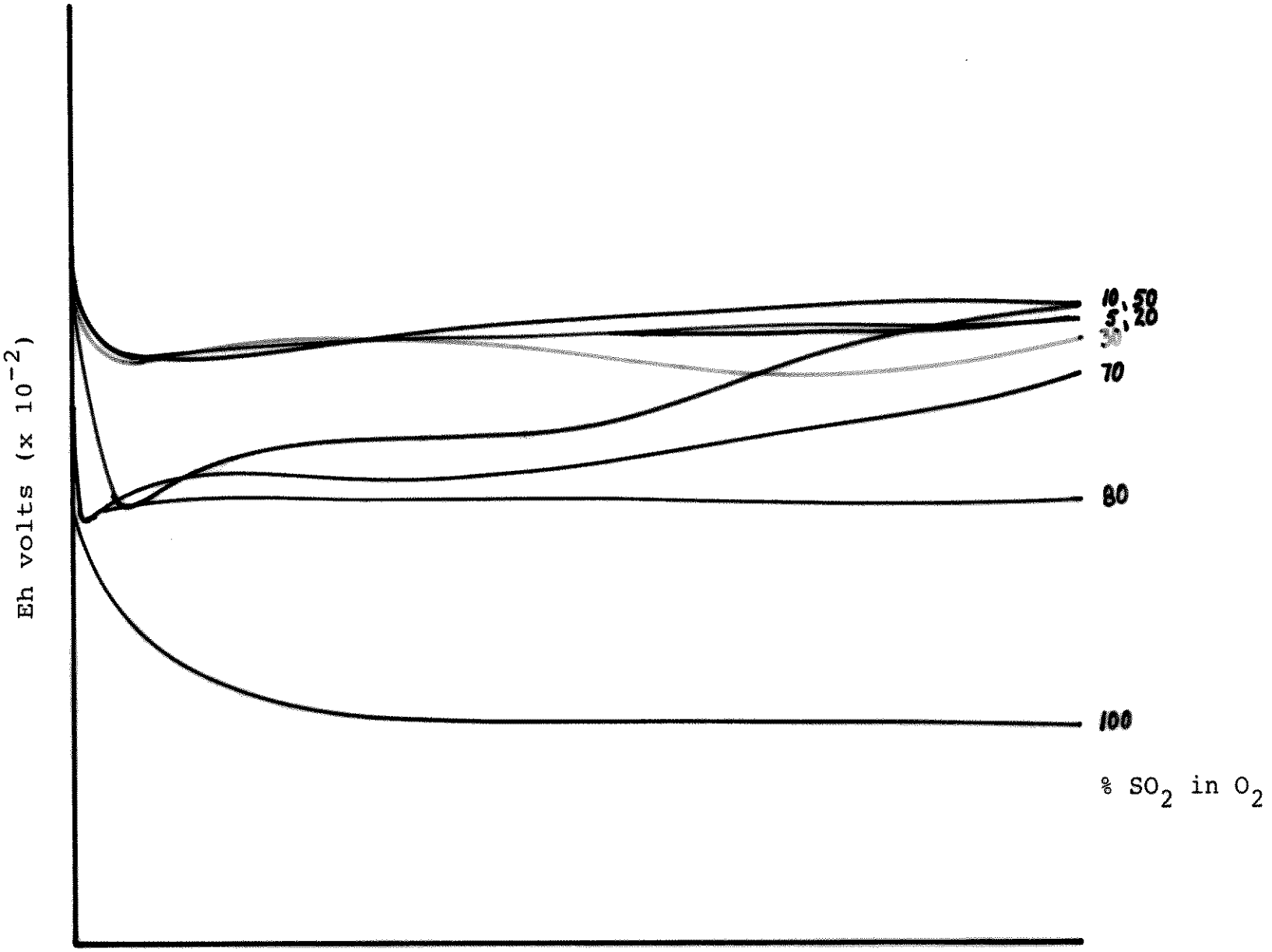
Eh volts (x 10^{-2})
10, 50
5, 20
30
70
80
100
% SO_2 in O_2

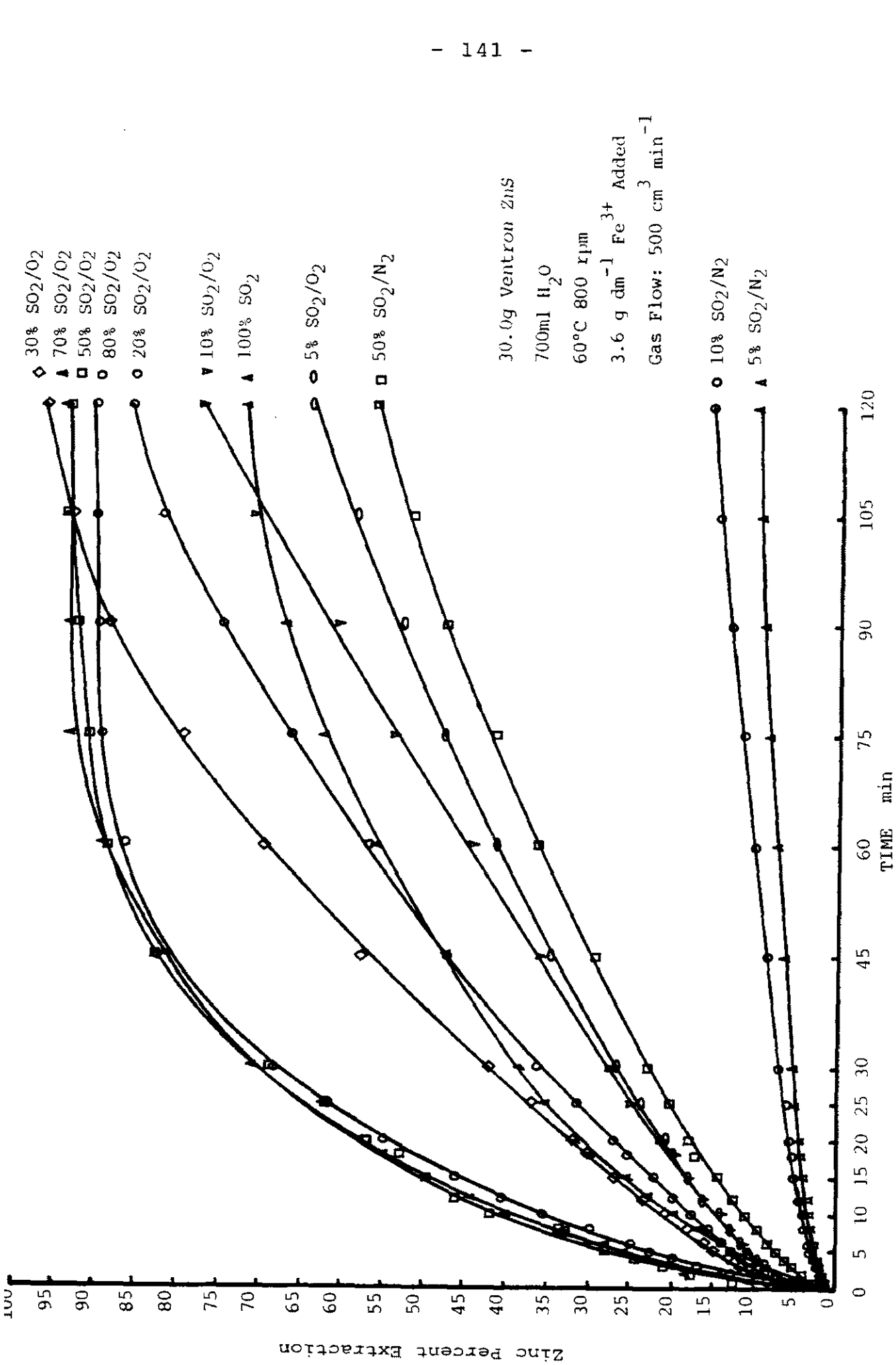

FIGURE 38. Dissolution of sphalerite with SO_2/O_2 and SO_2/N_2 mixtures in the presence of dissolved iron.

3.6 g dm^{-3}. Tests were conducted with SO_2/O_2 and SO_2/N_2 mixtures at various sulphur dioxide partial pressures. The resulting kinetic dissolution data are plotted in Figure 38.

Table 22 summarizes a series of leaching experiments employing a mixture of three gases, denoted with their percentages by $SO_2/O_2/N_2$. In this series of experiments, the sulphur dioxide partial pressure was held constant at 0.10 atm. Various oxygen and nitrogen flowrates were then used to obtain the desired oxygen partial pressure in the reactant gas. The experiments were designed to evaluate the effect of oxygen in the dissolution of sphalerite with SO_2/O_2 mixtures in the presence of dissolved iron. The kinetic dissolution data obtained are plotted in Figure 39.

Table 23 summarizes a similar series of experiments where the oxygen partial pressure was held constant at 0.30 atm. The sulphur dioxide and nitrogen flowrates were then varied to obtain the desired sulphur dioxide partial pressure in the reactant gas. This series of experiments was designed to evaluate the effect of sulphur dioxide in the SO_2/O_2 leaching of sphalerite in the presence of dissolved iron. The resulting kinetic dissolution data are plotted in Figure 40.

Table 24 presents a set of experiments which elucidates the difference between initially adding soluble iron to an experiment in the form of Fe^{2+} or Fe^{3+}. Contained in this table are two pairs of experiments where one pair employed a SO_2/O_2 mixture as the reactant gas and the other pair used SO_2/N_2. One test in each pair was run by initially adding soluble iron in the form of ferric sulphate and to the other test was added ferrous sulphate. Also, Table 24 presents duplicate pairs of experiments which demonstrates the typical reproducibility of the experimental work.

Since the presence of dissolved iron significantly

TABLE 22

VARIATION OF OXYGEN PARTIAL PRESSURE

Conditions: 30.0g Ventron sphalerite, 3.6g dm^{-3} Fe^{3+} added
60°C, 800 rpm, gas flow = 500 $cm^3 min^{-1}$

TEST NO.	GAS COMPOSITION	AFTER 30 min. Zn^{2+} g dm^{-3}	AFTER 30 min. PERCENT EXTN.	AFTER 2 hrs. LEACHING Zn^{2+} g dm^{-3}	AFTER 2 hrs. LEACHING PERCENT EXTN.	Eh	pH	H_2SO_4 g dm^{-3}	Fe^{2+} g dm^{-3}	SO_2 mol dm^{-3}	EXIT GAS BUBBLER
75	10%SO_2/90%O_2/0%N_2	7.72	27.7	21.58	77.2	676	0.56	45		0.0005	S°
103	10%SO_2/40%O_2/50%N_2	6.48	23.2	19.93	71.3	722	0.89	36	0.45	---	S°
98	10%SO_2/30%O_2/60%N_2	6.57	23.5	20.40	73.0	723	0.94	36	0.39	---	S°
101	10%SO_2/20%O_2/70%N_2	5.92	20.7	16.88	60.4	637	1.05	33	2.64	0.0028	S°
100	10%SO_2/10%O_2/80%N_2	3.63	13.0	10.25	36.7	507	1.05	24		0.014	S°
93	10%SO_2/0%O_2/90%N_2	2.12	7.6	4.63	16.6	266	1.39	6.6	4.27	0.031	Clear

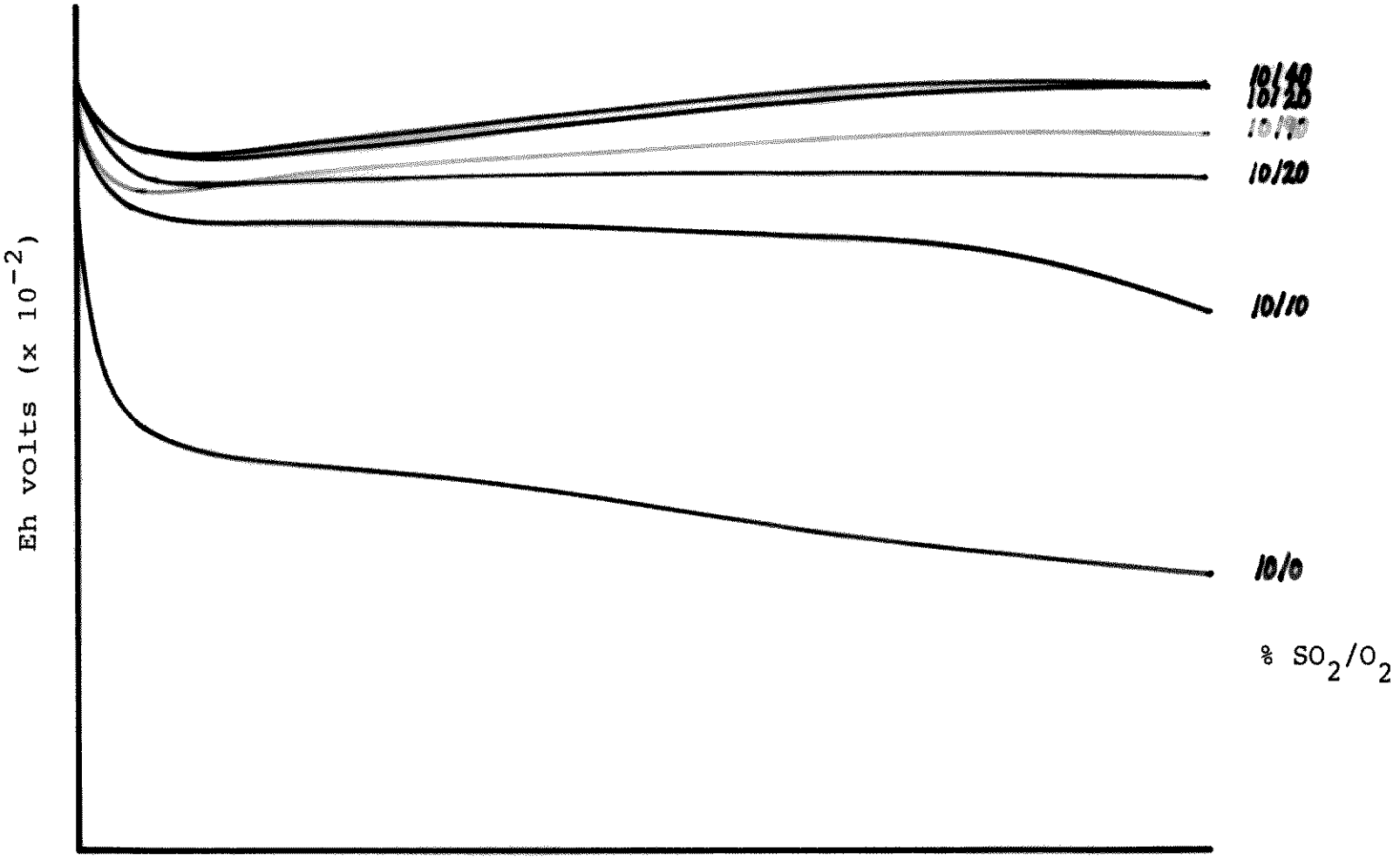
Eh volts (x 10^{-2})
10/20
10/10
10/0
% SO_2/O_2

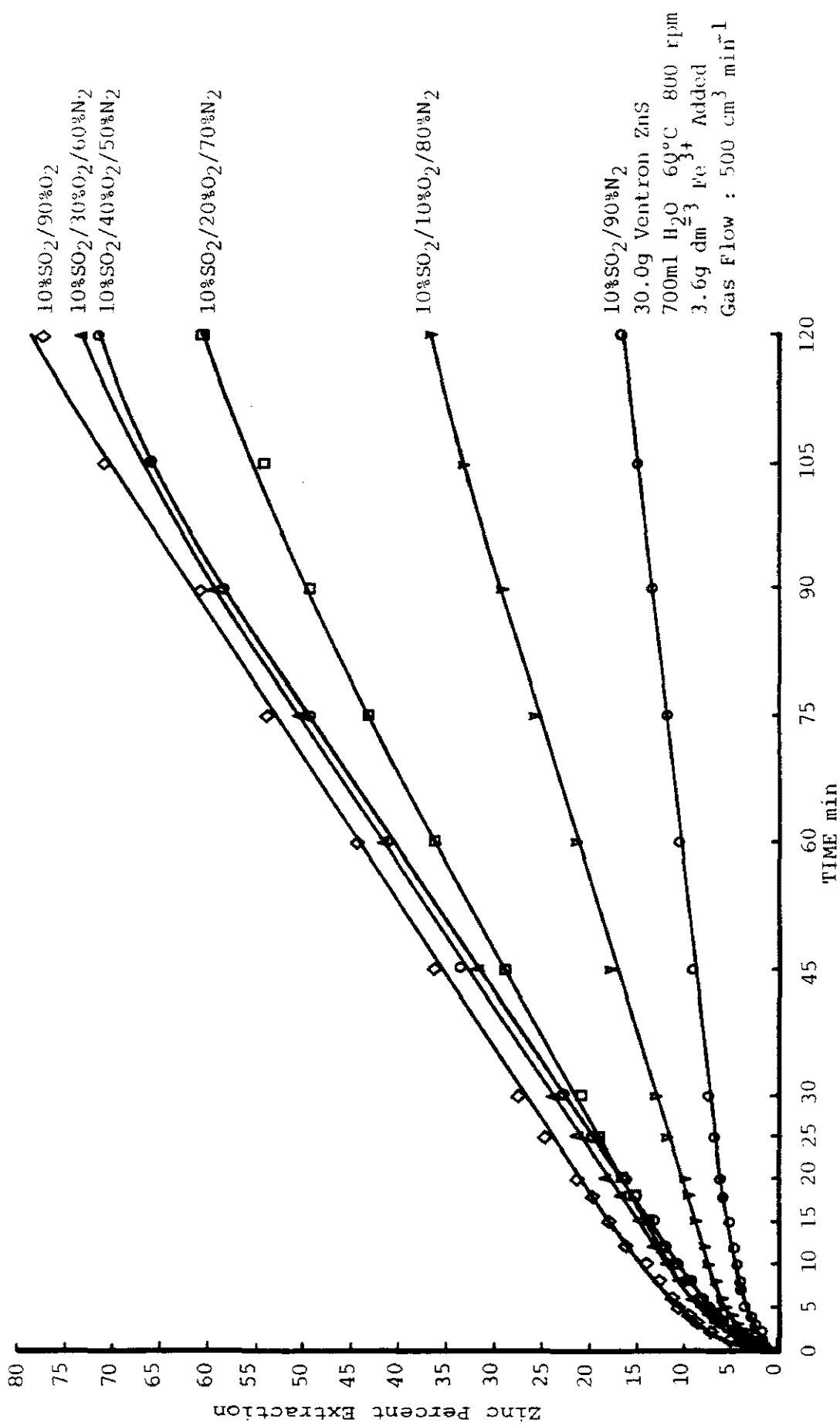

FIGURE 39. Dissolution of sphalerite with $SO_2/O_2/N_2$ mixtures at a constant SO_2 partial pressure in the presence of dissolved iron.

TABLE 23

VARIATION OF SULPHUR DIOXIDE PARTIAL PRESSURE

Conditions: 30.0g Ventron sphalerite, 3.6g dm^{-3} Fe^{3+} added
60°C, 800 rpm, gas flow = 500 $cm^3 min^{-1}$

TEST NO.	GAS COMPOSITION	AFTER 30 min. Zn^{2+} g dm^{-3}	AFTER 30 min. PERCENT EXTN.	AFTER 2 hrs. LEACHING Zn^{2+} g dm^{-3}	AFTER 2 hrs. LEACHING PERCENT EXTN.	Eh	pH	H_2SO_4 g dm^{-3}	Fe^{2+} g dm^{-3}	SO_2 mol dm^{-3}	EXIT GAS BUBBLER
98	10%SO_2/30%O_2/60%N_2	6.57	23.5	20.40	73.0	723	0.94	36	0.39	---	S° (high)
120	20%SO_2/30%O_2/50%N_2	8.22	31.6	22.15	79.3	519	0.84	50	3.59	0.029	S° (high)
121	30%SO_2/30%O_2/40%N_2	10.37	37.1	24.04	86.1	524	0.76	43	3.63	0.035	S° (low)
122	40%SO_2/30%O_2/30%N_2	12.64	45.3	26.56	95.1	524	0.75	49	3.64	0.063	Clear
124	50%SO_2/30%O_2/20%N_2	18.19	65.2	26.43	94.6	605	0.51	83	2.88	0.097	Clear
126	60%SO_2/30%O_2/10%N_2	18.74	67.1	25.78	92.6	628	0.42	98	2.88	0.10	Clear
123	70%SO_2/30%O_2/0%N_2	19.78	70.8	25.97	93.0	581	0.67	90	3.27	0.15	Clear

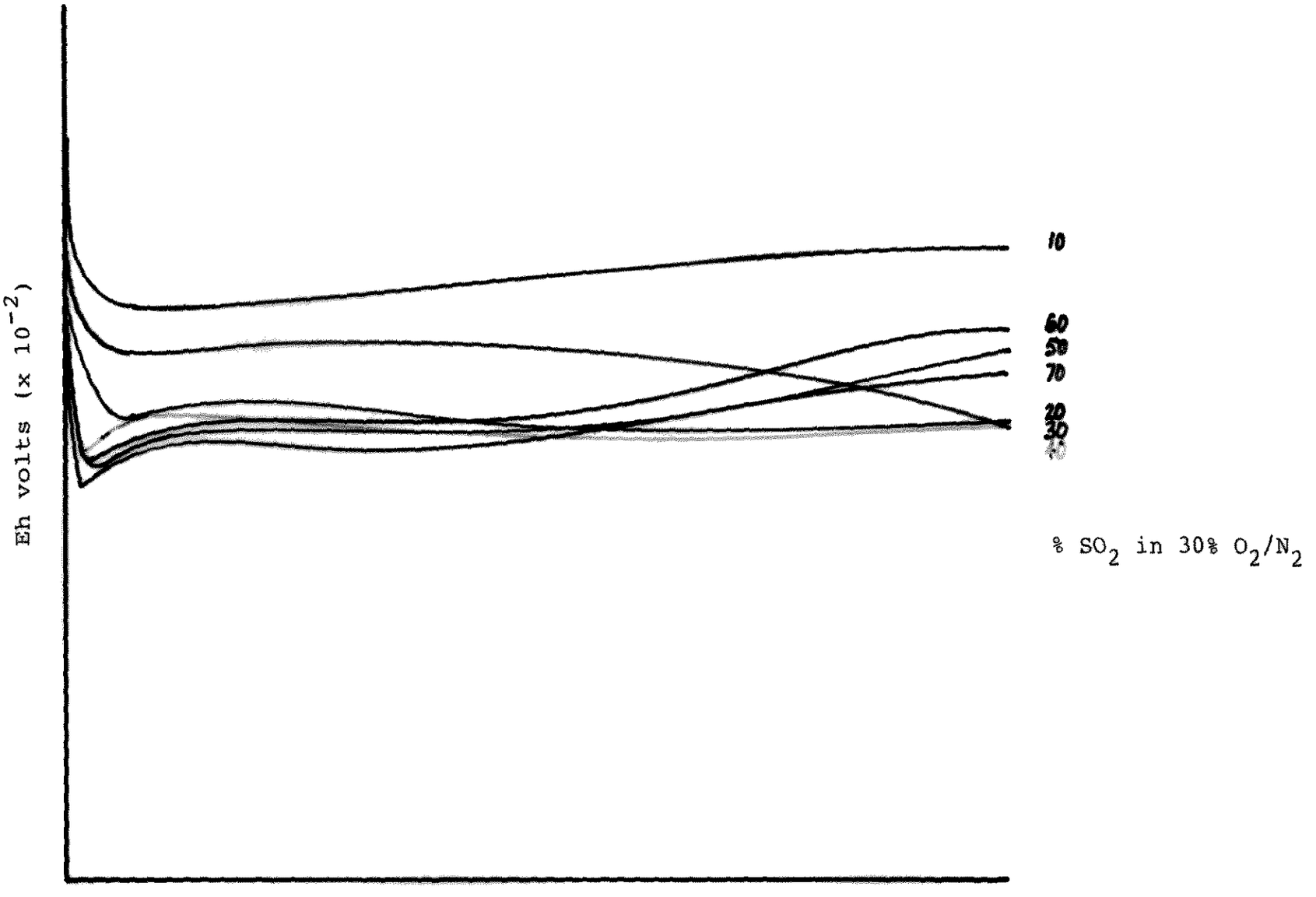
Eh volts (x 10^{-2})
10
60
50
70
20
30
% SO_2 in 30% O_2/N_2

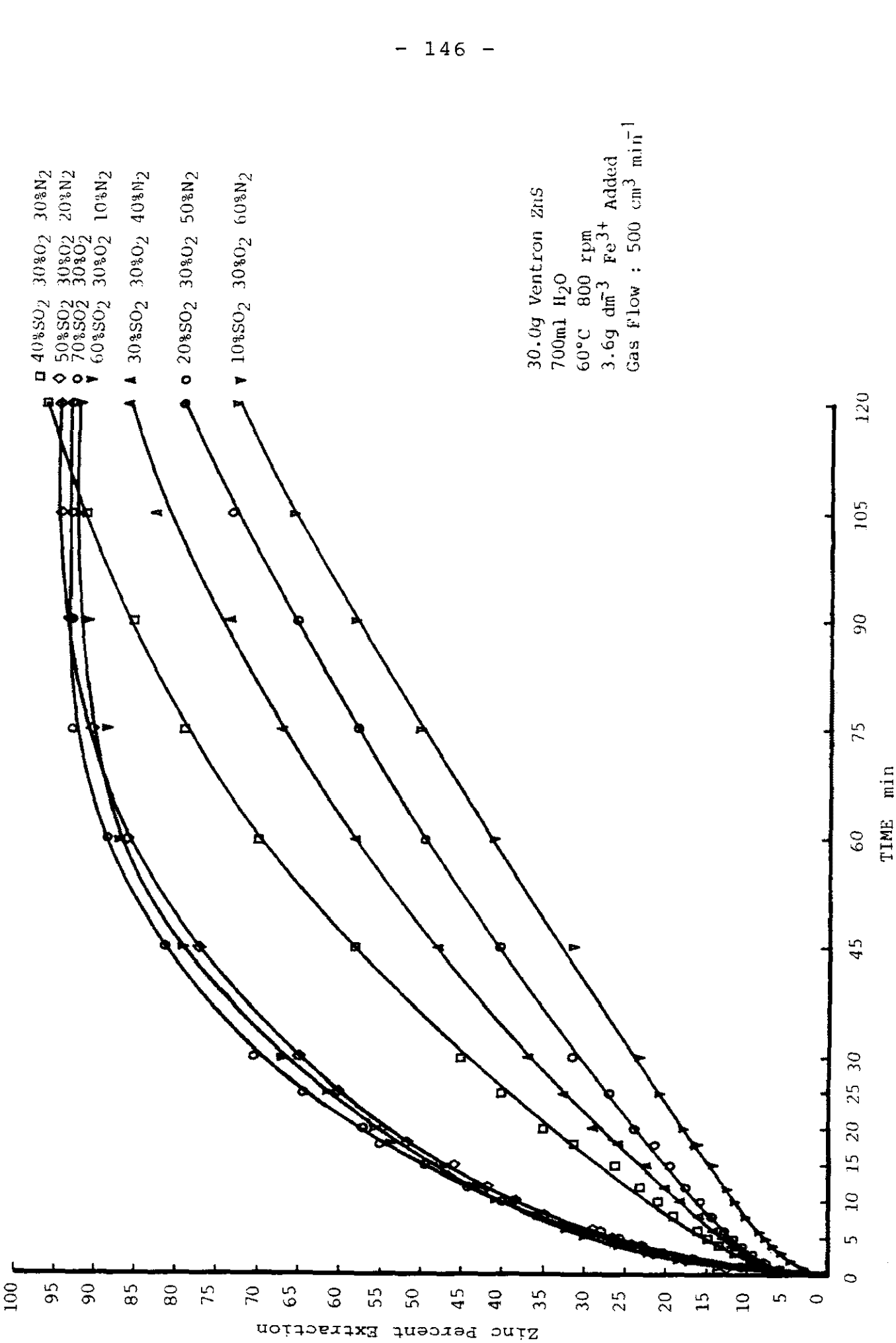

FIGURE 40. Dissolution of sphalerite with $SO_2/O_2/N_2$ mixtures at a constant O_2 partial pressure in the presence of dissolved iron.

TABLE 24

EFFECT OF IRON OXIDATION STATE

Conditions: 30.0g Ventron sphalerite, 60°C, 800 rpm
gas flow = 500 $cm^3 min^{-1}$

TEST NO.	GAS COMPOSITION	Fe Added g dm^{-3}	AFTER 30 min. Zn^{2+} g dm^{-3}	AFTER 30 min. PERCENT EXTN.	AFTER 2 hrs. LEACHING Zn^{2+} g dm^{-3}	AFTER 2 hrs. LEACHING PERCENT EXTN.	Eh	pH	H_2SO_4 g dm^{-3}	Fe^{2+} g dm^{-3}	$S_4O_6^{2-}$ g dm^{-3}	SO_2 mol dm^{-3}	EXIT GAS BUBBLER
75	10% SO_2/O_2	3.6 Fe^{3+}	7.72	27.7	21.58	77.2	676	0.56	45			0.0005	S°
89	10% SO_2/O_2	3.6 Fe^{2+}	6.89	24.8	21.38	77.0	732	1.07	30		0.28	---	S°
92	10% SO_2/O_2	3.6 Fe^{2+}	8.39	30.1	21.78	78.0	732	0.90	36	0.53		---	S°
88	10% SO_2/N_2	3.6 Fe^{2+}	0.59	2.1	1.90	6.9	265	1.86	2.4		4.88	0.043	Clear
83	10$ SO_2/N_2	3.6 Fe^{3+}	1.96	7.1	4.34	15.6	265	1.53	5.8		8.68	0.023	Clear
93	10% SO_2/N_2	3.6 Fe^{3+}	2.12	7.6	4.63	16.6	266	1.39	6.6	4.27		0.031	Clear
97	100% N_2	3.6 Fe^{3+}	2.15	7.7	2.30	8.2	428	1.75	4.8	3.66		---	Clear

affects the kinetics of leaching with SO_2/O_2 gas mixtures, a series of tests were designed to evaluate the effect dissolved iron concentration. Table 25 summarizes experiments conducted with various concentrations of Fe^{3+}, up to 20.0 g dm^{-3}, added as ferric sulphate. The corresponding kinetic data are plotted in Figure 41. Ferrous iron analyses were performed on the leach liquor at half hour intervals by the method given in Appendix 5.5. The ferrous iron concentration at the conclusion of each test is given in Table 25, with the remainder of this data tabulated in Appendix 7.

It was found in the preliminary studies that, under certain conditions, quantities of sulphuric acid were generated within the leaching media during the course of the experiments. Consequently, an analysis scheme was devised to quantitatively measure the acid generated at the conclusion of each experiment. The method for analysis of sulphuric acid in leach liquors is presented in Appendix 5.4. The quantity of sulphuric acid generated during each experiment is included in all of the tables of results in this section. Furthermore, a series of experiments were conducted with a quantity of sulphuric acid added to the leach media. Table 26 summarizes this series of experiments. One experiment, test no. 129, was aborted at 12 minutes into the run as stated. It was evident that the 316 grade stainless steel impeller and other internal reactor parts were being attacked by the leach medium in this test. No damage to the reactor stainless steel parts was apparent in any of the other experiments. Figure 42 and Figure 43 present plots of the kinetic data obtained from the tests with added sulphuric acid.

Table 27 and Table 28 present two series of tests designed to evaluate the hindering effect of the accumulated zinc concentration in the leach medium on the overall rate of dissolution. The tests presented in Table 27 were conducted in aqueous sulphur dioxide media

TABLE 25

VARIATION OF IRON ADDITION

Conditions: 30.0g Ventron sphalerite, 60°C, 800 rpm
gas flow = 10% SO_2/O_2 at 500 $cm^3 min^{-1}$

TEST NO.	Fe^{3+} ADDED g dm^{-3}	AFTER 30 min. Zn^{2+} g dm^{-3}	AFTER 30 min. PERCENT EXTN.	AFTER 2 hrs LEACHING Zn^{2+} g dm^{-3}	AFTER 2 hrs LEACHING PERCENT EXTN.	Eh	pH	H_2SO_4 g dm^{-3}	Fe^{2+} g dm^{-3}	SO_2 g dm^{-3}	EXIT GAS BUBBLER
79	0.0	0.71	2.6	1.88	6.8	330	1.65	0.7		0.034	Clear
119	1.0	4.69	16.8	14.00	50.1	502	0.90	34	1.00	0.012	S° (high)
75	3.6	7.72	27.7	21.58	77.2	676	0.56	45		0.0005	S°
117	10.0	9.94	35.6	22.51	80.6	773	1.01	40	0.27	---	S° (low)
125	20.0	12.70	45.5	24.53	87.1	728	0.86	62	1.06	---	Clear

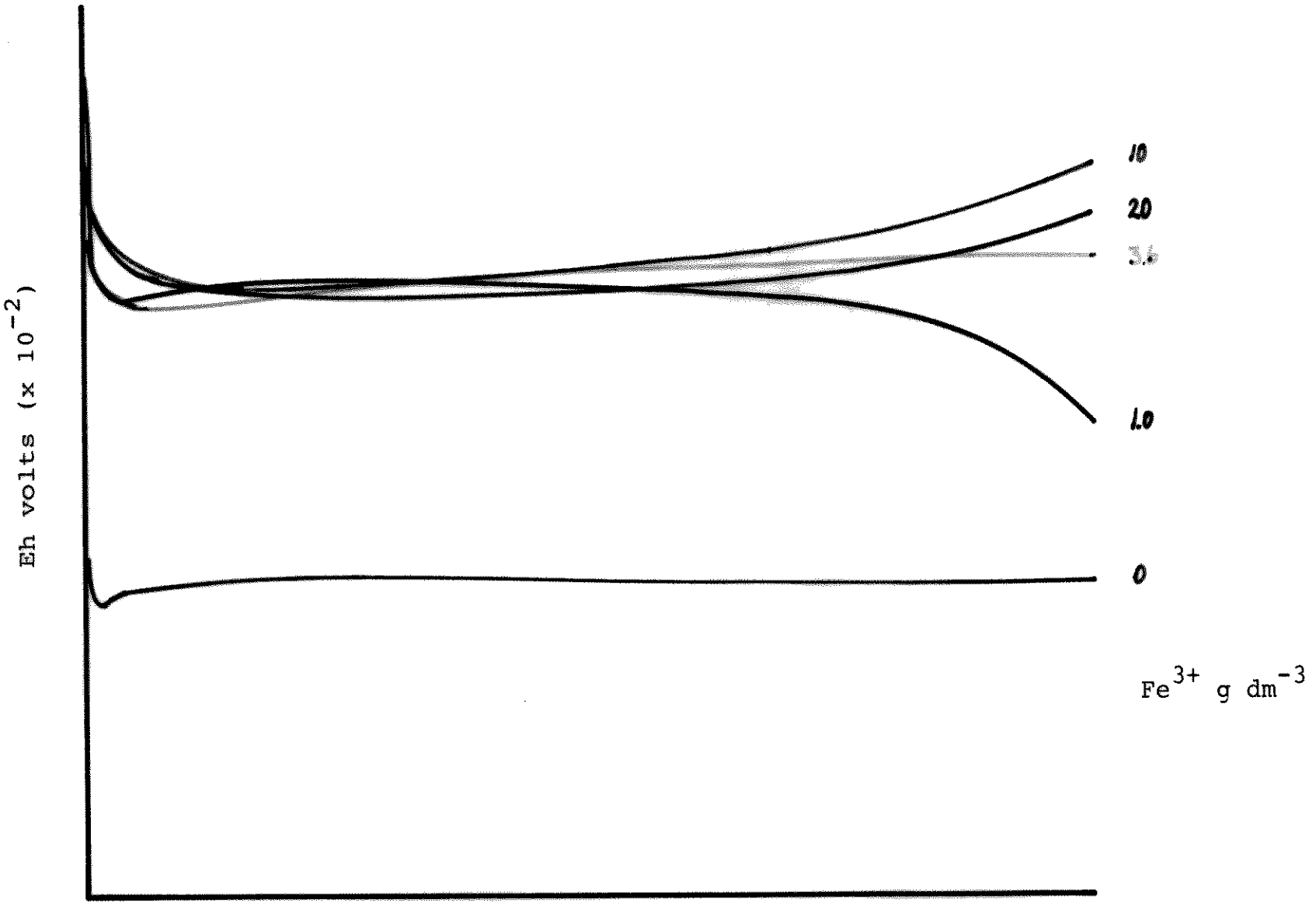
Eh volts (x 10^{-2})
10
20
5.6
1.0
0
Fe^{3+} g dm^{-3}

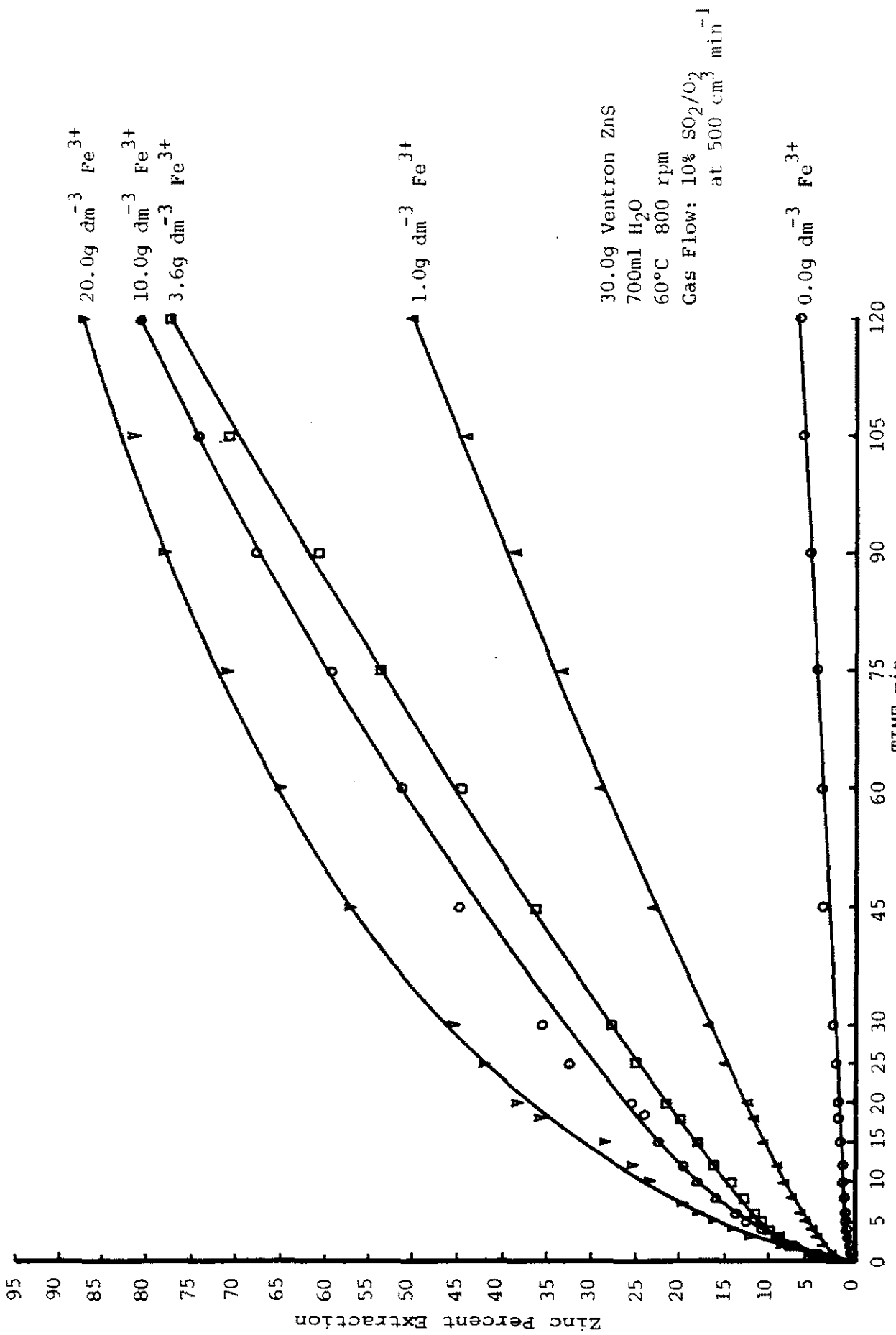

FIGURE 41. Effect of dissolved iron on the dissolution of sphalerite with SO_2/O_2 mixtures.

TABLE 26

EFFECT OF ACID ADDITION

Conditions: 30.0g Ventron sphalerite, 60°C, 800 rpm
gas flow = 500 $cm^3 min^{-1}$

TEST NO.	GAS COMPOSITION	H_2SO_4 ADDED g dm^{-3}	AFTER 30 min. Zn^{2+} g dm^{-3}	AFTER 30 min. PERCENT EXTN.	AFTER 2 hrs LEACHING Zn^{2+} g dm^{-3}	AFTER 2 hrs LEACHING PERCENT EXTN.	Eh	pH	H_2SO_4 g dm^{-3}	SO_2 mol dm^{-3}	EXIT GAS BUBBLER
82	10% SO_2/N_2	0.0	0.61	2.2	1.54	5.6	220	1.74	0.3	0.039	Clear
130	10% SO_2/N_2	20.0	5.51	19.9	8.75	31.5	264	1.15	10.8	0.028	S° (low)
131	10% SO_2/O_2	20.0	5.16	18.6	9.2	33.4	248	0.93	10.0	0.020	S°
129	10% SO_2/N_2	50.0	7.17	25.8	At 10 min. test aborted						S° (high)
81	50% SO_2/N_2	0.0	3.79	13.7	10.24	36.9	225	0.81	0.8	0.17	Clear
127	50% SO_2/N_2	10.0	6.91	24.9	15.76	56.8	248	0.99	7.2	0.24	Clear

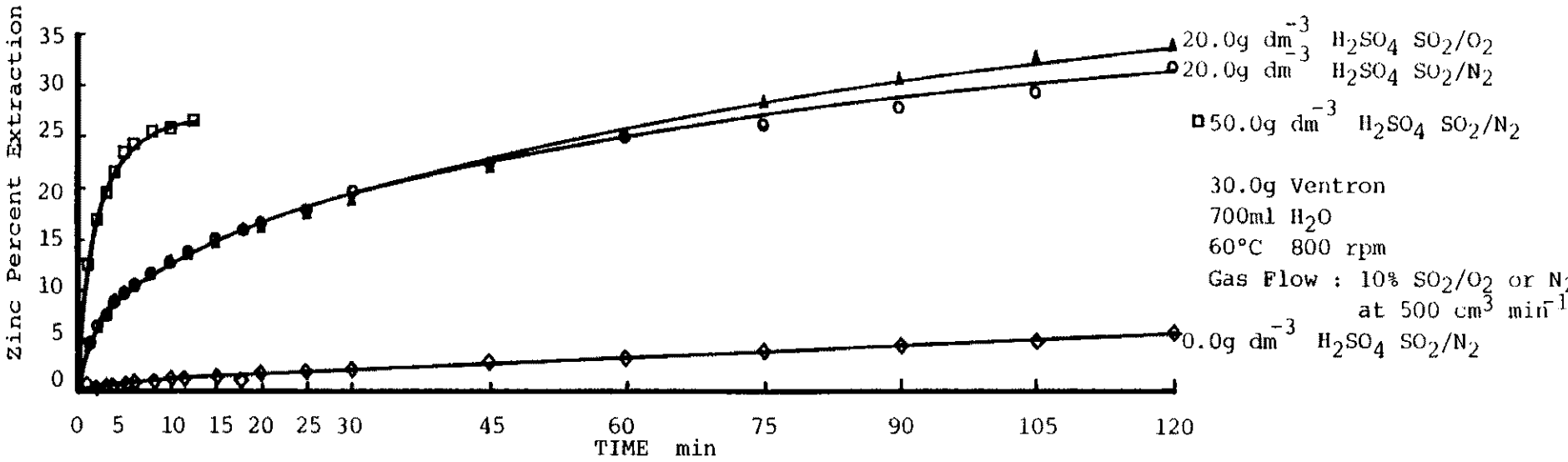

FIGURE 42. Effect of sulphuric acid addition on the dissolution of sphalerite with SO_2/O_2 and SO_2/N_2 mixtures in the absence of dissolved iron.

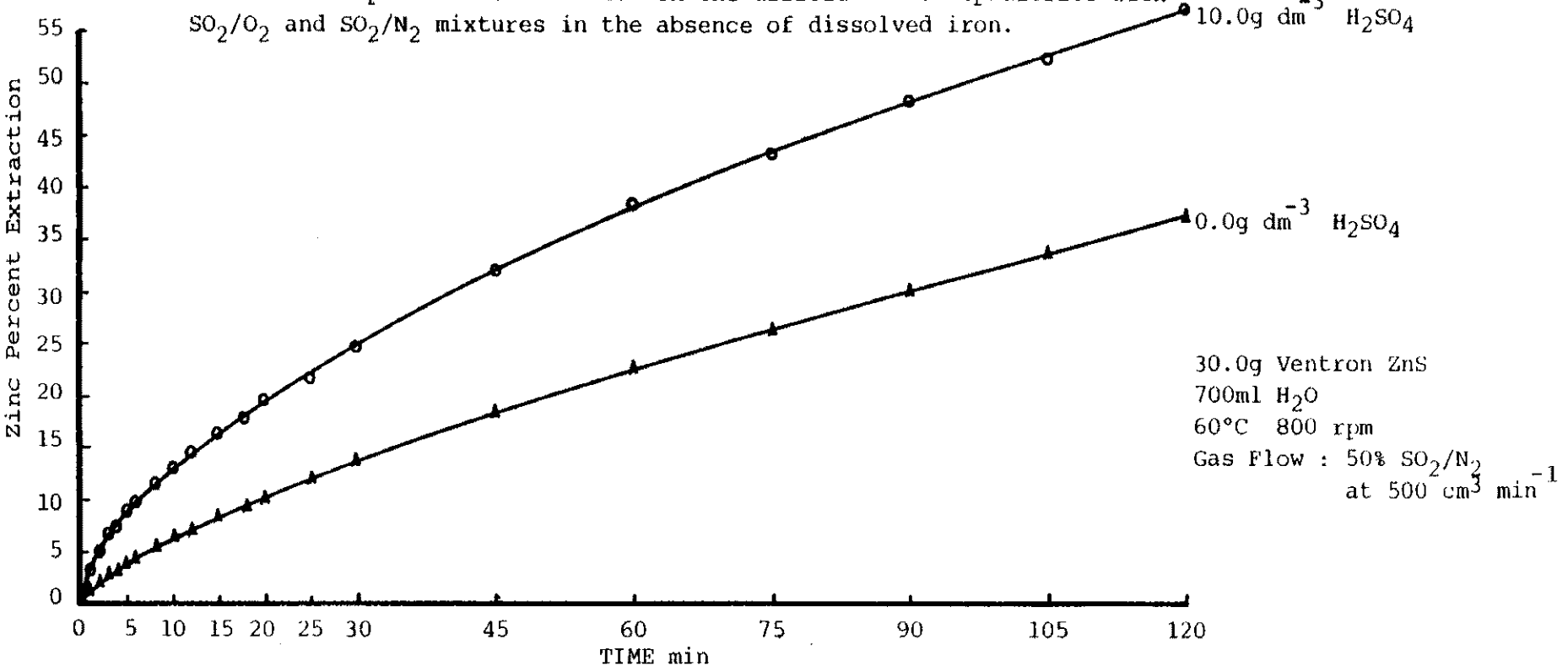

FIGURE 43. Effect of sulphuric acid addition on the dissolution of sphalerite with SO_2/O_2 mixtures in the absence of dissolved iron.

TABLE 27

EFFECT OF AQUEOUS ZINC IN LEACH MEDIA

Conditions: 30.0g Ventron sphalerite Lot No. 080581
800 rpm, gas flow = 100% SO_2 at 500 $cm^3 min^{-1}$

TEST NO.	TEMP. °C	Zn^{2+} ADDED g dm^{-3}	AFTER 30 min Zn^{2+} g dm^{-3}	AFTER 30 min PERCENT EXTN.	AFTER 2 hrs. LEACHING Zn^{2+} g dm^{-3}	AFTER 2 hrs. LEACHING PERCENT EXTN.	Eh	pH	H_2SO_4 g dm^{-3}	$S_2O_6^{2-}$ g dm^{-3}	SO_2 mol dm^{-3}	EXIT GAS BUBBLER
64	25	0.0	4.21	15.2	8.62	31.1	287	0.90	0.2	11.8	0.96	Clear
70	25	7.0	1.01	3.6	2.33	8.3	331	1.13	---	7.0	0.16	Clear
68	60	0.0	4.89	17.6	10.05	36.2	222	0.73	1.8	29.7	0.35	Clear
69	60	7.0	0.86	3.1	1.71	6.1	225	1.29	---	1.8	0.47	Clear

TABLE 28

EFFECT OF AQUEOUS ZINC IN LEACH MEDIA

Conditions: 30.0g Ventron sphalerite, 60°C, 800 rpm
3.6 g dm^{-3} Fe^{3+} added, gas flow = 10% SO_2/O_2 at 500 $cm^3 min^{-1}$

		AFTER 30 min		AFTER 2 hrs. LEACHING							
TEST NO.	Zn^{2+} ADDED g dm^{-3}	Zn^{2+} g dm^{-3}	PERCENT EXTN.	Zn^{2+} g dm^{-3}	PERCENT EXTN.	Eh	pH	H_2SO_4 g dm^{-3}	Fe^{2+} g dm^{-3}	SO_2 mol dm^{-3}	EXIT GAS BUBBLER
75	0.0	7.72	27.7	21.58	77.2	676	0.56	45		0.0005	S°
102	5.0	5.86	20.1	18.05	64.6	710	1.06	41	0.53	---	S°
116	10.0	2.11	7.6	12.53	44.9	710	0.94	39	0.61	---	S° (low)
118	20.0	0.85	3.0	10.74	38.4	684	0.84	47	1.01	0.0006	S° (low)

in the absence of iron and are four of the tests performed using the Ventron sphalerite from lot no. 080581. The kinetic data for these tests, two of which have 7.0 g dm^{-3} of Zn^{2+} ion added at the start of the test, are plotted in Figure 44. Table 28 presents a series of experiments with an initial quantity of Zn^{2+} ion added at concentrations up to 20 g dm^{-3}. A 10% SO_2/O_2 gas mixture was used in these experiments conducted in the presence of dissolved iron. The resulting kinetic dissolution curves are shown in Figure 45. Both Figure 44 and Figure 45 demonstrate that an initial concentration of dissolved zinc significantly hinders the dissolution kinetics.

Table 29 summarizes a series of tests designed to assess the effect of slurry density on the rate of dissolution. Two of the tests were performed with half the normal mass of sphalerite (15g ZnS) added to the reactor yielding a slurry density of 21.43 g dm^{-3} (kg m^{-3}). All other conditions were held constant. These tests were conducted in the presence of dissolved iron using SO_2/O_2 gas mixtures. The resulting kinetic data is plotted in Figure 46.

A single experiment was performed in the presence of an organic solvent for sulphur. Its purpose was to determine if a product layer of elemental sulphur formed on the sphalerite particles retards the rate of dissolution. In this experiment, 50.0 cm^3 of xylene was added to a test using sulphur dioxide gas only and in the absence of aqueous iron. If elemental sulphur is deposited on the surface of the sphalerite particles and inhibits the rate of dissolution, the xylene, being a solvent of elemental sulphur, should remove this product layer and the rate of dissolution should increase. The resulting dissolution curves obtained for two equivalent tests with and without added xylene are presented in Figure 47.

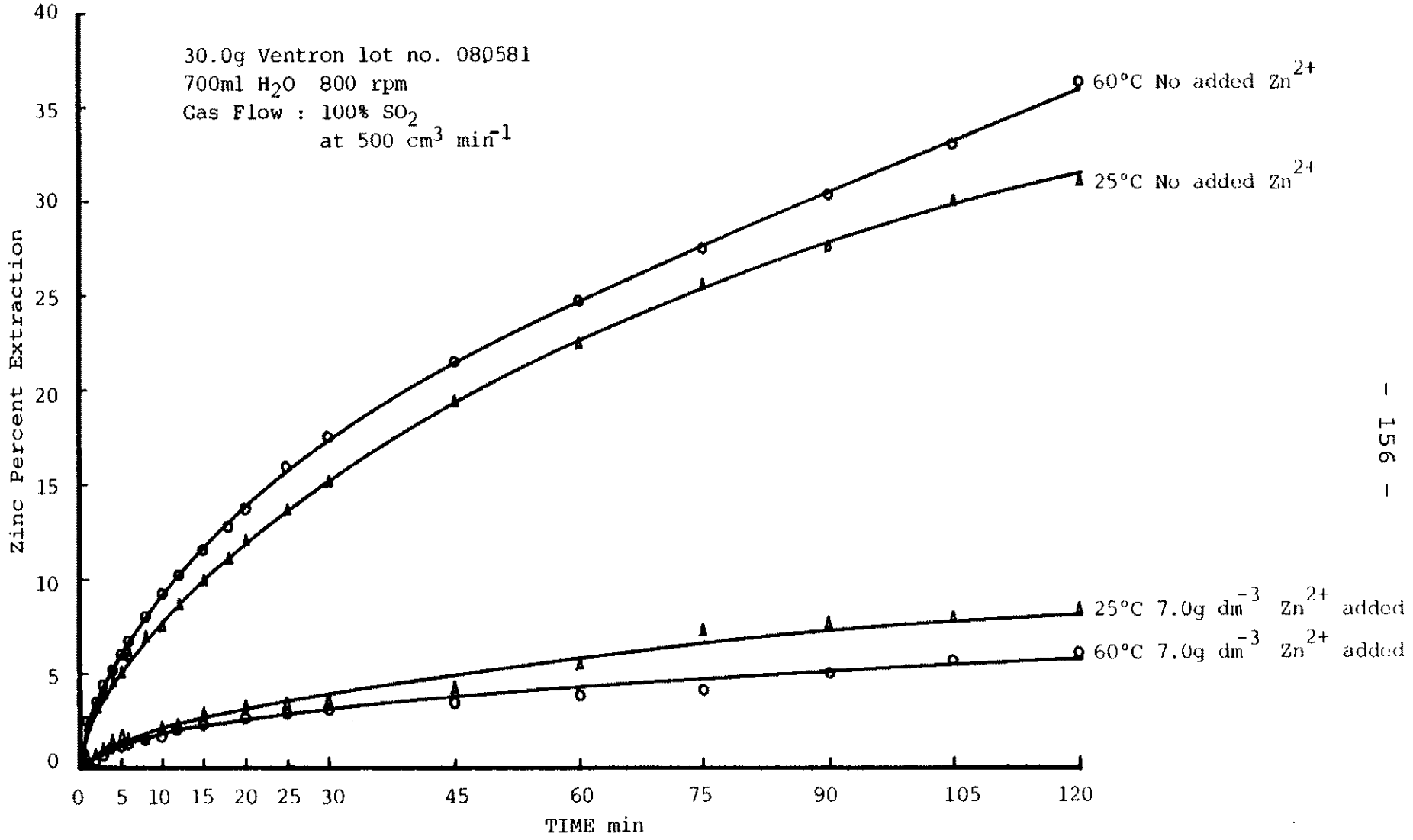

FIGURE 44. Effect of dissolved zinc on the dissolution of sphalerite in aqueous SO_2 media in the absence of dissolved iron.

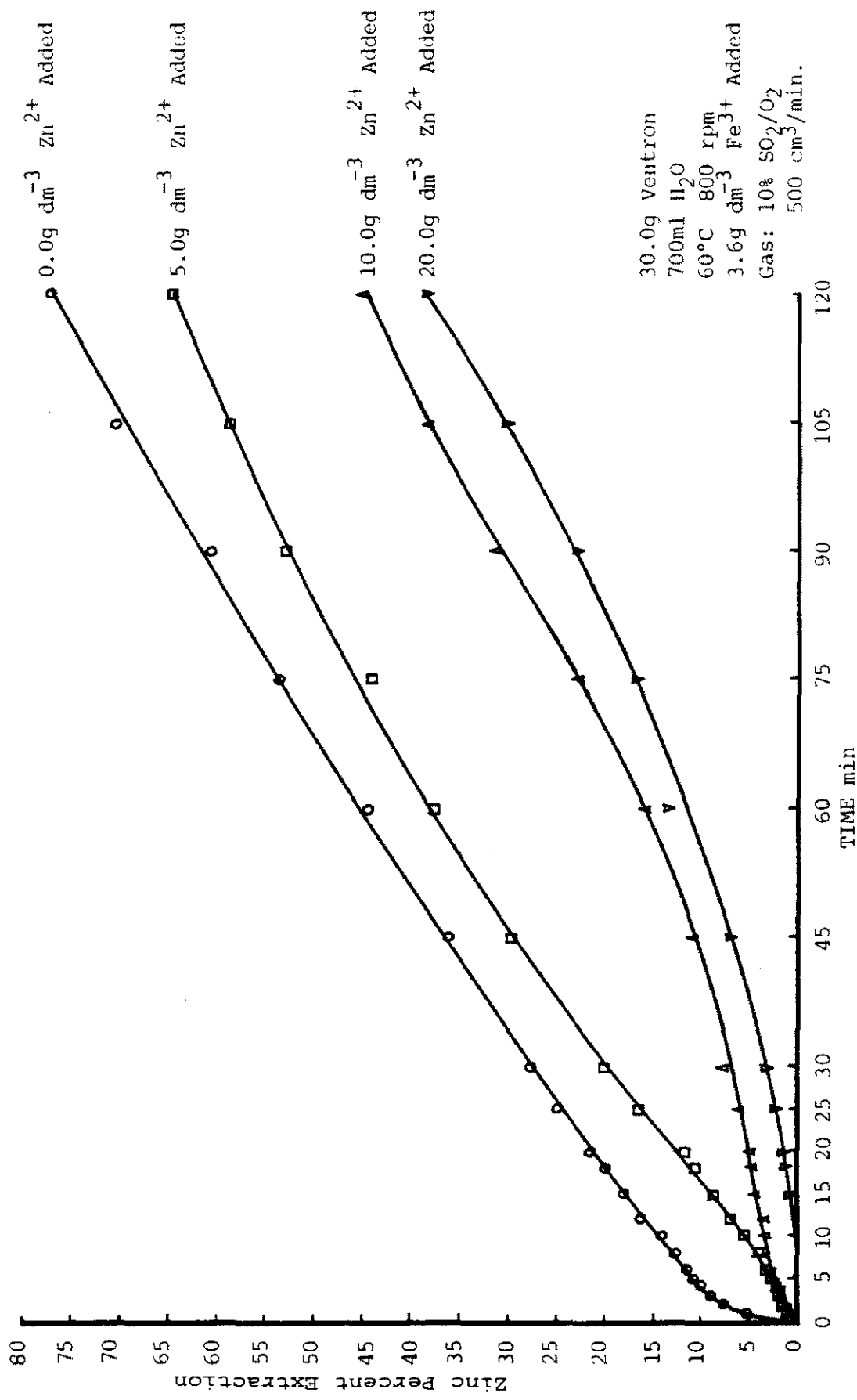

FIGURE 45. Effect of dissolved zinc on the dissolution of sphalerite with SO_2/O_2 mixtures in the presence of dissolved iron.

TABLE 29

VARIATION OF SLURRY DENSITY

Conditions: 60°C, 800 rpm, 3.6 g dm^{-3} Fe^{3+} Added
gas flow = 500 $cm^3 min^{-1}$

TEST NO.	GAS COMPOSITION	ZnS ADDED g	SLURRY DENSITY ZnS g dm^{-3}	AFTER 30 min Zn^{2+} g dm^{-3}	AFTER 30 min EXTN. %	AFTER 2 hrs. LEACHING Zn^{2+} g dm^{-3}	AFTER 2 hrs. LEACHING EXTN. %	Eh	pH	H_2SO_4 g dm^{-3}	Fe^{2+} g dm^{-3}	So_2 mol dm^{-3}	EXIT GAS BUBBLER
75	10% SO_2/O_2	30.0	42.8	7.72	27.7	21.58	77.2	676	0.56	45		0.0005	S°
113	10% SO_2/O_2	15.0	21.4	6.36	49.5	12.34	100.0	816	0.97	39	0.014	---	S°
76	50% SO_2/O_2	30.0	42.8	18.81	67.8	25.64	92.4	675	0.10	132		0.05	S°
114	50% SO_2/O_2	15.0	21.4	11.64	90.6	12.20	96.3	707	0.62	172	0.29	0.065	S°

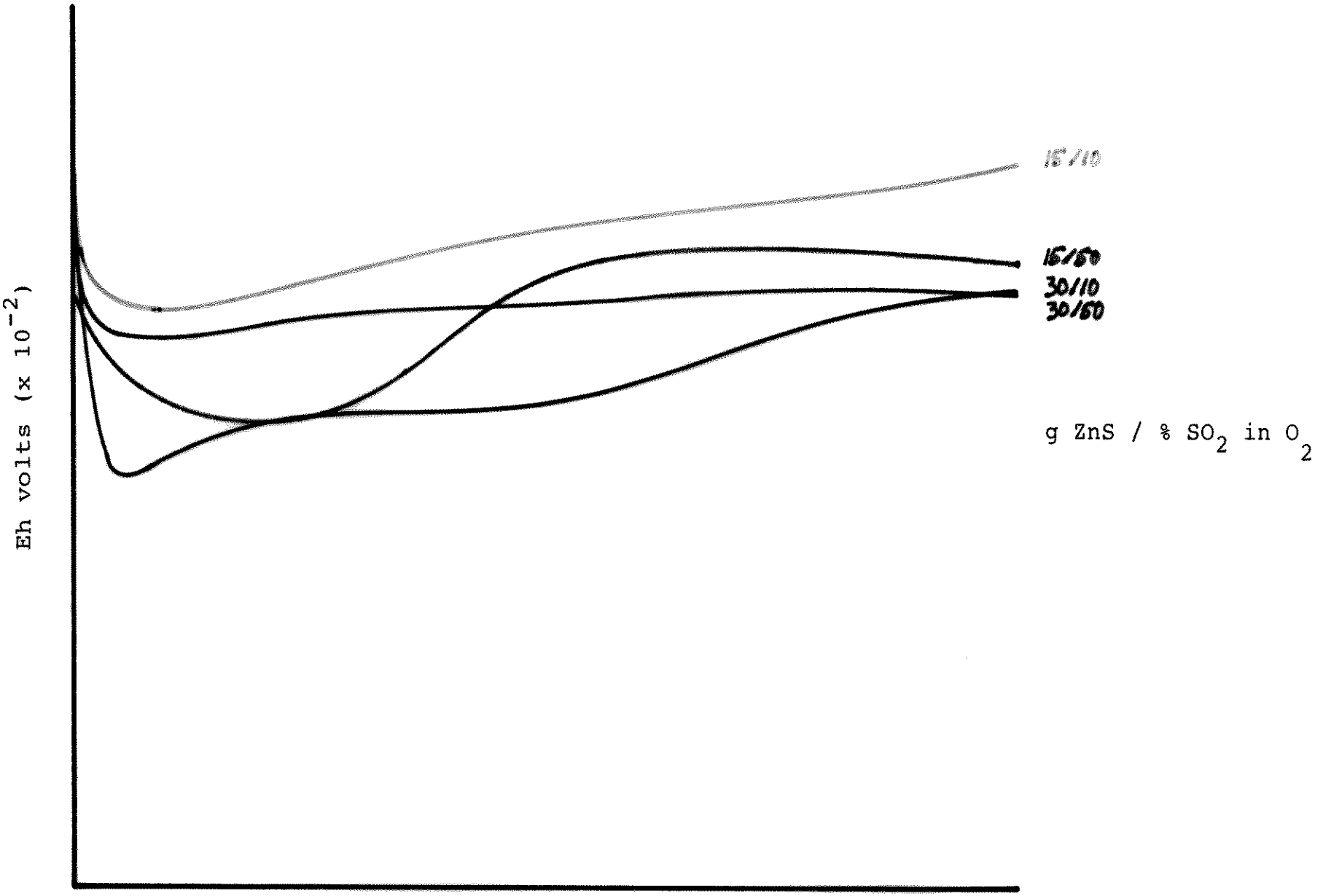
Eh volts (x 10^{-2})
15/10
15/60
30/10
30/60
g ZnS / % SO_2 in O_2

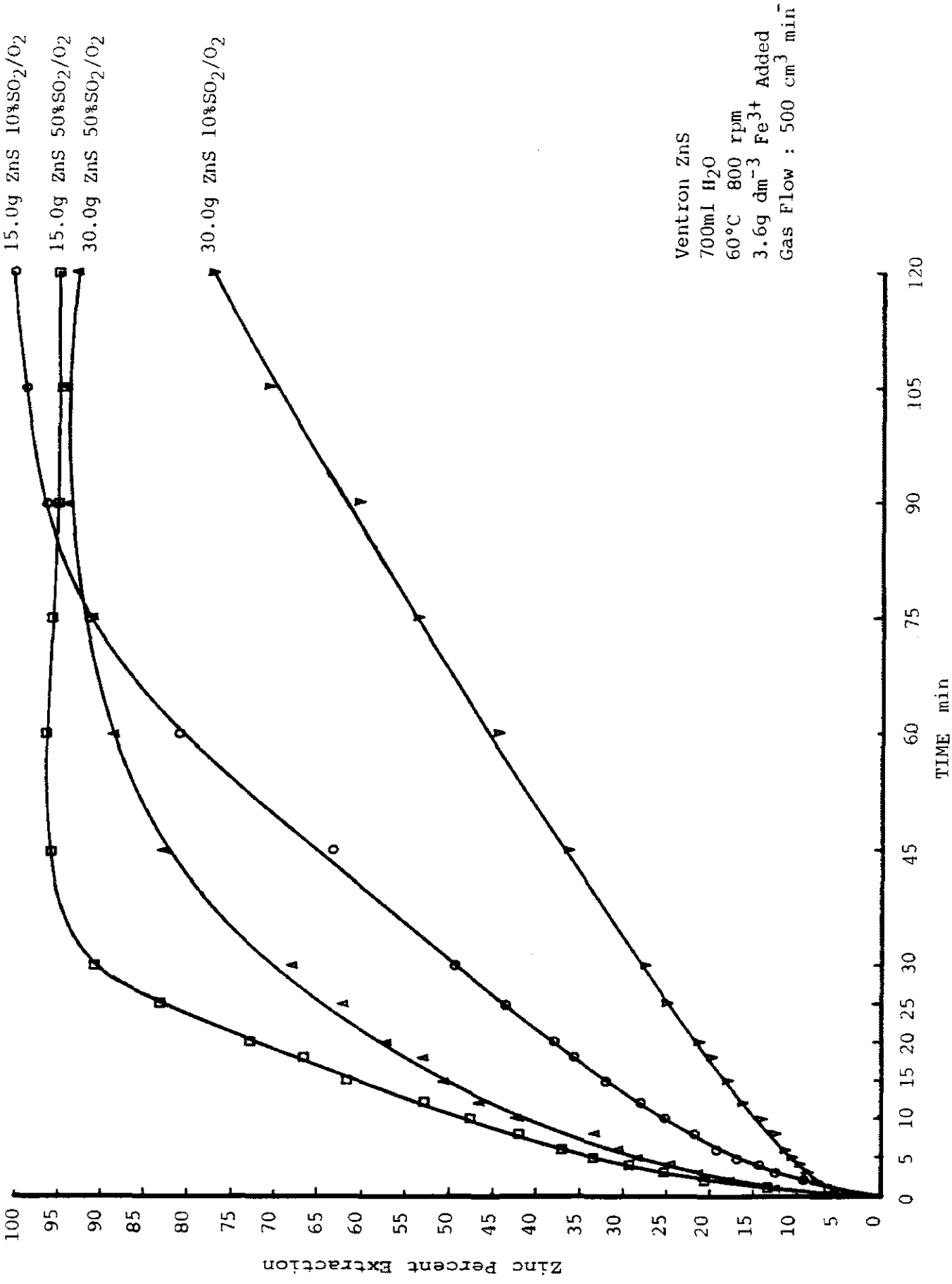

FIGURE 46. Effect of slurry density on the dissolution of sphalerite with SO_2/O_2 mixtures in the presence of dissolved iron.

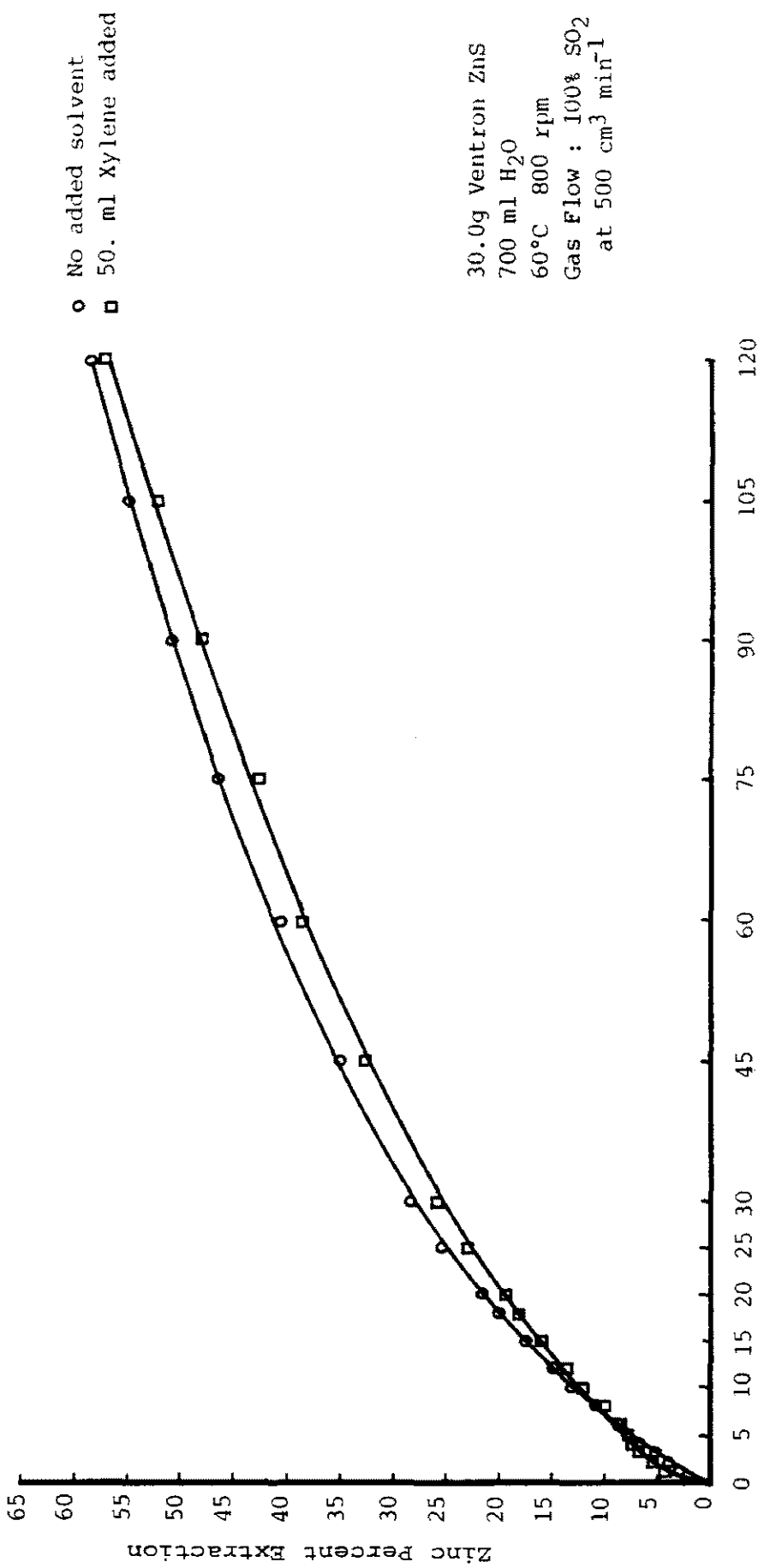

FIGURE 47. Effect of adding an organic solvent for sulphur on the dissolution of sphalerite in aqueous SO_2 media in the absence of dissolved iron.

Figure 48 presents the percent zinc extraction versus time data from a leaching test carried out to completion over a 28 hour time period. Sulphur dioxide only is used as a reagent gas in this experiment performed on Ventron sphalerite from lot no. 080581 in the absence of aqueous iron. The concentration of the tetrathionate species in the leach liquor was quantitatively analyzed throughout the experiment and is also plotted in Figure 48. The method of analysis of the tetrathionate species is given in Appendix 5.3. As seen in Figure 48 the tetrathionate species was formed immediately at the start of the reaction and its concentration continued to increase well into the test. At long times, when the sphalerite dissolution reaction was nearing completion, the tetrathionate concentration decreased.

Figure 49 presents the result of a two stage leaching experiment also performed on Ventron sphalerite, lot no. 080581, with sulphur dioxide gas only and in the absence of dissolved iron. The first stage of this experiment was conducted by the normal leaching test procedure. The solid residue from the first stage leach was filtered and washed with distilled water. The washed solids were then returned to the second stage leach. The second stage was begun with a fresh leach liquor and conducted by the standard procedure. This experiment was designed to determine if a product layer of elemental sulphur is deposited on the sphalerite particles and inhibits the rate of dissolution. If diffusion through a layer of elemental sulphur on the surface of the sphalerite particles controls the rate of dissolution, it was expected that the second stage of leaching would follow the dissolution curve projected from stage one. Since a sulphur layer formed on the sphalerite particles in stage one would not be removed and would be present at the start of stage two, it was expected that no increase in the rate of dissolution would occur at the start of the second stage. The resulting dissolution

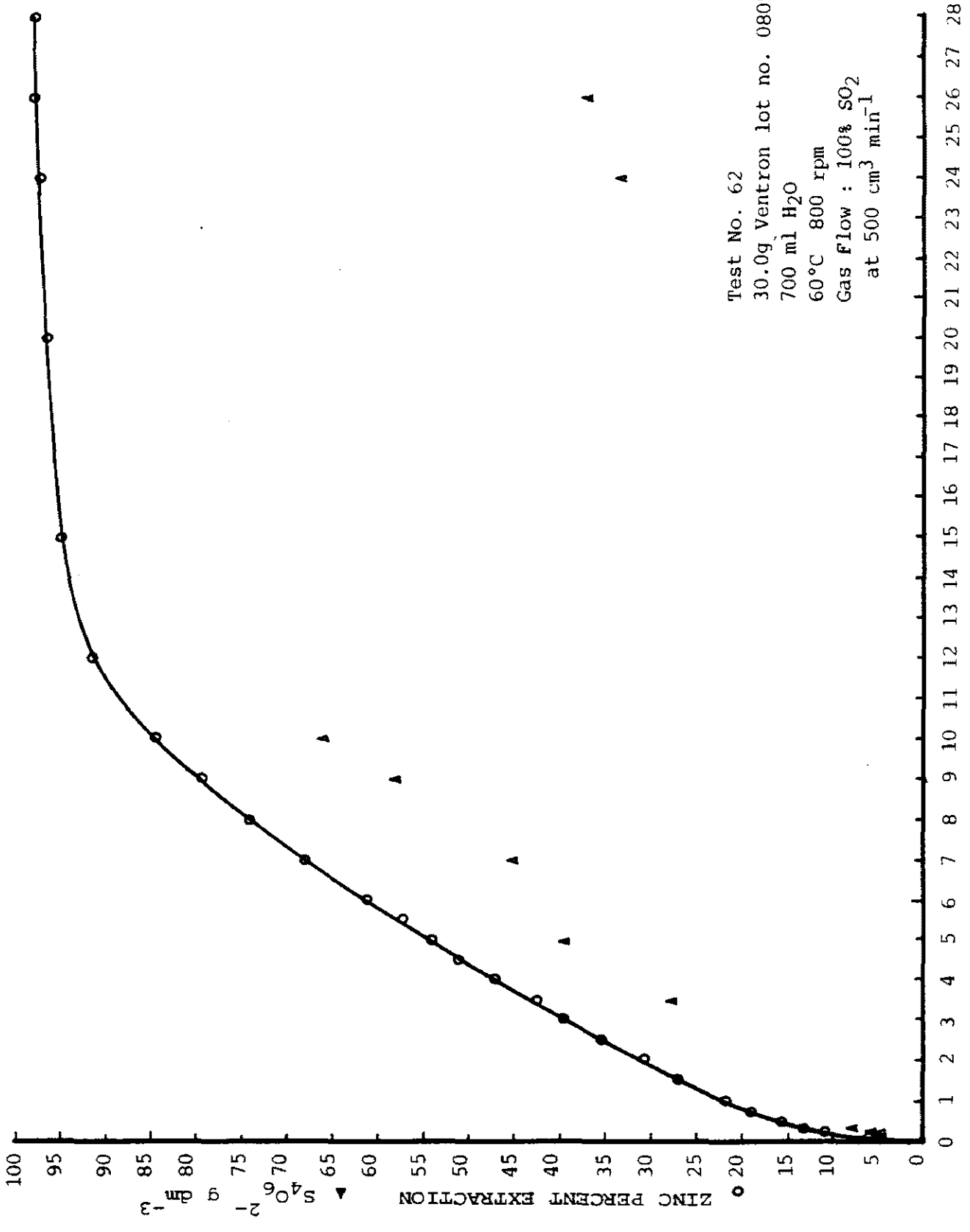

FIGURE 48. Dissolution of sphalerite in aqueous SO_2 media in the absence of dissolved iron.

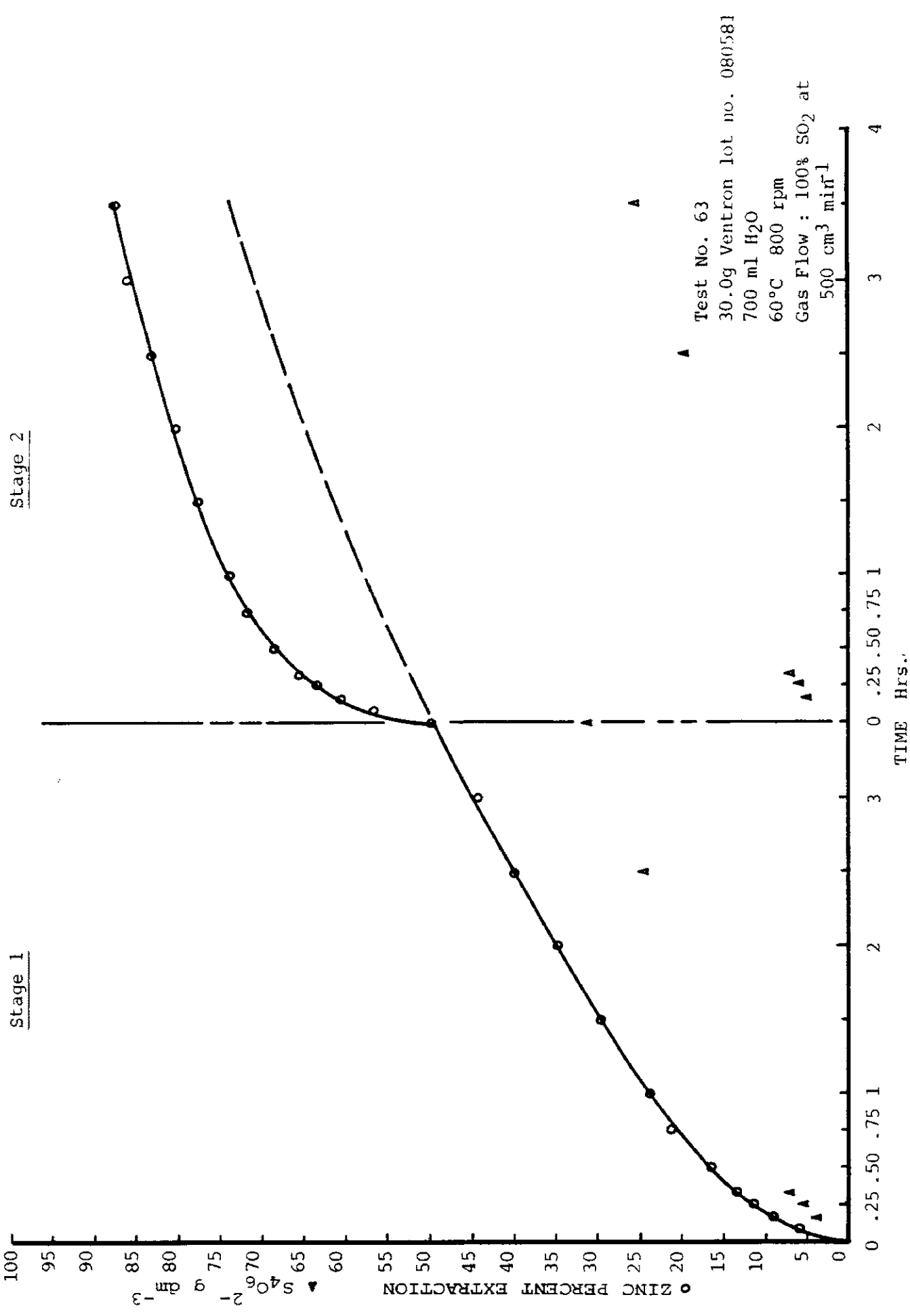

FIGURE 49. Two stage dissolution of sphalerite in aqueous SO_2 media in the absence of dissolved iron.

curves of both stage one and stage two are shown in Figure 49 along with the projected curve from stage one. Figure 49 also shows the concentration of the tetrathionate species as quantitatively analyzed during both stages.

Another two stage experiment, test no. 105, was conducted in a manner similar to test no. 63 shown in Figure 49 using the same experimental conditions. The second stage of test no. 105, however, was carried out in a fresh leach liquor to which zinc sulphate was added. The concentration of the Zn^{2+} ion at the start of stage two was equal to that measured at the end of stage one. It was found that very little additional dissolution of the sphalerite occurred in stage two. The kinetic data for test no. 105 is presented in Appendix 7.

A single experiment, test no. 128 was conducted to determine if dissolved nickel could have the same effect on the kinetics of dissolution as dissolved iron. The result of test no. 128, which is compiled in Appendix 7 with all of the experimental dissolution data, shows that dissolved nickel at a concentration of 4.0 g dm^{-3} has no effect on the rate of dissolution.

CHAPTER SIX

DISCUSSION OF THE KINETICS OF DISSOLUTION OF ZINC SULPHIDE IN AQUEOUS SULPHUROUS ACID

The review on the present knowledge of the leaching of sphalerite in Chapter Four highlights the numerous proposals by previous researchers for a mechanism to describe the kinetics of the sulphurous, ferric and sulphuric leaching systems. Several of these previous studies are built upon an experimental programme of limited scope and consequently many of the theories proposed diverge in premise. The aim of the present chapter is to shed more light on these proposed theories, elucidate the true active role of each component of the sulphurous acid leaching system and assess the kinetic aspects of the overall leaching process. The considerable body of experimental data presented in Chapter Five to describe the dissolution of sphalerite in aqueous sulphurous acid media will be used as the basis for this evaluation.

The experimental results are summarized in the convenient form of Tables and Figures in Chapter Five. The actual test number has been given with each result reported and these correspond to the complete set of experimental data compiled in Appendix 7. Approximately sixty preliminary experiments were carried out, during which ideas were formulated on what were the important aspects of the leaching process to be investigated. The experimentation sequence was altered several times from its original plan as the knowledge of the leaching system expanded during the experimentation. It is for this reason then, that the test numbers appear to be completely scattered when the results are assembled in a logical fashion as in Chapter Five. The discussion of the results in this chapter follows a logical sequence to the complete description of sulphurous acid dissolution of sphalerite

and refers to the appropriate set of experimental results presented in Chapter Five in evidence as required.

6.1 DISSOLUTION IN THE ABSENCE OF IRON

Table 20 presents a series of tests employing various SO_2/O_2 and SO_2/N_2 gas mixtures as the leaching reagent. Clearly, Table 20 demonstrates that the greater the partial pressure of sulphur dioxide employed (P_{SO_2}), the greater the rate of extraction. The corresponding kinetic plots presented in Figure 37 reveal that the rate of dissolution is identical whether oxygen or nitrogen is mixed with the sulphur dioxide. Therefore, oxygen, in the absence of dissolved iron, is not an active reagent in the dissolution process. This effect is further demonstrated in Figure 42 for a SO_2/O_2 and SO_2/N_2 mixture with added sulphuric acid. Both oxygen and nitrogen act only as a diluent of the sulphur dioxide gas. The rate of extraction is dependent upon the partial pressure of sulphur dioxide only and not the partial pressure of oxygen (or nitrogen). Although, as Table 20 shows, the Eh of the leach media increases as the oxygen content of reagent gas increases, oxygen does not act as an additional oxidizing agent in the leaching system.

Generally, two reaction paths have been proposed to describe the dissolution of sphalerite in aqueous sulphur dioxide media. The acid dissolution path can be described by the following reactions:

$$ZnS + 2H^+ = Zn^{2+} + H_2S \qquad (31)$$

$$SO_2 + 2H_2S = 2H_2O + 3S^\circ$$

where the second reaction is the sum of Reactions 44 and 47 of Appendix 1. As previously discussed in Chapter Two, Figure 13 demonstrates that Reaction 31 requires a high

acid concentration to occur to any appreciable extent. The injection of sulphur dioxide gas alone, or $SO_2/O_2/N_2$ gas mixtures under atmospheric pressure into the leach media, does not drive the pH low enough for this reaction sequence to occur to any great extent. As Table 20 shows, there is no visible evidence from the exit gas bubbler that hydrogen sulphide is being evolved from the reactor in any test using SO_2, SO_2/O_2 or SO_2/N_2 gases without added acid or iron. Thermodynamically, Figure 13 predicts that hydrogen sulphide should not be evolved since the acidity of the leach media is not great enough. Experimentally, there is no evidence that hydrogen sulphide is produced since elemental sulphur is not found in the leach residues or precipitated in the exit gas bubbler by the Wackenrhoder Reaction. Therefore, in the absence of added sulphuric acid, the acid dissolution of sphalerite in aqueous sulphurous does not appear to occur to any great extent.

Tiwari (1976) proposed the reaction sequence discussed above (acidic decomposition) for the dissolution of sphalerite in aqueous sulphur dioxide media. However, Tiwari carried out all of his experiments in the presence of added sulphuric acid. Table 26 along with Figures 42 and 43 present several tests employing SO_2/O_2 and SO_2/N_2 mixtures as the leachant with added sulphuric acid. It can be seen in Figures 42 and 43 that added acid accelerates the leaching reaction. Table 26 demonstrates that hydrogen sulphide is evolved from the reactor when sulphuric acid is an additional reagent, since elemental sulphur is precipitated in the exit gas bubbler. Therefore, in the case of added sulphuric acid, the acid dissolution path will become predominant, whereas, without the added acid it occurs only to a minor extent.

The second reaction path that has been proposed is the direct oxidation of zinc sulphide by the sulphur

dioxide, represented by:

$$ZnS = Zn^{2+} + S^\circ + 2e^- \quad (32)$$

$$\tfrac{1}{2}SO_2 + 2H^+ + 2e^- = \tfrac{1}{2}S^\circ + H_2O \quad (44)$$

The Eh and pH of the leach media recorded during the tests as shown in Table 20, fall in the proximity of Line 32 of Figure 13 where the ZnS and Zn^{2+} predominance areas meet within the elemental sulphur region. Also, since no hydrogen sulphide is detected as being generated in any experiment without added acid, it is probable that the reaction path predominating is the oxidative dissolution path. Both reaction paths given above, however, lead to the same overall reaction,

$$ZnS + \tfrac{1}{2}SO_2 + 2H^+ = Zn^{2+} + \tfrac{3}{2}S^\circ + H_2O \ .$$

The stoichiometry given above corresponds to the overall reaction proposed by Tiwari (1976). The elemental sulphur produced in this reaction was proposed by Tiwari to form a tenacious film of sulphur on the surface of the zinc sulphide particles and restrict the dissolution. The method used by Tiwari in his experimentation was quite different from the methods used in the present study. Tiwari did not use a continuous flow of reagent gas mixtures to the leaching vessel. Rather, Tiwari saturated the leach media with a particular SO_2/N_2 gas mixture and then the gas flow was ceased before the zinc sulphide was introduced to the leach media. Tiwari also added sulphuric acid to the leach solution used in his kinetic studies. Although the form of the experiments in the present study is different to that used by Tiwari (1976), an investigation was made to determine if a surface film of sulphur is formed on the zinc sulphide during leaching and if this product layer, if formed, contributes significant resistance to the dissolution process.

The residues of several of the tests presented in Table 20 were analysed by energy dispersive x-ray fluorescence spectrometry. Each residue, with up to 60 percent extraction, showed an assay that conformed to only zinc sulphide remaining in the leach residue without any additional elemental sulphur. Although no elemental sulphur could be detected in the leach residues, tests were carried out to determine if a sulphur product layer could be inhibiting the rate of dissolution.

Table 17 and Figure 33 present a series of tests at various impeller speeds using sulphur dioxide only as the leaching reagent. The identical kinetic dissolution curves obtained for low to high agitation indicates that the dissolution process is not controlled by mass transfer in the aqueous phase. Therefore, the rate of the dissolution process must be controlled either by the rate of the dissolution reaction or diffusion through a surface product layer.

Figure 47 presents a comparison of two tests employing sulphur dioxide only as the leachant. An organic solvent of sulphur, xylene, was added to the leach pulp in one of these two tests. If a layer of elemental sulphur is deposited on the surface of the sphalerite particles and restricts the dissolution kinetics, as proposed by Tiwari (1976), then the addition of the xylene would remove this sulphur layer and the rate of dissolution should increase. As shown in Figure 47, the rate of dissolution is essentially identical, both with and without the addition of the xylene. Therefore, this experiment demonstrates that a tenacious surface layer of elemental sulphur is not impeding the dissolution kinetics.

Figure 49 presents the results of a two stage leaching experiment also designed to test if a sulphur product layer is impeding the dissolution process. A sample of sphalerite was leached with sulphur dioxide until about 50 percent of

the material had reacted. The solid material remaining was then filtered from the leach media and releached in a fresh solution in a second stage of leaching. If a tenacious film of sulphur was formed on the sphalerite particles in stage one and impeded the rate of dissolution, then, this layer would be present at the start of stage two and the dissolution kinetics should follow the curve projected from stage one. As Figure 49 shows, the rate of dissolution at the start of stage two does not follow the curve projected from stage one but displays the same behaviour as at the start of stage one. This result is further evidence that the rate of dissolution of sphalerite in aqueous sulphurous acid media is not impeded by diffusion through a tenacious sulphur film deposited on the particle surface as proposed by Tiwari (1976). Furthermore, since the kinetic dissolution curve of stage 2 is very similar to stage 1, Figure 49 suggests that it is the rate of the dissolution reaction, and the products formed in the aqueous phase, that is controlling the kinetics of the leaching process.

The experimental results shown here, demonstrate that elemental sulphur is not being deposited on the sphalerite particles as a coherent tenacious film as a consequence of leaching in an aqueous pulp with sulphur dioxide. Furthermore, the analyses fail to show the production of any sulphur in the leach residue. Obviously, the sulphide component of the sphalerite in this type of leaching process must undergo a reaction and be produced in an elemental, aqueous or gaseous form. A more in depth investigation, therefore, was made on the thermodynamic principles developed in Chapter Two to explore the possible forms in which sulphur could be produced as a reaction product.

Figure 50 presents an Eh-pH diagram constructed at 25°C from the superimposition of Figures 4 and 6 of Chapter Two. As discussed in Chapter Two, Figures 4 and 6

are original diagrams developed by the author from experimental thermodynamic measurements (Figure 6) and the recently available thermodynamic data of Wagman, et al (1982). The incorporation of the metastable polythionate species into the Eh-pH diagram of the $Zn-S-SO_2-H_2O$ system has not been considered in the past. The reactions of Figure 50 also, have been extrapolated to elevated temperatures and the results are shown in Figures 51, 52 and 53. Since the bulk of the leaching test work was performed at 60°C, Figure 51 best describes the reaction products that should be formed in the leaching process under study.

Figure 51 shows that within the Eh and pH region, where the sulphur dioxide leaching of sphalerite occurs, lies a region of stability for the tetrathionate ion, $S_4O_6^{2-}$. Since the stable region of the tetrathionate species lies between the predominance areas of zinc sulphide and sulphur dioxide and is superimposed by the predominance area of the Zn^{2+} ion, Figure 51 predicts that the $S_4O_6^{2-}$ and Zn^{2+} species can be formed from a reaction between sphalerite and sulphur dioxide. Furthermore, Figure 51 demonstrates that in the absence of any strong oxidizing agents, the $S_4O_6^{2-}$ species may exist in the leach media as a metastable equilibrium species. Therefore, it has been shown by Figure 51 that it is theoretically possible that the tetrathionate ion may form as a product of the leaching process under study in preference to the formation of elemental sulphur. In order to test the validity of the thermodynamic predictions of Figure 51, it was necessary to devise a method for the quantitative analysis of the tetrathionate species in leach liquors. The analysis of polythionate mixtures, especially in the presence of sulphur dioxide, is a difficult task, but a method for the spectrophotometric estimation of tetrathionate in the presence of sulphur dioxide was developed from the work of Kelly, et al (1969) and Nietzel and DeSesa (1955). This analysis scheme is

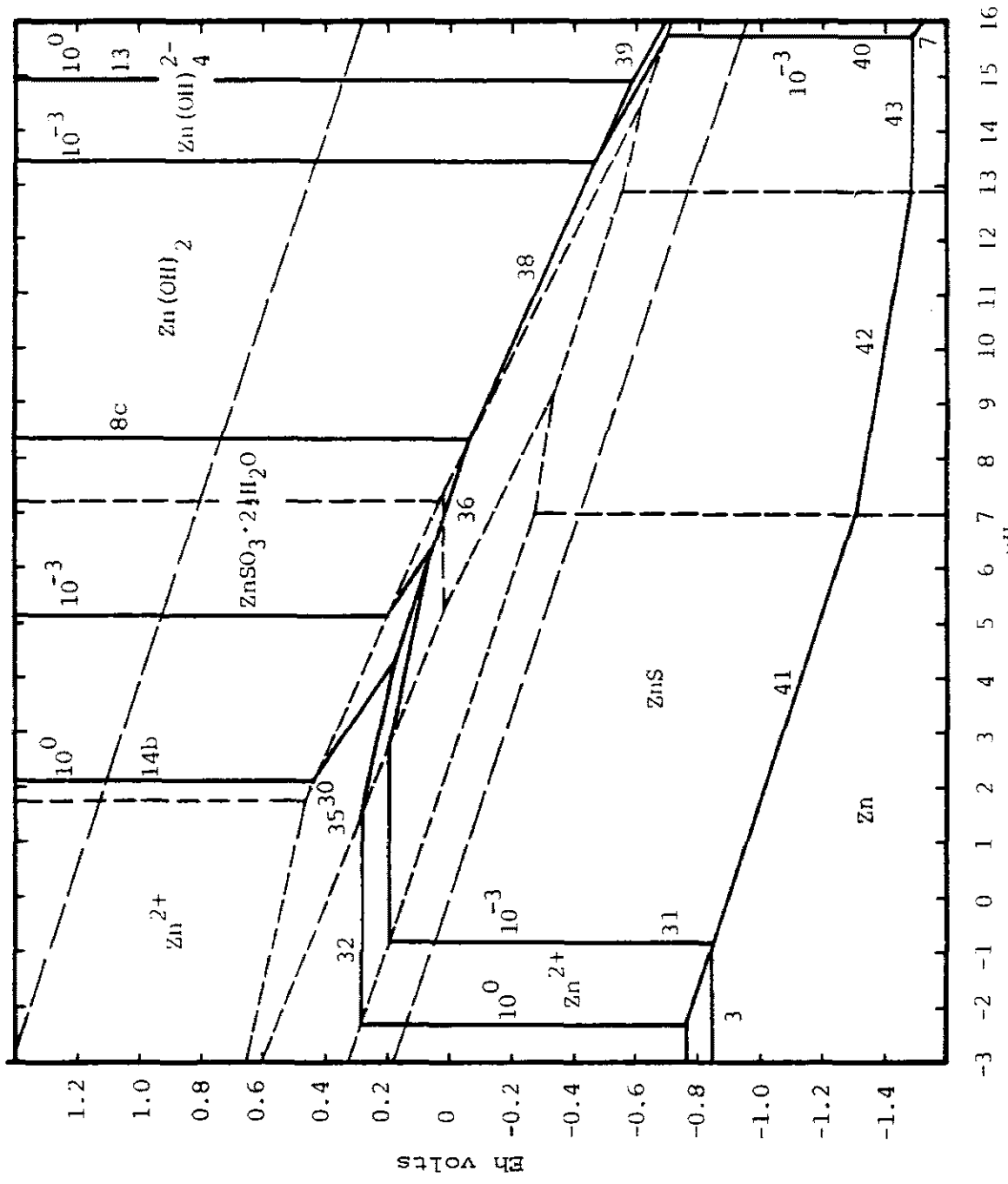

FIGURE 50. Potential -pH diagram of the Zn-S-SO_2-H_2O system at 25°C with polythionate species.

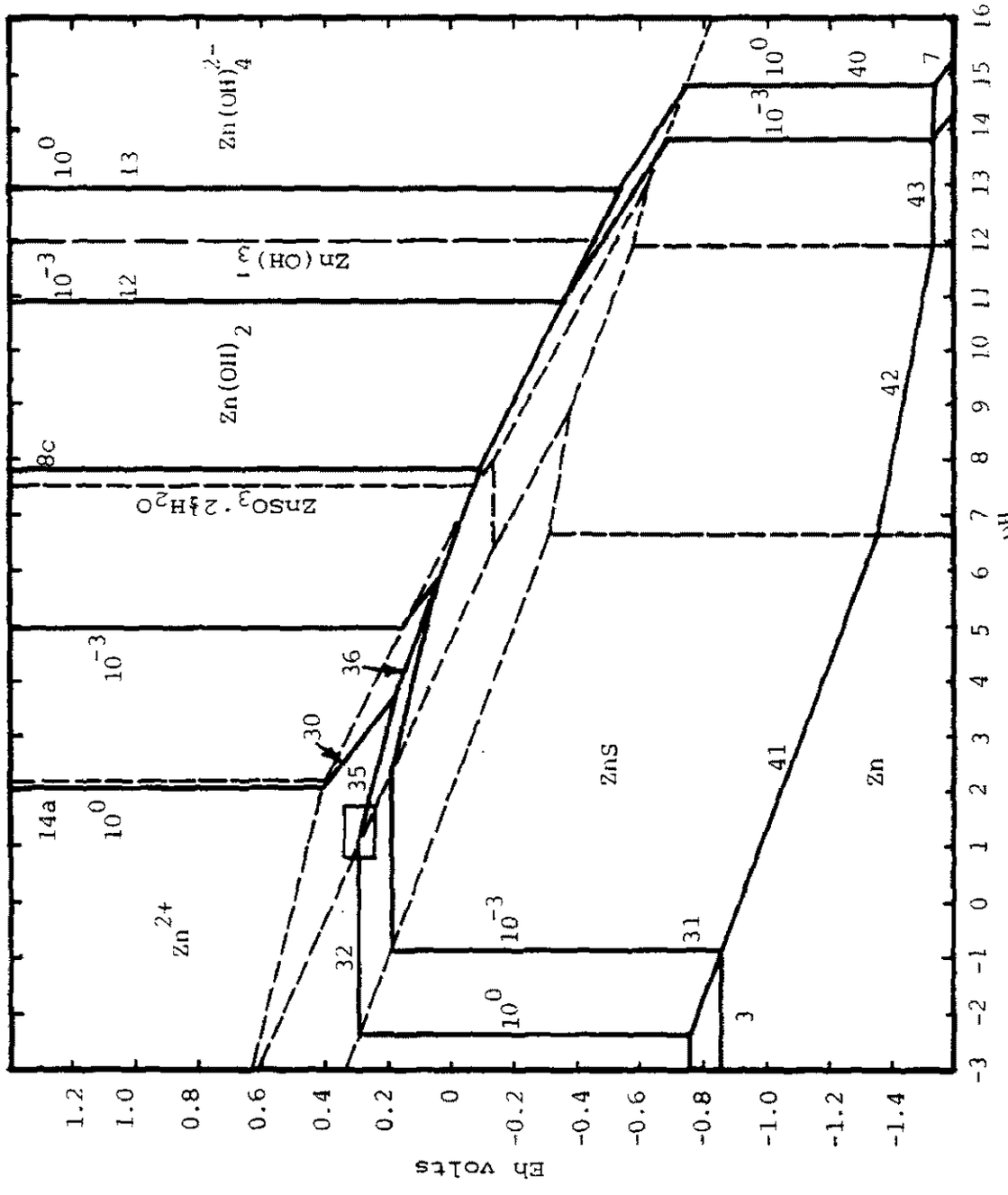

FIGURE 51 Potential -pH diagram of the Zn-S-SO_2-H_2O system at 60°C with polythionate species

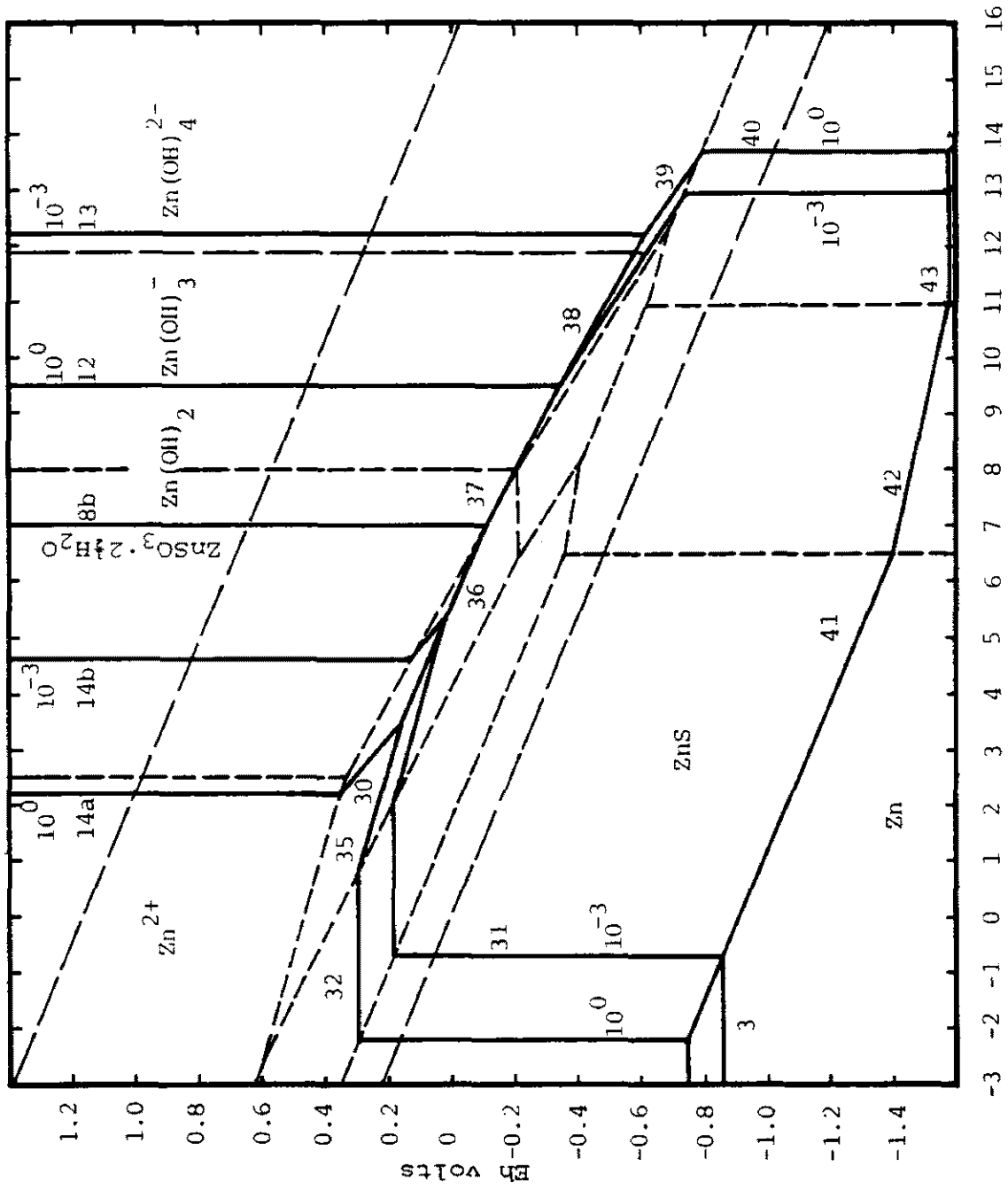

FIGURE 52. Potential -pH diagram of the Zn-S-SO_2-H_2O system at 100°C with polythionate species.

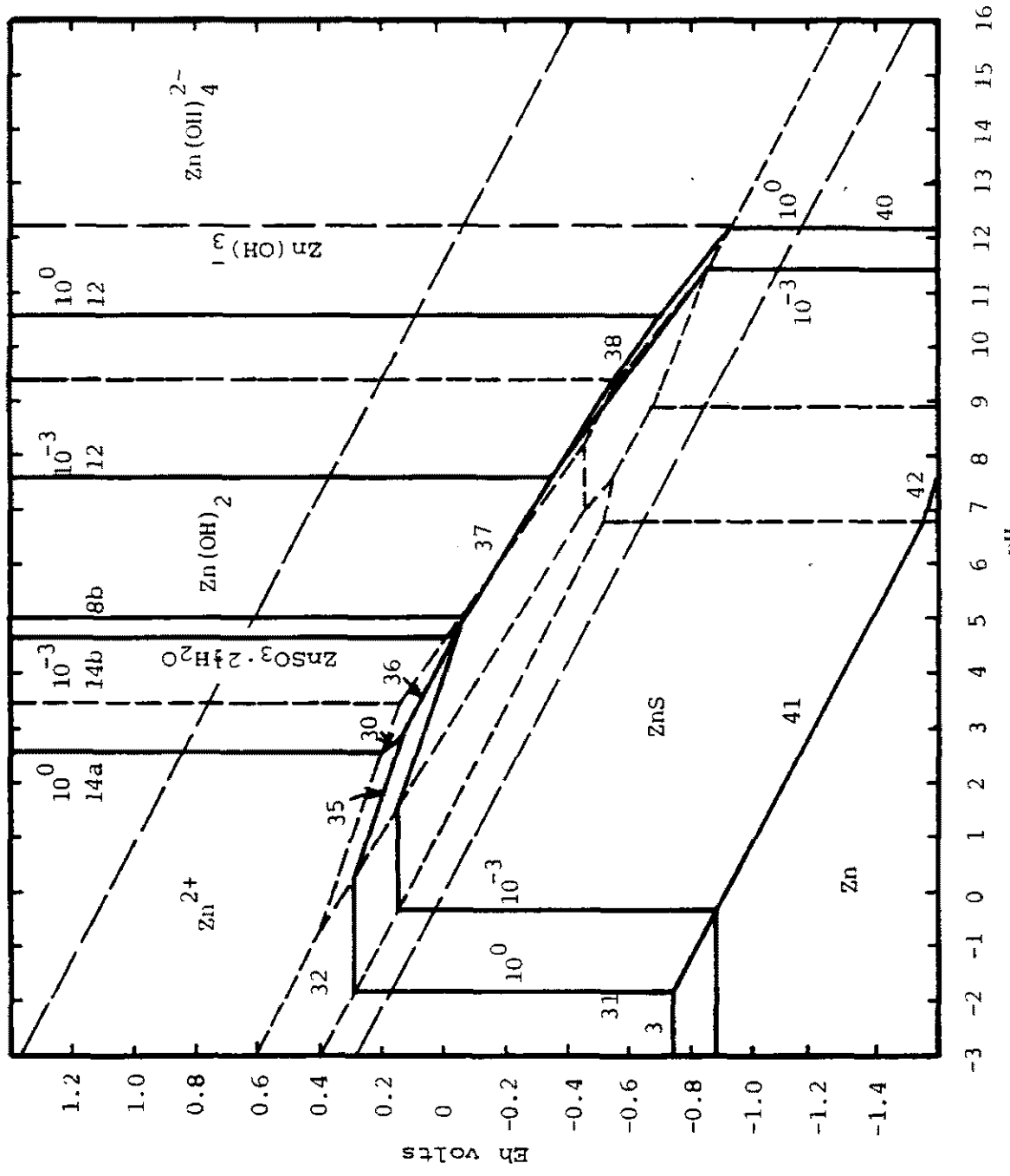

FIGURE 53. Potential -pH diagram of the Zn-S-SO_2-H_2O system at 200°C with polythionate species.

presented in detail in Appendix 5.3.

Figure 48 presents the results of a sulphur dioxide leaching test carried out over a 28 hour period to explore the formation of the tetrathionate species. The tetrathionate ion concentration was quantitatively measured throughout the duration of the test by the method described in Appendix 5.3. This information is plotted in Figure 48 along with the percent zinc extraction data. As Figure 48 shows, the tetrathionate species is formed in measurable quantities immediately at the start of the experiment and increases in concentration for at least 10 hours into the test. The greatest concentration of tetrathionate in the leach media was measured at 10 hours into the run as the percent zinc extraction was approaching 90 percent. The concentration of tetrathionate may have exceeded the 66 g dm^{-3} measured at 10 hours in the 10 to 15 hour time period. However, no analysis was made during this time interval. After 15 to 18 hours of leaching it became visually evident that elemental sulphur was being formed within the leaching reactor and was adhering to the reactor baffles. After 24 hours of leaching the tetrathionate concentration was again measured as the percent zinc extraction was approaching 100 percent. The tetrathionate concentration after 24 hours was found to have decreased to 34 g dm^{-3}, about one-half the value measured at 10 hours. In addition to the 28 hour test, tetrathionate is seen to form in all of the experiments involving sulphur dioxide as the sole reagent. Table 20 shows tetrathionate to be formed in all cases with SO_2/O_2 and SO_2/N_2 mixtures. The concentration $S_4O_6^{2-}$ measured at the end of a two hour leaching test is roughly proportional to the percent zinc extraction obtained. Furthermore, tetrathionate was seen to form in both the first and second stage of leaching in the two stage experiment shown in Figure 49. The levels of tetrathionate measured in the second stage compare very closely with those measured at the same time period in

the first stage.

The results presented above demonstrate conclusively that tetrathionate is a product of the dissolution reaction of sphalerite in a sulphur dioxide medium. Since it was concluded earlier that it is unlikely that sphalerite is decomposing by acidic dissolution in the presence of sulphur dioxide only, the leaching reactions must involve a direct oxidative decomposition of the sphalerite. Figure 51 elucidates the reactions which may be occurring. If sphalerite is being oxidized as already suggested by the reaction at Line 32,

$$ZnS = Zn^{2+} + S^{\circ} + 2e^{-} \quad , \qquad (32)$$

sulphur dioxide could be reducing to form the tetrathionate via the reaction at Line 61,

$$\tfrac{4}{3}SO_2 + \tfrac{4}{3}H^{+} + 2e^{-} = \tfrac{1}{3}S_4O_6^{2-} + \tfrac{2}{3}H_2O \quad . \qquad (61)$$

However, by the stoichiometry of Reaction 61 the maximum concentration of $S_4O_6^{2-}$ that could form is 33 g dm^{-3}. Since in several experiments tetrathionate concentrations well in excess of 33 g dm^{-3} and up to 66 g dm^{-3} were measured, it is likely that $S_4O_6^{2-}$ is being formed in some other reaction as well as Reaction 61. Furthermore, since no sulphur was detected as being formed until after 15 hours of leaching, it is likely that Reaction 32 is not occurring. From Figure 51 it can be seen that the two following reactions could be operative,

$$ZnS + \tfrac{3}{2}H_2O = Zn^{2+} + \tfrac{1}{4}S_4O_6^{2-} + 3H^{+} + \tfrac{9}{2}e^{-} \qquad (35)$$

$$3SO_2 + 3H^{+} + \tfrac{9}{2}e^{-} = \tfrac{3}{4}S_4O_6^{2-} + \tfrac{3}{2}H_2O \qquad (61)$$

where sphalerite decomposes by oxidation to form the Zn^{2+} and $S_4O_6^{2-}$ species at Line 35 in Figure 51. Sulphur dioxide functions as the oxidant in this process and is

consequently reduced to $S_4O_6^{2-}$ at Line 61. By the stoichiometry of Reactions 35 and 61, a maximum $S_4O_6^{2-}$ concentration of 99 g dm^{-3} could be formed in the leach media. Additionally, no elemental sulphur is formed via Reactions 35 and 61. Thus, the 28 hour leaching test (test no. 62) and those tests given in Table 20 substantiate that sphalerite is decomposing in a sulphur dioxide medium via Reactions 35 and 61. Furthermore, shown in Figure 51 is a small rectangle surrounding a segment of Line 35 near the intersection of Line 32 and Line 35. All of the Eh and pH values, measured in the leach media during all tests with the use of sulphur dioxide only, fall within this rectangular region. This indicates that the media Eh is being controlled by Reaction 35 and that Reaction 35 is the predominating reaction.

The experimental evidence demonstrates conclusively that the tetrathionate ion ($S_4O_6^{2-}$) is the primary sulphur product of the direct oxidation of sphalerite by sulphur dioxide in the short term (at least up to 10 hours leaching). After extended time periods (more than 15 to 18 hours), elemental sulphur is formed within the leaching medium. Since elemental sulphur is one of the ultimately stable states of sulphur, thermodynamic considerations predict that elemental sulphur must eventually be formed, as was observed within the leach medium. There are a number of reactions which could contribute to the observed formation of elemental sulphur. One possibility is that in the final stages of leaching, Reaction 63 could be working in conjunction with or replacing Reaction 61.

$$S_4O_6^{2-} + 12H^+ + 10e^- = 4S^\circ + 6H_2O \qquad (63)$$

The tetrathionate ion in this reaction is acting as an oxidant and is being reduced to elemental sulphur. The other and more probable possibility is that the

tetrathionate ion could be disproportionating to elemental sulphur and sulphur dioxide by the reaction

$$2S_4O_6^{2-} + 4H^+ = 3S^\circ + 2H_2O + 5SO_2$$

which is the sum of Reactions 61 and 44 of Appendix 1.

Overall, the dissolution reaction of zinc sulphide in a sulphur dioxide media by any of the reaction paths discussed in this section ultimately adds up to be

$$ZnS + \tfrac{1}{2}SO_2 + 2H^+ = Zn^{2+} + \tfrac{3}{2}S^\circ + H_2O$$

which is the reaction proposed by Tiwari (1976). Tiwari in his work, however, generalized from his limited experimental results to conclude that elemental sulphur was the primary dissolution reaction product. It was found in this work that elemental sulphur is not an immediate reaction product and does not contribute a controlling factor to the dissolution kinetics. Furthermore, it was found that the tetrathionate ion is formed as the primary product of the oxidation of sphalerite by sulphur dioxide and that elemental sulphur is formed only at extended time periods as the leaching reaction is reaching completion.

The experimental evidence for the formation of the tetrathionate ion, together with the experimentally measured media potentials and pH values being in agreement with Line 35 of Figure 51, demonstrates a very good correlation between the theoretical thermodynamic fundamentals and actual experimental observations. The thermodynamic diagrams developed in this work are based on the experimental solubility measurements in the zinc sulphite system and the available thermodynamic data. Pourbaix diagrams were then constructed from this data for the $Zn-S-SO_2-H_2O$ system and the metastable $S-H_2O$ system. Superimposing these two systems and extending

the calculations to elevated temperatures led to the development of the hybrid diagram of the $Zn-S-SO_2-H_2O$ system with the polythionate species shown in Figure 51. It was predicted with the aid of Figure 51 that the tetrathionate species should be a product of the dissolution of sphalerite in a sulphur dioxide medium. Subsequently, it was experimentally found, as expected, that the tetrathionate species was formed as the primary sulphur product in the dissolution reaction.

6.2 DISSOLUTION WITH $SO_2/O_2/N_2$ GAS MIXTURES IN THE PRESENCE OF IRON

Naturally occurring ores of sphalerite inherently contain significant quantities of iron. This impurity iron can occur both in the form of non-liberated iron sulphides, such as pyrite or pyrrhotite, and substitutional iron atoms within the sphalerite lattice. It was found in the preliminary experimentation that the addition of a soluble iron salt to an iron-free sulphur dioxide leach medium can greatly increase the rate of dissolution of synthetic zinc sulphide. Most of the leaching studies by previous researchers, as shown in Table 15, have been performed on zinc sulphide concentrates or in ferric sulphate leach liquors. Various dissolution mechanisms have been proposed in these previous studies to explain the role of iron in the leaching process [Verhulst (1974), Scott and Nicol (1978), Verbaan (1980) and Adams and Matthew (1981)] but none have been supported by a great deal of experimental evidence. Scott and Nicol (1978) conclude that more extensive investigations with synthetic materials of controlled composition and structure are necessary before the mechanisms can be established more firmly. The present discussion of the experimental work is aimed at elucidating the actual function of iron in sulphur dioxide leaching systems.

Table 21 and Figure 38 demonstrate the effect of adding ferric ion to sulphurous acid leach media as compared to Figure 37 in the absence of any iron. As Figure 38 shows, the addition of ferric ion to a leach medium using a SO_2/N_2 reactant gas mixture has little effect on the dissolution kinetics. However, the addition of ferric ion to a SO_2/O_2 leach media leads to a dramatic increase in the rate of leaching by comparison with Figure 37. Hence, it is obvious from Figure 38 that the combination of a SO_2/O_2 gas mixture with the addition of soluble iron is required to obtain the highest rate of leaching. This is in direct contrast to the result obtained in the absence of iron where oxygen functions only as a diluent of the sulphur dioxide gas. Generally, two schools of thought have been progressively developed by previous researchers to explain the role of iron in studies using ferric leach media. These two proposed dissolution processes are acidic dissolution and direct oxidative dissolution.

The acidic dissolution of sphalerite in an acidic ferric sulphate media has been proposed to proceed by the following reactions,

$$ZnS + 2H^+ = Zn^{2+} + H_2S \qquad (31)$$

$$H_2S + 2Fe^{3+} = S^\circ + 2Fe^{2+} + 2H^+ \ .$$

As previously discussed, Reaction 31 requires a strong acid concentration. However, in ferric sulphate media, the hydrogen sulphide produced in Reaction 31 will be oxidized by the ferric ion. The removal of the hydrogen sulphide from the leach media would pull the equilibrium of Reaction 31 to the right and increase the rate of dissolution. This principle is also shown through the rate expression developed by Romankiw and de Bruyn (1964). The above mechanism was supported by Verhulst (1974), who studied the kinetics of oxidation of hydrogen sulphide by

ferric iron and Scott and Nicol (1978), who studied the leaching of sphalerite concentrates in acidic solutions of ferric sulphate.

Verbaan (1980), who followed up the study of Scott and Nicol, presented evidence for the occurrence of direct oxidative dissolution of sphalerite concentrates in acidic ferric sulphate media. The dissolution via this mechanism occurs by the following two half-cell reactions,

$$\text{Anodic:} \qquad ZnS = Zn^{2+} + S^{\circ} + 2e^{-} \qquad (32)$$

$$\text{Cathodic:} \qquad Fe^{3+} + e^{-} = Fe^{2+}$$

The discharge of the Fe^{3+} ion to Fe^{2+} acts as the oxidant in the type of system studied by these researchers. Verbaan supported this mechanism on the basis of the close correlation he found between the initial rate of dissolution and the measured media potential which is controlled by the Fe^{3+}/Fe^{2+} couple. The direct oxidative dissolution mechanism requires the sphalerite to be conductive. Pawlek (1969) discussed some conductivity concepts with regard to the oxygen pressure leaching of sphalerite and concluded, as Scott and Nicol (1978), that both oxidative and non-oxidative processes are operative.

The oxidation of ferrous iron to ferric iron by mixtures of sulphur dioxide and oxygen in aqueous solution, accompanied by the oxidation of sulphur dioxide to sulphuric acid, has been known for some time. Keyes (1946) and Karraker (1963) investigated this so called "autoxidation process" for the production of sulphuric acid from sulphur dioxide. More recently, Tiwari, et al (1979) studied the oxidation of ferrous sulphate by a mixture of sulphur dioxide and oxygen in solution. The autocatalytic oxidation of ferrous iron by SO_2/O_2 gas

mixtures was found to proceed by the reaction,

$$2Fe^{2+} + SO_2 + O_2 = 2Fe^{3+} + SO_4^{2-} \quad .$$

The oxidation reaction is accompanied by a parallel and simultaneous reaction catalyzed by iron,

$$2SO_2 + O_2 + 2H_2O \xrightarrow{Fe^{3+}} 2\ H_2SO_4$$

which produces sulphuric acid in the leach media. However, an excess of sulphur dioxide over the stoichiometry given in the above reactions leads to the reduction of ferric iron by the following reaction,

$$2Fe^{3+} + SO_2 + 2H_2O = 2Fe^{2+} + SO_4^{2-} + 4H^+ \quad .$$

Therefore, if the leaching of zinc sulphide proceeds by reaction with the ferric ion as in either of the mechanisms discussed above, then, in the presence of SO_2/O_2 mixtures of the appropriate composition, it should be possible to regenerate the ferric ion for further reaction. Also, the regeneration of ferric iron should be accompanied by the production of sulphuric acid. This idea was suggested by Adams and Matthew (1981) who studied the leaching of sphalerite concentrates by sulphur dioxide and oxygen. However, no attempt was made to unravel the role of the iron in their experimental investigation. In light of these previous leaching studies, the present experimental programme is designed to investigate the role of each of the reactants in this leaching system (i.e., ZnS, SO_2, O_2 and Fe(aq)) and elucidate which mechanisms are active under various conditions.

6.2.1 SO_2/N_2 Mixtures in the Presence of Iron

The addition of the soluble salt, ferrous sulphate, to a leaching test with a SO_2/N_2 mixture has no effect upon the leaching performance. As seen by a comparison of test no. 82 (Table 20) with test no. 88 (Table 24), the same result is obtained both with and without ferrous iron added to a test using a 10% SO_2/N_2 mixture. However, the addition of ferric sulphate, which is soluble in sulphurous acid media, to tests using SO_2/N_2 gas mixtures leads to a small but significant increase in the rate of dissolution. This result is clearly seen by comparing the lower portion of Table 20 to that of Table 21. The reason for this behaviour can be deduced from the overlay to Figure 38. This overlay shows the Eh trace recorded during the experiment. The media Eh at the start of the tests with SO_2/N_2 mixtures is initially high in the range of 650 mV to 700 mV. As soon as the sphalerite is charged to the reactor, the Eh rapidly drops indicating that the Fe^{3+} in solution is being converted to Fe^{2+}. Some time later in the test, the Eh attains a value in the 220 mV to 250 mV region indicating that all the Fe^{3+} has been converted to Fe^{2+}. This is confirmed by the ferrous iron analysis given for test no. 93 in Table 24 which shows all the iron to be in the ferrous state.

Initially, in a test with ferric iron added, the dissolution could be occurring by the direct oxidative decomposition of the sphalerite with the reduction of Fe^{3+} to Fe^{2+}. Superimposed on this, leaching is probably also proceeding by the mechanism described in the previous section for dissolution in the absence of iron. This mechanism then continues after the Fe^{3+} ion supply is exhausted. In all cases when there is only Fe^{2+} present, the media Eh has a value in the 220 mV to 265 mV range which corresponds to that observed for studies made in the absence of iron. In those tests where Fe^{3+} was initially added, a small amount of elemental sulphur could be seen

adhering to the reactor baffles at the end of the run. This also indicates that some dissolution has occurred by direct oxidative dissolution. The tests shown in Table 21 performed with 100% SO_2 or SO_2/N_2 mixtures show that significant concentrations of tetrathionate ion are formed in the leach media. This indicates that the sphalerite has been undergoing decomposition by Reaction 35:

$$ZnS + \tfrac{3}{2}H_2O = Zn^{2+} + \tfrac{1}{4}S_4O_6^{2-} + 3H^+ + \tfrac{9}{2}e^- \quad . \qquad (35)$$

Therefore, the leaching of sphalerite by SO_2/N_2 mixtures in the presence of Fe^{2+} proceeds via the same mechanism as in the absence of iron. The presence of Fe^{3+} increases the extraction to a limited extent due to the additional direct oxidation of the sphalerite by the ferric ion.

Since there is no evidence from the exit gas bubbler that hydrogen sulphide has formed in any experiment using SO_2/N_2 gas mixtures in the presence of dissolved iron, it is reasonable to conclude that the acidic dissolution mechanism is inactive. Additionally, the fact that very little free sulphuric acid is present in the leach media with SO_2/N_2 gas mixtures, as shown in Table 21, would suggest that the acidic dissolution mechanism is not relevant under these leaching conditions.

6.2.2 $SO_2/O_2/N_2$ Mixtures in the Presence of Iron

Table 21 together with Figure 38 demonstrate the dramatic increase in the overall rate of dissolution obtained when soluble iron is added to the leach media where SO_2/O_2 gas mixtures are injected. Furthermore, Table 24 demonstrates that this high rate of leaching is obtained whether iron is added in the form of ferrous or ferric sulphate. The Eh trace overlay to Figure 38 shows that with the three reagents SO_2, O_2 and iron present,

the media attains, in most cases, a high potential in the region of 650 mV to 700 mV. The high media Eh indicates that the Fe^{3+}/Fe^{2+} electrochemical couple is active and maintaining a large oxidizing potential in the leach media. If the ferric ion is acting as an oxidant in the system, and is reduced to the ferrous state, then the ferric ion is being regenerated through the autoxidation reaction,

$$2Fe^{2+} + SO_2 + O_2 = 2Fe^{3+} + SO_4^{2-}$$

since the media Eh remains high throughout the tests.

Tables 21, 22 and 23 show that in all cases the leaching of sphalerite, with gas mixtures containing both sulphur dioxide and oxygen in the presence of iron, leads to the generation of significant concentrations (30 to 130 g dm^{-3}) of sulphuric acid. The free sulphuric acid data, listed in these Tables, were obtained by analysis at the conclusion of a two hour leaching test, using the method described in Appendix 5.4. As indicated, the maximum concentration of acid produced during a leaching test occurs with gas compositions of around 50% SO_2/O_2. The amount of acid produced, as shown in Table 21, increases with an increasing SO_2/O_2 ratio up to 0.5 and decreases at the high SO_2/O_2 ratios. The production of sulphuric acid within the leach media is further evidence that the autoxidation process is active and the ferric ion present is catalyzing the production of acid by the reaction,

$$2SO_2 + O_2 + 2H_2O \xrightarrow{Fe^{3+}} 2H_2SO_4 \ .$$

Several of the tests presented in Tables 21, 22 and 23 show that elemental sulphur was precipitated in the exit gas bubbler. This is evidence that hydrogen sulphide was generated in the leaching reaction and swept out of the reactor by the flow of gases to be oxidized, with sulphur dioxide in the exit bubbler, by the Wackenrhoder reaction:

$$SO_2 + H_2S = S^\circ + H_2O \quad .$$

Therefore, it is apparent that the sulphuric acid produced in the autoxidation process causes acidic dissolution of the sphalerite by Reaction 31

$$ZnS + 2H^+ = Zn^{2+} + H_2S \quad . \qquad (31)$$

The observations made of the solution in the exit gas bubbler are shown in the last column of Table 21. Consequently, as shown in Table 21, hydrogen sulphide is produced in the dissolution reaction and swept out of the reactor in tests using SO_2/O_2 mixtures from 5 to 50% sulphur dioxide.

Tiwari, et al (1979), in their study of the oxidation of ferrous sulphate in acid solution by a mixture of sulphur dioxide and oxygen, make three points relevant to the present study. Firstly, the greatest rate of ferrous ion oxidation by SO_2/O_2 mixtures (at 72°C) occurs with a 3.8% SO_2/O_2 mixture. Secondly, a given SO_2/O_2 ratio establishes in solution an equilibrium Fe^{3+}/Fe^{2+} ratio. The greater the SO_2/O_2 mixture, the lower the Fe^{3+}/Fe^{2+} ratio. The third point is that the rate of sulphuric acid production is greater using a SO_2/O_2 mixture rather than the same SO_2/air mixture. These authors, however, did not study the rate of H_2SO_4 production as a function of the sulphur dioxide partial pressure.

The Eh overlay sheets on Figures 38 and 39 show how the media potential varies with time for each test presented in these figures. The Eh values recorded, for those tests using a SO_2/O_2 ratio at the low end of the composition range, indicate that the Fe^{3+}/Fe^{2+} ratio in the leach media is high. This is also confirmed by the ferrous iron analyses given in Tables 21 and 22. The high Fe^{3+}/Fe^{2+} ratios obtained for the low SO_2/O_2 ratios, are in

agreement with the observation of Tiwari, et al (1979) that the highest rate of Fe^{2+} oxidation was obtained with a low (3.8% SO_2) SO_2/O_2 gas mixture. As seen in the overlay sheet on Figure 38 for the low SO_2/O_2 ratios ranging from 5% to 30% SO_2, the media Eh attains a value in the 650 mV to 700 mV region shortly after the start of the run. The Eh throughout these tests remains at this level, indicating that the iron is predominantly in the ferric state. At a 50% SO_2/O_2 mixture, the Eh initially drops at the start of the experiment but regains a high value toward the end of the run. Above a 50% SO_2/O_2 gas mixture, the Eh is less than about 500 mV indicating that a low Fe^{3+}/Fe^{2+} ratio is established. This experimental observation confirms the proposal of Tiwari, et al (1979) that a high SO_2/O_2 ratio tends to be reducing to the ferric ion by the reaction,

$$2Fe^{3+} + SO_2 + 2H_2O = 2Fe^{2+} + SO_4^{2-} + 4H^+ .$$

At 100% SO_2, the low Eh indicates that essentially all of the iron is in the ferrous state. The media Eh in this case no longer appears to be controlled by the Fe^{3+}/Fe^{2+} couple but by the interaction of sulphur dioxide with the zinc sulphide as in the case without iron present. Therefore, it is seen in the present work that a given SO_2/O_2 ratio establishes in the leach solution a particular Fe^{3+}/Fe^{2+} ratio as was proposed by Tiwari, et al (1979). The Fe^{3+}/Fe^{2+} ratio is the greatest at the low SO_2/O_2 ratios at the low end of the range and decreases as the proportion of sulphur dioxide is increased.

Since the Fe^{3+}/Fe^{2+} ratio is the greatest when leaching is carried out with gas mixtures of low SO_2/O_2 ratio, the oxidizing potential of the Fe^{3+}/Fe^{2+} electrochemical couple is the greatest with these low SO_2/O_2 ratios. However, it is clearly shown in Table 21 and Table 23 that hydrogen sulphide is evolved from the dissolution of the sphalerite and swept out of the reactor

when leaching is carried out with mixtures of a low SO_2/O_2 ratio. Therefore, for a concentration of 3.6 g dm^{-3} total dissolved iron present, the rate of the reaction

$$H_2S + 2Fe^{3+} = S^\circ + 2Fe^{2+} + 2H^+$$

is not great enough to completely oxidize all of the hydrogen sulphide as it is generated when the Fe^{3+}/Fe^{2+} ratio is the greatest. Also by the same reasoning, since copious quantities of hydrogen sulphide are being produced under conditions which yield the highest Fe^{3+}/Fe^{2+} ratio (or oxidizing potential), the zinc sulphide is dissolving by a non-oxidative mechanism and therefore, very little decomposition by direct oxidation is occurring. Although no attempt was made to quantitatively analyse the hydrogen sulphide evolved from the leaching reactor, it appears that the ferric ion is acting neither to directly oxidize the zinc sulphide nor to rapidly oxidize in-situ the hydrogen sulphide generated from the acid decomposition of the sphalerite.

In summary then, for low SO_2/O_2 gas mixtures, the sulphuric acid produced through the autoxidation process leads to the acidic decomposition of sphalerite by Reaction 31

$$ZnS + 2H^+ = Zn^{2+} + H_2S \qquad (31)$$

with the accompanying production of hydrogen sulphide. The Eh or media potential observed is the greatest at the low end of the range of SO_2/O_2 gas ratios. This shows that under the conditions which yield the greatest Fe^{3+}/Fe^{2+} ratios, the Fe^{3+} ion, at a total iron concentration of 3.6 g dm^{-3}, cannot oxidize the hydrogen sulphide produced from the non-oxidative decomposition rapidly enough to prevent it from being swept out of the reactor. Therefore, the ferric ion, at a total iron concentration of

3.6 g dm^{-3}, is not an effective in-situ oxidant of hydrogen sulphide nor is it acting directly as an oxidant of zinc sulphide.

The form or oxidation state of the dissolved iron, from the foregoing discussion has an obvious effect on the dissolution mechanism of sphalerite in aqueous sulphurous acid. Consequently, it is pertinent to consider the formation of aqueous complexes of ferrous and ferric iron in a sulphurous acid medium. Kao (1979) in his electrochemical study of the iron sulphite system, proposed the formation of sulphite complexes of iron in solutions reacted with SO_2/O_2 gas mixtures. Kao electrochemically measured and reported formation constants for the following iron sulphite species: $FeHSO_3^{2+}$, $FeSO_3^{+}$, $FeHSO_3^{+}$ and $FeSO_3^{o}$. The free energy of formation, calculated from the formation constants given by Kao, for each of these complex ions are presented in Table 5 (Chapter Two). Also, Table 5 gives the free energy of formation of crystalline iron sulphite, $FeSO_3.3H_2O$, determined experimentally from solubility experiments similar to those described in Chapter Three for zinc sulphite. Figure 54 presents a Pourbaix diagram of the $Fe-S-SO_2-H_2O$ system at 25°C which was developed from the thermodynamic data compiled in Table 5. An Eh-pH diagram of the type presented in Figure 54 is previously unpublished.

Figure 54 shows that in a sulphurous acid medium dissolved iron should in fact, as proposed by Kao (1979), form several aqueous complex sulphite species. Furthermore, Figure 54 shows that in the pH range of about 0 to 2, dissolved iron, in a sulphurous medium, will be present in the form of the $FeHSO_3^{2+}$ and $FeHSO_3^{+}$ complexes rather than the Fe^{3+} and Fe^{2+} ions, respectively. Figure 54, however, is drawn at a total sulphite activity of 1.0 mol dm^{-3}. At a lower sulphite activity, the $Fe^{3+}/FeHSO_3^{2+}$ boundary is shifted toward the right. This is shown in Figure 54 by the bold broken line which represents the $Fe^{3+}/FeHSO_3^{2+}$ and $Fe^{2+}/FeHSO_3^{+}$ boundaries at a total sulphite activity

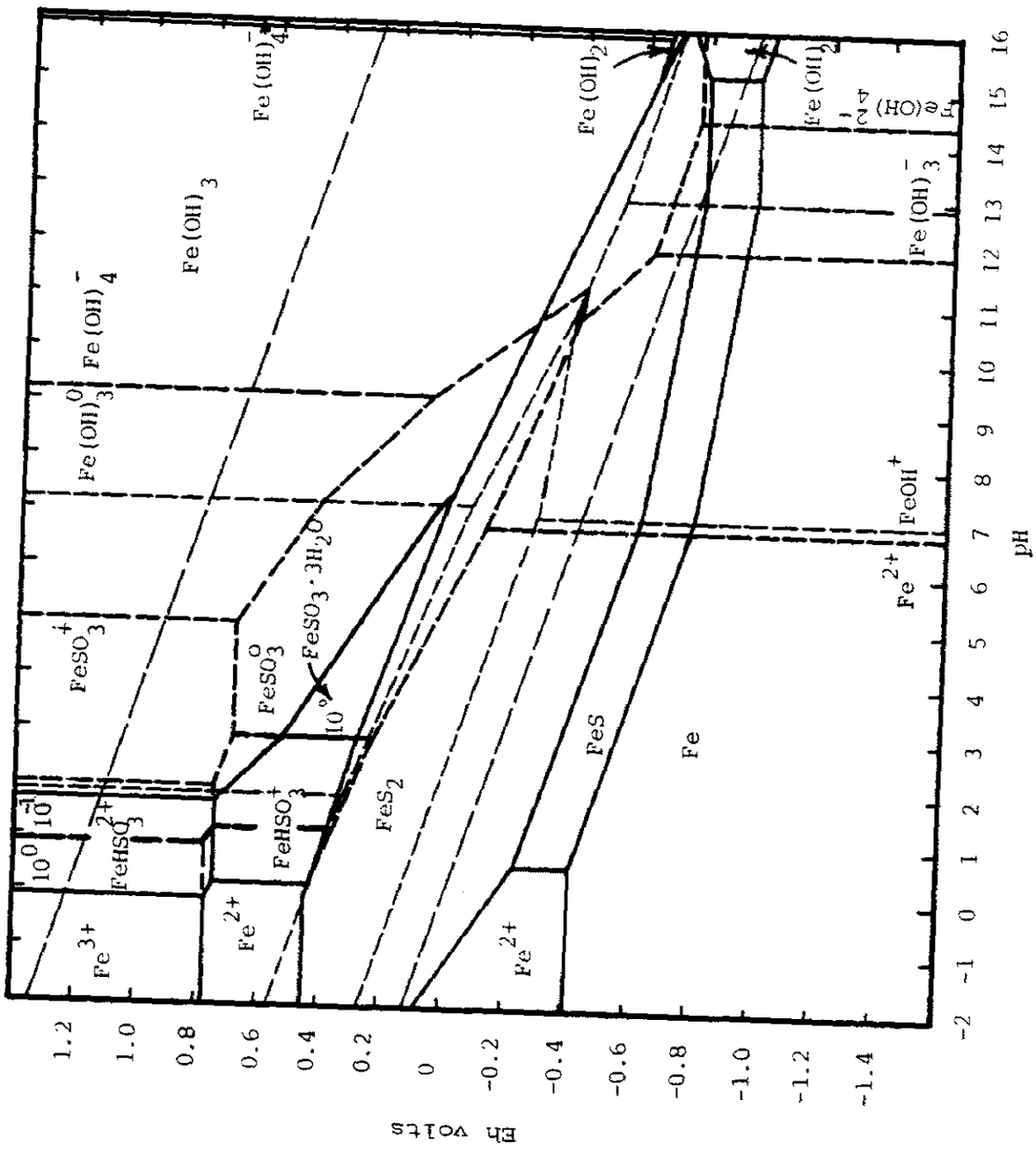

FIGURE 54. Potential -pH diagram of the Fe-S-SO_2-H_2O system at 25°C.

of 0.1 mol dm^{-3}. Therefore, Figure 54 demonstrates that within the range of pH measured in the leaching tests, the dissolved iron species will actually be present as the complex ions, $FeHSO_3^{2+}$ and $FeHSO_3^{+}$, if the aqueous sulphur dioxide concentration is greater than about 0.05 mol dm^{-3}. Below this concentration the dissolved iron will be present as the Fe^{3+} and Fe^{2+} ions.

Tables 21, 22 and 23 show that in leaching with SO_2/O_2 or $SO_2/O_2/N_2$ gas mixtures in the presence of iron, there is a significant increase in the concentration of aqueous sulphur dioxide, in the leach media, when the partial pressure of the sulphur dioxide in the gas mixture is greater than about 0.5 atm. The aqueous sulphur dioxide concentrations presented in Tables 21, 22 and 23 were measured at the conclusion of the two hour leaching tests by the analysis method given in Appendix 5.2. Table 30 presents some additional experimental data on the aqueous sulphur dioxide concentrations present and the quantity of sulphuric acid produced in the leach media. This data was obtained by analysing the leach media before the zinc sulphide was charged to the reactor in the standard start-up procedure described in Section 5.2.1. Table 30, then gives the conditions present in the leach media at the start of each of the tests given in Table 21. As in Tables 21, 22 and 23, Table 30 shows also that there is a significant increase in the concentration of aqueous sulphur dioxide present in the leach media with a sulphur dioxide partial pressure greater than 0.5 atm. Also, the sulphuric acid production increases with an increase in the SO_2/O_2 ratio to a maximum at 50% SO_2/O_2. At a high SO_2/O_2 ratio, the sulphuric acid production decreases. Therefore, Table 30 directly confirms the results given in Table 21. Further evidence of the sulphur dioxide concentration in the leach media was given by its smell. The odour of sulphur dioxide could be detected in the leaching media at the end of a test only when the SO_2/O_2 ratio was greater than 0.5.

TABLE 30

SULPHURIC ACID PRODUCTION WITH SO_2/O_2 MIXTURES IN THE PRESENCE OF IRON

Conditions: 60°C, 800 rpm, 3.6 g dm^{-3} Fe^{3+} added
gas flow = 500 cm^3 min^{-1}

GAS COMPOSITION	AFTER 15 min. OF REACTION			
	H_2SO_4 g dm^{-3}	Eh mv	pH	SO_2 mol dm^{-3}
5% SO_2/O_2	20.3	1072	1.10	---
10% SO_2/O_2	17.1	1014	1.41	0.001
20% SO_2/O_2	31.3	940	1.29	0.004
30% SO_2/O_2	43.8	896	1.35	0.007
50% SO_2/O_2	58.7	852	0.93	0.014
70% SO_2/O_2	42.5	653	1.20	0.224
80% SO_2/O_2	17.9	590	1.39	0.295

The reason behind the large increase in the aqueous sulphur dioxide concentration of the leach media, with SO_2/O_2 gas ratios above 50% SO_2/O_2, can be understood when it is considered that, sulphur dioxide is consumed in the autoxidation process both in the production of sulphuric acid and in the oxidation of ferrous iron. Sulphur dioxide, when leaching with the low SO_2/O_2 ratio gas mixtures, is entirely consumed by the production of acid and the oxidation of ferrous iron to maintain the high Eh (high Fe^{3+}/Fe^{2+} ratios) shown in Table 21. The production of acid increases with the sulphur dioxide content as seen in Tables 21, 23 and 30 and consequently all the sulphur dioxide is consumed. At the high SO_2/O_2 ratios, the production of acid decreases and the Eh drops indicating that a low Fe^{3+}/Fe^{2+} equilibrium ratio is established. Consequently, there is an excess of aqueous sulphur dioxide in the leach media with gas compositions above 50% SO_2/O_2. Therefore, as demonstrated in Figure 54 the soluble iron in the leach media will be present in the form of the aqueous complexes $FeHSO_3^{2+}$ and $FeHSO_3^{+}$ when a reactant gas mixture with a SO_2/O_2 ratio greater than 0.5 is used. Only with the high SO_2/O_2 ratios is the aqueous sulphur dioxide concentration great enough to form these complexes.

Figure 38 shows that the overall rate of dissolution of sphalerite with SO_2/O_2 mixtures in the presence of soluble iron increases with the partial pressure of sulphur dioxide up to 50% SO_2/O_2. The dissolution curves are essentially identical for gas mixtures of 50% to 80% SO_2/O_2 and the rate decreases finally at a sulphur dioxide partial pressure of 1 atm. The increase in the rate of leaching with gas mixtures in the range of 5 to 50% SO_2/O_2 is directly linked to an increase in the rate of sulphuric acid production. As the SO_2/O_2 ratio increases in this range, the acid production increases and the rate of dissolution increases. This observation is in direct agreement with the rate equation of Romankiw and

de Bruyn (1964):

$$\frac{d[Zn^{2+}]}{dt} = A_o(k_f[H^+] - k_r[Zn^{2+}]^{\frac{1}{2}} P_{H_2S}^{\frac{1}{2}}) . \quad (35)$$

This equation describing the acid dissolution of sphalerite shows that an increase in the hydrogen ion concentration will lead to a greater rate of extraction. The appearance of elemental sulphur in the exit gas bubbler indicates that hydrogen sulphide is being evolved in the dissolution process faster than it can be oxidized by the ferric iron present. Since, as already shown, there is no residual sulphur dioxide present to oxidize the hydrogen sulphide when using the low SO_2/O_2 ratio gas mixtures, the Fe^{3+} ion is the only available oxidant in the system for hydrogen sulphide. Combined with the observation that a high constant potential (Fe^{3+}/Fe^{2+} ratio) is established in the solution for all tests with low SO_2/O_2 ratio gas mixtures, it is evident from these facts, that the predominant route for zinc sulphide dissolution is through acidic decomposition accompanied by hydrogen sulphide production, with the ferric ion acting as a catalyst for the production of sulphuric acid.

The rate of the decomposition of sphalerite, as seen in Figure 38, is essentially identical for SO_2/O_2 gas mixtures, above 50% sulphur dioxide and at least up to 80% sulphur dioxide, used together with dissolved iron as the leaching reagents. The quantity of sulphuric acid produced, however, significantly decreases above the 50% SO_2/O_2 mark even though the rate of extraction remains high, as shown in Table 21 and Table 30. Also, with gas mixtures above the 50% SO_2/O_2 ratio, hydrogen sulphide is not swept out of the leaching reactor as evidenced by the clear exit gas bubbler, shown in Tables 21 and 23, for those gas compositions. It therefore may be postulated, that the excess sulphur dioxide, shown to be available in solution

when using SO_2/O_2 gas mixtures at the high end of the range, is able to increase the oxidation rate of hydrogen sulphide. Furthermore, the reaction rate is rapid enough to result in complete oxidation within the reactor vessel. Consequently, the removal of hydrogen sulphide from the leach media, by oxidation with sulphur dioxide, allows the leaching rate to remain high, although, there is less acid present with the high SO_2/O_2 ratio gas mixtures. Such a conclusion is also consistent with the rate equation proposed by Romankiw and de Bruyn (1964) which was given by Equation (35). This equation demonstrates that a reduction in the partial pressure of hydrogen sulphide, decreases the inhibiting effect of the reverse reaction, leading to an increase in the rate of dissolution. Thus, the rate of dissolution with SO_2/O_2 ratios greater than about 0.5 is balanced between the decrease in sulphuric acid production, and the increase in the rate of oxidation of hydrogen sulphide by sulphur dioxide in the leach media.

The potential or Eh of the leaching media is established at a low equilibrium value, with the high SO_2/O_2 ratio gas mixtures, as shown in the Eh overlay to Figure 38. Furthermore, with the SO_2/O_2 mixtures greater than 50% sulphur dioxide, the dissolved iron in the leach media should be present as the bisulphite complex species due to the available aqueous sulphur dioxide in the leach media. Since the Eh is low in the region of 450 mV to 550 mV with the high SO_2/O_2 gas mixtures, Figure 54 indicates that the $FeHSO_3^+$ ion is the predominant form of dissolved iron.

Although no attempt was made to elucidate the mechanism whereby hydrogen sulphide is oxidized in the presence of relatively high levels of aqueous sulphur dioxide, it is useful to note the possible routes. Sulphur dioxide could be oxidizing hydrogen sulphide directly via the multiple step Wackenrhoder reaction,

$$2H_2S + SO_2 = 3S^\circ + 2H_2O$$

within the leach media. Alternatively, hydrogen sulphide could be oxidizing via a mechanism linked to the ferric bisulphite species. A possible reaction path for the oxidation of hydrogen sulphide is,

$$H_2S + 2FeHSO_3^{2+} = S^\circ + 2FeHSO_3^{+} + 2H^{+}$$

where the $FeHSO_3^{2+}$ ion is regenerated by the reaction

$$SO_2 + O_2 + 2FeHSO_3^{+} = 2FeHSO_3^{2+} + SO_4^{2-} \quad .$$

None of the above reactions are necessarily elementary. Thus, hydrogen sulphide could be oxidized by sulphur dioxide, directly in the Wackenrhoder reaction, by a combination of sulphur dioxide and oxygen indirectly via the iron bisulphite complex species, or by a combination of both.

The kinetic data presented in Figures 39 and 40 supplement and directly confirm the results shown in Figure 38. Figure 39, which is an extension of test no. 75 in Figure 38, shows the effect of reducing the oxygen partial pressure by dilution with nitrogen at a constant sulphur dioxide partial pressure of 0.10 atm. The data in Table 22 and Figure 39 show that when the oxygen partial pressure is decreased significantly, the production of sulphuric acid is hindered and the rate of extraction decreases. The results given in Figure 40 and Table 23 at a constant oxygen partial pressure of 0.3 atm are very similar to the results and trends observed in Figure 38 and Table 21.

6.2.3 Variation of the Soluble Iron Addition

Table 25 and Figure 41 demonstrate the effect of the dissolved iron concentration on the rate of dissolution

in the leaching of sphalerite with a 10% SO_2/O_2 gas mixture. As shown in Figure 41, the addition of a small amount of iron (1.0 g dm^{-3}) leads to a dramatic increase in the rate of dissolution over that obtained in the absence of iron. A greater rate of extraction is obtained with further increases in the soluble iron addition although, the effect is less pronounced at the higher levels of iron (20 g dm^{-3}). As the Eh overlay sheet to Figure 41 shows, with any concentration of dissolved iron present, the Eh is consistently in the 650 mV to 700 mV range indicating a reasonably constant Fe^{3+}/Fe^{2+} ratio is established in the leach media. Since a low gas ratio of 10% SO_2/O_2 is used in this series of runs, a high Fe^{3+}/Fe^{2+} ratio and high Eh are consequently established in each case with iron present. The greater the amount of soluble iron present, the greater is the ferric ion concentration which leads to a greater production of sulphuric acid by the autocatalytic reaction. Table 25 indicates this trend, and the resulting increase of the sphalerite dissolution rate with the higher acid concentrations, corresponding to the higher soluble iron additions, is shown by Figure 41.

The other factor contributing to the increase in the rate of dissolution with a greater soluble iron addition is the removal of hydrogen sulphide from the leach liquor. As shown by the last column in Table 25, a large quantity of hydrogen sulphide is swept out of the reactor with 1.0 g dm^{-3} dissolved iron present, whereas, with 20 g dm^{-3} of dissolved iron, all of the hydrogen sulphide produced in the dissolution reaction is oxidized within the reactor. Furthermore, Table 25 shows that there is very little sulphur dioxide present in the leach media in any of these tests with a 10% SO_2/O_2 gas mixture. It is probable then, that the higher concentrations of Fe^{3+} ion, available with a greater soluble iron addition, increase the rate of oxidation of hydrogen sulphide and result in the higher sphalerite dissolution rates obtained. At 20 g dm^{-3} of

dissolved iron, the complete oxidation of hydrogen sulphide, as it is produced, and the high concentration of acid produced, both contribute to the high level of sphalerite dissolution shown in Figure 41.

6.3 ANALYSIS OF THE KINETIC DATA

The previous two sections of this chapter have qualitatively developed, from the kinetic experiments, a mechanistic picture of the fundamental processes involved in the dissolution of sphalerite in aqueous sulphurous acid media. The present section further develops these ideas by quantitatively analyzing the kinetic data in terms of generally accepted heterogeneous reaction models. In general, the study of reaction rate data can provide two kinds of information. Experimentation carried out on a given system approximating conditions to be encountered commercially, provide valuable engineering data, leading from bench-scale to pilot tests and finally to full-scale operation. Extrapolation of results of previous experiments to new conditions is a economical substitute for complete experimentation, the inconvenience and cost of which normally precludes full-scale testwork. A more fundamental benefit of the analysis of reaction rate data arises from the interpretation of rates in terms of a mechanistic model. The fundamental approach, with sufficient information, inherently has the ability to predict results under a variety of conditions as well as to indicate fundamental concepts.

The majority of hydrometallurgical and pyrometallurgical processes are heterogeneous, that is, they are characterized by having an interface between the reactants. In the case of the reaction of a solid mineral particle in an aqueous suspension, with a dissolved reactant, the interface is the solid-liquid boundary. A simple idealized model has been developed for the noncatalytic reaction of particles in a

surrounding fluid which seems to reasonably represent reality in a wide variety of situations, Levenspiel (1972). In this unreacted-core or shrinking-core model, it is visualized that a reaction first occurs at the outer surface of a particle. The zone of reaction then progressively moves into the solid and may or may not leave behind a layer of completely converted product material. Thus, at any time there exists an unreacted core of material which shrinks in size during the reaction. The shrinking core model was discussed in detail in the literature review of Chapter Four.

Figure 26 of Chapter Four illustrates the shrinking core heterogeneous reaction model. Indicated in the diagram are five steps, any one of which could control the overall rate of the dissolution process. These five steps, as described in Chapter Four include, the diffusion of reactant materials through the solution film and product layer to the particle surface, reaction at the particle surface and diffusion of the products back through the residue layer and solution film to the bulk fluid. A mathematical expression relating the time, to the fraction of the solids reacted at that time, for each situation where film diffusion, product layer diffusion or the chemical reaction are exhibiting control over the process, also is presented in Figure 26. The derivation of these equations describing the shrinking core model are summarized in Appendix 3.4.

If a conceptual picture or model for the progress of a reaction process corresponds closely to the processes actually occurring in reality, then, the rate expression of the model will closely predict and describe the actual reaction kinetics. The assumptions of any model, however, may not match reality precisely. As an example for the shrinking core model, the reaction may occur along a diffuse front rather than along a sharp interface between the product layer and the unreacted solid. In the extreme

case of a slow reaction of a fluid with a very porous solid, the solid reactant may be converted continuously and progressively throughout the particle at all times. This is known as the progressive-conversion model, Levenspiel (1972). Thus, if the reaction is occurring along a diffuse front, the kinetics may exhibit behaviour intermediate between the shrinking core and the continuous reaction models. Despite such complications Wen (1968) and Ishida, et al (1971) conclude, on the basis of studies of numerous systems, that the shrinking core model is the best simple representation of fluid-solid heterogeneous reaction systems.

6.3.1 Heterogeneous Reaction Model Analysis

Figures 33 and 34 show, as briefly discussed in the previous two sections, that reactant diffusion through the stagnant film of solution surrounding the zinc sulphide particles does not significantly hinder the rate of decomposition. At impeller speeds of 300 rpm to 800 rpm the kinetic dissolution curves obtained in the absence of iron are identical as shown in Figure 33. Thus mass transfer in the aqueous phase does not control the rate of sphalerite decomposition by aqueous sulphur dioxide in the absence of iron. Figure 34, however, reveals that the rate of dissolution has some dependency on the degree of agitation when leaching is carried out in the presence of iron. The dependency upon stirring speed is significant around 300 rpm, but, this diminishes to a negligible effect at 800 rpm. It is highly probable that the decreased kinetics at low agitation could be the result of a slow mass transfer of sulphur dioxide or oxygen from the gas phase to the liquid phase due to inefficient gas distribution in the leach pulp at low impeller speeds. Since all other experiments were carried out at an impeller speed of 800 rpm, mass transfer effects in the aqueous phase were minimal throughout the experimentation of the present study.

Figure 26 presents the conventionally accepted models for the heterogeneous reaction of a particle in a fluid medium. The experimental results have shown that solution film diffusion is not a rate controlling process under the agitation conditions used in the experimentation. The Jander approximation for product layer diffusion control shown in Figure 26 is applicable only to flat surfaces or to situations where a residue film is very thin compared to the curvature of the particle surface. Since many of the leaching experiments were carried out to high degrees of extraction, the general solution for product layer diffusion control is more suitable for analysing the experimental data than Jander's approximation. The experimental data, therefore, were analysed in terms of the generally accepted heterogeneous reaction models for product layer diffusion control and surface chemical reaction control which are presented in Figure 26. Analysis of the rate data, in terms of the simple heterogeneous models, suggested that the best representation of the reaction process was the shrinking core model with a surface reaction as the rate limiting step.

Figure 55 presents a plot of the surface reaction control function of conversion, $1-(1-\alpha)^{\frac{1}{3}}$, against time for the data given in Figure 37. The fraction of the solid material reacted at any particular time, α, is equivalent to the fraction of zinc extracted (zinc percent extraction $x10^{-2}$) at that time. The numerical data for the $1-(1-\alpha)^{\frac{1}{3}}$ parameter are compiled with each test in Appendix 7. Figure 55 shows a good fit of the data, for the leaching of sphalerite with SO_2/O_2 gas mixtures in the absence of dissolved iron, to the surface reaction control model for gas mixtures up to 50% SO_2/O_2.

Figures 56, 57 and 58 present plots of the $1-(1-\alpha)^{\frac{1}{3}}$ parameter against time for the leaching experiments using various SO_2/O_2 and $SO_2/O_2/N_2$ gas mixtures in the presence of dissolved iron. The corresponding percent extraction versus time data are plotted in Figures 38, 40 and 39,

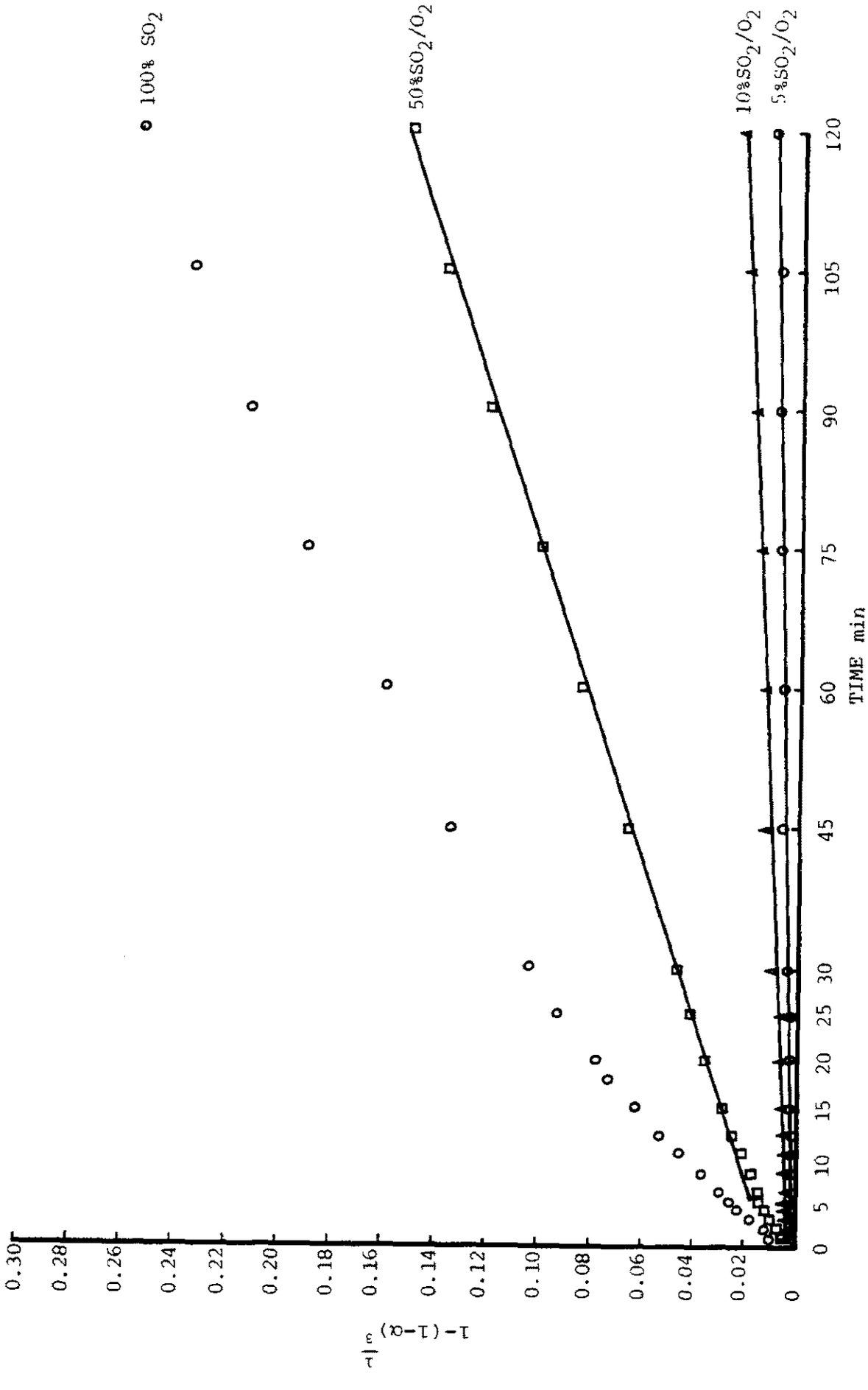

FIGURE 55. Surface reaction model for the dissolution data presented in Fig. 37.

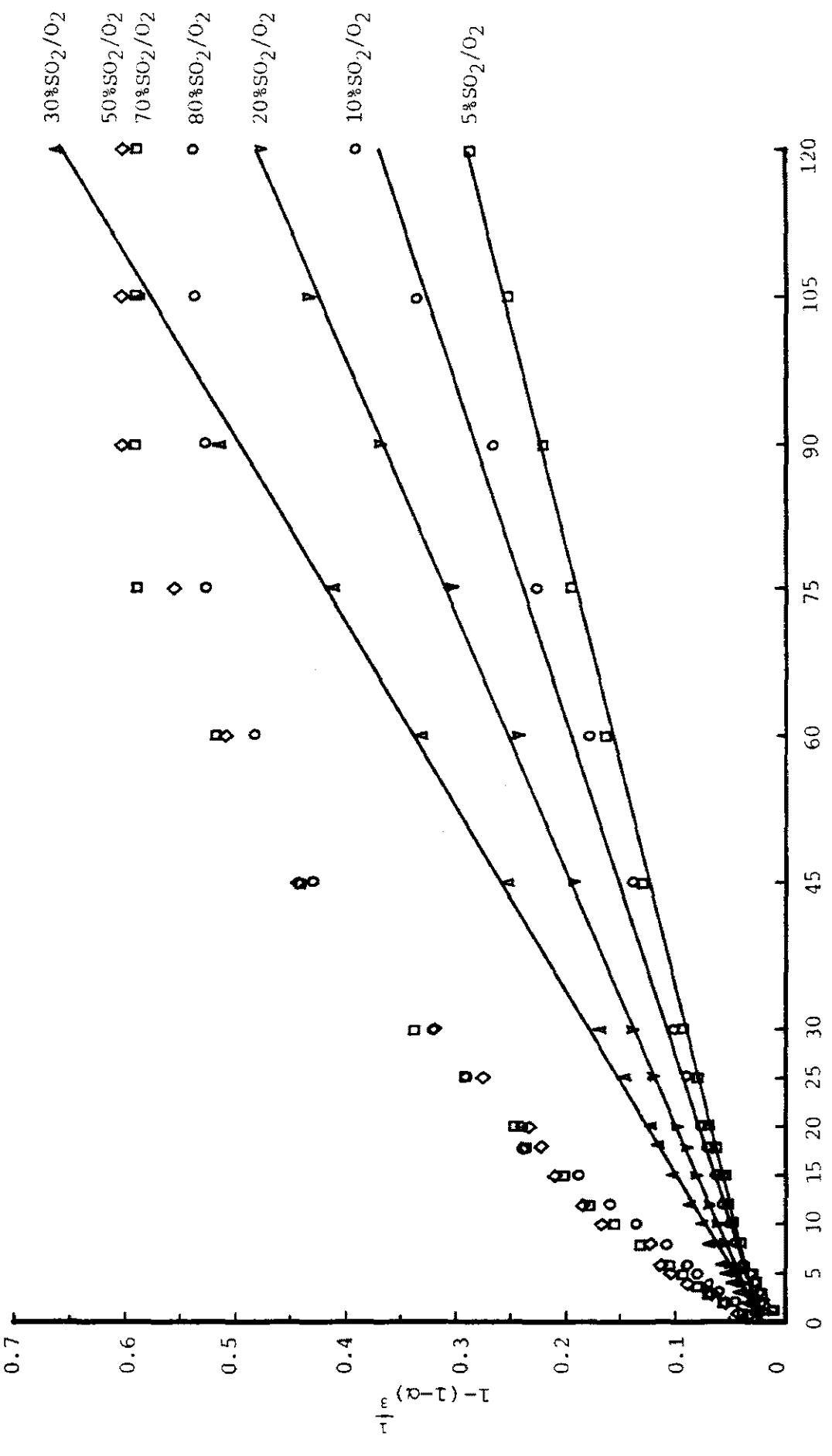

FIGURE 56. Surface reaction model for the dissolution data presented in Fig. 38.

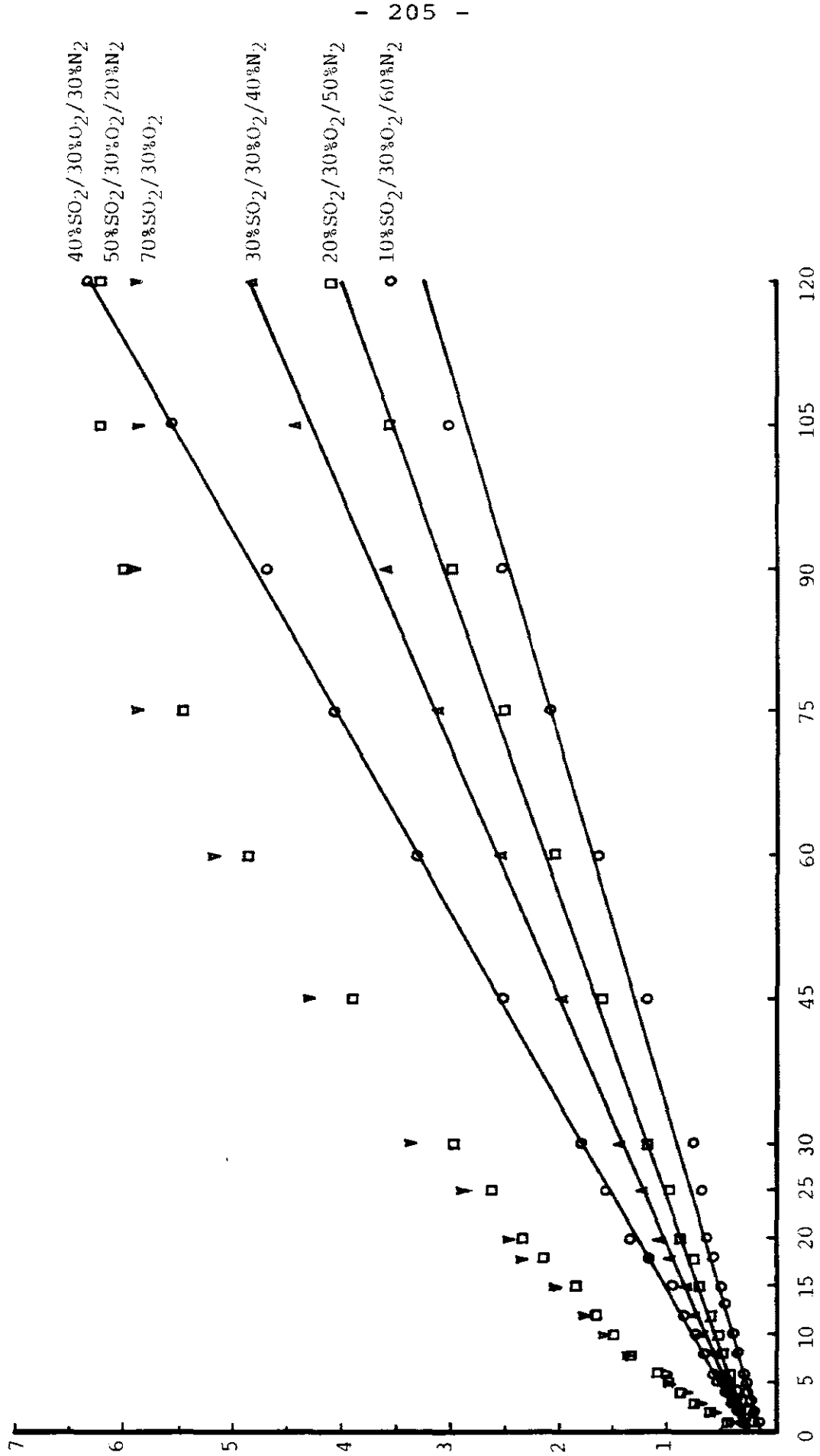

FIGURE 57. Surface reaction model for the dissolution data presented in Fig. 40.

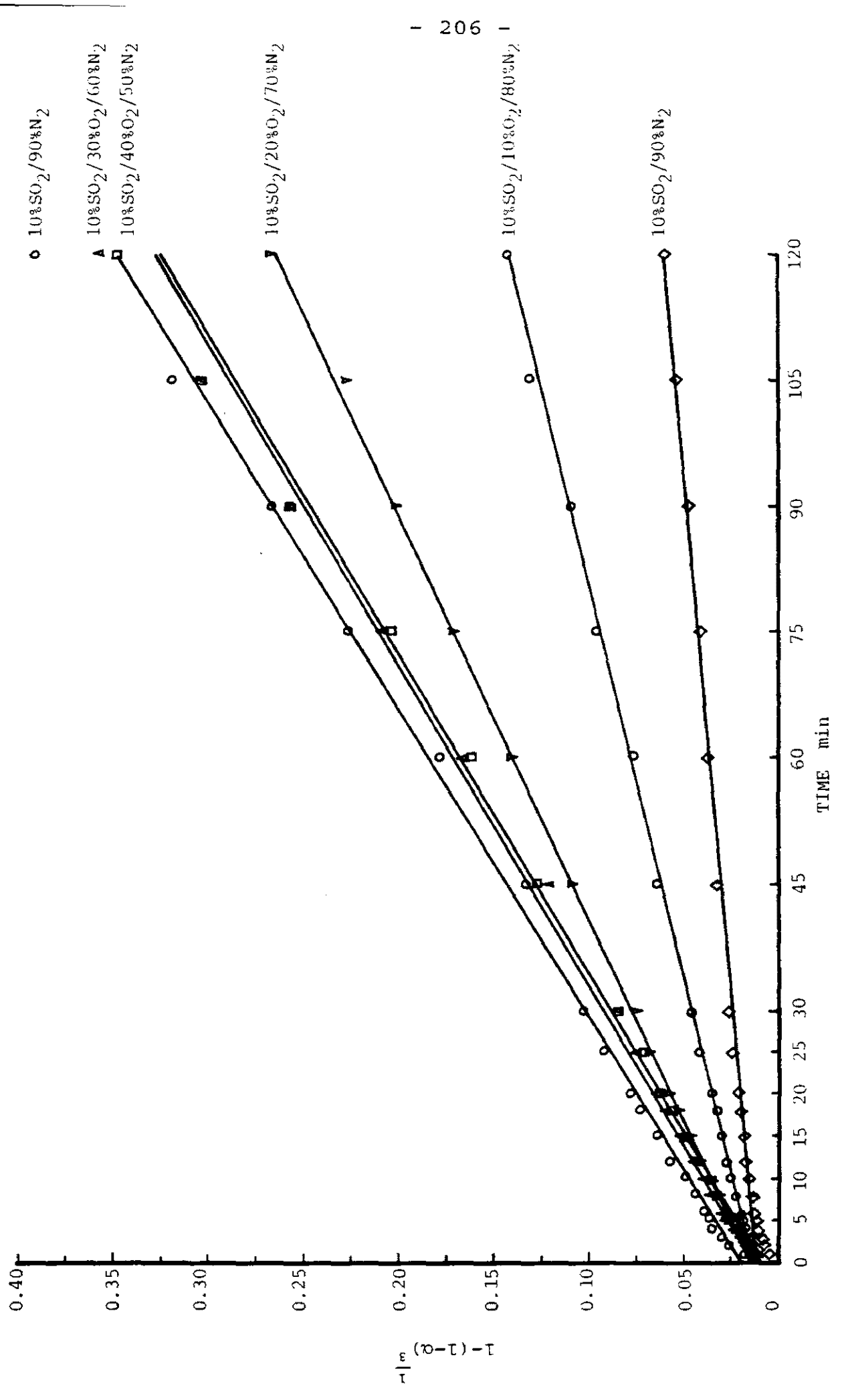

FIGURE 58. Surface reaction model for the dissolution data presented in Fig. 39.

respectively. These figures show a good fit of the experimental data to the surface reaction control model for gas mixtures containing up to 40 percent sulphur dioxide. At gas mixtures containing 50 percent sulphur dioxide and above, the data no longer correlates with the surface reaction control equation, nor does it correlate with the product layer diffusion control model. This further demonstrates the obvious change in the mechanism of dissolution, discussed in the previous section, for leaching with a SO_2/O_2 or $SO_2/O_2/N_2$ gas mixture of 50 percent sulphur dioxide or more. The lines of best fit to the data, by the least-squares method, are shown in Figures 55, 56, 57 and 58. The correlation coefficient in each case was greater than 0.99.

Figure 59 presents a plot of $1-(1-\alpha)^{\frac{1}{3}}$ against time for leaching experiments using 10% SO_2/O_2 mixtures in the presence of dissolved iron at various temperatures. The experimental data shows a good fit to surface reaction control model in the temperature range of 25°C to 90°C. At temperatures above 60°C, however, the data begins to lose linearity above 70 percent zinc extraction. The lines of best fit to the experimental data over the range indicated, by the least-squares method, are shown in Figure 59. Again, a correlation coefficient greater than 0.99 was obtained in each case.

The experimental data presented in Figures 56, 57 and 58 were used to evaluate the order of the leaching reaction with respect to sulphur dioxide, and the apparent activation energy of the dissolution process in the presence of dissolved iron. The equation for a rate limiting surface reaction for the shrinking core model was given in Figure 26 as:

$$\frac{b\ k_r C}{r_o\ \rho}\ t \quad = \quad 1-(1-\alpha)^{\frac{1}{3}} \quad .$$

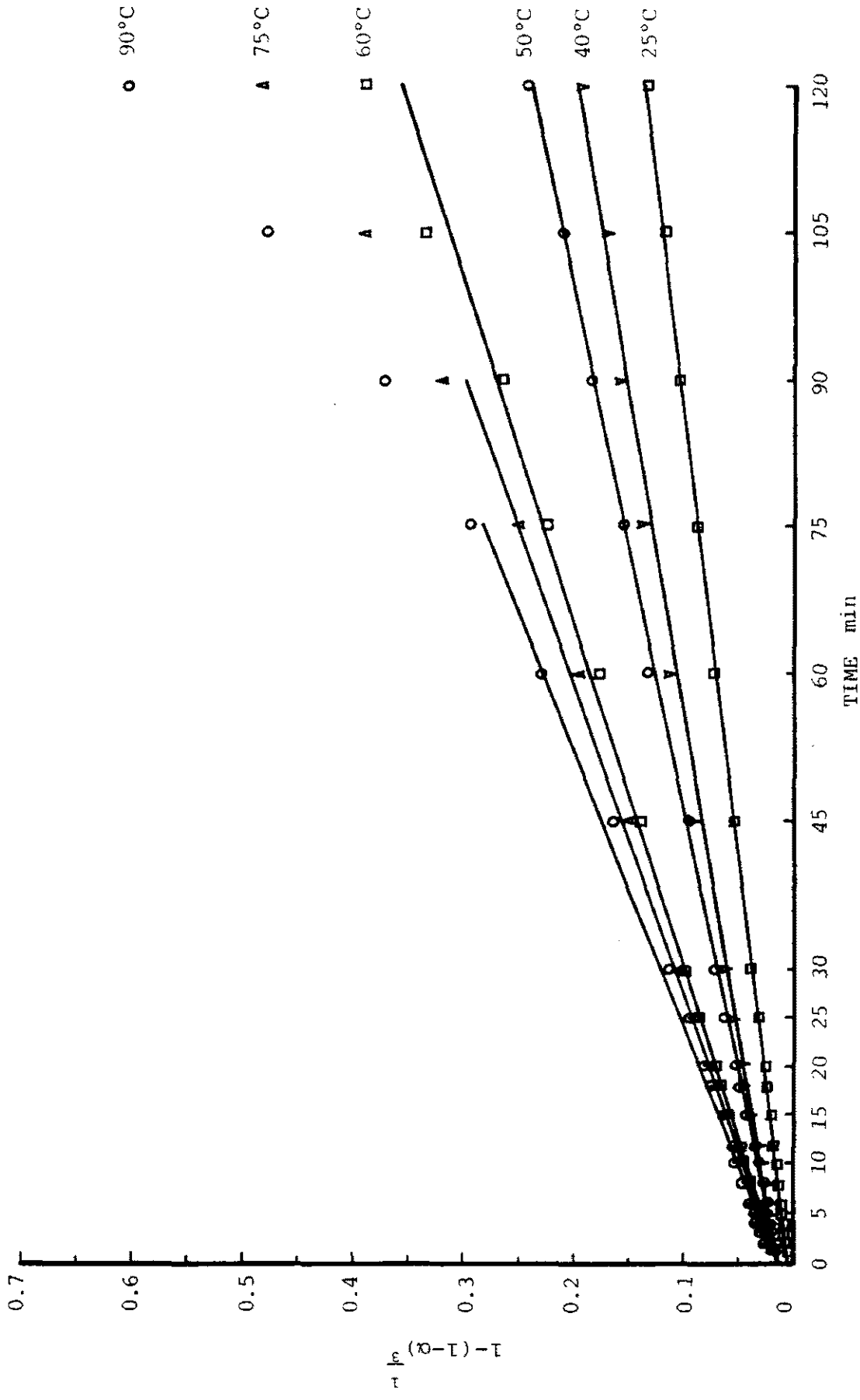

FIGURE 59. Surface reaction model for the dissolution data presented in Fig.36.

Collecting all of the constants into one apparent rate constant yields,

$$kt = k' C_{SO_2}^{n} t = 1-(1-\alpha)^{\frac{1}{3}}$$

where $C_{SO_2}^{n}$ is the total concentration of aqueous sulphur dioxide as defined by Equation (23) in Chapter Three. The two apparent rate constants, k and k', are related by

$$k = k' C_{SO_2}^{n} .$$

Taking the logarithm of both sides of this equation yields

$$\log k = \log k' + n \log C_{SO_2} .$$

Consequently, the slope of a plot of log k against log C_{SO_2} is equal to the order of the reaction with respect to sulphur dioxide, n. Table 31 lists the apparent rate constants, k, obtained from the slopes of the lines in Figures 56 and 57 for leaching with SO_2/O_2 gas mixtures and $SO_2/30\%O_2/N_2$ gas mixtures, respectively. Table 31 also gives the total sulphur dioxide concentrations in water at the various partial pressures of sulphur dioxide in the reagent gas mixture. This information is taken from the experimentally determined sulphur dioxide solubility plot in Figure 60(a). The sulphur dioxide solubility data presented in Figure 60 was experimentally determined from equilibrium measurements of total sulphur dioxide concentration under the various conditions shown in the diagrams. Figure 61(a) presents the resulting plot of log k against log C_{SO_2} for the two sets of data given in Table 31. The data for leaching with SO_2/O_2 gas mixtures yielded a reaction order of n = 0.65. The best fit line to the data by least-squares gave a correlation coefficient of 0.99. Similarly, the data for leaching with $SO_2/30\%O_2/N_2$ gas mixtures gave a reaction order of n = 0.58 with a

TABLE 31

DETERMINATION OF REACTION ORDER

TEST NO.	GAS COMPOSITION	k min^{-1}	P_{SO_2} atm	C_{SO_2} $g(kgH_2O)^{-1}$	log k	log Cso_2
84	5% SO_2/O_2	2.16×10^{-3}	0.05	2.3	-2.67	0.361
75	10% SO_2/O_2	2.73×10^{-3}	0.10	3.7	-2.56	0.568
111	20% SO_2/O_2	3.79×10^{-3}	0.20	6.3	-2.42	0.799
110	30% SO_2/O_2	5.29×10^{-3}	0.30	8.8	-2.28	0.944
98	10% SO_2/30% O_2/60% N_2	2.59×10^{-3}	0.10	3.7	-2.59	0.568
120	20% SO_2/30% O_2/50% N_2	3.13×10^{-3}	0.20	6.3	-2.51	0.799
121	30% SO_2/30% O_2/40% N_2	3.81×10^{-3}	0.30	8.8	-2.42	0.944
122	40% SO_2/30% O_2/30% N_2	5.02×10^{-3}	0.40	11.0	-2.30	1.041

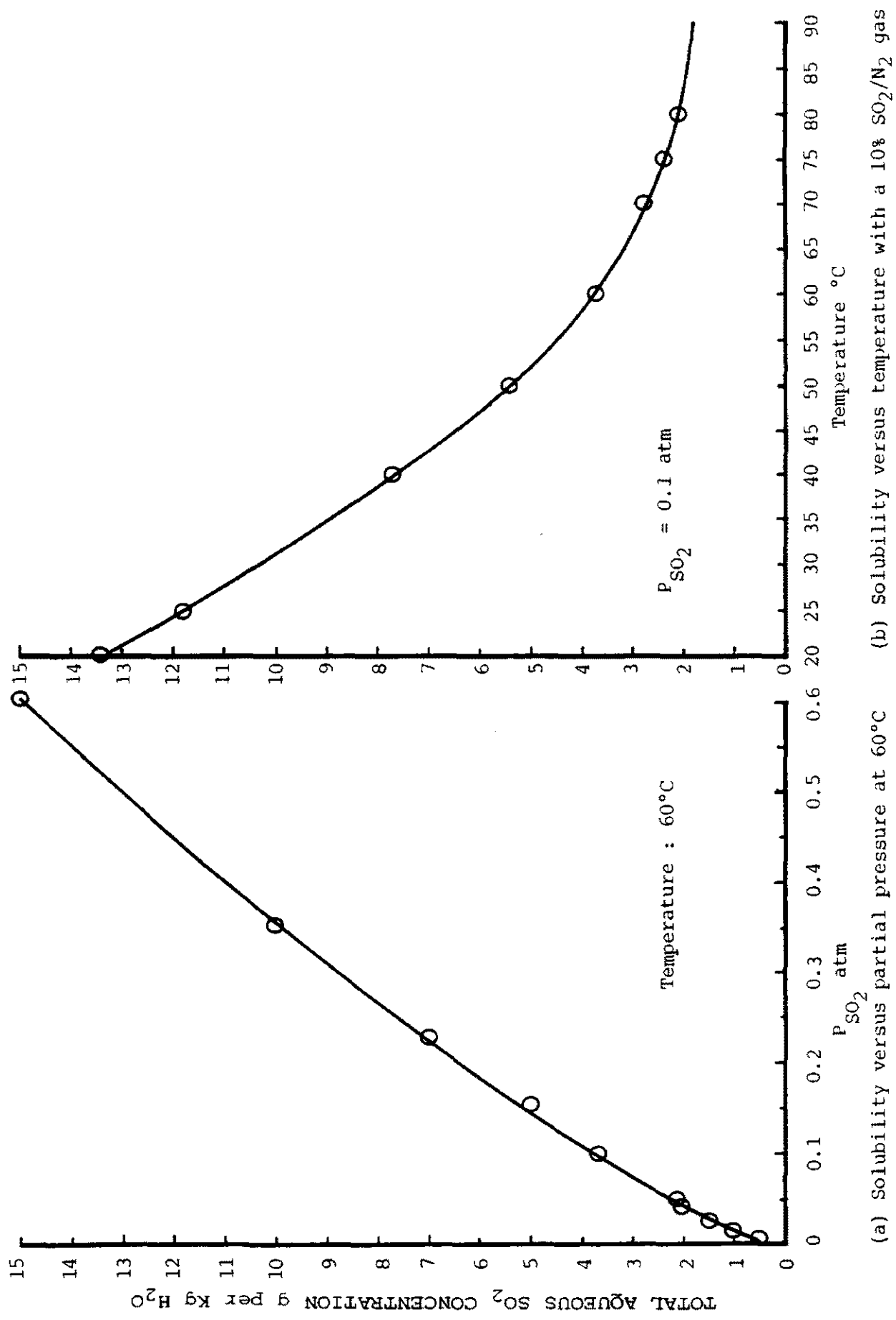

(a) Solubility versus partial pressure at 60°C (b) Solubility versus temperature with a 10% SO_2/N_2 gas mixture

FIGURE 60. Solubility of Sulphur dioxide in Water

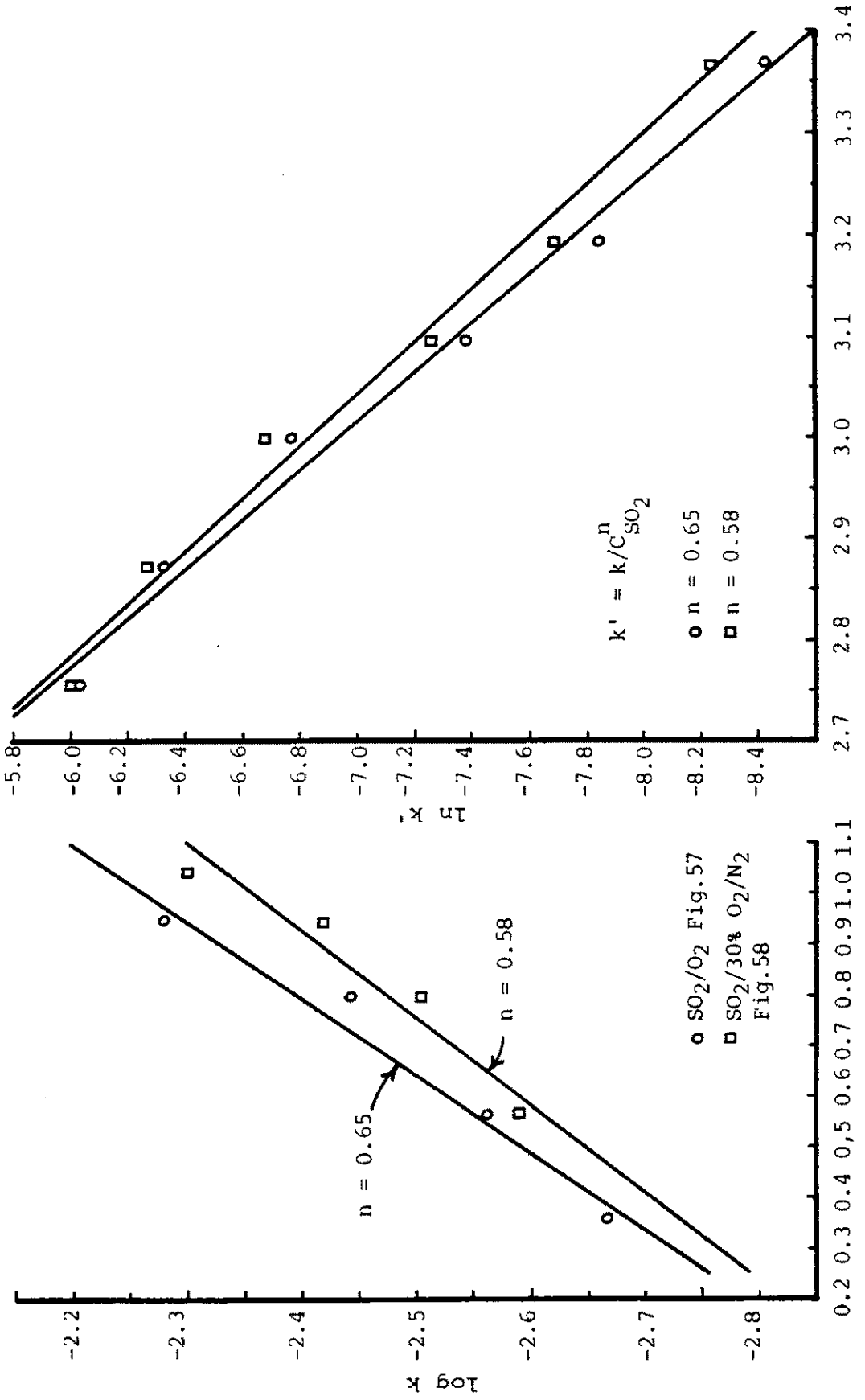

FIGURE 61. (a) Log-log plot of the reaction rate constant k versus sulphur dioxide concentration

(b) Arrhenius plot : natural logarithm of reaction rate constant k' versus inverse absolute temperature.

correlation coefficient of 0.96. Therefore, a reaction order of about 0.6, with respect to sulphur dioxide, is indicated by the experimental data.

The apparent activation energy of the dissolution process can be determined from the slopes of the lines in Figure 59. However, the solubility of sulphur dioxide in water changes by an order of magnitude over the temperature range under study, as shown in Figure 60(b). Consequently, an activation energy calculated directly from the rate constant k, the slopes of the lines in Figure 59, would also be incorporating the sulphur dioxide solubility function with temperature. The rate constant k', as it has been defined, is independent of the sulphur dioxide concentration and can be used to calculate the activation energy independent of the sulphur dioxide concentration. The Arrhenius equation, after incorporation of the rate constant k' becomes,

$$k' = k_o' \; e^{-E/RT} \; .$$

Thus, the slope of a plot of ln k' against the reciprocal absolute temperature yields the activation energy of the dissolution process, E. Table 32 lists the rate constant k, from Figure 59, over the temperature range of 25°C to 90°C along with the corresponding sulphur dioxide solubility from Figure 60(b). The rate constant k' is calculated in Table 32 for both cases where n = 0.65 and n = 0.58. The resulting Arrhenius plot is shown in Figure 61(b). An activation energy of 34.5 kJ mol^{-1} and 32.4 kJ mol^{-1} was calculated for n = 0.65 and 0.58, respectively. Thus the activation energy of the dissolution process is about 33 kJ mol^{-1} (8 k cal mol^{-1}).

The effect of sulphur dioxide concentration and temperature observed in the experimental data can be incorporated into the surface reaction equation of the shrinking core model to yield the kinetic expression,

TABLE 32

DETERMINATION OF ACTIVATION ENERGY

TEST NO.	TEMP °C	k min^{-1}	C_{SO_2} $g(kgH_2O)^{-1}$	$k' = k/C_{SO_2}^{0.65}$		$k' = k/C_{SO_2}^{0.58}$		T^{-1} $°K^{-1}$
				k' min^{-1}	ln k'	k' min^{-1}	ln k'	
108	25	1.10×10^{-3}	11.8	2.21×10^{-4}	-8.42	2.63×10^{-4}	-8.24	3.37×10^{-3}
106	40	1.49×10^{-3}	7.7	3.95×10^{-4}	-7.84	4.56×10^{-4}	-7.69	3.19×10^{-3}
115	50	1.87×10^{-3}	5.4	6.25×10^{-4}	-7.38	7.03×10^{-4}	-7.26	3.10×10^{-3}
75	60	2.73×10^{-3}	3.8	1.15×10^{-3}	-6.77	1.26×10^{-3}	-6.68	3.00×10^{-3}
107	75	3.16×10^{-3}	2.4	1.79×10^{-3}	-6.32	1.90×10^{-3}	-6.26	2.87×10^{-3}
109	90	3.55×10^{-3}	1.8	2.41×10^{-3}	-6.03	2.52×10^{-3}	-5.98	2.76×10^{-3}

$$\left[\frac{k_r}{r_o\rho}\exp\frac{-E}{RT}\,C_{SO_2}\right]t = 1-(1-\alpha)^{\frac{1}{3}} \quad . \qquad (36)$$

The observed reaction order, n, is about 0.6 and the activation energy is approximately 33 kJ mol^{-1} (8 k cal mol^{-1}). These two observations directly support the conclusion that the dissolution process is limited by the chemical reaction at the zinc sulphide surface. A diffusion controlled process would be expected, from Fick's first law of diffusion, to have a first order dependence on the reactant concentration. Thus, the fractional order dependence observed experimentally supports surface reaction control. Furthermore, the observed activation energy is of a magnitude more in keeping with a chemical reaction controlled process than that for a diffusion controlled process.

The reversible nature of the sphalerite decomposition process is apparent in the experiments incorporating the addition of soluble zinc to the initial leach reagent liquor. The kinetic model can be modified by the incorporation of a back reaction term such as,

$$\frac{1}{A}\frac{d[Zn^{2+}]}{dt} = k_f[H^+] - k_r[H_2S][Zn^{2+}] \quad . \qquad (37)$$

If the term $k_r[H_2S][Zn^{2+}]$ does not vary significantly then, the general relationship found for the shrinking core model is valid, and a linear relationship between $1-(1-\alpha)^{\frac{1}{3}}$ and t is obtained. Throughout the experimentation, the hydrogen sulphide generated was continuously purged from the reactor system by a steady flow of inlet gas. Consequently, the term $k_r[H_2S][Zn^{2+}]$ was relatively constant and this condition was generally realized.

The second term of Equation (37), on the other hand, may become significant when an appreciable quantity of soluble zinc is added to the leach liquor initially. Such an effect is shown in Figures 44 and 45, where the extraction rate decreases with an increase in added soluble zinc. The variation of extraction with the zinc sulphide slurry density can be seen in Figure 46. This result can be attributed to the initial increase in the bulk concentration of soluble zinc with high slurry densities, thus, causing a decrease in the rate of extraction.

6.3.2 Electrochemical Kinetics

A quantitative description of the kinetics of dissolution of sphalerite under various conditions has been presented,with the aid of the shrinking core model which incorporates both surface reaction and diffusion control considerations. Although it is beyond the scope of this thesis to present a full treatment, it is informative to consider the surface reaction of being electrochemical in nature and develop the mathematical description in terms of electrochemical parameters. Wadsworth (1981) has reviewed such techniques in considering the leaching of a number of minerals.

As an example, consider the dissolution of sphalerite according to the tetrathionate producing reaction

$$ZnS + 3SO_2 = Zn^{2+} + S_4O_6^{2-} \quad .$$

This reaction could be considered to be electrochemical in nature with an anodic reaction,

$$4ZnS + 6H_2O = 4Zn^{2+} + S_4O_6^{2-} + 12H^+ + 18e^- \qquad (35)$$

and a cathodic reaction,

$$12SO_2(aq) + 12H^+ + 18e^- = 3S_4O_6^{2-} + 6H_2O \quad . \qquad (61)$$

The rate of the anodic reaction, R_a, is given by

$$R_a = k_a - k_a' \; C_{Zn^{2+}} \; C_{S_4O_6^{2-}} \; C_{H^+}$$

and for the cathodic reaction

$$R_c = k_c \; C_{SO_2} \; C_{H^+} - k_c' \; C_{S_4O_6^{2-}} \quad .$$

These rates can be expressed in electrochemical terms, for charge transfer in simple reversible reactions, by means of the Butler-Volmer equation. This fundamental equation of electrodics relates the current density at a solid solution interface to the established over-potential. Thus, for a single electron transfer process, application of this equation to the anodic and cathodic reactions yields,

$$I_a = 18A_a \, F[k_a^{\circ} \; \exp(\beta_a \frac{FE}{RT}) - k_a' \; C_{Zn^{2+}} \; C_{S_4O_6^{2-}} \; C_{H^+} \exp(-(1-\beta_a)\frac{FE}{RT})]$$

and

$$I_c = 18A_c \, F[k_c^{\circ\prime} \; C_{S_4O_6^{2-}} \exp(\beta_c \frac{FE}{RT}) - k_c^{\circ} \; C_{SO_2} \; C_{H^+} \; \exp(-(1-\beta_c)\frac{FE}{RT}]$$

Several simplifying assumptions help in the development of the rate equations. For example, if the anodic current due to the anodic oxidation of ZnS is much greater than the partial anodic current for the anodic oxidation of $S_4O_6^{2-}$ (i.e., both I_a and I_c fall within their respective

"Tafel regions" and $k_a^{\circ} >> k_a^{\circ'}$, $k_c^{\circ} >> k_c^{\circ'}$) and if $A_a = A_c = A$, the following is obtained:

$$-\frac{dN_{ZnS}}{dt} = A\, k_a^{\circ(1-\phi)}\, k_c^{\circ\phi}\, C_{SO_2}^{\phi}\, C_{H^+}^{\phi}$$

where,

$$\phi = \frac{\beta_a}{1+\beta_a-\beta_c} .$$

Since,

$$-\frac{1}{A}\frac{dN_{ZnS}}{dt} = -\frac{1}{4\pi r^2}\frac{4\pi\rho r^2 dr}{dt} = -\rho\frac{dr}{dt}$$

where ρ is the molar density of zinc sulphide, the above relationship becomes,

$$-\rho\frac{dr}{dt} = k_a^{\circ(1-\phi)}\, k_c^{\circ\phi}\, C_{SO_2}^{\phi}\, C_{H^+}^{\phi} .$$

Integration of this equation in the manner shown in Appendix 3.4 yields,

$$\frac{1}{r_o\rho} k_a^{\circ(1-\phi)}\, k_c^{\circ\phi}\, C_{SO_2}^{\phi}\, C_{H^+}^{\phi}\, t = 1-(1-\alpha)^{\frac{1}{3}} \qquad (38)$$

Thus, the electrochemical model yields the same format as the shrinking core model expressed in surface reaction terms. Additionally, the dependency upon the reactant concentrations are inherently expressed by the electrochemical approach.

The parameter ϕ is a function of β_a and β_c, the charge transfer coefficients, and this function is fractional. For the case of symmetrical "charge transfer barriers", $\beta_a = \beta_c = 0.5$ which yields $\phi = 0.5$ and hence,

$$\frac{1}{r_o \rho} \left(k_a^{\circ} \, k_c^{\circ}\right)^{0.5} C_{SO_2}^{0.5} \, C_{H^+}^{0.5} \, t = 1-(1-\alpha)^{\frac{1}{3}} \quad .$$

Obviously then, this approach is consistent with the experimental results and provides a means of analysing the rate of dissolution in terms of an electrochemical mechanism. Furthermore, the postulation of the surface reaction rate limiting step being an electrochemical reaction allows some of the kinetic parameters to be obtained independently, using polarization techniques, as discussed by Wadsworth (1981). The use of simplifying assumptions other than those used in this analysis results in the same function of α, $1-(1-\alpha)^{\frac{1}{3}}$, with modified expressions for the dependency on reactant concentrations.

CHAPTER SEVEN

SUMMARY AND CONCLUSIONS

An intensive study was made on the properties of zinc in aqueous sulphur dioxide media. It was found that zinc could be readily precipitated from a sulphur dioxide solution as a sulphite corresponding to the composition $ZnSO_3.2\frac{1}{2}H_2O$ at 25°C. The precipitated material, when filtered from its parent solution and dried, was a coarse, well crystallized, free flowing solid which was stable in air. The Gibb's standard free energy of formation of zinc sulphite, determined experimentally by measuring the solubility of the salt as a function of pH, is:

$$\Delta G^{\circ}_{f,ZnSO_3.2\frac{1}{2}H_2O} = -1256 \pm 4 \text{ kJ mol}^{-1} .$$

The experimentally determined free energy of formation for zinc sulphite has been incorporated into the concise and convenient form of a potential -pH diagram of the $Zn-SO_2-H_2O$ system and extrapolated to temperatures up to 200°C.

The thermodynamic potential -pH diagrams developed in this study for the $Zn-SO_2-H_2O$ system provide a basic understanding and summarize the relevant chemistry to aid in development of effective process strategies. These diagrams, along with their subsidiary solubility diagrams, allow prediction of the optimum conditions for the precipitation of zinc sulphite and the maximum depletion obtainable from a number of process variables such as temperature, sulphurous acid concentration and media pH. At 25°C the maximum depletion of zinc from an aqueous solution by precipitation of the sulphite salt in the pH

range of approximately 7 to 8 was found to yield a residual zinc concentration of 0.53 mg dm^{-3}. Since zinc sulphite can be precipitated at a much lower pH than zinc hydroxide from acidic media, the reduced reagent requirements for precipitation combined with the favourable filtering and handling characteristics make zinc sulphite an attractive alternative to zinc hydroxide production.

The phase and solubility relationships in the $Zn-SO_2-H_2O$ system were investigated by a method described by Ricci (1952). It was determined in this investigation that zinc sulphite is an incongruently soluble salt. This implies several physical characteristics for this salt in water. Pure zinc sulphite cannot be precipitated from a water solution containing a 1:1 ratio of zinc to sulphite ions. Concentration of such a solution by evaporation will result in the co-precipitation of zinc hydroxide along with zinc sulphite. An excess of the sulphite species over the zinc species is required to prevent precipitation of zinc hydroxide. Also, zinc sulphite salt cannot be washed with water without heterogeneous decomposition resulting in precipitation of zinc hydroxide.

The leaching of sphalerite in aqueous sulphurous acid media was experimentally investigated in a 1.3 dm^{-3} stirred reactor system. The role of the various reagents in the leaching process have been elucidated under a variety of conditions. Emphasis was placed on exploration of the key processes involved to expand the present knowledge of sulphurous acid reagent systems, along with the development of a kinetic leaching model to form a basis for process design.

The experimentation was carried out on a synthetically prepared pure sphalerite in the form of a fine powder. Sulphur dioxide, oxygen and nitrogen gases in various mixtures were injected into the zinc sulphide-water slurry

as the principal leaching reagents. Both ferrous and ferric sulphate, as well as sulphuric acid in some cases, were used as secondary reagents. It was found that in the absence of dissolved iron or added sulphuric acid, the dissolution of the sphalerite proceeded by an oxidative dissolution process with the formation of the tetrathionate species as the principal sulphur reaction product. Oxygen as well as nitrogen gases were shown to act only as diluents of the sulphur dioxide and play no role in the dissolution mechanism. Furthermore, the rate of reaction was observed to increase with the sulphur dioxide partial pressure.

The formation of the tetrathionate species as a dissolution reaction product was thermodynamically predicted from a Pourbaix diagram of the metastable $Zn-S-SO_2-H_2O$ system developed in this work. The tetrathionate ion was experimentally observed to form immediately and continuously throughout the dissolution process. At prolonged reaction times (greater than 15 hours) elemental sulphur was observed to form at the expense of the tetrathionate species. The reaction kinetics were observed to be surface reaction controlled and the dissolution process appears to occur by the reaction,

$$ZnS + 3SO_2 = Zn^{2+} + S_4O_6^{2-} .$$

This reaction could be composed of the two following electrochemical reactions,

$$\text{Anodic:} \quad ZnS + \tfrac{3}{2} H_2O = Zn^{2+} + \tfrac{1}{4} S_4O_6^{2-} + 3H^+ + \tfrac{9}{2}e^-$$

$$\text{Cathodic:} \quad 3SO_2 + 3H^+ + \tfrac{9}{2}e^- = \tfrac{3}{4} S_4O_6^{2-} + \tfrac{3}{2} H_2O \quad .$$

The potentials and pH observed in the leach media support these reactions on the basis of the thermodynamic diagrams. At prolonged times tetrathionate may disproportionate to

elemental sulphur by the reaction,

$$2S_4O_6^{2-} + 4H^+ = 3S^\circ + 2H_2O + 5SO_2 \quad .$$

The addition of sulphuric acid (20 g dm^{-3}) accelerated the rate of dissolution and hydrogen sulphide was observed to be swept out of the reactor by the flow of gases. This observation indicates that with sulphuric acid added, an acidic dissolution mechanism becomes active, whereby hydrogen sulphide is produced by the reaction,

$$ZnS + 2H^+ = Zn^{2+} + H_2S \quad .$$

In some cases elemental sulphur was found adhering to the reactor baffles indicating that some of the hydrogen sulphide was being oxidized within the reactor by sulphur dioxide,

$$SO_2 + 2H_2S = 2H_2O + 3S^\circ \quad .$$

The overall reaction indicated by either of the reaction paths mentioned above is,

$$ZnS + \tfrac{1}{2}SO_2 + 2H^+ = Zn^{2+} + \tfrac{3}{2}S^\circ + H_2O \quad .$$

The addition of a soluble form of ferrous iron to the leaching media using sulphur dioxide alone or SO_2/N_2 gas mixtures does not alter the above mentioned dissolution processes. However, the addition of ferric iron does increase the rate of reaction to a limited extent. The increase is probably due to the direct oxidation of the sphalerite through the reaction,

Anodic: $ZnS + \tfrac{3}{2}H_2O = Zn^{2+} + \tfrac{1}{4}S_4O_6^{2-} + 3H^+ + \tfrac{9}{2}e^-$

Cathodic: $Fe^{3+} + e^- = Fe^{2+}$

acting in conjunction with the tetrathionate producing reactions which occur in the absence of iron. After complete conversion of ferric to ferrous iron, the dissolution proceeds via reaction with sulphur dioxide to produce tetrathionate. This conclusion is supported by the increased formation of the tetrathionate species in the presence of sulphur dioxide and ferric iron without the evolution of hydrogen sulphide.

It was observed that the reagent combination of sulphur dioxide, oxygen and soluble iron leads to a dramatic increase in the rate of sphalerite dissolution. Identical results were obtained when soluble iron was added either as ferrous or ferric ions. The high rate of dissolution was attributed directly to the production of sulphuric acid by the autoxidation process:

$$2Fe^{2+} + SO_2 + O_2 = 2Fe^{3+} + SO_4^{2-}$$

$$2SO_2 + O_2 + 2H_2O \xrightarrow{Fe^{3+}} 2H_2SO_4$$

where, SO_2/O_2 gas mixtures can oxidize ferrous iron to ferric iron and are simultaneously catalyzed by the ferric ion to form sulphuric acid. Sulphuric acid production was observed to increase with an increase in the SO_2/O_2 ratio of the reactant gas mixture to a maximum around 50% SO_2/O_2 and then decrease with greater SO_2/O_2 ratios. The rate of dissolution of the sphalerite accordingly increased with an increase in the SO_2/O_2 ratio of the gas mixture up to 50% SO_2/O_2 but, remained rapid and relatively constant for gas mixtures with 50% SO_2/O_2 and up to at least 80% SO_2/O_2. The rate of dissolution then decreased using 100% sulphur dioxide. Two different modes of dissolution were concluded to occur depending on the SO_2/O_2 ratio in the reactant gas mixture.

For SO_2/O_2 gas mixtures below 50% sulphur dioxide, hydrogen sulphide resulted, due to the production of sulphuric acid, and was swept out of the reactor by the flow of gas. This indicated that the dissolution was occurring by the reaction,

$$ZnS + 2H^+ = Zn^{2+} + H_2S \quad .$$

The increase in the rate of extraction directly followed the increase in sulphuric acid production with higher SO_2/O_2 gas ratios up to 50% SO_2/O_2. Sulphur dioxide, it was found, was completely consumed in the reactor vessel by the production of sulphuric acid. A high Fe^{3+}/Fe^{2+} ratio was established in the leach media with low SO_2/O_2 ratio gas mixtures. Since hydrogen sulphide was carried out of the reactor, it was concluded that the rate of oxidation of hydrogen sulphide by the ferric ion at a total iron concentration of 3.6 g dm^{-3} was slow.

Hydrogen sulphide, on the other hand, was not swept out of the reactor using SO_2/O_2 gas mixtures above 50% sulphur dioxide. Sulphur dioxide was observed to be present in the leach media and a low Fe^{3+}/Fe^{2+} ratio was established. It is postulated that the available sulphur dioxide is able to increase the rate of oxidation of hydrogen sulphide resulting in complete oxidation within the reactor vessel. Consequently, the removal of hydrogen sulphide from the leach media by oxidation with sulphur dioxide allows the rate of dissolution of sphalerite to remain high, although, there is less sulphuric acid present using SO_2/O_2 gas mixtures above 50% sulphur dioxide.

A thermodynamic Pourbaix diagram of the $Fe-S-SO_2-H_2O$ system was developed in this work from experimental solubility measurements on iron sulphite and from the data of Kao (1979). This diagram predicts that dissolved iron will be present in the leach medium in the form of the iron bisulphite complex ions, $FeHSO_3^{2+}$ and $FeHSO_3^{+}$, rather

than Fe^{3+} and Fe^{2+}, respectively, when leaching is carried out using an SO_2/O_2 gas mixture with more than 50% sulphur dioxide. Thus, the high rate of hydrogen sulphide oxidation observed when leaching with SO_2/O_2 gases with greater than 50% sulphur dioxide can be directly attributed to the sulphur dioxide available in the leach media. Although no attempt was made to identify a specific mechanism, two possible routes are indicated. Hydrogen sulphide oxidation could be occurring directly by the multi-step Wackenrhoder reaction,

$$2H_2S + SO_2 = 3S^\circ + 2H_2O$$

or, via a mechanism linked to the ferric bisulphite species. A possible reaction process is,

$$H_2S + 2FeHSO_3^{2+} = S^\circ + 2FeHSO_3^{+} + 2H^{+}$$

where the $2FeHSO_3^{2+}$ ion is regenerated by the reaction

$$SO_2 + O_2 + 2FeHSO_3^{+} = 2FeHSO_3^{2+} + SO_4^{2-} .$$

Therefore, the rate of dissolution with SO_2/O_2 ratios greater than about 0.5 is balanced between the decrease in sulphuric acid production and the increase in the rate of oxidation of hydrogen sulphide by sulphur dioxide in the leach media.

The kinetic data of the leaching experiments were analysed in terms of the generally accepted heterogeneous reaction models. The most suitable form of model appeared to be the surface reaction control equation of the shrinking core model. This applies to leaching carried out both in the presence and absence of dissolved iron. The rate of the dissolution reaction was found to be completely independent of the reactor stirrer speed in the absence of dissolved iron. In the presence of dissolved iron, reaction rates were independent of the stirrer speed above 500 rpm.

Consequently, all experiments were carried out at a stirrer speed of 800 rpm to ensure minimization of mass transfer effects.

The shrinking core model adequately describes the dissolution rate for SO_2/O_2 mixtures up to 50% SO_2 in the presence of soluble iron over the temperature range of 25°C to 90°C. The kinetics are determined by an equation of the form,

$$\left[\frac{k_r}{r_o \rho} \exp \frac{-E}{RT} \; C_{SO_2}^{n}\right] t = 1-(1-\alpha)^{\frac{1}{3}} \quad .$$

The observed reaction order with respect to sulphur dioxide, n, is about 0.6 and the activation energy is approximately 33 kJ mol^{-1} (8 kcal mol^{-1}). Therefore, it can be concluded that the dissolution rate of sphalerite in aqueous sulphurous acid is controlled by the rate of the reaction at the zinc sulphide surface. This is supported by: (1) the independence of the reaction rate on the stirring speed, (2) the fractional order dependence of the reaction rate with respect to the sulphur dioxide concentration and (3) an apparent activation energy of 33 kJ mol^{-1} (8 kcal mol^{-1}).

REFERENCES

Adams, R.W. and Matthew, I.G. (1981), "Leaching of Metal Sulphide Concentrates at Atmospheric Pressure Using SO_2/O_2 Mixtures", Proc.Australas.Inst.Min.Metall., No. 280, pp. 41-53.

Anon. (1977), Mt. Isa Mines Ltd. Staff, "Mount Isa Probes McArthur Deposits", Mine and Quarry Mechanisation, Publicity Press, Sydney, pp. 178-179.

Barin, I., Knacke, O. and Kubaschewski, O. (1977), Thermochemical Properties of Inorganic Substances, Springer-Verlag. Berlin.

Barner, H.E. and Scheuerman, R.N. (1978), Handbook of Thermochemical Data for Compounds and Aqueous Species, John Wiley and Sons, New York, N.Y.

Biernat, R.J. and Robins, R.G. (1969), "High Temperature Potential/pH Diagrams For The Sulphur-Water System", Electrochim.Acta, Vol. 14, pp 809-820.

Biernat, R.J. and Robins, R.G. (1972), "High Temperature Potential/pH Diagrams For The Iron-Water and Iron-Water-Sulphur Systems", Electrochim.Acta, Vol. 17, pp1261-1283.

Bolton, G.L., Zubrychkyj, N. and Veltman, H. (1981), "Pressure Leaching Process for Complex Zinc-Lead Concentration", Mineral Processing, Laskowski, J. ed., Elsevier Sci.Publ.Co., New York, pp 993-1019.

Burkin, A.R. (1966), The Chemistry of Hydrometallurgical Processes, Spon, London.

Cobble, J.W. (1953a), "The Entropies of Oxy-anions and Related Species", J.Chem.Phys., Vol. 21, pp 1443-1445.

Cobble, J.W.,(1953b), "Empirical Considerations of Entropy: The Entropies of Inorganic Complex Ions", J.Chem.Phys., Vol. 21, pp 1446-1450.

Connick, R.E. and Powell, R.E.,(1953), "The Entropy of Aqueous Oxy-anions", J.Chem.Phys., Vol. 21, pp2206-2207.

Couture, A.M. and Laidler, K.H. (1957), Can.J.Chem., Vol. 35, p 202.

Criss, C.M. and Cobble, J.W. (1964a), "The Thermodynamic Properties of High Temperature Aqueous Solutions. IV: Entropies of the Ions up to 200°C and The Correspondence Principal", J.Am.Chem.Soc., Vol. 86, pp 5385-5390.

Criss, C.M. and Cobble, J.W. (1964b), "The Thermodynamic Properties of High Temperature Aqueous Solutions. V: The Calculation of Ionic Heat Capacities up to 200°C, Entropies and Heat Capacities Above 200°C", J.Am.Chem.Soc., Vol. 86, pp 5390-5393.

Debus, H. (1888), "Chemical Investigation of Wackenrhoder's Solution, and Explanation of the Formation of its Constituents", Chapt. 25, Trans.J.Chem.Soc., Vol. 53, pp. 278-357.

Dewing, H.H. and Cochran, A.A. (1978), "Sulphuric Acid Extraction Technique for Recovering Zinc and Sulfur from Sphalerite", U.S. Bureau of Mines, R.I. 8322, 14p.

Dewing, H.H., Lay, S.E. and Cochran, A.A. (1982), "Recovery of Zinc and Sulfur from Sphalerite Concentrates by Reaction with Sulphuric Acid", U.S. Bureau of Mines, R.I. 8690, 16p.

Dutrizac, J.E. and MacDonald, R.J.C. (1974), "Ferric Ion as a Leaching Medium", Minerals Sci.Engng., Vol. 6, no. 2, pp 59-100.

Esdaile, J.D. and Walters, G.W. (1969), "Studies of Sulphite Processes For The Treatment of McArthur River Ore", CSIRO Australia Report R17, 43p.

Feitknecht, W. and Schindler, P. (1963), "Solubility Constants of Metal Oxides, Metal Hydroxides and Metal Hydroxide Salts in Aqueous Solution", Pure Applied Chemistry, Vol. 6, Butterworths, London, pp 134-198.

Ferreira, R.C.H. (1975), "High-Temperature E-pH Diagrams For The Systems S-H_2O, Cu-S-H_2O and Fe-S-H_2O", Leaching and Reduction in Hydrometallurgy, A.R. Burkin ed., I.M.M., London, pp 67-83.

Foreward, F.A. and Veltman, H. (1959), "Direct Leaching of Zinc-Sulfide Concentrates by Sherritt Gordon", J.Metals, Vol. 11, pp 836-840.

Foreward, F.A. and Warren, I.H., (1960), "Extraction of Metals from Sulphide Ores by Wet Methods", Metall. Revs., Vol. 5, no. 18, pp 137-164.

Garrels, R.M. and Christ, C.L. (1965), Solutions, Minerals and Equilibria, Harper and Row, New York, N.Y.

Gerlach, J. and Pawlek, F. (1968), "On the Kinetics of Pressure Leaching of Metal Sulfides and Ores", TMS Paper Selection A68-4, The Metallurgical Society of AIME, 16p.

Habashi, F. (1969), "Principals of Extractive Metallurgy", Gordon and Breach, New York, N.Y.

Habashi, F. (1971), "The Electrometallurgy of Sulphides in Aqueous Solutions", Minerals Sci.Engng., Vol. 3, no. 3, pp 3-12.

Halpern, J. (1957), "Some Aspects of the Physical Chemistry of Hydrometallurgy", J.Metals, pp 280-289.

Heuston, F.T. and Tichborne, C.R. (1890), "A Non-Poisonous, Non-Irritative, Antiseptic Dressing", Brit.Med.J., pp 1063-1064.

Hiskey, J.B. and Wadsworth, M.E. (1981), "Electrochemical Processes in the Leaching of Metal Sulphides and Oxides", Chapter 26, Process and Fundamental Considerations of Selected Hydrometallurgical Systems, Ed. M.C. Kuhn, AIME, New York, N.Y., pp 303-325.

Ishida, M. and Wen, C.Y. (1971), Chem.Eng.Sci., Vol. 26, p 1031.

Jackson, K.J. and Strickland, J.D.H. (1958), "The Dissolution of Sulfide Ores in Acid Chlorine Solutions; A Study of the More Common Sulfide Minerals", Trans. Met.Soc. of AIME, Vol. 212, pp 373-379.

Johnstone, H.F. and Singh, A.D. (1940), "Recovery of Sulfur Dioxide from Waste Gases: Regeneration of the Absorbent by Treatment with Zinc Oxide", Industrial and Engineering Chemistry, Vol. 32, no. 8, pp 1037-1049.

Joint Committee on Powder Diffraction Standards, 1601 Park Lane, Swarthmore, Pa. 19081.

Kao, C.F. (1979), "Thermodynamic and Kinetic Studies of the Iron-Sulphite System by Electrochemical Methods", Eng.Sc.D. Thesis, Columbia University, NYC, New York.

Karraker, P.G. (1963), "The Kinetics of the Reaction Between Sulfurous Acid and Ferric Ion", J.Phys.Chem., Vol. 67, pp 871-874.

Kelly, D.P., Chambers, L.A. and Trudinger, P.A. (1969), "Cyanolysis and Spectrophotometric Estimation of Trithionate in Mixture with Thiosulphate and Tetrathionate", Analytical Chemistry, Vol. 47, no. 7, pp 898-901.

Keyes, H.E. (1946), "Autoxidation Process for Sulphuric Acid and Sulphate Production", Chem. & Metall. Engng., Vol. 53, pp 126-130.

Kielland, (1937), J.Am.Chem.Soc., Vol. 59, p 1675.

Kopp, H. (1864), Ann.Chem.Pharm.Suppl., Vol. 3, no. 1, p 289.

Kuzminkh, I.N. and Yakhontova, E.L. (1950a), "Action of Solutions of Ferric Sulfate on Zinc Sulfide", Zh. Priklad.Khim., Vol. 23, pp 1121-1126.

Kuzminkh, I.N. and Yakhontova, E.L. (1950b), "Wet Extraction of Zinc From Mixtures of Sulfides", Zh. Priklad.Khim., Vol. 23, pp 1142-1148.

Kwok, O.J. and Robins, R.G. (1973), "Thermal Precipitation in Aqueous Solutions", Intern.Symposium of Hydrometallurgy, Chicago 1973, Ed. Evans and Shoemaker, AIME, New York, N.Y.

Langmuir, D. (1971), "Eh-pH Determination", Ch. 26 in: Methods in Sedimentary Petrology, R.E. Carver, ed., John Wiley and Sons, New York, pp 597-634.

Latimer, W.M. (1921), J.Am.Chem.Soc., Vol. 43, p 818.

Latimer, W.M. (1951), J.Am.Chem.Soc., Vol. 73, p 1480.

Latimer, W.M. (1952), Oxidation Potentials, 2nd ed., Prentice-Hall, Inc., Englewood Cliffs, N.J., p 392.

Levenspiel, O. (1972), Chemical Reaction Engineering , 2nd ed., John Wiley and Sons, New York.

Linkson, P.B. (1983), "Precipitation of Metal Sulphites From Aqueous Liquors", Hydrometallurgy: Research, Development and Plant Practice, Ed., K.Osseo-Asare and J.D. Miller, Proc. 3rd Int. Symp. on Hydrometallurgy, Atlanta, Ga., AIME, New York, N.Y., pp 311-327.

Linkson, P.B., Phillips, B.D. and Rowles, C.D. (1979), "Computer Methods For The Generation of Eh-pH Diagrams", Min.Sci.Eng., Vol. 11, no. 2, p 77.

Lowson, R.T. (1971), "Potential-pH Diagrams At Temperatures Above 298.16°K. Part 1: Theoretical Background", Report AAEC-E219 pt. 1.

Majima, H. and Peters, E. (1966), "Oxidation Rates of Sulfide Minerals by Aqueous Oxidation at Elevated Temperatures", Trans.Met.Soc. AIME, Vol. 236, pp 1409-1413.

McDonald, D.D., et al (1972), "The Thermodynamics of Metal-Water Systems at Elevated Temperatures. Part 1: The Water and Water-Copper Systems", Report AECL-4136.

Mizoguchi, T. and Habashi, F. (1983), "Aqueous Oxidation of Zinc Sulphide, Pyrite and Their Mixtures in Hydrochloric Acid", Trans.Instn.Min.Metall.Sect. C, Vol. 92, pp C14-C19.

Narasagoudar, R.A., Johnson, J.W. and O'Keefe, T.J. (1982), "The Anodic Dissolution of ZnS Electrodes in Sulfuric Acid Solutions", Hydrometallurgy, 9, pp 37-55.

Naumov, G.B., Ryzhenko, B.N. and Khodakovsky, I.L., (1974), Handbook of Thermodynamic Data, U.S. Dept. of Commerce, NTIS, PB-226 722.

Nietzel, O.A. and DeSesa, M.A. (1955), "Spectrophotometric Determination of Tetrathionate", Analytical Chemistry, Vol. 47, no. 7, pp 898-901.

Nobbs, D.M. and Linkson, P.B. (1981), "A New Two-Stage Hydrometallurgical Process for the Recovery of Metallic Copper from Sulfite Leach Liquors", Extraction Metallurgy '81, Inst. of Min. and Met., London, pp 49-56.

Parker, A.J. and Muir, D.M. (1981), "Recovery of Copper Powder from Copper Concentrates and from Solutions of Copper (II) Sulfates using Sulfur Dioxide and Aqueous Acetonitrile", Hydrometallurgy, Vol. 6, pp 239-260.

Pauling, L. (1952), "Interatomic Distances and Bond Character in the Oxygen Acids and Related Substances", J.Phys.Chem., Vol. 56, pp 361-365.

Pawlek, F.E. (1969), "Research in Pressure Leaching", J.South African Inst.Min.and Metl., Vol. 69, no. 12, pp 632-654.

Peters, E. (1976), "Direct Leaching of Sulfides: Chemistry and Applications", Metallurgical Transactions B, Vol. 7B, pp 505-517.

Peters, E. (1977), "The Electrochemistry of Sulphide Minerals", Trends in Electrochmistry, Ed. J.O'M. Bockris, D.A.J. Rand and B.J. Welch, Plenum Publishing Corp., pp 267-290.

Peters, E. and Majima, H. (1968), "The Physical Chemistry of Leaching of Sulphide Minerals", TMS Paper Selection A68-32, The Metallurgical Society of AIME, New York, N.Y.

Pourbaix, M. (1949), Thermodynamics of Dilute Aqueous Solutions, Edward Arnold and Co., London.

Pourbaix, M., ed. (1966), Atlas of Electrochemical Equilibria in Aqueous Solutions, Pergamon Press, New York, N.Y.

Pourbaix, M. and Yang, X.Z. (1981), "Chemical and Electrochemical Equilibria in the Presence of a Gaseous Phase. Part 5, Oxygen-Hydrogen", Rapports Techniques CEBELCOR, Vol. 140, RT 260.

Powell, R.E. and Latimer, W.M. (1951), "The Entropy of Aqueous Solutes", J.Chem.Phys., Vol. 19, pp 1139-1142.

Rath, P.C., Paramguru, R.K. and Jena, P.K. (1981), "Kinetics of Dissolution of Zinc Sulphide in Aqueous Ferric Chloride Solution", Hydrometallurgy 6, pp 219-225.

Ricci, J.E. (1952), Hydrogen Ion Concentration, Princeton University Press, Princeton, N.J., p 460.

Romankiw, L.T. and de Bruyn, P.L. (1964), "Kinetics of Dissolution of Zinc Sulfide in Aqueous Sulfuric Acid", Unit Processes in Hydrometallurgy, Ed. M.E. Wadsworth and F.T. Davis, TMS of AIME. Conferences Volume 24, Gordon and Breach, Science Publishers, Inc. New York, N.Y., pp 45-66.

Schroeter, L.C. (1966), Sulfur Dioxide: Applications in Foods, Beverages and Pharmaceuticals, Pergamon Press, New York, N.Y., pp 92-93.

Scott, P.D. and Nicol, M.J. (1977), "The Kinetics and Mechanisms of the Non-Oxidative Dissolution of Metal Sulphides", Trends in Electrochemistry, Ed. J.O'M Bockris, D.A.J. Rand and B.J. Welch, Plenum Publishing Corp., pp 303-316.

Scott, P.D. and Nicol, M.J. (1978), "The Kinetics of the Leaching of Zinc Sulphide Concentrates in Acidic Solutions Containing Ferric Sulphate", National Institute for Metallurgy, South Africa, rpt. no. 1949, 12p.

Scott, T.R. and Dyson, N.F. (1968), "The Catalyzed Oxidation of Zinc Sulfide under Acid Pressure Leaching Conditions", Trans.Met.Soc. AIME, Vol. 242, pp 1815-1821.

Sobol, S.I. and Frash, T.M. (1974), "Sulfur Dioxide in the Autoclave Technology of Processing Sulfide Raw Material", Tsvetnye Metally, Vol. 47, no. 2, pp 14-20.

Stanczyk, M.H. and Rampacek, C. (1961), "Dissolution of Zinc from Sphalerite at Elevated Temperatures and Pressures". U.S. Bureau of Mines, R.I. 5848, 23p.

Sudderth, R.B., Clitheroe, J.B. and Kordosky, G.A. (1978), "The Sulfite System - A New Hydrometallurgical Process for Zinc", presented at AIME Annual Meeting, Denver, Co..

Thorne, P.C.L. and Roberts, E.R. (1948), "Fritz Ephraim Inorganic Chemistry", 5th ed., Interscience, New York, p 573.

Tiwari, B.L. (1976), "The Kinetics of Oxidation of Zinc Sulfide and Hydrogen Sulfide by Sulfur Dioxide in Aqueous Sulfuric Acid", Eng.Sc.D. Thesis, Columbia University, NYC, N.Y.

Tiwari, B.L., Kolbe, J. and Hayden, H.W. (1979), "Oxidation of Ferrous Sulfate in Acid Solution by a Mixture of Sulfur Dioxide and Oxygen", Metallurgical Transactions B, Vol. 10B, pp 607-612.

Trudinger, P.A. (1961), Biochemical Journal, Vol. 78, pp 680-686.

Valensi, G. (1950), "Contribution au diagramme potential-pH du soufre", Proc. 2nd Meeting CITCE, Milan, pp 51-68.

Veltman, H. and Bolton, G.L. (1980), "Direct Pressure Leaching of Zinc Blends with Simultaneous Production of Elemental Sulphur. A State-of-the-Art Review", Erzmetall. 33, no. 2, pp 77-83.

Venkataswamy, Y. and Khangaonkar, P.R. (1981), "Ferric Chloride Leaching of Sphalerite in the Presence of an Organic Solvent for Sulphur", Hydrometallurgy 7, pp 1-5.

Verbaan, B. (1980), "The Leaching of Sphalerite in Acidic Ferric Sulphate Media in the Absence of Elemental Oxygen", National Institute for Metallurgy, South Africa, rpt.no. 2038, 34p.

Verhulst, D. (1974), "The Kinetics of Oxidation of Hydrogen Sulfide and Zinc Sulfide by Ferric Iron in Sulfuric Acid Solution", Eng.Sc.D.Thesis, Columbia University, N.Y.C., N.Y.

Vogel, A.I., (1961), "Quantitative Inorganic Analysis", 3rd ed., Longmans, Green and Co. Ltd., London.

Wadsworth, M.E. (1972), "Advances in the Leaching of Sulphide Minerals", Minerals Sci.Engng., Vol. 4, no. 4, pp 36-47.

Wadsworth, M.E. (1981), "Electrochemical Reactions in Hydrometallurgy", in Metallurgical Treatises, Tien, J.K. and Elliott, J.F., ed., The Metallurgical Society of AIME, pp 1-22.

Wagman, D.D., Evans, W.H., Parker, V.B., Schumm, R.H., Halow, I., Bailey, S.M., Churney, K.L. and Nuttal, R.L. (1982), "The NBS Tables of Chemical Thermodynamic Properties", J.Phys. and Chem.Ref.Data, Vol. 11, no. 2, The American Chemical Society and The NBS, Washington, D.C..

Wells, A.F. (1949), "Bond Lengths in Some Inorganic Molecules and Complex Ions", J.Chem.Soc., pp 55-67.

Wen, C.Y. (1968), Ind.Eng.Chem., Vol. 60, p 34.

Woodcock, J.T. (1961), "Some Aspects of the Oxidation of Sulphide Minerals in Aqueous Suspension", Proc.Aus. I.M.M., no. 198, pp 47-84.

APPENDIX 1

REACTIONS BETWEEN THE SPECIES OF THE $Zn-S-SO_2-H_2O$ SYSTEM

Zinc Species

1. $Zn(OH)_2 = Zn + 2H_2O$
2a. $ZnSO_3 \cdot 2\frac{1}{2}H_2O + 2H^+ + 2e^- = Zn + SO_2(aq) + 3\frac{1}{2}H_2O$
2b. $ZnSO_3 \cdot 2\frac{1}{2}H_2O + H^+ + 2e^- = Zn + HSO_3^- + 2\frac{1}{2}H_2O$
2c. $ZnSO_3 \cdot 2\frac{1}{2}H_2O + 2e^- = Zn + SO_3^{2-} + 2\frac{1}{2}H_2O$
3. $Zn^{2+} + 2e^- = Zn$
4. $ZnOH^+ + H^+ + 2e^- = Zn + H_2O$
5. $Zn(OH)_2(aq) + 2H^+ + 2e^- = Zn + 2H_2O$
6. $Zn(OH)_3^- + 3H^+ + 2e^- = Zn + 3H_2O$
7. $Zn(OH)_4^{2-} + 4H^+ + 2e^- = Zn + 4H_2O$
8a. $ZnSO_3 \cdot 2\frac{1}{2}H_2O = Zn(OH)_2 + SO_2(aq) + 1\frac{1}{2}H_2O$
8b. $ZnSO_3 \cdot 2\frac{1}{2}H_2O = Zn(OH)_2 + HSO_3^- + H^+ + \frac{1}{2}H_2O$
8c. $ZnSO_3 \cdot 2\frac{1}{2}H_2O = Zn(OH)_2 + SO_3^{2-} + 2H^+ + \frac{1}{2}H_2O$
9. $Zn^{2+} + 2H_2O = Zn(OH)_2 + 2H^+$
10. $ZnOH^+ + H_2O = Zn(OH)_2 + H^+$
11. $Zn(OH)_2 = Zn(OH)_2(aq)$
12. $Zn(OH)_2 + H_2O = Zn(OH)_3^- + H^+$
13. $Zn(OH)_2 + 2H_2O = Zn(OH)_4^{2-} + 2H^+$
14a. $Zn^{2+} + SO_2(aq) + 3\frac{1}{2}H_2O = ZnSO_3 \cdot 2\frac{1}{2}H_2O + 2H^+$
14b. $Zn^{2+} + HSO_3^- + 2\frac{1}{2}H_2O = ZnSO_3 \cdot 2\frac{1}{2}H_2O + H^+$
14c. $Zn^{2+} + SO_3^{2-} + 2\frac{1}{2}H_2O = ZnSO_3 \cdot 2\frac{1}{2}H_2O$
15a. $ZnOH^+ + SO_2(aq) + 2\frac{1}{2}H_2O = ZnSO_3 \cdot 2\frac{1}{2}H_2O + H^+$
15b. $ZnOH^+ + HSO_3^- + 1\frac{1}{2}H_2O = ZnSO_3 \cdot 2\frac{1}{2}H_2O$
15c. $ZnOH^+ + SO_3^{2-} + H^+ + 1\frac{1}{2}H_2O = ZnSO_3 \cdot 2\frac{1}{2}H_2O$

16a. $ZnSO_3 \cdot 2\frac{1}{2}H_2O = Zn(OH)_2(aq) + SO_2(aq) + 1\frac{1}{2}H_2O$

16b. $ZnSO_3 \cdot 2\frac{1}{2}H_2O = Zn(OH)_2(aq) + HSO_3^- + H^+ + \frac{1}{2}H_2O$

16c. $ZnSO_3 \cdot 2\frac{1}{2}H_2O = Zn(OH)_2(aq) + SO_3^{2-} + 2H^+ + \frac{1}{2}H_2O$

17a. $ZnSO_3 \cdot 2\frac{1}{2}H_2O = Zn(OH)_3^- + SO_2(aq) + H^+ + \frac{1}{2}H_2O$

17b. $ZnSO_3 \cdot 2\frac{1}{2}H_2O + \frac{1}{2}H_2O = Zn(OH)_3^- + HSO_3^- + 2H^+$

17c. $ZnSO_3 \cdot 2\frac{1}{2}H_2O + \frac{1}{2}H_2O = Zn(OH)_3^- + SO_3^{2-} + 3H^+$

18a. $ZnSO_3 \cdot 2\frac{1}{2}H_2O + \frac{1}{2}H_2O = Zn(OH)_4^{2-} + SO_2(aq) + 2H^+$

18b. $ZnSO_3 \cdot 2\frac{1}{2}H_2O + 1\frac{1}{2}H_2O = Zn(OH)_4^{2-} + HSO_3^- + 3H^+$

18c. $ZnSO_3 \cdot 2\frac{1}{2}H_2O + 1\frac{1}{2}H_2O = Zn(OH)_4^{2-} + SO_3^{2-} + 4H^+$

19. $Zn^{2+} + H_2O = ZnOH^+ + H^+$

20. $Zn^{2+} + 2H_2O = Zn(OH)_2(aq) + 2H^+$

21. $Zn^{2+} + 3H_2O = Zn(OH)_3^- + 3H^+$

22. $Zn^{2+} + 4H_2O = Zn(OH)_4^{2-} + 4H^+$

23. $ZnOH^+ + H_2O = Zn(OH)_2(aq) + H^+$

24. $ZnOH^+ + 2H_2O = Zn(OH)_3^- + 2H^+$

25. $ZnOH^+ + 3H_2O = Zn(OH)_4^{2-} + 3H^+$

26. $Zn(OH)_2(aq) + H_2O = Zn(OH)_3^- + H^+$

27. $Zn(OH)_2(aq) + 2H_2O = Zn(OH)_4^{2-} + 2H^+$

28. $Zn(OH)_3^- + H_2O = Zn(OH)_4^{2-} + H^+$

29. $ZnSO_3 \cdot 2\frac{1}{2}H_2O + 6H^+ + 4e^- = Zn^{2+} + S + 5\frac{1}{2}H_2O$

30. $4ZnSO_3 \cdot 2\frac{1}{2}H_2O + 12H^+ + 6e^- = 4Zn^{2+} + S_4O_6^{2-} + 16H_2O$

31. $ZnS + 2H^+ = Zn^{2+} + H_2S\ (aq)$

32. $Zn^{2+} + S + 2e^- = ZnS$

33. $Zn^{2+} + SO_2(aq) + 4H^+ + 6e^- = ZnS + 2H_2O$

34. $Zn^{2+} + HSO_3^- + 5H^+ + 6e^- = ZnS + 3H_2O$

35. $4Zn^{2+} + S_4O_6^{2-} + 12H^+ + 18e^- = 4ZnS + 6H_2O$

36. $ZnSO_3 \cdot 2\frac{1}{2}H_2O + 6H^+ + 6e^- = ZnS + 5\frac{1}{2}H_2O$

37. $Zn(OH)_2 + HSO_3^- + 7H^+ + 6e^- = ZnS + 5H_2O$

38. $Zn(OH)_2 + SO_3^{2-} + 8H^+ + 6e^- = ZnS + 5H_2O$

39. $Zn(OH)_4^{2-} + SO_3^{2-} + 10H^+ + 6e^- = ZnS + 7H_2O$

40. $Zn(OH)_4^{2-} + S^{2-} + 4H^+ = ZnS + 4H_2O$

41. $ZnS + 2H^+ + 2e^- = Zn + H_2S(aq)$

42. $ZnS + H^+ + 2e^- = Zn + HS^-$

43. $ZnS + 2e^- = Zn + S^{2-}$

Sulfur Species

44. $SO_2(aq) + 4H^+ + 4e^- = S + 2H_2O$

45. $HSO_3^- + 5H^+ + 4e^- = S + 3H_2O$

46. $SO_3^{2-} + 6H^+ + 4e^- = S + 3H_2O$

47. $S + 2H^+ + 2e^- = H_2S(aq)$

48. $S + H^+ + 2e^- = HS^-$

49. $SO_3^{2-} + 7H^+ + 6e^- = HS^- + 3H_2O$

50. $SO_3^{2-} + 6H^+ + 6e^- = S^{2-} + 3H_2O$

51. $SO_2(aq) + H_2O = HSO_3^- + H^+$

52. $HSO_3^- = SO_3^{2-} + H^+$

53. $H_2S(aq) = HS^- + H^+$

54. $HS^- = S^{2-} + H^+$

55. $2HSO_3^- + 4H^+ + 4e^- = S_2O_3^{2-} + 3H_2O$

56. $2SO_3^{2-} + 6H^+ + 4e^- = S_2O_3^{2-} + 3H_2O$

57. $S_2O_3^{2-} + 6H^+ + 4e^- = 2S + 3H_2O$

58. $S_2O_3^{2-} + 8H^+ + 8e^- = 2HS^- + 3H_2O$

59. $S_2O_3^{2-} + 6H^+ + 8e^- = 2S^{2-} + 3H_2O$

60. $S_4O_6^{2-} + 2e^- = 2S_2O_3^{2-}$

61. $4SO_2(aq) + 4H^+ + 6e^- = S_4O_6^{2-} + 2H_2O$

62. $4HSO_3^- + 8H^+ + 6e^- = S_4O_6^{2-} + 6H_2O$

63. $S_4O_6^{2-} + 12H^+ + 10e^- = 4S + 6H_2O$

Aqueous Species

64. $2H^+ + 2e^- = H_2$

65. $O_2 + 4H^+ + 4e^- = 2H_2O$

APPENDIX 2

EQUILIBRIUM EQUATIONS FOR THE REACTIONS OF APPENDIX 1

$$AEh = B + CpH + D \log R^*$$

REACTION	T(°C)	A	B	C	D	R^*
1	25	1	-0.419	-0.0592		
	60	1	-0.426	-0.0661		
	100	1	-0.430	-0.0740		
	150	1	-0.431	-0.0839		
	200	1	-0.430	-0.0939		
2a	25	1	-0.647	-0.0592	-0.0296	$SO_2(aq)$
	60	1	-0.624	-0.0661	-0.0330	$SO_2(aq)$
	100	1	-0.595	-0.0740	-0.0370	$SO_2(aq)$
	150	1	-0.553	-0.0839	-0.0420	$SO_2(aq)$
	200	1	-0.505	-0.0939	-0.0469	$SO_2(aq)$
2b	25	1	-0.699	-0.0296	-0.0296	HSO_3^-
	60	1	-0.694	-0.0330	-0.0330	HSO_3^-
	100	1	-0.687	-0.0370	-0.0370	HSO_3^-
	150	1	-0.681	-0.0420	-0.0420	HSO_3^-
	200	1	-0.668	-0.0469	-0.0469	HSO_3^-
2c	25	1	-0.913	0	-0.0296	SO_3^{2-}
	60	1	-0.943	0	-0.0330	SO_3^{2-}
	100	1	-0.984	0	-0.0370	SO_3^{2-}
	150	1	-1.041	0	-0.0420	SO_3^{2-}
	200	1	-1.112	0	-0.0469	SO_3^{2-}
3	25	1	-0.762	0	0.0296	Zn^{2+}
	60	1	-0.759	0	0.0330	Zn^{2+}
	100	1	-0.755	0	0.0370	Zn^{2+}
	150	1	-0.750	0	0.0420	Zn^{2+}
	200	1	-0.747	0	0.0469	Zn^{2+}
4	25	1	-0.482	-0.0296	0.0296	$ZnOH^+$
	60	1	-0.516	-0.0330	0.0330	$ZnOH^+$
	100	1	-0.535	-0.0370	0.0370	$ZnOH^+$
	150	1	-0.556	-0.0420	0.0420	$ZnOH^+$
	200	1	-0.578	-0.0469	0.0469	$ZnOH^+$

NOTE: R^* = activity ratio, written in terms of species formula.

REACTION	T(°C)	A	B	C	D	R*
5	25	1	-0.251	-0.0591	0.0296	$Zn(OH)_2(aq)$
	60	1	-0.308	-0.0661	0.0330	$Zn(OH)_2(aq)$
	100	1	-0.292	-0.0740	0.0370	$Zn(OH)_2(aq)$
	150	1	-0.270	-0.0839	0.0420	$Zn(OH)_2(aq)$
	200	1	-0.249	-0.0939	0.0469	$Zn(OH)_2(aq)$
6	25	1	0.089	-0.0887	0.0296	$Zn(OH)_3^-$
	60	1	0.034	-0.0991	0.0330	$Zn(OH)_3^-$
	100	1	0.036	-0.1110	0.0370	$Zn(OH)_3^-$
	150	1	0.049	-0.1259	0.0420	$Zn(OH)_3^-$
	200	1	0.068	-0.1408	0.0469	$Zn(OH)_3^-$
7	25	1	0.466	-0.1183	0.0296	$Zn(OH)_4^{2-}$
	60	1	0.431	-0.1322	0.0330	$Zn(OH)_4^{2-}$
	100	1	0.476	-0.1480	0.0370	$Zn(OH)_4^{2-}$
	150	1	0.547	-0.1679	0.0420	$Zn(OH)_4^{2-}$
	200	1	0.644	-0.1877	0.0469	$Zn(OH)_4^{2-}$
8a	25	0	7.71	0	1	$SO_2(aq)$
	60	0	6.00	0	1	$SO_2(aq)$
	100	0	4.46	0	1	$SO_2(aq)$
	150	0	2.90	0	1	$SO_2(aq)$
	200	0	1.59	0	1	$SO_2(aq)$
8b	25	0	-9.47	1	-1	HSO_3^-
	60	0	-8.11	1	-1	HSO_3^-
	100	0	-6.97	1	-1	HSO_3^-
	150	0	-5.95	1	-1	HSO_3^-
	200	0	-5.06	1	-1	HSO_3^-
8c	25	0	-16.69	2	-1	SO_3^{2-}
	60	0	-15.66	2	-1	SO_3^{2-}
	100	0	-14.99	2	-1	SO_3^{2-}
	150	0	-14.52	2	-1	SO_3^{2-}
	200	0	-14.53	2	-1	SO_3^{2-}
9	25	0	-11.60	2	1	Zn^{2+}
	60	0	-10.08	2	1	Zn^{2+}
	100	0	-8.80	2	1	Zn^{2+}
	150	0	-7.59	2	1	Zn^{2+}
	200	0	-6.74	2	1	Zn^{2+}

REACTION	T(°C)	A	B	C	D	R*
10	25	0	-2.13	1	1	$ZnOH^+$
	60	0	-2.72	1	1	$ZnOH^+$
	100	0	-2.85	1	1	$ZnOH^+$
	150	0	-2.98	1	1	$ZnOH^+$
	200	0	-3.14	1	1	$ZnOH^+$
11	25	0	5.67	0	1	$Zn(OH)_2(aq)$
	60	0	3.56	0	1	$Zn(OH)_2(aq)$
	100	0	3.70	0	1	$Zn(OH)_2(aq)$
	150	0	3.84	0	1	$Zn(OH)_2(aq)$
	200	0	3.87	0	1	$Zn(OH)_2(aq)$
12	25	0	-17.16	1	-1	$Zn(OH)_3^-$
	60	0	-13.91	1	-1	$Zn(OH)_3^-$
	100	0	-12.57	1	-1	$Zn(OH)_3^-$
	150	0	-11.43	1	-1	$Zn(OH)_3^-$
	200	0	-10.62	1	-1	$Zn(OH)_3^-$
13	25	0	-29.92	2	-1	$Zn(OH)_4^{2-}$
	60	0	-15.92	2	-1	$Zn(OH)_4^{2-}$
	100	0	-24.48	2	-1	$Zn(OH)_4^{2-}$
	150	0	-23.30	2	-1	$Zn(OH)_4^{2-}$
	200	0	-22.89	2	-1	$Zn(OH)_4^{2-}$
14a	25	0	-3.90	2	1	$Zn^{2+} . SO_2(aq)$
	60	0	-4.08	2	1	$Zn^{2+} . SO_2(aq)$
	100	0	-4.34	2	1	$Zn^{2+} . SO_2(aq)$
	150	0	-4.69	2	1	$Zn^{2+} . SO_2(aq)$
	200	0	-5.14	2	1	$Zn^{2+} . SO_2(aq)$
14b	25	0	-2.13	1	1	$Zn^{2+} . HSO_3^-$
	60	0	-1.97	1	1	$Zn^{2+} . HSO_3^-$
	100	0	-1.63	1	1	$Zn^{2+} . HSO_3^-$
	150	0	-1.64	1	1	$Zn^{2+} . HSO_3^-$
	200	0	-1.68	1	1	$Zn^{2+} . HSO_3^-$
14c	25	0	5.06	0	1	$Zn^{2+} . SO_3^{2-}$
	60	0	5.58	0	1	$Zn^{2+} . SO_3^{2-}$
	100	0	6.19	0	1	$Zn^{2+} . SO_3^{2-}$
	150	0	6.93	0	1	$Zn^{2+} . SO_3^{2-}$
	200	0	7.79	0	1	$Zn^{2+} . SO_3^{2-}$

REACTION	T(°C)	A	B	C	D	R*
15a	25	0	5.58	1	1	$ZnOH^+ . SO_2(aq)$
	60	0	3.29	1	1	$ZnOH^+ . SO_2(aq)$
	100	0	1.62	1	1	$ZnOH^+ . SO_2(aq)$
	150	0	-0.08	1	1	$ZnOH^+ . SO_2(aq)$
	200	0	-1.55	1	1	$ZnOH^+ . SO_2(aq)$
15b	25	0	7.34	0	1	$ZnOH^+ . HSO_3^-$
	60	0	5.39	0	1	$ZnOH^+ . HSO_3^-$
	100	0	4.12	0	1	$ZnOH^+ . HSO_3^-$
	150	0	2.97	0	1	$ZnOH^+ . HSO_3^-$
	200	0	1.92	0	1	$ZnOH^+ . HSO_3^-$
15c	25	0	14.56	-1	1	$ZnOH^+ . SO_3^{2-}$
	60	0	12.94	-1	1	$ZnOH^+ . SO_3^{2-}$
	100	0	12.14	-1	1	$ZnOH^+ . SO_3^{2-}$
	150	0	11.54	-1	1	$ZnOH^+ . SO_3^{2-}$
	200	0	11.39	-1	1	$ZnOH^+ . SO_3^{2-}$
16a	25	0	13.37	0	1	$Zn(OH)_2(aq) . SO_2(aq)$
	60	0	9.47	0	1	$Zn(OH)_2(aq) . SO_2(aq)$
	100	0	8.16	0	1	$Zn(OH)_2(aq) . SO_2(aq)$
	150	0	6.74	0	1	$Zn(OH)_2(aq) . SO_2(aq)$
	200	0	5.47	0	1	$Zn(OH)_2(aq) . SO_2(aq)$
16b	25	0	15.14	-1	1	$Zn(OH)_2(aq) . HSO_3^-$
	60	0	11.67	-1	1	$Zn(OH)_2(aq) . HSO_3^-$
	100	0	10.66	-1	1	$Zn(OH)_2(aq) . HSO_3^-$
	150	0	9.78	-1	1	$Zn(OH)_2(aq) . HSO_3^-$
	200	0	8.93	-1	1	$Zn(OH)_2(aq) . HSO_3^-$
16c	25	0	22.36	-2	1	$Zn(OH)_2(aq) . SO_3^{2-}$
	60	0	19.22	-2	1	$Zn(OH)_2(aq) . SO_3^{2-}$
	100	0	18.69	-2	1	$Zn(OH)_2(aq) . SO_3^{2-}$
	150	0	18.36	-2	1	$Zn(OH)_2(aq) . SO_3^{2-}$
	200	0	18.40	-2	1	$Zn(OH)_2(aq) . SO_3^{2-}$
17a	25	0	24.87	-1	1	$Zn(OH)_3^- . SO_2(aq)$
	60	0	19.92	-1	1	$Zn(OH)_3^- . SO_2(aq)$
	100	0	17.04	-1	1	$Zn(OH)_3^- . SO_2(aq)$
	150	0	14.34	-1	1	$Zn(OH)_3^- . SO_2(aq)$
	200	0	12.22	-1	1	$Zn(OH)_3^- . SO_2(aq)$

REACTION	T(°C)	A	B	C	D	R*
17b	25	0	26.63	-2	1	$Zn(OH)_3^- . HSO_3^-$
	60	0	22.02	-2	1	$Zn(OH)_3^- . HSO_3^-$
	100	0	19.54	-2	1	$Zn(OH)_3^- . HSO_3^-$
	150	0	17.38	-2	1	$Zn(OH)_3^- . HSO_3^-$
	200	0	15.68	-2	1	$Zn(OH)_3^- . HSO_3^-$
17c	25	0	33.86	-3	1	$Zn(OH)_3^- . SO_3^{2-}$
	60	0	29.57	-3	1	$Zn(OH)_3^- . SO_3^{2-}$
	100	0	27.57	-3	1	$Zn(OH)_3^- . SO_3^{2-}$
	150	0	25.95	-3	1	$Zn(OH)_3^- . SO_3^{2-}$
	200	0	25.15	-3	1	$Zn(OH)_3^- . SO_3^{2-}$
18a	25	0	37.63	-2	1	$Zn(OH)_4^{2-} . SO_2(aq)$
	60	0	31.93	-2	1	$Zn(OH)_4^{2-} . SO_2(aq)$
	100	0	28.94	-2	1	$Zn(OH)_4^{2-} . SO_2(aq)$
	150	0	26.21	-2	1	$Zn(OH)_4^{2-} . SO_2(aq)$
	200	0	24.49	-2	1	$Zn(OH)_4^{2-} . SO_2(aq)$
18b	25	0	39.39	-3	1	$Zn(OH)_4^{2-} . HSO_3^-$
	60	0	34.03	-3	1	$Zn(OH)_4^{2-} . HSO_3^-$
	100	0	31.44	-3	1	$Zn(OH)_4^{2-} . HSO_3^-$
	150	0	29.25	-3	1	$Zn(OH)_4^{2-} . HSO_3^-$
	200	0	27.95	-3	1	$Zn(OH)_4^{2-} . HSO_3^-$
18c	25	0	46.62	-4	1	$Zn(OH)_4^{2-} . SO_3^{2-}$
	60	0	41.58	-4	1	$Zn(OH)_4^{2-} . SO_3^{2-}$
	100	0	39.47	-4	1	$Zn(OH)_4^{2-} . SO_3^{2-}$
	150	0	37.83	-4	1	$Zn(OH)_4^{2-} . SO_3^{2-}$
	200	0	37.42	-4	1	$Zn(OH)_4^{2-} . SO_3^{2-}$
19	25	0	-9.47	1	-1	$ZnOH^+/Zn^{2+}$
	60	0	-7.36	1	-1	$ZnOH^+/Zn^{2+}$
	100	0	-5.95	1	-1	$ZnOH^+/Zn^{2+}$
	150	0	-4.61	1	-1	$ZnOH^+/Zn^{2+}$
	200	0	-3.59	1	-1	$ZnOH^+/Zn^{2+}$
20	25	0	17.27	-2	1	$Zn(OH)_2(aq)/Zn^{2+}$
	60	0	13.64	-2	1	$Zn(OH)_2(aq)/Zn^{2+}$
	100	0	12.50	-2	1	$Zn(OH)_2(aq)/Zn^{2+}$
	150	0	11.43	-2	1	$Zn(OH)_2(aq)/Zn^{2+}$
	200	0	10.61	-2	1	$Zn(OH)_2(aq)/Zn^{2+}$

REACTION	T(°C)	A	B	C	D	R*
21	25	0	-28.77	3	-1	$Zn(OH)_3^-/Zn^{2+}$
	60	0	-23.99	3	-1	$Zn(OH)_3^-/Zn^{2+}$
	100	0	-21.37	3	-1	$Zn(OH)_3^-/Zn^{2+}$
	150	0	-19.02	3	-1	$Zn(OH)_3^-/Zn^{2+}$
	200	0	-17.36	3	-1	$Zn(OH)_3^-/Zn^{2+}$
22	25	0	-41.53	4	-1	$Zn(OH)_4^{2-}/Zn^{2+}$
	60	0	-36.00	4	-1	$Zn(OH)_4^{2-}/Zn^{2+}$
	100	0	-33.28	4	-1	$Zn(OH)_4^{2-}/Zn^{2+}$
	150	0	30.89	4	-1	$Zn(OH)_4^{2-}/Zn^{2+}$
	200	0	-29.63	4	-1	$Zn(OH)_4^{2-}/Zn^{2+}$
23	25	0	7.80	-1	1	$Zn(OH)_2(aq)/ZnOH^+$
	60	0	6.28	-1	1	$Zn(OH)_2(aq)/ZnOH^+$
	100	0	6.54	-1	1	$Zn(OH)_2(aq)/ZnOH^+$
	150	0	6.82	-1	1	$Zn(OH)_2(aq)/ZnOH^+$
	200	0	7.01	-1	1	$Zn(OH)_2(aq)/ZnOH^+$
24	25	0	-19.29	2	-1	$Zn(OH)_3^-/ZnOH^+$
	60	0	-16.63	2	-1	$Zn(OH)_3^-/ZnOH^+$
	100	0	-15.42	2	-1	$Zn(OH)_3^-/ZnOH^+$
	150	0	-14.41	2	-1	$Zn(OH)_3^-/ZnOH^+$
	200	0	-13.76	2	-1	$Zn(OH)_3^-/ZnOH^+$
25	25	0	-32.05	3	-1	$Zn(OH)_4^{2-}/ZnOH^+$
	60	0	-28.64	3	-1	$Zn(OH)_4^{2-}/ZnOH^+$
	100	0	-27.32	3	-1	$Zn(OH)_4^{2-}/ZnOH^+$
	150	0	-26.29	3	-1	$Zn(OH)_4^{2-}/ZnOH^+$
	200	0	-26.03	3	-1	$Zn(OH)_4^{2-}/ZnOH^+$
26	25	0	-11.50	1	1	$Zn(OH)_2(aq)/Zn(OH)_3^-$
	60	0	-10.35	1	1	$Zn(OH)_2(aq)/Zn(OH)_3^-$
	100	0	-8.88	1	1	$Zn(OH)_2(aq)/Zn(OH)_3^-$
	150	0	-7.59	1	1	$Zn(OH)_2(aq)/Zn(OH)_3^-$
	200	0	-6.75	1	1	$Zn(OH)_2(aq)/Zn(OH)_3^-$
27	25	0	-24.26	2	1	$Zn(OH)_2(aq)/Zn(OH)_4^{2-}$
	60	0	-22.36	2	1	$Zn(OH)_2(aq)/Zn(OH)_4^{2-}$
	100	0	-20.78	2	1	$Zn(OH)_2(aq)/Zn(OH)_4^{2-}$
	150	0	-19.47	2	1	$Zn(OH)_2(aq)/Zn(OH)_4^{2-}$
	200	0	-19.02	2	1	$Zn(OH)_2(aq)/Zn(OH)_4^{2-}$

REACTION	T(°C)	A	B	C	D	R*
28	25	0	-12.76	1	-1	$Zn(OH)_4^{2-}/Zn(OH)_3^-$
	60	0	-12.01	1	-1	$Zn(OH)_4^{2-}/Zn(OH)_3^-$
	100	0	-11.90	1	-1	$Zn(OH)_4^{2-}/Zn(OH)_3^-$
	150	0	-11.87	1	-1	$Zn(OH)_4^{2-}/Zn(OH)_3^-$
	200	0	-12.27	1	-1	$Zn(OH)_4^{2-}/Zn(OH)_3^-$
29	25	1	0.507	-0.0887	-0.0148	Zn^{2+}
	60	1	0.495	-0.0991	-0.0165	Zn^{2+}
	100	1	0.481	-0.1110	-0.0185	Zn^{2+}
	150	1	0.468	-0.1259	-0.0210	Zn^{2+}
	200	1	0.459	-0.1408	-0.0235	Zn^{2+}
30	25	1	0.693	-0.1183	-0.0099	$(Zn^{2+})_4 . S_4O_6^{2-}$
	60	1	0.684	-0.1321	-0.0110	$(Zn^{2+})_4 . S_4O_6^{2-}$
	100	1	0.677	-0.1480	-0.0123	$(Zn^{2+})_4 . S_4O_6^{2-}$
	150	1	0.675	-0.1678	-0.0140	$(Zn^{2+})_4 . S_4O_6^{2-}$
	200	1	0.683	-0.1877	-0.0156	$(Zn^{2+})_4 . S_4O_6^{2-}$
31	25	0	4.62	2	1	$Zn^{2+} . H_2S(aq)$
	60	0	4.73	2	1	$Zn^{2+} . H_2S(aq)$
	100	0	4.39	2	1	$Zn^{2+} . H_2S(aq)$
	150	0	4.01	2	1	$Zn^{2+} . H_2S(aq)$
	200	0	3.61	2	1	$Zn^{2+} . H_2S(aq)$
32	25	1	0.281	0	0.0296	Zn^{2+}
	60	1	0.294	0	0.0330	Zn^{2+}
	100	1	0.295	0	0.0370	Zn^{2+}
	150	1	0.295	0	0.0420	Zn^{2+}
	200	1	0.293	0	0.0469	Zn^{2+}
33	25	1	0.394	-0.0394	0.0099	$Zn^{2+} . SO_2(aq)$
	60	1	0.383	-0.0440	0.0110	$Zn^{2+} . SO_2(aq)$
	100	1	0.366	-0.0493	0.0123	$Zn^{2+} . SO_2(aq)$
	150	1	0.345	-0.0560	0.0140	$Zn^{2+} . SO_2(aq)$
	200	1	0.323	-0.0626	0.0156	$Zn^{2+} . SO_2(aq)$
34	25	1	0.411	-0.0493	0.0099	$Zn^{2+} . HSO_3^-$
	60	1	0.406	-0.0551	0.0110	$Zn^{2+} . HSO_3^-$
	100	1	0.397	-0.0617	0.0123	$Zn^{2+} . HSO_3^-$
	150	1	0.387	-0.0699	0.0140	$Zn^{2+} . HSO_3^-$
	200	1	0.377	-0.0782	0.0156	$Zn^{2+} . HSO_3^-$

REACTION	T(°C)	A	B	C	D	R*
35	25	1	0.345	-0.0394	0.0033	$(Zn^{2+})^4 . S_4O_6^{2-}$
	60	1	0.342	-0.0440	0.0037	$(Zn^{2+})^4 . S_4O_6^{2-}$
	100	1	0.333	-0.0493	0.0041	$(Zn^{2+})^4 . S_4O_6^{2-}$
	150	1	0.322	-0.0559	0.0047	$(Zn^{2+})^4 . S_4O_6^{2-}$
	200	1	0.311	-0.0626	0.0052	$(Zn^{2+})^4 . S_4O_6^{2-}$
36	25	1	0.432	-0.0592	0	
	60	1	0.429	-0.0661	0	
	100	1	0.419	-0.0740	0	
	150	1	0.410	-0.0839	0	
	200	1	0.404	-0.0939	0	
37	25	1	0.525	-0.0690	0.0099	HSO_3^-
	60	1	0.517	-0.0771	0.0110	HSO_3^-
	100	1	0.505	-0.0863	0.0123	HSO_3^-
	150	1	0.494	-0.0979	0.0140	HSO_3^-
	200	1	0.483	-0.1095	0.0156	HSO_3^-
38	25	1	0.597	-0.0789	0.0099	SO_3^{2-}
	60	1	0.600	-0.0881	0.0110	SO_3^{2-}
	100	1	0.604	-0.0987	0.0123	SO_3^{2-}
	150	1	0.613	-0.1119	0.0140	SO_3^{2-}
	200	1	0.631	-0.1251	0.0156	SO_3^{2-}
39	25	1	0.892	-0.0986	0.0099	$SO_3^{2-} . Zn(OH)_4^{2-}$
	60	1	0.886	-0.1102	0.0110	$SO_3^{2-} . Zn(OH)_4^{2-}$
	100	1	0.906	-0.1233	0.0123	$SO_3^{2-} . Zn(OH)_4^{2-}$
	150	1	0.939	-0.1399	0.0140	$SO_3^{2-} . Zn(OH)_4^{2-}$
	200	1	0.989	-0.1564	0.0156	$SO_3^{2-} . Zn(OH)_4^{2-}$
40	25	0	16.51	-1	0.250	$Zn(OH)_4^{2-} . S^{2-}$
	60	0	14.48	-1	0.250	$Zn(OH)_4^{2-} . S^{2-}$
	100	0	13.79	-1	0.250	$Zn(OH)_4^{2-} . S^{2-}$
	150	0	12.84	-1	0.250	$Zn(OH)_4^{2-} . S^{2-}$
	200	0	12.24	-1	0.250	$Zn(OH)_4^{2-} . S^{2-}$
41	25	1	-0.899	-0.0591	-0.0295	$H_2S(aq)$
	60	1	-0.915	-0.0661	-0.0330	$H_2S(aq)$
	100	1	-0.918	-0.0740	-0.0370	$H_2S(aq)$
	150	1	-0.918	-0.0839	-0.0420	$H_2S(aq)$
	200	1	-0.916	-0.0939	-0.0469	$H_2S(aq)$

REACTION	T(°C)	A	B	C	D	R*
42	25	1	-1.106	-0.0296	-0.0296	HS^-
	60	1	-1.135	-0.0331	-0.0331	HS^-
	100	1	-1.158	-0.0370	-0.0370	HS^-
	150	1	-1.193	-0.0420	-0.0420	HS^-
	200	1	-1.235	-0.0469	-0.0469	HS^-
43	25	1	-1.488	0	-0.0296	S^{2-}
	60	1	-1.530	0	-0.0331	S^{2-}
	100	1	-1.564	0	-0.0370	S^{2-}
	150	1	-1.608	0	-0.0420	S^{2-}
	200	1	-1.654	0	-0.0469	S^{2-}
44	25	1	0.450	-0.0592	0.0148	$SO_2(aq)$
	60	1	0.427	-0.0661	0.0165	$SO_2(aq)$
	100	1	0.401	-0.0740	0.0185	$SO_2(aq)$
	150	1	0.369	-0.0839	0.0210	$SO_2(aq)$
	200	1	0.338	-0.0939	0.0235	$SO_2(aq)$
45	25	1	0.476	-0.0740	0.0148	HSO_3^-
	60	1	0.462	-0.0826	0.0165	HSO_3^-
	100	1	0.448	-0.0952	0.0185	HSO_3^-
	150	1	0.433	-0.1049	0.0210	HSO_3^-
	200	1	0.420	-0.1173	0.0235	HSO_3^-
46	25	1	0.583	-0.0887	0.0148	SO_3^{2-}
	60	1	0.586	-0.0991	0.0165	SO_3^{2-}
	100	1	0.596	-0.1110	0.0185	SO_3^{2-}
	150	1	0.613	-0.1259	0.0210	SO_3^{2-}
	200	1	0.642	-0.1408	0.0235	SO_3^{2-}
47	25	1	0.144	-0.0592	-0.0296	$H_2S(aq)$
	60	1	0.138	-0.0661	-0.0330	$H_2S(aq)$
	100	1	0.132	-0.0740	-0.0370	$H_2S(aq)$
	150	1	0.127	-0.0839	-0.0430	$H_2S(aq)$
	200	1	0.124	-0.0939	-0.0469	$H_2S(aq)$
48	25	1	-0.062	-0.0296	-0.0296	HS^-
	60	1	-0.082	-0.0330	-0.0330	HS^-
	100	1	-0.109	-0.0370	-0.0370	HS^-
	150	1	-0.148	-0.0420	-0.0420	HS^-
	200	1	-0.195	-0.0469	-0.0469	HS^-

REACTION	T(°C)	A	B	C	D	R*
49	25	1	0.368	-0.0690	0.0099	SO_3^{2-}/HS^-
	60	1	0.363	-0.0771	0.0110	SO_3^{2-}/HS^-
	100	1	0.361	-0.0869	0.0123	SO_3^{2-}/HS^-
	150	1	0.359	-0.0979	0.0140	SO_3^{2-}/HS^-
	200	1	0.363	-0.1095	0.0156	SO_3^{2-}/HS^-
50	25	1	0.240	-0.0592	0.0099	SO_3^{2-}/S^{2-}
	60	1	0.232	-0.0661	0.0110	SO_3^{2-}/S^{2-}
	100	1	0.224	-0.0740	0.0123	SO_3^{2-}/S^{2-}
	150	1	0.221	-0.0839	0.0140	SO_3^{2-}/S^{2-}
	200	1	0.0223	-0.0939	0.0156	SO_3^{2-}/S^{2-}
51	25	0	1.76	-1	1	$HSO_3^-/SO_2(aq)$
	60	0	2.11	-1	1	$HSO_3^-/SO_2(aq)$
	100	0	2.50	-1	1	$HSO_3^-/SO_2(aq)$
	150	0	3.04	-1	1	$HSO_3^-/SO_2(aq)$
	200	0	3.47	-1	1	$HSO_3^-/SO_2(aq)$
52	25	0	7.22	-1	1	SO_3^{2-}/HSO_3^-
	60	0	7.55	-1	1	SO_3^{2-}/HSO_3^-
	100	0	8.03	-1	1	SO_3^{2-}/HSO_3^-
	150	0	8.58	-1	1	SO_3^{2-}/HSO_3^-
	200	0	9.47	-1	1	SO_3^{2-}/HSO_3^-
53	25	0	6.99	-1	1	$HS^-/H_2S(aq)$
	60	0	6.67	-1	1	$HS^-/H_2S(aq)$
	100	0	6.50	-1	1	$HS^-/H_2S(aq)$
	150	0	6.56	-1	1	$HS^-/H_2S(aq)$
	200	0	6.80	-1	1	$HS^-/H_2S(aq)$
54	25	0	12.91	-1	1	S^{2-}/HS^-
	60	0	11.95	-1	1	S^{2-}/HS^-
	100	0	10.98	-1	1	S^{2-}/HS^-
	150	0	9.89	-1	1	S^{2-}/HS^-
	200	0	8.92	-1	1	S^{2-}/HS^-
55	25	1	0.462	-0.0592	0.0148	$(HSO_3^-)^2/(S_2O_3^{2-})$
	60	1	0.417	-0.0661	0.0165	$(HSO_3^-)^2/(S_2O_3^{2-})$
	100	1	0.388	-0.0740	0.0185	$(HSO_3^-)^2/(S_2O_3^{2-})$
	150	1	0.357	-0.0839	0.0210	$(HSO_3^-)^2/(S_2O_3^{2-})$
	200	1	0.319	-0.0939	0.0235	$(HSO_3^-)^2/(S_2O_3^{2-})$

REACTION	T(°C)	A	B	C	D	R*
56	25	1	0.676	-0.0887	0.0148	$(SO_3^{2-})^2/(S_2O_3^{2-})$
	60	1	0.664	-0.0991	0.0165	$(SO_3^{2-})^2/(S_2O_3^{2-})$
	100	1	0.684	-0.1110	0.0185	$(SO_3^{2-})^2/(S_2O_3^{2-})$
	150	1	0.716	-0.1259	0.0210	$(SO_3^{2-})^2/(S_2O_3^{2-})$
	200	1	0.762	-0.1408	0.0235	$(SO_3^{2-})^2/(S_2O_3^{2-})$
57	25	1	0.489	-0.0887	0.0148	$S_2O_3^{2-}$
	60	1	0.508	-0.0991	0.0165	$S_2O_3^{2-}$
	100	1	0.507	-0.1110	0.0185	$S_2O_3^{2-}$
	150	1	0.510	-0.1259	0.0210	$S_2O_3^{2-}$
	200	1	0.521	-0.1408	0.0235	$S_2O_3^{2-}$
58	25	1	0.213	-0.0592	0.0074	$(S_2O_3^{2-})/(HS^-)^2$
	60	1	0.213	-0.0661	0.0083	$(S_2O_3^{2-})/(HS^-)^2$
	100	1	0.199	-0.0740	0.0093	$(S_2O_3^{2-})/(HS^-)^2$
	150	1	0.181	-0.0839	0.0105	$(S_2O_3^{2-})/(HS^-)^2$
	200	1	0.163	-0.0939	0.0117	$(S_2O_3^{2-})/(HS^-)^2$
59	25	1	0.022	-0.0444	0.0074	$(S_2O_3^{2-})/(S^{2-})^2$
	60	1	0.016	-0.0496	0.0083	$(S_2O_3^{2-})/(S^{2-})^2$
	100	1	-0.004	-0.0555	0.0093	$(S_2O_3^{2-})/(S^{2-})^2$
	150	1	-0.027	-0.0630	0.0105	$(S_2O_3^{2-})/(S^{2-})^2$
	200	1	-0.047	-0.0704	0.0117	$(S_2O_3^{2-})/(S^{2-})^2$
60	25	1	0.024	0	0.0296	$(S_4O_6^{2-})/(S_2O_3^{2-})^2$
	60	1	-0.129	0	0.0330	$(S_4O_6^{2-})/(S_2O_3^{2-})^2$
	100	1	-0.211	0	0.0370	$(S_4O_6^{2-})/(S_2O_3^{2-})^2$
	150	1	-0.322	0	0.0420	$(S_4O_6^{2-})/(S_2O_3^{2-})^2$
	200	1	-0.459	0	0.0470	$(S_4O_6^{2-})/(S_2O_3^{2-})^2$
61	25	1	0.539	-0.0349	0.0099	$(SO_2(aq))^4/(S_4O_6^{2-})$
	60	1	0.504	-0.0441	0.0110	$(SO_2(aq))^4/(S_4O_6^{2-})$
	100	1	0.464	-0.0493	0.0123	$(SO_2(aq))^4/(S_4O_6^{2-})$
	150	1	0.413	-0.0560	0.0140	$(SO_2(aq))^4/(S_4O_6^{2-})$
	200	1	0.360	-0.0626	0.0156	$(SO_2(aq))^4/(S_4O_6^{2-})$
62	25	1	0.608	-0.0789	0.0099	$(HSO_3^-)^4/(S_4O_6^{2-})$
	60	1	0.598	-0.0881	0.0110	$(HSO_3^-)^4/(S_4O_6^{2-})$
	100	1	0.587	-0.0987	0.0123	$(HSO_3^-)^4/(S_4O_6^{2-})$
	150	1	0.583	-0.1119	0.0140	$(HSO_3^-)^4/(S_4O_6^{2-})$
	200	1	0.578	-0.1252	0.0156	$(HSO_3^-)^4/(S_4O_6^{2-})$

REACTION	T(° C)	A	B	C	D	R*
63	25	1	0.396	-0.0710	0.0059	$S_4O_6^{2-}$
	60	1	0.381	-0.0793	0.0066	$S_4O_6^{2-}$
	100	1	0.364	-0.0888	0.0074	$S_4O_6^{2-}$
	150	1	0.344	-0.1007	0.0084	$S_4O_6^{2-}$
	200	1	0.325	-0.1126	0.0094	$S_4O_6^{2-}$
64	25	1	0	-0.0591	0.0296	P_{H_2}
	60	1	0	-0.0661	0.0330	P_{H_2}
	100	1	0	-0.0740	0.0370	P_{H_2}
	150	1	0	-0.0839	0.0420	P_{H_2}
	200	1	0	-0.0939	0.0469	P_{H_2}
65	25	1	1.229	-0.0591	0.0148	Po_2
	60	1	1.200	-0.0661	0.0165	Po_2
	100	1	1.167	-0.0740	0.0185	Po_2
	150	1	1.127	-0.0829	0.0210	Po_2
	200	1	1.088	-0.0939	0.0235	Po_2

APPENDIX 3

SAMPLE CALCULATIONS

A.3.1 ENTROPY ESTIMATION

The use of Equation (18) for the calculation of the free energy of formation of a particular species at elevated temperatures requires a knowledge of the entropy at 298°K, S°_{298}. In the absence of such data this may be estimated from one of several empirical equations describing the entropy correspondence between ions at 298°K.

Solid Compounds

Latimer (1921) presented an equation for the contribution of each element to the entropy of a solid compound,

$$S^{\circ}_{298} = \frac{3}{2}R \ln(\text{atomic weight}) - 3.93 \quad \text{J mol}^{-1}\text{K}^{-1}$$

where R is the universal gas constant (8.314 J $mol^{-1}K^{-1}$). Latimer (1951) later refined this approximation to take into account the size and charge of the ions constituting the solid and presented a table of entropies of the elements in solid compounds at 298°K. Latimer (1951) also prepared, from experimental data, a table of entropies of negative ions in which the entropy value is modified by the charge on the positive ion. Thus, the entropy of a salt may be estimated by combining the values for negative ions with the values for positive ions. The entropies of hydrates may be estimated by assigning the value 39.3 kJ $mol^{-1}K^{-1}$ to the contribution of a mole of hydrated water. The following calculation for $ZnSO_3 . 2\frac{1}{2}H_2O$ is given as an example:

ion	contribution
Zn^{2+}	45.6
SO_3^{2-} (for +2 ion)	62.4
H_2O	39.3 x 2.5
	206.3 kJ $mol^{-1}K^{-1}$

Anions

Couture and Laidler (1957) developed the following empirical relationship for the entropy of oxy-anions,

$$S^\circ_{298} = 168-23\ |z| + \frac{3}{2} R \ln M - \frac{455\ z^2}{nr}\ J\ mol^{-1}K^{-1}$$

where n is the number of free oxygen atoms and r is equal to $(r_{12} + 1.40)$. The interatomic distance between the central atom and peripherical oxygen atom in angstroms, r_{12}, is available from Wells (1949) or Pauling (1952) and 1.40Å is the Van der Waals radius of oxygen. Therefore, r represents the radius of a sphere which completely circumscribes the anion and Z is the ionic charge. The method of Couture and Laidler was used to estimate the entropy of the $Zn(OH)_3^-$ and $Zn(OH)_4^{2-}$ ions. The calculation of the entropy of the $Zn(OH)_3^-$ ion is given as an example.

$$S^\circ_{298}(HZnO_2^-) = 168 - 23(1) + \frac{3}{2}(8.314)\ln(98.4) - \frac{455(1)^2}{(1)3.54}$$

$$= 74.1\ J\ mol^{-1}K^{-1}$$

$$S^\circ_{298}(Zn(OH)_3^-) = S^\circ_{298}(HZnO_2^-) + S^\circ_{298}(H_2O)$$

$$= 74.1 + 69.91$$

$$= 144\ J\ mol^{-1}K^{-1}$$

Complex Ions

Cobble (1953)b has presented a method for estimating the entropies of inorganic complex ions. It is applicable to both negative and positive complex ions alike and a treatment for nondissociated netural complex ions is also presented. Hydroxy complexes of the form $M(OH)^{n+}$ fit well into this treatment, whereas, they do not fit the methods for oxy-anions discussed above. The entropy, S°_{298}, is given by the relationship,

$$S^{\circ}_{298} = 205 - 414 \frac{|z|f}{r_{12}} + n\, S^{\circ}_{298}(H_2O) \quad J\ mol^{-1}K^{-1}$$

where n represents the number of water molecules replaced from the normal coordinated aquated ion by the complexing agent. $S^{\circ}_{298}(H_2O)$ is the molar entropy of water which at 298°K is 69.91 J $mol^{-1}K^{-1}$. r_{12} is the interatomic distance between the central atom and the ligand and f is a structural factor given by Cobble (1953)a. This method was used to estimate the entropy of the $ZnOH^{+}$ ion by the following calculation:

$$S^{\circ}_{298} = 205 - 414 \frac{(1)\ (1.00)}{(0.74+1.40)} + (1)\ 69.91$$

$$= 81.6 \quad J\ mol^{-1}K^{-1}.$$

The method of Cobble (1953)b can be extended to neutral species by the relationship,

$$S^{\circ}_{298} = 552 - \frac{1480}{r_{12}} + nS^{\circ}_{298}(H_2O) \quad J\ mol^{-1}K^{-1}$$

A.3.2 HIGH TEMPERATURE EXTRAPOLATION

The calculation of the free energy of formation of a species at an elevated temperature requires the use of average heat capacity data. Equation (18), in addition to

the entropy of a species at 298°K, requires that the mean heat capacity of the particular species over the temperature range of 298°K to T be known or estimated. In the absence of published data, heat capacity estimates may be made from one of the following correlations.

Solid Compounds

Kopp's rule (1864) states that at room temperature the sum of the heat capacities of the individual elements is approximately equal to the heat capacity of a solid compound. Where Kopp's rule has been employed for the estimation of heat capacity of solids, the estimated value has been assumed constant over the temperature range of 298°K to T. The heat capacities assigned to each element by Kopp are given below.

VALUES FOR KOPP'S RULE

Atomic Heat Capacity at 20°C $J(g\text{-atom})^{-1}K^{-1}$	
C	7.5
H	9.6
B	11.3
Si	15.9
O	16.7
F	20.9
P or S	22.6
All others	25.9

Ions and Neutral Species in Solution

Criss and Cobble (1964) derived a principal of entropy correspondence for ions between different temperatures. This "Correspondence Principal" states that a standard state can be chosen at every temperature such that the partial molar entropies of one class of ions at that temperature are linearly related to the corresponding

entropies at some reference temperature. Mathematically this is represented by,

$$S^{\circ}_{T_2} = c_{T_2} + d_{T_2} S^{\circ}_{T_1} .$$

Criss and Cobble (1964) present a table of the constants c and d for different ionic classes. Thus, the linear correspondence of entropy for ions between 298°K and T can be written as,

$$S^{\circ}_{T} = c_T + d_T \bar{S}^{\circ}_{298}$$

where $\bar{S}^{\circ}_{298}$ refers to the absolute ionic entropy. The absolute ionic entropy, $\bar{S}^{\circ}_{298}$, is defined by Criss and Cobble (1964) as,

$$\bar{S}^{\circ}_{298} = S^{\circ}_{298} - Z\, \bar{S}^{\circ}_{298}(H^+)$$

where Z is the ionic charge of the species and $\bar{S}^{\circ}_{298}(H^+)$ refers to the absolute entropy of H^+ ion.
At 298°K, $\bar{S}^{\circ}_{298}(H^+)$ = 20.9 J $mol^{-1}K^{-1}$. The average value of partial molar heat capacity between 298°K and T from basic relationships is,

$$\bar{C}^{\circ}_{p}\Big|^{T}_{298} = \frac{S^{\circ}_{T} - S^{\circ}_{298}}{\ln(T/298)} .$$

Combining the above equations then yields,

$$\bar{C}^{\circ}_{p}\Big|^{T}_{298} = a_T + b_T \bar{S}^{\circ}_{298} .$$

The following values for the constants a and b are reproduced from Criss and Cobble (1964).

HEAT CAPACITY PARAMETERS

T(°C)	Cations		OH^- and Anions		Oxy-anions		Acid Oxy-anions		$C_p \Big\vert_{298}^{T}$ H^+
	a	b	a	b	a	b	a	b	
60	146	-0.41	192	-0.28	531	1.96	510	3.44	96
100	192	-0.55	243	0.00	577	2.24	565	3.97	130
150	192	-0.59	255	-0.03	556	2.27	598	3.95	138
200	209	-0.63	272	-0.04	607	2.53	636	4.24	146

Hence, the average value of the heat capacity of an ionic species over the temperature range of 298°K to T can be estimated up to 473°K from the above equation with the given parameters.

Example Free Energy Calculations

Consider Reaction 4 of Appendix 1,

$$ZnOH^+ + H^+ + 2e^- = Zn + H_2O$$

At 298°K, the free energy change of Reaction 4 is calculated from Equation (10) with the standard free energy of formation data of Tables 3 and 7. Thus,

$$\Delta G^\circ_{298} = \Delta G^\circ_{f,Zn} + \Delta G^\circ_{f,H_2O} - \Delta G^\circ_{f,ZnOH^+} - \Delta G^\circ_{f,H^+}$$

$$= 0 + (-237129) - (-330100) - 0$$

$$= 92970 \text{ J mol}^{-1}.$$

Equation (12) then yields the potential -pH relationship given in Appendix 2,

$$Eh_{298} = \frac{-92970 \text{ J mol}^{-1}}{2 \cdot 96487 \text{ C mol}^{-1}} + \frac{8.314 \text{ J mol}^{-1}\text{K}^{-1} \cdot 298 \text{ K}}{2 \cdot 96487 \text{ C mol}^{-1}} \ln(ZnOH^+)(H^+)$$

or,

$$Eh_{298}(\text{volts}) = -0.482 - 0.0296 \text{ pH} + 0.0296 \log(ZnOH^+) .$$

The calculation of Eh_T at elevated temperatures, similarly, requires that the standard free energy of formation be known for each species of interest at the elevated temperature, T. Consider the $ZnOH^+$ species as an example. The formation reaction of the $ZnOH^+$ species from the elements is,

$$Zn + \tfrac{1}{2}O_2 + \tfrac{1}{2}H_2 = ZnOH^+ + e^- .$$

The standard reference state at all temperatures has been defined as the standard hydrogen electrode which is,

$$H^+ + e^- = \tfrac{1}{2}H_2 .$$

The formation reaction with respect to the standard reference state is, then, the sum of the above two reactions, or

$$Zn + \tfrac{1}{2}O_2 + H^+ = ZnOH^+ .$$

The standard free energy change of this formation reaction, using the free energy data of Naramov, et al (1974) is,

$$\Delta G^\circ_{f,298} = -333260 - 0 - \tfrac{1}{2}(0) - 0 = -333260 \text{ J mol}^{-1} .$$

The entropy of the $ZnOH^+$ species was estimated in the previous section as, $S^\circ_{298} = 81.6$ J $mol^{-1}K^{-1}$, or on the absolute scale $\overline{S}^\circ_{298} = 60.7$ J $mol^{-1}K^{-1}$. The standard entropy change of the formation reaction, using the data of Tables 3 and 7, is

$$\Delta S^\circ_{f,298} = 81.6 - 41.63 - \tfrac{1}{2}(205.138) - 0$$

$$= -62.6 \text{ J mol}^{-1}\text{K}^{-1} .$$

Using the Correspondence Principal of Criss and Cobble (1964), the average molar heat capacity of the $ZnOH^+$ species between 298°K and 473°K is calculated as follows:

$$\overline{C}^\circ_p \Big|_{298}^{473} = 209 - 0.63(60.7)$$

$$= 171 \text{ J mol}^{-1}\text{K}^{-1} .$$

The average molar heat capacities of all species of interest can be calculated in this manner and compiled as shown in Table 8. Using the data in Table 8, then, the average heat capacity change of the formation reaction between 298°K and 473°K is,

$$\Delta\overline{C}^\circ_{p,f} \Big|_{298}^{473} = 171 - 26.15 - \tfrac{1}{2}(30.1) - 146$$

$$= -16.2 \text{ J mol}^{-1}\text{K}^{-1}$$

The standard free energy of formation for the $ZnOH^+$ species at 473°K is then calculated using Equation (18),

$$\Delta G^{\circ}_{f,473} = -333260 - (-62.6)(473 - 298.15) + (-16.2)(473 - 298.15 - 473 \ln \frac{473}{298.15})$$

$$= -333260 + 10946 + 705$$

$$= -321600 \text{ J mol}^{-1}\text{K}^{-1}$$

The standard free energy of formation of all the species of the Zn-S-SO_2-H_2O system at four elevated temperatures were calculated in this manner and are compiled in Table 8. The free energy change of Reaction 4 can then be calculated with Equation (10) using the data in Table 8. At 473°K the free energy change of Reaction 4 is,

$$\Delta G^{\circ}_{473} = 0 + (-210040) - (-321500) - 0$$

$$= 111460 \text{ J mol}^{-1}$$

Equation (12) then yields the potential -pH relationship at 473°K as given in Appendix 2,

$$Eh_{473} = \frac{-111460 \text{ J mol}^{-1}}{2 \cdot 96487 \text{ C mol}^{-1}} + \frac{8.314 \text{ J mol}^{-1}\text{K}^{-1} \cdot 473^{\circ}\text{K}}{2 \cdot 96487 \text{ C mol}^{-1}} \ln (ZnOH^{+})(H^{+})$$

or,

$$Eh(\text{volts}) = -0.578 - 0.0469 \text{ pH} + 0.0469 \log(ZnOH^{+}).$$

The calculation of all the potential -pH relationships presented in Appendix 2 for the Zn-S-SO_2-H_2O system were accomplished in this manner.

A.3.3 CALCULATION OF PERCENT ZINC EXTRACTION

Percent zinc extraction, as used in this study, is defined as the percentage of the available zinc dissolved into solution. In a standard two hour leaching experiment, 20 samples were withdrawn from the reactor each containing about $4cm^3$ of slurry. After completing several tests it was found that the average mass of solids lost through the extraction of samples was approximately 0.17g per sample. A formula for the calculation of percent zinc extraction was devised to account for the loss of solids and solution from the reactor due to sampling. Since the reactor in the standard test contained 700.0 cm^3 of water and 30.0 g of ZnS, the devised formula is,

$$\%EXTN = \frac{C(0.704-0.004n)}{0.647(30.17-0.17n)} \cdot 100\%$$

where C is the solution concentration of zinc in g dm^{-3} measured by AAS (Appendix 5.1) and n is the sample number. 0.647 is the mass fraction of zinc in the Ventron sphalerite determined by repeated assays (Appendix 4). For example if a zinc concentration of 0.80 g dm^{-3} is measured in the first sample taken at one minute in a standard test, the percent zinc extraction is,

$$\%EXTN = \frac{0.80 \text{ g } dm^{-3} \cdot 0.700 \text{ } dm^3}{0.647 \cdot 30.0g} \cdot 100\%$$

$$= 2.9 \text{ percent extraction .}$$

If a zinc concentration of 22.45 g dm^{-3} is measured after 120 minutes of leaching (i.e., sample number 20) the

percent zinc extraction is,

$$\%EXTN = \frac{22.45 \text{ g dm}^{-3} \cdot 620 \text{ dm}^3}{0.647 \cdot 26.6\text{g}} \cdot 100\%$$

$$= 80.9 \text{ percent extraction .}$$

This method was found to account reasonably for the losses incurred through sampling.

A.3.4 DEVELOPMENT OF THE SHRINKING CORE MODEL

A fluid-solid heterogeneous reaction may be represented by the following reaction,

$$A(\text{fluid}) + bB(\text{solid}) \rightarrow \text{Products .}$$

The shrinking core model of the reaction process can be visualized to occur by the five steps given in Chapter Four. At times some of these steps do not exist. For instance, if no solid product is formed by the reaction, no product layer can be formed on the particle surface. Consequently, product layer diffusion (Steps 2 and 4) does not apply, and this case is referred to as the shrinking particle model. In the basic treatment of the shrinking core model, conversion equations are developed for elementary irreversible reactions and Steps 4 and 5 do not apply. Therefore, the equations of Figure 26 are derived for each case in which Steps 1, 2 and 3, in turn, are rate limiting.

Whenever the resistance of the solution film is rate controlling, the concentration gradient for the reactant A is given by $(C_A - O)$ which is the concentration of A in the bulk solution less its concentration at the particle surface. Based on the available surface area, s, which is

unchanging when a product layer is formed, the rate of mass transfer by the stoichiometry of the above reaction is,

$$-\frac{1}{s}\frac{dN_B}{dt} = -\frac{1}{4\pi r_o^2}\frac{dN_B}{dt} = -\frac{b}{4\pi r_o^2}\frac{dN_A}{dt} = b\, k_d\, C_A \ .$$

If ρ_B is the molar density of B in the solid, the above equation becomes,

$$-\frac{1}{s}\frac{dN_B}{dt} = -\frac{1}{4\pi r_o^2}\rho_B\frac{d(\frac{4}{3}\pi r^3)}{dr}\frac{dr}{dt} = \frac{\rho_B r^2}{r_o^2}\frac{dr}{dt} = b\, k_d C_A$$

Rearranging and integrating as unreacted core shrinks with time,

$$-\frac{\rho_B}{r_o^2}\int_{r_o}^{r} r^2 dr = b\, k_d C_A \int_o^t dt$$

or

$$t = \frac{\rho_B\, r_o}{3b\, k_d C_A}\left[1-\left(\frac{r}{r_o}\right)^3\right]$$

The time required for complete reaction, τ, is given when r = 0, or

$$\tau = \frac{\rho_B\, r_o}{3b\, k_d C_A} \ .$$

The radius of unreacted core in terms of fractional time for complete conversion is then,

$$\frac{t}{\tau} = 1 - \left(\frac{r}{r_o}\right)^3 \ .$$

If α is defined as the fraction of the solid material reacted, then

$$\alpha = \frac{\rho_B \frac{4}{3}\pi r_o^3 - \rho_B \frac{4}{3}\pi r^3}{\rho_B \frac{4}{3}\pi r_o^3} = \frac{r_o^3 - r^3}{r_o^3} = 1 - \left(\frac{r}{r_o}\right)^3$$

Therefore, $t/\tau = \alpha$ and

$$\frac{3b\ k_D C_A}{\rho_B\ r_o}\ t = \alpha \quad .$$

This equation represents the time, conversion relationship when solution film diffusion is rate controlling.

Since the progress of the reaction is unaffected by the presence of any surrounding layers in the case of chemical reaction control, the quantity of material reacting is proportional to the available surface of unreacted core. Thus, based on unit surface area, the rate of reaction is given by,

$$-\frac{1}{s}\frac{dN_B}{dt} = -\frac{1}{4\pi r^2}\frac{dN_B}{dt} = -\frac{b}{4\pi r^2}\frac{dN_A}{dt} = b\ k_r C_A$$

where k_r is the first-order rate constant of the surface reaction. If N_B is written in terms of the shrinking radius then,

$$-\frac{1}{4\pi r^2}\rho_B \frac{d(\frac{4}{3}\pi r^3)}{dt}\frac{dr}{dt} = -\frac{1}{4\pi r^2}\rho_B\ 4\pi r^2 = -\rho_B \frac{dr}{dt} = b\ k_r C$$

Upon integration this equation becomes

$$-\rho_B \int_{r_o}^{r} dr = b\ k_r C_A \int_o^t dt$$

or

$$t = \frac{\rho_B}{b\ k_r C_A}(r_o - r) \ .$$

The time required for complete conversion, τ, is given when r = 0, or

$$\tau = \frac{\rho_B r_o}{b\, k_r C_A}$$

The fraction of solid material reacted, α, as derived above is,

$$\alpha = 1 - \left(\frac{r}{r_o}\right)^3 .$$

The decrease in radius or increase in fractional conversion is then,

$$\frac{t}{\tau} = \frac{r_o - r}{r_o} = 1 - \frac{r}{r_o} = 1 - (1-\alpha)^{\frac{1}{3}}$$

or,

$$\frac{b\, k_r C_A}{\rho_B r_o}\, t = 1 - (1-\alpha)^{\frac{1}{3}} .$$

This equation represents the time conversion relationship when the surface reaction is rate limiting.

The situation in which resistance to diffusion through the product layer controls the rate of reaction requires a two-step analysis. First, the flux relationships for a typical partially leached particle are developed. Then, this relationship is applied to all values of r by integrating r from r_o to O. The rate of reaction of A at any instant is given by its rate of diffusion to the reaction surface. The flux of A, Q_A,

is constant at all radial positions, or

$$-\frac{dN_A}{dt} = 4\pi r^2 Q_A = \text{constant} .$$

The flux of A in the product layer may be expressed by Fick's law as,

$$Q_A = D_e \frac{dC_A}{dr}$$

where D_e is the effective diffusion coefficient. Combining these two equations yields,

$$-\frac{dN_A}{dt} = 4\pi r^2 D_e \frac{dC_A}{dr} = \text{constant} .$$

Integrating across the ash layer from r_o to r gives,

$$-\frac{dN_A}{dt} = \int_{r_o}^{r} \frac{dr}{r^2} = 4\pi D_e \int_{C_A}^{0} dC_A$$

or,

$$-\frac{dN_A}{dt}\left(\frac{1}{r} - \frac{1}{r_o}\right) = 4\pi D_e C_A .$$

This expression represents the conditions of a reacting particle at any time. As with film diffusion, N_A can be written in terms of r. Separating variables and integrating then yields,

$$-\rho_B \int_{r_o}^{r} \left(\frac{1}{r} - \frac{1}{r_o}\right) r^2 \, dr = b D_e C_A \int_{o}^{t} dt$$

or

$$t = \frac{\rho_B r_o^2}{6b D_e C_A}\left[1 - 3\left(\frac{r}{r_o}\right)^2 + 2\left(\frac{r}{r_o}\right)^3\right]$$

The time required for complete conversion is

$$\tau = \frac{\rho_B r_o^2}{6b\ D_e C_A} .$$

The progression of the reaction in terms of the time required for complete conversion is

$$\frac{t}{\tau} = 1 - 3\left(\frac{r}{r_o}\right)^2 + 2\left(\frac{r}{r_o}\right)^3$$

In terms of fractional conversion, α, the above equation becomes

$$\frac{t}{\tau} = 1 - 3(1-\alpha)^{\frac{2}{3}} + 2(1-\alpha)$$

or

$$\frac{2b\ D_e C_A}{r_o^2\ \rho_B} = 1 - \tfrac{2}{3}\alpha - (1-\alpha)^{\frac{2}{3}}$$

This equation represents the time conversion relationship when product layer diffusion is limiting the reaction process.

APPENDIX 4

MATERIALS AND REAGENTS

Sphalerite

Electronic grade zinc sulphide in the form of a fine powder was supplied by VENTRON GMBH, D-7500 Karlsruhe -1. Two bulk samples of this material with different lot numbers were supplied by the manufacturer. Both samples were shown to be composed entirely of well crystallized sphalerite by x-ray diffraction. Repeated assays, by both the author and by other laboratories, revealed both samples to be free of iron and have the following composition:

	Percent Mass
Zn	64.7
S	35.0

A particle size distribution was obtained on each sample with a SediGraph Particle Size Analyzer manufactured by Micromeritics Instrument Corporation and are shown in the following graphs. The sample with lot no. 080581 was somewhat coarser, with a mean particle size of 4.4 μm as compared to lot no. 031220608 with a mean particle size of 2.2 μm. Also, a specific surface area of 17.3 m^2g^{-1} was determined on lot no. 031220608 by nitrogen adsorption according to the B.E.T. method. The majority of the experimental work was carried out on the Ventron sphalerite with lot no. 031220608.

Reagent Gases

All gases were supplied in commercial gas cylinders

PARTICLE SIZE DISTRIBUTION

SAMPLE IDENTIFICATION Ventron ZnS Lot No. 080581 DATE November, 1982

Density 4.08 g/cc LIQUID Sedisperse A-12 Density 0.803 g/cc Viscosity 3.45 cp BY D. Larsen

Preparation Blunge and Ultrasonic TEMPERATURE 35 °C

RATE 762 START DIA 90 µm

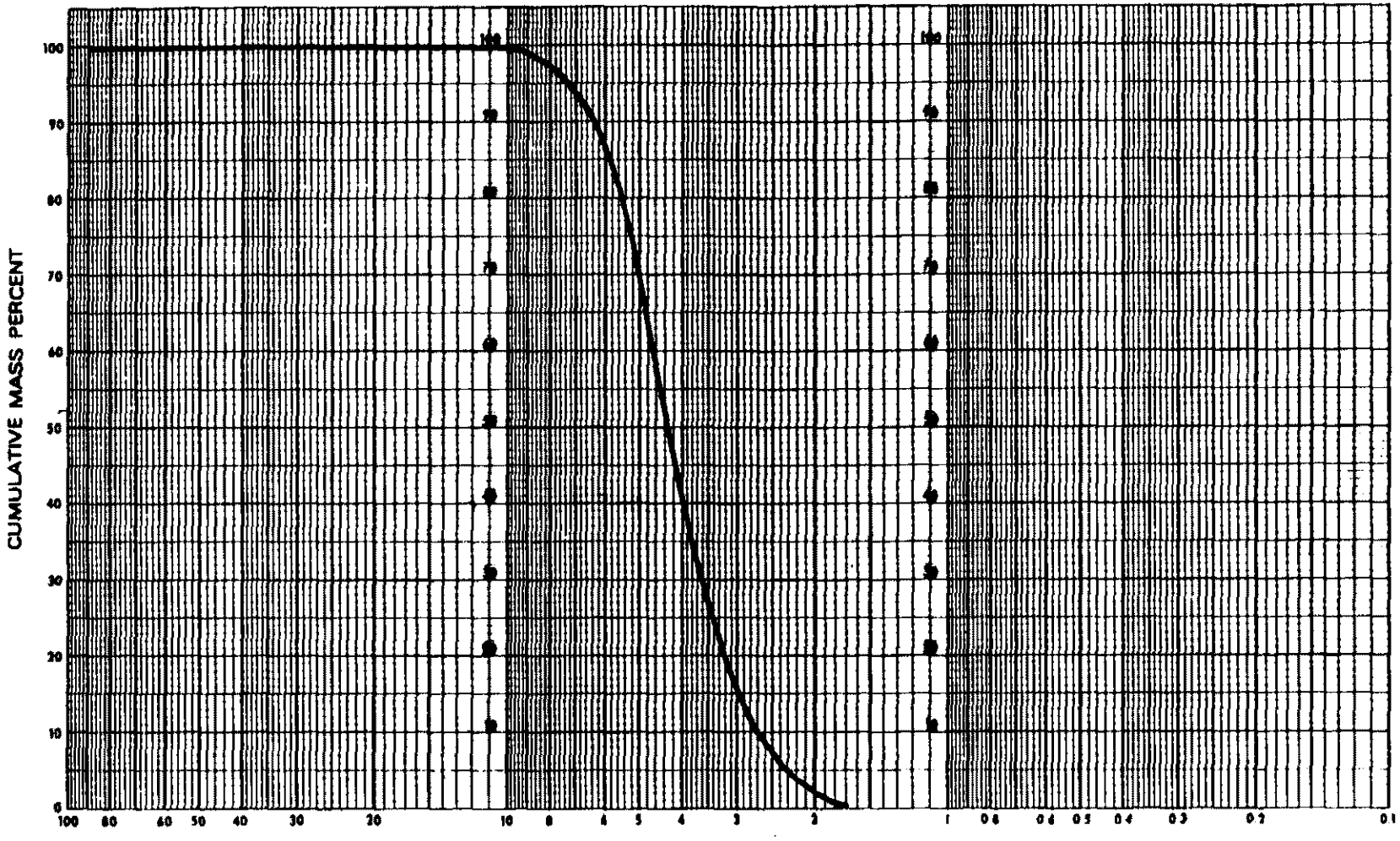

micromeritics instrument corporation

PARTICLE SIZE DISTRIBUTION

SAMPLE IDENTIFICATION Ventron ZnS Lot No. 031220608 DATE November, 1982

Density 4.08 g/cc LIQUID Sedisperse A-12 Density 0.803 g/cc Viscosity 3.45 cp BY D. Larsen

Preparation Blunge and Ultrasonic TEMPERATURE 35 °C

RATE 762 START DIA. 90 µm

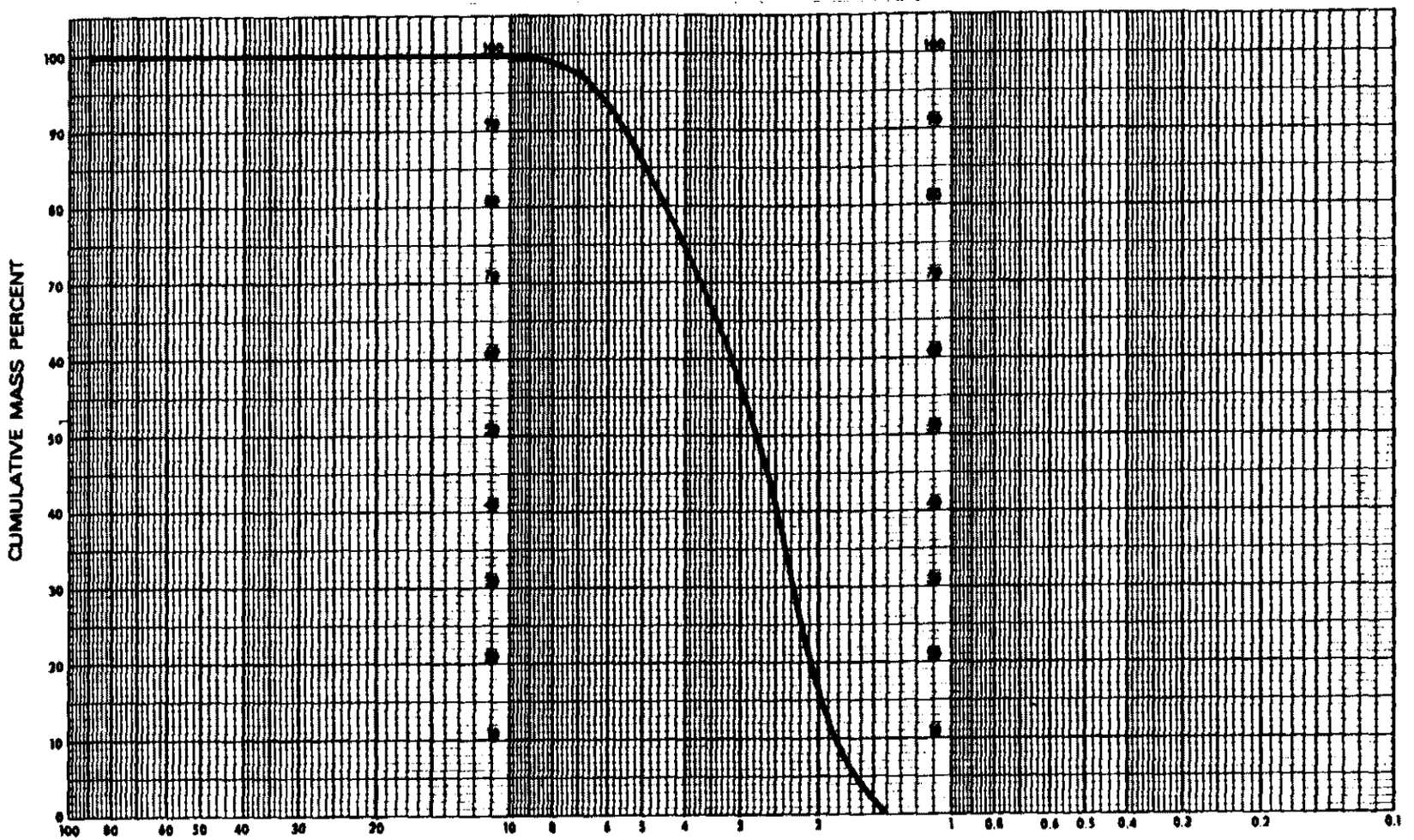

micromeritics instrument corporation

by CIG Ltd., Sydney. The sulphur dioxide used was anhydrous purified industrial grade. The oxygen was standard industrial grade and the nitrogen was a high purity grade.

Other Reagents

All other reagents used including ferric sulphate, ferrous sulphate, zinc oxide, sodium sulphite, sodium thiosulphate, zinc sulphate and sulphuric acid were analytical grade reagents.

APPENDIX 5

ANALYTICAL METHODS

A.5.1 DETERMINATION OF ZINC AND IRON BY ATOMIC ABSORPTION SPECTROPHOTOMETRY

Aliquots of leach liquor samples, or solutions from equilibrium studies, were diluted with hydrochloric acid as required and analyzed by atomic absorption spectrophotometry. The instrument used for analysis was a Techtron Type AA-5 atomic absorption spectrophotometer. Standard metal solutions, for calibration purposes, were prepared from Merck analytical grade zinc metal and Merck Titrisol standard iron solution. The following wavelengths and conditions were used to measure zinc and iron:

	Zinc	Zinc	Iron
Lamp Current mA	5	5	5
Slit Width μm	100	100	50
Fuel/Support	acetylene/air	acetylene/air	acetylene/air
Wavelength nm	213.9	307.6	248.3
Working Range Used	0.5-3ppm	0.50-6.0g dm^{-3}	5-20ppm

A.5.2 VOLUMETRIC DETERMINATION OF AQUEOUS SULPHUR DIOXIDE AND THIOSULPHATE

The total concentration of aqueous sulphur dioxide (i.e., total concentration of all sulphite species) and thiosulphate was determined using the iodometric titration method described by Vogel (1961). In this method, thiosulphate is oxidized by iodine in an acid medium to

tetrathionate by the reaction,

$$2S_2O_3^{2-} + I_2 = S_4O_6^{2-} + 2I^-$$

and sulphite (i.e., $SO_2(aq)$, HSO_3^- and SO_3^{2-}) is oxidized to sulphate by,

$$SO_3^{2-} + I_2 + H_2O = SO_4^{2-} + 2H^+ + 2I^- .$$

The total equivalents of sulphite and thiosulphate are determined by adding an aliquot of sample to an excess of standard iodine solution. The excess iodine is then determined by back titration with a standard thiosulphate solution, using starch as an indicator. A second aliquot can then be added to an alkaline solution of formaldehyde to deactivate the sulphite. The solution is then acidified and titrated with a standard iodine solution. The difference in the two titrations represents the total sulphite concentration. Since thiosulphate is unstable in a low pH leach liquor, the second titration was seldom carried out. Depending on the sulphite concentration in the solutions being examined, 0.1N or 0.01N sodium thiosulphate and iodine solutions were employed and the aliquots varied from 1.0 to 50.0 cm^3.

A.5.3 SPECTROPHOTOMETRIC DETERMINATION OF TETRATHIONATE

A method was required for the estimation of tetrathionate in aqueous sulphur dioxide leach liquors to confirm the postulated formation of tetrathionate in such leach liquors. The formation of the tetrathionate species from the decomposition of sphalerite in aqueous sulphurous acid is predicted on a thermodynamic basis by the Eh-pH diagram of Figure 51. A literature search revealed a promising sensitive method for the estimation of tetrathionate in a mixture with thiosulphate.

Consequently, an investigation was made into its possible application to sulphur dioxide leach liquors.

The spectrophotometric method described by Nietzel and DeSesa (1955) and Kelly, et al (1969) is based on the formation of thiocyanate from tetrathionate by reaction with cyanide in an alkaline medium. Subsequently, a red ferric thiocyanate complex is developed with ferric nitrate and is read with a spectrophotometer at 460 nm. Tetrathionate and thiosulphate react with cyanide according to the following reactions:

$$S_4O_6^{2-} + 3CN^- + H_2O = S_2O_3^{2-} + SO_4^{2-} + 2HCN + SCN^-$$

$$S_2O_3^{2-} + CN^- \xrightarrow{Cu^{2+}} SO_3^{2-} + SCN^-$$

The first reaction occurs spontaneously at low temperatures (approximately 5°C) while the second reaction occurs at low temperatures in the presence of cupric ions.

The analysis method described by Kelly, et al (1969) includes the estimation of the trithionate species. Since the trithionate and thiosulphate species are unstable under the acidic conditions of a sulphur dioxide leach medium, the procedure was adapted for the estimation of tetrathionate only. The matrix interference effects of sulphur dioxide, zinc and ferrous ion were then evaluated in the modified procedure.

As no tetrathionate standard was available, potassium tetrathionate was prepared as described by Trudinger (1961). This involves the reaction of sodium thiosulphate with a KI/I_2 solution and precipitation of potassium tetrathionate with ethanol. Calibration standards for the spectrophotometric method were made using a standard potassium

thiocyanate solution. Trial analyses with potassium tetrathionate in a acidified solution showed a quantitative recovery of the tetrathionate. No interference effects from zinc or ferrous iron were found. Sulphur dioxide, on the other hand, appears to affect the analysis. It was determined, however, that with a suitable dilution and using the method of standard additions this interference affect was minimal. The method used for spectrophotometric calibration and for analysis of tetrathionate is presented with a summary of the reagents required.

REAGENTS

Potassium Thiocyanate: 1.000g KSCN diluted to 1.00 dm^3 with water. 1.00 cm^3 = 598 µg SCN^- .

Tetrathionate Solution: 0.6000 g $K_2S_4O_6$ diluted to 1.00 dm^3 with water. 1.00 cm^3 = 444.5 µg $S_4O_6^{2-}$
= 2.000 µmol $S_4O_6^{2-}$.

NaH_2PO_4-NaOH Buffer: A mixture of 0.2N NaOH and 0.2 M NaH_2PO_4. pH approximately 7.4.

Cyanide: 0.1 M KCN in water.

Ferric Nitrate: 1.5 M $Fe(NO_3)_3$ in 4 N $HClO_4$. Dissolve 60.6 g $Fe(NO_3)_3 . 9H_2O$ in a minimum amount of water. Heat if necessary. Cool and add 34 cm^3 of concentrated perchloric acid, $HClO_4$ (70% w/w, s.g. 1.70) and dilute to 100 cm^3 with water.

PROCEDURE

1. To each of four 25 cm^3 volumetric flasks add 4 cm^3 of buffer.

2. CALIBRATION: To three of the flasks add 0.200, 0.400 and 0.600 cm^3 respectively of the standard KSCN solution (equivalent to 119.6 µg, 239.2 µg and 358.8 µg of SCN^- respectively). Add water to give a total volume of 10 cm^3. One volumetric flask is used as a reagent blank.

   ANALYSIS: To each of three flasks add the appropriate aliquot of leach liquor containing around 1 µmol (224 µg) of $S_4O_6^{2-}$. To the three flasks add, respectively, 0.0, 0.500 and 1.000 cm^3 of standard tetrathionate solution (0.0 µg, 222.5 µg and 445 µg of $S_4O_6^{2-}$, respectively). The fourth flask is used as a reagent blank. Add water to give each flask a total volume of 10 cm^3.

3. Cool the flasks to 5°C in ice water. Add 5 cm^3 of 0.1 M KCN to each flask. Mix rapidly and maintain the mixture at 5°C for 20 mintues.

4. Add 3 cm^3 of ferric nitrate solution to each flask with continuous agitation. Warm each flask up to room temperature with constant shaking to redissolve any precipitate. Make up to the 25 cm^3 mark with water.

5. Read at once the ferric thiocyanate color which develops at 460 nm in 1 cm cells in a spectrophotometer against the blank.

The aliquot of sample taken in step 2 should contain approximately 1 µmol of $S_4O_6^{2-}$ for optimum sensitivity in this procedure. It is recommended that for unknown solutions, a run be first carried out to establish the level of $S_4O_6^{2-}$ present and then the method of standard additions be applied to a suitable aliquot to minimize matrix effects.

The instrument used in the experimental work was a Varian Techtron model 635 UV-VIS spectrophotometer. Small volume aliquots were taken with a Gilson variable volume pipette. The method of standard additions has been described by Vogel (1961).

A.5.4 VOLUMETRIC DETERMINATION OF SULPHURIC ACID

The concentration of sulphuric acid in leach liquor was determined by titration against sodium hydroxide. To minimize interference effects, ferric iron was first reduced by reaction with potassium iodide and then the acid was titrated with 0.5 N NaOH using bromocresol green - methyl orange indicator.

Procedure

1. Pipette 20.0 cm^3 of leach liquor into a tall beaker and dilute to approximately 100 cm^3 with water.

2. Boil gently on a hotplate for 15 minutes to expel any SO_2.

3. Cool to ambient temperature. Add a 50% W/V KI solution drop by drop until no more iodine is liberated and allow to stand for 10 minutes.

4. Add from a drop bottle a sufficient quantity of 10% W/V sodium thiosulphate solution to decolorize the iodine.

5. Add 5 drops of indicator and titrate to a green end point with 0.5 N NaOH.

The 0.5 N NaOH solution was calibrated against a Merck Titrisol 9.808 g dm^{-3} standard H_2SO_4 solution. The indicator can be prepared in the following manner:

triturate 0.1 g bromocresol green and 0.02 g methyl orange in 2 cm^3 of 0.25 N NaOH in an agate mortar and dilute to 100 cm^3 with water.

A.5.5 VOLUMETRIC DETERMINATION OF FERROUS/FERRIC IRON

Ferrous iron was determined in sulphur dioxide leach liquors in the presence of ferric iron by oxidation with potassium dichromate. The method as described by Vogel (1961) is based on the quantitative oxidation of ferrous iron in cold acid solution (HCl or H_2SO_4) to the ferric oxidation state by potassium dichromate according to the reaction

$$6Fe^{2+} + Cr_2O_7^{2-} + 14H^+ = 6Fe^{3+} + 2Cr^{3+} + 7H_2O$$

In acid solution, the reduction of potassium dichromate may be represented as:

$$Cr_2O_7^{2-} + 14H^+ + 6e^- = 2Cr^{3+} + 7H_2O$$

from which it follows that the equivalent weight is one-sixth the molecular weight, 294.2216 or 49.037. A 0.1 N solution therefore contains 4.9037 g dm^{-3} $K_2Cr_2O_7$.

Either diphenylamine, or potassium or barium diphenylamine sulphonate is employed as the internal redox indicator. A slight excess of the oxidant ($K_2Cr_2O_7$) causes the indicator to change to an intense violet-blue color. Since the standard oxidation potential of diphenylamine and diphenylamine sulphonate are close to the standard oxidation potential of the iron couple, it is necessary to add PO_4^{3-} or F^- to complex the Fe^{3+} causing it to be more readily oxidized. This also serves to remove the yellow color of ferric iron which would interfere with the color change at the endpoint. Each 0.1 cm^3 of a 0.5%

indicator solution requires approximately 0.2 cm^3 of 0.02 N oxidant and this correction should be made when oxidants of this strength are used for titration. The standard procedure given by Vogel (1961) was modified in the present work since sulphur dioxide would also be oxidized by the potassium dichromate.

REAGENTS

Potassium Dichromate: A 0.1 N $K_2Cr_2O_7$ stock solution was prepared as described by Vogel (1961). This solution was further diluted to a 0.02 N $K_2Cr_2O_7$ working solution. Thus, 1.0 cm^3 of the 0.02 N $K_2Cr_2O_7$ solution equals 1.117 mg Fe^{2+}.

Barium Diphenylamine Sulphonate: 0.50 g of the reagent is diluted to 100 cm^3 with water.

Sulphuric - Phosphoric Acid Solution: 20% (V/V) concentrated H_2SO_4 and 20% (V/V) concentrated H_3PO_4 in water.

PROCEDURE

1. Pipette 4.00 cm^3 of leach liquor into a 125 cm^3 Philips beaker with a magnetic stirrer. Add 100 cm^3 distilled water and 20 cm^3 of the H_2SO_4/H_3PO_4 solution.

2. Place the beaker on a hot plate and introduce nitrogen gas into the solution through a gas sparger at a steady rate while stirring. Quickly bring the solution to a boil for 7 to 10 minutes to completely expel any residual SO_2.

3. Cool the contents to room temperature in ice water keeping the beaker covered by a watch glass or foil to avoid contamination with air.

4. Add 3 drops of the indicator solution and titrate with 0.02 N $K_2Cr_2O_7$ to the first permanent violet-blue endpoint. Subtract 0.2 cm^3 from the titre reading and calculate the mg Fe^{2+} in the 4.0 cm^3 aliquot titrated by,

$$1\ cm^3 \text{ of } 0.02\ N\ K_2Cr_2O_7 = 1.117\ mg\ Fe^{2+}\ .$$

The total iron can then be determined by atomic absorption spectrophotometry on an aliquot of the same sample.

APPENDIX 6

Eh AND pH STANDARDIZATION

The pH measurement system used in the experimental work consisted of an Orion Research digital pH/millivolt meter, model 611 with a Phillips CH21 high temperature combination pH electrode. The Orion meter, when properly calibrated with a particular electrode, has an internal temperature compensation, based on the resistance of the electrode, that automatically adjusts itself to the temperature of electrode environment. Therefore, accurate pH measurements were obtained in the temperature range of 10°C to 90°C by standardizing the measurement system with two NBS standard buffer solutions at 20°C and 60°C. Vogel (1961) describes the NBS standard buffer solutions and their method of preparation. The two standards used and their pH at various temperatures are summarized below.

VALUES OF pH FOR NBS STANDARD BUFFERS: VOGEL (1961)

TEMP. °C	20	25	30	40	50	60	70	80	90
A	4.00	4.01	4.01	4.03	4.06	4.09	4.12	4.16	4.20
B	6.88	6.86	6.85	6.84	6.83	6.84	6.85	6.86	6.88

A: KH phthalate, M = 0.05 mol dm^{-3}

B: KH_2PO_4, M = 0.025 mol dm^{-3}

Na_2HPO_4, M = 0.025 mol dm^{-3}

M denotes molarity and the solvent is water.

The solution potential or Eh was measured using an Anax pH/millivolt meter with a 1.0 M KCl, silver/silver chloride platinum redox electrode. The potential of the electrode was checked using Zobell solution as described by Langmuir (1971). Zobell solution is composed of 0.003M potassium ferrocyanide and 0.003M potassium ferricyanide in 0.1M KCl. The potassium ferrocyanide and ferricyanide may be prepared as two separate solutions and mixed in equal volumes as required. The potential of Zobell solution with respect to the 1.0M KCl, Ag/AgCl electrode is 192 mV at 25°C, Langmuir (1971). If the potential of the electrode is significantly different from this value, all measurements must be adjusted by adding a value dE to the measured potential where,

$$dE = 192 - E_Z \text{ mV}$$

if E_Z is the observed potential of the electrode in Zobell solution. The potential of the Ag/AgCl electrode varies with temperature. Since Eh is defined as the potential with respect to the standard hydrogen electrode at all temperatures, a value E' must be added to the measured potential to obtain the Eh. The potential of a 1.0M KCl, Ag/AgCl electrode relative to a standard hydrogen electrode, E', is given below at various temperatures as calculated from the data of Langmuir (1971).

TEMP °C	25	40	60	75	90
E' mV	237	227	215	206	196

As an example, consider a leach liquor at 60°C. The potential of the leach media is 365 mV as measured with a 1.0M KCl Ag/AgCl electrode. This electrode at 25°C gave a potential of 199 mV in freshly mixed Zobell solution.

The Eh of the leach liquor, therefore, is

$$Eh = E_{Ag/AgCl} + E' + dE$$

$$= 365 + 215 + (-7)$$

$$= 573 \text{ mV} .$$

Solution Eh was calculated in this manner throughout the experimental work.

APPENDIX 7

EXPERIMENTAL DATA

Solubility Data

The data below represents the solubility of $ZnSO_3 \cdot 2\frac{1}{2}H_2O$ by direct measurement. Various quantities of ZnO were dissolved in excess aqueous SO_2. Precipitation of $ZnSO_3 \cdot 2\frac{1}{2}H_2O$ occurred when the excess SO_2 was removed. The following data was measured when equilibrium was established after several hours in the reactor.

ZnO g	Time hrs	Temp °C	$[Zn^{2+}]_{-3}$ mol dm	$\log_{2+}$ $[Zn^{2+}]$	$[SO_3^{2-}]_{-3}$ mol dm	$\log_{2-}$ $[SO_3^{2-}]$	pH	$n=\frac{[SO_3^{2-}]}{[Zn^{2+}]}$
10.0	18	25	0.315	-0.51	0.557	-0.25	3.12	1.77
5.0	240	25	0.130	-0.88	0.222	-0.65	3.68	1.71
6.0	40	25	0.191	-0.72	0.351	-0.45	3.36	1.84
3.0	25	25	0.0735	-1.13	0.115	-0.94	4.12	1.52
1.0	133	25	0.0400	-1.39	0.062	-1.21	4.49	1.55
8.0	120	25	0.142	-0.85	0.255	-0.59	3.42	1.80
10.0	43	25	0.152	-0.82	0.278	-0.56	3.67	1.83
4.0	135	25	0.132	-0.88	0.241	-0.62	3.46	1.83
14.0	96	25	0.198	-0.70	0.371	-0.43	3.48	1.87

The data below represents the solubility of $ZnSO_3 \cdot 2\frac{1}{2}H_2O$. Crystalline zinc sulphite was suspended in water and allowed to dissolve until equilibrium was achieved. The various measurements were made as the solid approached equilibrium with the solution. The two experiments presented below summarize six experiments performed in this manner.

Time hrs.	Temp °C	$[Zn^{2+}]$ mol dm^{-3}	$\log_{[Zn^{2+}]}$	$[SO_3^{2-}]$ mol dm^{-3}	$\log_{[SO_3^{2-}]}$	pH	$n=\frac{[SO_3^{2-}]}{[Zn^{2+}]}$
2.5	25.9	0.0113	-1.95	0.0162	-1.79	5.93	1.43
14	25.0	0.0116	-1.94	0.0179	-1.75	5.86	1.54
16.5	25.0	0.0123	-1.91	0.0179	-1.75	5.85	1.46
18.5	25.5	0.0123	-1.91	0.0182	-1.74	5.84	1.48
42	25.0	0.0127	-1.90	0.0185	-1.73	5.84	1.46
138	25.2	0.0124	-1.90	0.0189	-1.72	5.81	1.52
2	25.4	0.0106	-1.97	0.0151	-1.82	5.99	1.42
4.5	27.0	0.0117	-1.93	0.0173	-1.76	5.78	1.48
7	26.0	0.0117	-1.93	0.0175	-1.76	5.74	1.50
50	25.2	0.0126	-1.90	0.0190	-1.72	5.81	1.51
56	25.6	0.0129	-1.89	0.0192	-1.72	5.83	1.49
70	25.2	0.0126	-1.90	0.0188	-1.72	5.86	1.49
73	25.1	0.0127	-1.90	0.0192	-1.72	5.83	1.51

Leaching Data

The following data represents the kinetic study on the dissolution of sphalerite in aqueous sulphurous acid media.

TEST 62

30.0 g ZnS 700 cm^3 H_2O 60°C 800 rpm
50% SO_2/O_2 at 500 cm^3 min^{-1}

TIME hours	Eh	pH	Zn^{2+} g dm^{-3}	% EXTN	$1-(1-\alpha)^{\frac{1}{3}}$	$S_4O_6^{2-}$ g dm^{-3}
0	328	1.36	---	--	---	
5 min.	276	1.41	1.62	5.8	0.020	
10 min.	254	1.46	2.45	8.8	0.030	4.6
15 min.	251	1.47	3.07	11.0	0.038	5.8
20 min.	248	1.47	3.72	13.3	0.046	7.8
30 min.	241	1.43	4.45	15.9	0.056	
45 min.	236	1.39	5.36	19.1	0.068	
1	233	1.38	6.16	21.9	0.079	
1½	230	1.33	7.67	27.2	0.100	
2	228	1.31	8.73	30.9	0.116	
2½	226	1.28	10.08	35.5	0.136	
3	225	1.27	11.30	39.7	0.155	
3½	225	1.24	12.17	42.7	0.169	27.8
4	226	1.23	13.53	47.3	0.192	
4½	226	1.20	14.74	51.4	0.214	
5	226	1.19	15.65	54.4	0.230	39.5
5½	227	1.17	16.56	57.5	0.248	
6	228	1.17	17.80	61.6	0.273	
7	230	1.16	19.78	68.3	0.318	45.0
8	232	1.14	21.59	74.3	0.364	
9	233	1.14	23.17	79.5	0.410	58.1
10	234	1.15	24.75	84.7	0.465	66.0
12	235	1.17	26.86	91.7	0.564	
15	234	1.20	27.91	95.0	0.632	
20	234	1.22	28.44	96.5	0.672	
24	231	1.24	28.96	98.0	0.729	33.5
26	229	1.23	28.96	98.0	0.729	37.0
28	229	1.23	28.96	98.0	0.729	

TEST 63

30.0 g ZnS 700 cm^3 H_2O 60°C 800 rpm
50% SO_2/O_2 at 500 cm^3 min^{-1}

STAGE 1 LEACH

TIME hours	Eh	pH	Zn^{2+} g dm^{-3}	% EXTN	$1-(1-\alpha)^{\frac{1}{3}}$	$S_4O_6^{2-}$ g dm^{-3}
0	315	1.27	---	--	---	
5 min.	259	1.25	1.65	6.0	0.020	
10 min.	264	1.24	2.53	9.1	0.031	3.84
15 min.	259	1.23	3.24	11.6	0.040	5.36
20 min.	257	1.22	3.78	13.5	0.047	7.20
30 min.	253	1.20	4.68	16.7	0.059	
45 min.	247	1.17	6.00	21.4	0.077	
1	243	1.14	6.73	23.9	0.087	
1½	239	1.09	8.41	29.8	0.111	
2	236	1.04	9.85	34.8	0.133	
2½	233	1.00	11.35	40.0	0.157	24.5
3	232	0.97	12.61	44.4	0.178	
3½	231	0.93	14.24	50.0	0.206	31.3

STAGE 2 LEACH

Solid residue from Stage 1, same conditions, cumulative % EXTN.

0	252	1.15	--	--	--	
5 min.	264	1.22	1.88	56.8	0.244	
10 min.	259	1.19	2.94	60.6	0.267	5.08
15 min.	256	1.19	3.78	63.6	0.286	5.88
20 min.	252	1.18	4.38	65.6	0.299	7.20
30 min.	244	1.16	5.23	68.6	0.320	
45 min.	238	1.13	6.12	71.8	0.344	
1	235	1.10	6.73	73.9	0.361	
1½	232	1.12	7.81	77.7	0.394	
2	226	1.12	8.53	80.2	0.417	
2½	226	1.10	9.37	83.0	0.446	19.5
3	224	1.10	10.27	86.1	0.482	
3½	224	1.09	10.63	87.3	0.497	25.6

TEST 64

30.0 g ZnS 700 cm³ H_2O 25°C 800 rpm

100% SO_2 at 500 cm³ min^{-1}

TIME Min.	Eh	pH	Zn^{2+} g dm^{-3}	% EXTN	$1-(1-\alpha)^{\frac{1}{3}}$	$S_4O_6^{2-}$ g dm^{-3}
0	346	1.14	---	--	---	
1	281	1.13	0.65	2.3	0.008	
2	296	1.13	0.90	3.2	0.011	
3	301	1.14	1.11	4.0	0.014	
4	307	1.15	1.26	4.5	0.015	
5	315	1.15	1.42	5.1	0.017	0.80
6	319	1.15	1.63	5.9	0.020	
8	322	1.14	1.90	6.9	0.023	
10	317	1.14	2.05	7.4	0.025	1.56
12	307	1.13	2.42	8.7	0.030	
15	289	1.13	2.74	9.9	0.034	3.40
18	287	1.12	3.06	11.0	0.038	
20	285	1.10	3.33	12.0	0.042	
25	285	1.10	3.79	13.7	0.047	
30	284	1.10	4.21	15.2	0.053	
45	286	1.08	5.37	19.4	0.069	
60	289	1.05	6.22	22.4	0.081	
75	289	1.03	7.10	25.6	0.093	10.0
90	289	0.95	7.64	27.5	0.102	
105	289	0.91	8.30	29.9	0.112	
120	287	0.90	8.62	31.1	0.117	11.8

TEST 65

30.0 g ZnS 700 cm³ H_2O 40°C 800 rpm

100% SO_2 at 500 cm³ min^{-1}

TIME Min.	Eh	pH	Zn^{2+} g dm^{-3}	% EXTN	$1-(1-\alpha)^{\frac{1}{3}}$	$S_4O_6^{2-}$ g dm^{-3}
0	341	1.19	--	--	---	
1	271	1.18	0.61	2.2	0.007	
2	271	1.20	0.94	3.4	0.011	
3	272	1.21	1.11	4.0	0.014	
4	273	1.20	1.32	4.8	0.016	
5	274	1.19	1.53	5.5	0.019	2.5
6	275	1.19	1.74	6.3	0.021	
8	273	1.18	2.05	7.4	0.025	
10	271	1.17	2.32	8.4	0.029	3.7
12	272	1.17	2.63	9.5	0.033	
15	271	1.16	3.00	10.8	0.037	4.8
18	274	1.16	3.44	12.4	0.043	
20	277	1.16	3.60	13.0	0.045	
25	271	1.16	4.11	14.8	0.052	
30	272	1.16	4.53	16.3	0.058	
45	271	1.14	5.68	20.5	0.074	
60	268	1.11	6.44	23.2	0.084	
75	265	1.08	7.21	26.0	0.095	11.6
90	263	1.06	7.64	27.5	0.102	
105	260	1.05	8.08	29.1	0.108	
120	258	1.02	8.52	30.7	0.115	20.0

TEST 66

30.0 g ZnS 700 cm^3 H_2O 75°C 800 rpm

100% SO_2 at 500 cm^3 min^{-1}

TIME Min.	Eh	pH	Zn^{2+} g dm^{-3}	% EXTN	$1-(1-\alpha)^{\frac{1}{3}}$	$S_4O_6^{2-}$ g dm^{-3}
0	238	1.26	--	--	---	
1	243	1.26	0.50	1.8	0.006	
2	246	1.30	0.72	2.6	0.009	
3	248	1.30	0.89	3.2	0.011	
4	248	1.29	1.05	3.8	0.013	
5	244	1.28	1.22	4.4	0.015	2.9
6	245	1.27	1.32	4.8	0.016	
8	247	1.28	1.54	5.6	0.019	
10	243	1.28	1.76	6.3	0.021	3.8
12	241	1.27	1.97	7.1	0.024	
15	240	1.27	2.24	8.1	0.027	5.0
18	240	1.26	2.52	9.1	0.031	
20	239	1.26	2.68	9.7	0.033	
25	237	1.24	3.08	11.1	0.038	
30	237	1.22	3.52	12.7	0.044	
45	234	1.18	4.60	16.6	0.058	
60	232	1.14	5.68	20.5	0.074	
75	231	1.13	6.76	24.4	0.089	19.7
90	231	1.12	7.72	27.8	0.103	
105	230	1.11	8.69	31.3	0.118	
120	231	1.11	9.65	34.8	0.133	26.8

TEST 67

30.0 g ZnS 700 cm^3 H_2O 90°C 800 rpm

100% SO_2 at 500 cm^3 min^{-1}

TIME Min.	Eh	pH	Zn^{2+} g dm^{-3}	% EXTN	$1-(1-\alpha)^{\frac{1}{3}}$	$S_4O_6^{2-}$ g dm^{-3}
0	242	1.06	--	--	---	
1	226	1.12	0.30	1.1	0.0037	
2	229	1.16	0.43	1.6	0.0054	
3	227	1.16	0.55	2.0	0.0067	
4	226	1.17	0.60	2.2	0.0074	
5	225	1.16	0.65	2.3	0.0077	1.48
6	224	1.16	0.70	2.5	0.0084	
8	221	1.15	0.75	2.7	0.0091	
10	221	1.15	0.80	2.9	0.0097	1.76
12	221	1.14	0.90	3.2	0.0108	
15	220	1.12	0.95	3.4	0.0115	2.64
18	220	1.10	1.00	3.6	0.0121	
20	217	1.10	1.06	3.8	0.0128	
25	213	1.10	1.18	4.3	0.0145	
30	209	1.08	1.29	4.6	0.0156	
45	204	1.08	1.65	5.9	0.0201	
60	206	1.05	1.94	7.0	0.0239	
75	208	1.02	2.30	8.3	0.0285	7.10
90	209	0.99	2.71	9.8	0.0338	
105	212	0.97	3.00	10.8	0.0374	
120	213	0.93	3.39	12.2	0.0424	9.05

TEST 68

30.0 g ZnS 700 cm³ H_2O 60°C 800 rpm

100% SO_2 at 500 cm³ min^{-1}

TIME Min.	Eh	pH	Zn^{2+} g dm^{-3}	% EXTN	$1-(1-\alpha)^{\frac{1}{3}}$	$S_4O_6^{2-}$ g dm^{-3}
0	252	1.07	--	--	---	
1	240	1.06	0.67	2.4	0.008	
2	243	1.13	1.00	3.6	0.012	
3	244	1.14	1.22	4.4	0.015	
4	246	1.14	1.44	5.2	0.018	
5	245	1.13	1.67	6.0	0.020	3.04
6	244	1.13	1.89	6.8	0.023	
8	244	1.13	2.22	8.0	0.027	
10	245	1.12	2.56	9.2	0.032	3.60
12	246	1.12	2.84	10.2	0.035	
15	246	1.10	3.22	11.6	0.040	6.52
18	245	1.08	3.55	12.8	0.045	
20	245	1.06	3.82	13.8	0.048	
25	243	1.04	4.45	16.0	0.056	
30	243	1.00	4.89	17.6	0.062	
45	239	0.92	6.00	21.6	0.077	
60	236	0.87	6.88	24.8	0.091	
75	233	0.83	7.64	27.5	0.101	17.5
90	229	0.79	8.41	30.3	0.113	
105	225	0.77	9.17	33.0	0.125	
120	222	0.74	10.05	36.2	0.139	29.7

TEST 69

30.0 g ZnS 700 cm³ H_2O 60°C 800 rpm

100% SO_2 at 500 cm³ min^{-1} 7.0 g dm^{-3} Zn^{2+} added

TIME Min.	Eh	pH	Zn^{2+} g dm^{-3}	% EXTN	$S_4O_6^{2-}$ g dm^{-3}
0	240	1.56	--	--	
1	256	1.50	0.19	0.7	
2	257	1.50	0.23	0.8	
3	252	1.51	0.26	0.9	
4	241	1.51	0.29	1.0	
5	240	1.51	0.35	1.2	--
6	235	1.51	0.40	1.4	
8	225	1.50	0.42	1.5	
10	224	1.50	0.44	1.6	0.56
12	221	1.49	0.47	1.7	
15	222	1.48	0.50	1.8	0.84
18	220	1.47	0.65	2.2	
20	222	1.46	0.71	2.5	
25	222	1.44	0.79	2.8	
30	223	1.43	0.86	3.1	
45	223	1.39	0.96	3.4	
60	221	1.37	1.05	3.8	
75	214	1.38	1.15	4.1	1.50
90	218	1.34	1.36	4.9	
105	224	1.31	1.58	5.7	
120	225	1.29	1.71	6.1	1.80

TEST 70

30.0 g ZnS 700 cm^3 H_2O 25°C 800 rpm

100% SO_2 at 500 cm^3 min^{-1} 7.0 g dm^{-3} Zn^{2+} added

TIME Min.	Eh	pH	Zn^{2+} g dm^{-3}	% EXTN	$S_4O_6^{2-}$ g dm^{-3}
0	368	1.31	--	--	
1	367	1.31	0.06	0.2	--
2	388	1.31	0.18	0.6	
3	399	1.31	0.25	0.9	
4	387	1.30	0.30	1.1	
5	371	1.30	0.30	1.1	--
6	344	1.29	0.34	1.2	
8	320	1.27	0.42	1.5	
10	308	1.26	0.58	2.1	--
12	303	1.25	0.64	2.3	
15	299	1.23	0.76	2.7	--
18	298	1.22	0.81	2.9	
20	297	1.22	0.88	3.2	
25	296	1.21	0.91	3.3	
30	297	1.20	1.01	3.6	
45	299	1.17	1.17	4.2	
60	303	1.15	1.50	5.4	
75	311	1.14	2.03	7.3	3.60
90	318	1.14	2.12	7.6	
105	324	1.14	2.20	7.9	
120	331	1.13	2.33	8.3	7.00

TEST 74

30.0 g ZnS 700 cm^3 H_2O 60°C 800 rpm

50% SO_2/O_2 at 500 cm^3 min^{-1}

TIME Min.	Eh	pH	Zn^{2+} g dm^{-3}	% EXTN	$1-(1-\alpha)^{\frac{1}{3}}$
0	331	1.27	--	--	---
1	285	1.25	0.39	1.4	0.005
2	287	1.27	0.61	2.2	0.007
3	289	1.28	0.83	3.0	0.010
4	291	1.29	0.98	3.5	0.012
5	293	1.20	1.12	4.0	0.014
6	295	1.29	1.22	4.4	0.015
8	297	1.29	1.49	5.4	0.018
10	298	1.29	1.76	6.3	0.021
12	300	1.29	2.02	7.3	0.025
15	300	1.28	2.33	8.4	0.029
18	301	1.28	2.65	9.6	0.033
20	301	1.28	2.87	10.3	0.036
25	201	1.28	3.33	12.0	0.042
30	300	1.26	3.87	13.9	0.047
45	297	1.26	5.20	18.7	0.066
60	290	1.17	6.45	23.2	0.084
75	285	1.11	7.56	27.2	0.100
90	281	1.06	8.80	31.7	0.119
105	276	1.01	9.87	35.6	0.136
120	273	1.00	10.41	37.5	0.145

TEST 75

30.0 g ZnS 700 cm^3 H_2O 60°C 800 rpm

10% SO_2/O_2 at 500 cm^3 min^{-1} 3.6 g dm^{-3} Fe^{3+}

TIME Min.	Eh	pH	Zn^{2+} g dm^{-3}	% EXTN	$1-(1-\alpha)^{\frac{1}{3}}$
0	941	0.68	--	--	
1	681	0.68	1.47	5.3	0.018
2	655	0.73	2.14	7.7	0.026
3	643	0.74	2.47	8.9	0.031
4	633	0.75	2.75	9.9	0.034
5	628	0.75	3.00	10.8	0.037
6	625	0.76	3.22	11.5	0.040
8	623	0.76	3.56	12.8	0.044
10	624	0.77	3.93	14.1	0.049
12	626	0.78	4.56	16.3	0.058
15	630	0.78	5.04	18.1	0.064
18	633	0.79	5.53	19.8	0.071
20	637	0.79	6.00	21.5	0.078
25	642	0.79	7.00	25.1	0.092
30	645	0.78	7.72	27.7	0.102
45	653	0.76	10.13	36.3	0.139
60	660	0.73	12.39	44.4	0.178
75	668	0.67	15.01	53.7	0.226
90	675	0.62	16.89	60.5	0.266
105	678	0.57	19.71	70.6	0.335
120	676	0.56	21.58	77.2	0.389

TEST 76

30.0 g ZnS 700 cm^3 H_2O 60°C 800 rpm

50% SO_2/O_2 at 500 cm^3 min^{-1} 3.6 g dm^{-3} Fe^{3+}

TIME Min.	Eh	pH	Zn^{2+} g dm^{-3}	% EXTN	$1-(1-\alpha)^{\frac{1}{3}}$
0	840	0.43	---	--	
1	631	0.41	3.52	12.7	0.044
2	588	0.44	4.82	17.4	0.061
3	535	0.46	5.81	21.0	0.075
4	500	0.47	6.73	24.3	0.088
5	474	0.48	7.80	28.1	0.104
6	465	0.48	8.41	30.3	0.113
8	468	0.50	9.17	33.1	0.125
10	479	0.52	11.71	42.2	0.167
12	491	0.53	12.85	46.3	0.187
15	509	0.54	14.00	50.5	0.209
18	516	0.55	14.68	52.9	0.222
20	521	0.54	15.83	57.1	0.245
25	525	0.54	17.20	62.0	0.275
30	533	0.53	18.81	67.8	0.315
45	540	0.46	22.95	82.7	0.443
60	552	0.43	24.47	88.2	0.510
75	579	0.35	25.24	90.9	0.550
90	626	0.25	26.00	93.7	0.602
105	660	0.15	26.00	93.7	0.602
120	675	0.10	26.00	93.7	0.602

TEST 77

30.0 g ZnS 700 cm^3 H_2O 60°C 800 rpm

100% SO_2 at 500 cm^3 min^{-1}

TIME Min.	Eh	pH	Zn^{2+} g dm^{-3}	% EXTN	$1-(1-\alpha)^{\frac{1}{3}}$	$S_4O_6^{2-}$
0	340	1.13	--	--	---	
1	314	1.16	0.81	2.9	0.010	
2	315	1.21	1.05	3.8	0.013	
3	315	1.24	1.45	5.2	0.018	
4	319	1.21	1.83	6.6	0.023	4.28
5	319	1.27	2.14	7.7	0.026	
6	321	1.28	2.45	8.8	0.030	
8	333	1.29	3.00	10.8	0.037	
10	326	1.29	3.70	13.3	0.046	6.96
12	321	1.28	4.16	15.0	0.053	
15	318	1.28	4.85	17.5	0.062	10.8
18	315	1.27	5.62	20.3	0.073	
20	314	1.25	6.01	21.7	0.078	
25	308	1.21	7.08	25.5	0.093	
30	301	1.15	7.85	28.3	0.104	
45	285	1.02	9.70	35.0	0.134	
60	274	0.92	11.24	40.5	0.159	
75	265	0.84	12.94	46.6	0.189	29.0
90	257	0.79	14.09	50.8	0.211	
105	249	0.75	15.25	54.9	0.233	
120	242	0.69	16.17	58.3	0.253	

TEST 78

30.0 g ZnS 700 cm^3 H_2O 60°C 800 rpm

100% SO_2 at 500 cm^3 min^{-1} 3.6 g dm^{-3} Fe^{3+}

TIME Min.	Eh	pH	Zn^{2+} g dm^{-3}	% EXTN	$1-(1-\alpha)^{\frac{1}{3}}$	$S_4O_6^{2-}$ g dm^{-3}
0	536	0.92	---	--		
1	433	0.93	1.06	3.8	0.013	
2	402	0.98	1.71	6.2	0.021	
3	385	1.01	2.32	8.4	0.029	
4	369	1.02	2.93	10.6	0.037	
5	368	1.02	3.44	12.4	0.043	6.76
6	358	1.03	3.88	14.0	0.049	
8	328	1.03	4.76	17.2	0.061	
10	308	1.04	5.49	19.8	0.071	10.9
12	297	1.04	6.35	22.9	0.083	
15	290	1.04	7.13	25.7	0.094	16.4
18	281	1.04	8.50	30.6	0.115	
20	276	1.04	8.94	32.2	0.121	
25	258	1.02	9.82	35.4	0.136	
30	248	1.01	10.70	38.6	0.150	
45	239	0.96	13.23	47.7	0.194	
60	236	0.93	15.53	56.0	0.239	
75	236	0.91	17.29	62.3	0.277	41.5
90	234	0.92	18.46	66.5	0.305	
105	232	0.90	19.63	70.7	0.335	
120	232	0.90	19.92	71.8	0.344	53.6

TEST 79

30.0 g ZnS 700 cm^3 H_2O 60°C 800 rpm

10% SO_2/O_2 at 500 cm^3 min^{-1}

TIME Min.	Eh	pH	Zn^{2+} g dm^{-3}	% EXTN	$\frac{1}{1-(1-\alpha)^3}$	$S_4O_6^{2-}$ g dm^{-3}
0	366	1.37	--	--		
1	322	1.38	0.15	0.54	0.0018	
2	317	1.40	0.25	0.90	0.0030	
3	320	1.42	0.27	0.97	0.0032	
4	325	1.43	0.29	1.0	0.0033	
5	326	1.44	0.31	1.1	0.0037	--
6	327	1.44	0.32	1.2	0.0040	
8	333	1.46	0.37	1.3	0.0044	
10	335	1.48	0.42	1.5	0.0050	--
12	337	1.49	0.44	1.6	0.0054	
15	338	1.51	0.50	1.8	0.0060	0.80
18	338	1.53	0.57	2.0	0.0067	
20	339	1.54	0.59	2.1	0.0070	
25	339	1.56	0.64	2.3	0.0077	
30	339	1.57	0.71	2.6	0.0087	
45	337	1.60	1.05	3.8	0.0128	
60	336	1.65	1.10	4.0	0.0135	
75	333	1.66	1.24	4.5	0.0152	2.80
90	331	1.65	1.44	5.2	0.0176	
105	330	1.64	1.66	6.0	0.0204	
120	330	1.65	1.88	6.8	0.0232	4.20

TEST 80

30.0 g ZnS 700 cm^3 H_2O 60°C 800 rpm

50% SO_2/N_2 at 500 cm^3 min^{-1} 3.6 g dm^{-3} Fe^{3+}

TIME Min.	Eh	pH	Zn^{2+} g dm^{-3}	% EXTN	$S_4O_6^{2-}$ g dm^{-3}
0	559	1.19	---	--	
1	402	1.19	0.78	2.8	
2	329	1.24	1.23	4.4	
3	331	1.27	1.53	5.5	
4	319	1.29	1.78	6.4	
5	311	1.30	2.08	7.5	3.68
6	304	1.31	2.33	8.4	
8	300	1.33	2.73	9.8	
10	296	1.33	3.09	11.1	5.60
12	296	1.33	3.49	12.6	
15	289	1.33	3.99	14.4	7.80
18	283	1.32	4.77	17.2	
20	282	1.32	5.07	18.3	
25	269	1.31	5.67	20.4	
30	258	1.30	6.37	23.0	
45	234	1.25	8.18	29.5	
60	233	1.22	10.14	36.5	
75	224	1.25	11.54	41.6	32.3
90	222	1.27	13.15	47.4	
105	222	1.32	14.35	51.7	
120	220	1.37	15.55	56.0	40.5

TEST 81

30.0 g ZnS 700 cm^3 H_2O 60°C 800 rpm

50% SO_2/N_2 at 500 cm^3 min^{-1}

TIME Min.	Eh	pH	Zn^{2+} g dm^{-3}	% EXTN	$1-(1-\alpha)^{\frac{1}{3}}$	$S_4O_6^{2-}$ g dm^{-3}
0	329	1.25	---	--		
1	292	1.27	0.36	1.3	0.005	
2	294	1.30	0.59	2.1	0.007	
3	294	1.32	0.79	2.8	0.009	
4	295	1.34	0.92	3.3	0.011	
5	296	1.36	1.08	3.9	0.013	1.84
6	296	1.37	1.24	4.5	0.015	
8	297	1.38	1.49	5.4	0.018	
10	298	1.38	1.73	6.2	0.021	3.04
12	299	1.38	1.98	7.1	0.024	
15	296	1.37	2.31	8.3	0.029	4.28
18	294	1.36	2.55	9.2	0.031	
20	295	1.36	2.80	10.1	0.035	
25	290	1.35	3.30	11.9	0.041	
30	286	1.33	3.79	13.7	0.048	
45	270	1.25	5.10	18.4	0.066	
60	255	1.16	6.25	22.5	0.081	
75	244	1.08	7.29	26.3	0.096	15.3
90	236	1.01	8.27	29.8	0.111	
105	229	0.90	9.25	33.3	0.126	
120	225	0.81	10.24	36.9	0.142	21.8

TEST 82

30.0 g ZnS 700 cm^3 H_2O 60°C 800 rpm

10% SO_2/N_2 at 500 cm^3 min^{-1}

TIME Min.	Eh	pH	Zn^{2+} g dm^{-3}	% EXTN	$1-(1-\alpha)^{\frac{1}{3}}$	$S_4O_6^{2-}$ g dm^{-3}
0	244	1.62	--	--		
1	241	1.64	0.14	0.50	0.0016	
2	242	1.65	0.17	0.61	0.0020	
3	240	1.67	0.19	0.69	0.0023	
4	240	1.68	0.22	0.79	0.0026	
5	239	1.68	0.24	0.87	0.0029	--
6	239	1.69	0.26	0.94	0.0031	
8	238	1.69	0.29	1.05	0.0035	
10	237	1.70	0.33	1.19	0.0040	0.48
12	236	1.70	0.36	1.30	0.0044	
15	235	1.70	0.42	1.51	0.0050	0.80
18	234	1.70	0.47	1.69	0.0056	
20	233	1.70	0.49	1.77	0.0058	
25	233	1.70	0.54	1.95	0.0065	
30	233	1.70	0.61	2.20	0.0074	
45	233	1.71	0.77	2.77	0.0093	
60	229	1.72	0.93	3.35	0.0113	
75	227	1.73	1.10	3.96	0.0133	2.40
90	222	1.73	1.23	4.43	0.0149	
105	221	1.74	1.37	4.94	0.0168	
120	220	1.74	1.54	5.55	0.0188	3.60

TEST 83

30.0 g ZnS 700 cm³ H_2O 60°C 800 rpm

10% SO_2/N_2 at 500 cm³ min^{-1} 3.6 g dm^{-3} Fe^{3+}

TIME Min.	Eh	pH	Zn^{2+} g dm^{-3}	% EXTN	$S_4O_6^{2-}$ g dm^{-3}
0	624	1.30	--	--	
1	581	1.33	0.46	1.66	
2	530	1.35	0.63	2.27	
3	458	1.38	0.72	2.60	
4	385	1.40	0.80	2.88	
5	358	1.41	0.89	3.21	0.92
6	347	1.42	0.95	3.43	
8	313	1.43	1.06	3.82	
10	303	1.44	1.15	4.15	1.04
12	298	1.44	1.23	4.43	
15	286	1.45	1.40	5.05	1.40
18	280	1.46	1.49	5.37	
20	282	1.47	1.62	5.84	
25	273	1.48	1.79	6.45	
30	270	1.51	1.96	7.06	
45	260	1.56	2.44	8.79	
60	257	1.59	2.83	10.2	
75	258	1.59	3.28	11.8	5.60
90	253	1.57	3.64	13.1	
105	253	1.55	4.07	14.7	
120	265	1.53	4.34	15.6	8.68

TEST 84

30.0 g ZnS 700 cm³ H_2O 60°C 800 rpm

5% SO_2/O_2 at 500 cm³ min^{-1} 3.6 g dm^{-3} Fe^{3+}

TIME Min.	Eh	pH	Zn^{2+} g dm^{-3}	% EXTN	$1-(1-\alpha)^{\frac{1}{3}}$	$S_4O_6^{2-}$ g dm^{-3}
0	893	0.93	--	--	---	
1	683	0.95	1.46	5.3	0.018	
2	660	1.00	2.08	7.5	0.026	
3	647	1.03	2.53	9.1	0.031	
4	638	1.05	2.81	10.1	0.034	
5	634	1.06	3.15	11.4	0.040	0.48
6	629	1.09	3.26	11.8	0.041	
8	627	1.11	3.71	13.4	0.047	
10	627	1.13	3.99	14.4	0.051	0.56
12	628	1.16	4.50	16.2	0.057	
15	631	1.18	5.06	18.2	0.064	0.60
18	635	1.19	5.62	20.3	0.073	
20	636	1.18	5.85	21.1	0.076	
25	638	1.15	6.63	23.9	0.087	
30	639	1.15	7.42	26.7	0.098	
45	642	1.12	9.67	34.8	0.132	
60	647	1.07	11.47	41.3	0.163	
75	651	1.03	13.27	47.8	0.195	1.72
90	656	1.00	14.62	52.7	0.221	
105	652	0.96	16.19	58.3	0.253	
120	667	0.90	17.77	64.0	0.287	1.68

TEST 85

30.0 g ZnS 700 cm³ H_2O 60°C 800 rpm

5% SO_2/O_2 at 500 cm³ min^{-1}

TIME Min.	Eh	pH	Zn^{2+} g dm^{-3}	% EXTN	$(1-(1-\alpha)^{\frac{1}{3}}$	$S_4O_6^{2-}$ g dm^{-3}
0	390	1.61	--	--	---	
1	360	1.62	0.14	0.50	0.0017	
2	360	1.62	0.15	0.54	0.0018	
3	359	1.63	0.16	0.58	0.0019	
4	359	1.64	0.17	0.61	0.0020	
5	360	1.65	0.19	0.69	0.0023	0.40
6	360	1.65	0.21	0.76	0.0025	
8	361	1.66	0.23	0.83	0.0028	
10	361	1.67	0.26	0.94	0.0031	0.40
12	361	1.68	0.27	0.97	0.0033	
15	361	1.70	0.31	1.12	0.0037	0.40
18	359	1.72	0.34	1.23	0.0038	
20	358	1.73	0.35	1.26	0.0042	
25	356	1.76	0.39	1.41	0.0046	
30	354	1.78	0.43	1.55	0.0052	
45	348	1.84	0.52	1.87	0.0062	
60	344	1.86	0.60	2.16	0.0072	
75	342	1.86	0.67	2.41	0.0081	1.48
90	341	1.86	0.71	2.56	0.0086	
105	337	1.87	0.75	2.70	0.0091	
120	335	1.87	0.88	3.17	0.0106	2.24

TEST 86

30.0 g ZnS 700 cm³ H_2O 60°C 800 rpm

5% SO_2/N_2 at 500 cm³ min^{-1} 3.6 g dm^{-3} Fe^{3+}

TIME Min.	Eh	pH	Zn^{2+} g dm^{-3}	% EXTN	$S_4O_6^{2-}$ g dm^{-3}
0	634	1.37	--	--	
1	606	1.38	0.45	1.6	
2	577	1.41	0.62	2.2	
3	549	1.32	0.67	2.4	
4	520	1.43	0.74	2.7	
5	478	1.43	0.78	2.8	0.60
6	427	1.44	0.83	3.0	
8	367	1.45	0.91	3.3	
10	351	1.45	0.99	3.6	0.60
12	336	1.47	1.08	3.9	
15	329	1.47	1.16	4.2	0.88
18	315	1.47	1.24	4.5	
20	312	1.48	1.28	4.6	
25	305	1.48	1.41	5.1	
30	298	1.48	1.53	5.5	
45	279	1.50	1.83	6.6	
60	268	1.52	2.08	7.5	
75	260	1.53	2.33	8.4	2.92
90	255	1.54	2.49	9.0	
105	252	1.55	2.66	9.6	
120	243	1.56	2.87	10.4	4.32

TEST 87

30.0 g ZnS 700 cm^3 H_2O 60°C 800 rpm

5% SO_2/N_2 at 500 cm^3 min^{-1}

TIME Min.	Eh	pH	Zn^{2+} g dm^{-3}	% EXTN	$S_4O_6^{2-}$ g dm^{-3}
0	329	1.82	---	--	
1	278	1.81	0.073	0.26	
2	273	1.80	0.096	0.35	
3	272	1.80	0.107	0.39	
4	269	1.80	0.116	0.42	
5	268	1.81	0.121	0.44	--
6	266	1.80	0.130	0.47	
8	262	1.80	0.141	0.51	
10	260	1.80	0.164	0.59	--
12	259	1.80	0.176	0.63	
15	256	1.80	0.198	0.71	--
18	254	1.80	0.210	0.76	
20	253	1.80	0.233	0.84	
25	250	1.79	0.255	0.92	
30	247	1.80	0.290	1.05	
45	232	1.81	0.369	1.33	
60	239	1.82	0.438	1.58	
75	235	1.83	0.495	1.78	0.92
90	233	1.83	0.563	2.03	
105	231	1.83	0.609	2.19	
120	228	1.84	0.678	2.44	1.48

TEST 88

30.0 g ZnS 700 cm^3 H_2O 60°C 800 rpm

10% SO_2/N_2 at 500 cm^3 min^{-1} 3.6 g dm^{-3} Fe^{3+}

TIME Min.	Eh	pH	Zn^{2+} g dm^{-3}	% EXTN	$S_4O_6^{2-}$ g dm^{-3}
0	428	1.90	--	--	
1	427	1.87	0.13	0.47	
2	355	1.89	0.16	0.58	
3	326	1.89	0.17	0.62	
4	319	1.90	0.20	0.71	
5	313	1.90	0.22	0.80	0.36
6	312	1.91	0.25	0.91	
8	314	1.90	0.28	1.03	
10	313	1.90	0.31	1.14	0.48
12	311	1.90	0.34	1.25	
15	313	1.91	0.39	1.43	0.88
18	314	1.91	0.42	1.51	
20	314	1.91	0.47	1.69	
25	311	1.91	0.53	1.91	
30	311	1.91	0.59	2.11	
45	303	1.91	0.83	3.02	
60	294	1.90	1.08	3.91	
75	286	1.89	1.26	4.58	3.32
90	278	1.87	1.48	5.35	
105	272	1.87	1.66	6.02	
120	266	1.86	1.90	6.90	4.88